HAL
open science

Modélisation et conception des micro commutateurs RF MEMS a actionnement électrostatique et/ou piezoélectrique

Hikmat Achkar

To cite this version:

Hikmat Achkar. Modélisation et conception des micro commutateurs RF MEMS a actionnement électrostatique et/ou piezoélectrique. Micro and nanotechnologies/Microelectronics. Université Paul Sabatier - Toulouse III, 2009. English. NNT : . tel-00462560

HAL Id: tel-00462560

https://theses.hal.science/tel-00462560v1

Submitted on 10 Mar 2010

HAL is a multi-disciplinary open access archive for the deposit and dissemination of scientific research documents, whether they are published or not. The documents may come from teaching and research institutions in France or abroad, or from public or private research centers.

L'archive ouverte pluridisciplinaire **HAL**, est destinée au dépôt et à la diffusion de documents scientifiques de niveau recherche, publiés ou non, émanant des établissements d'enseignement et de recherche français ou étrangers, des laboratoires publics ou privés.

THÈSE

En vue de l'obtention du

DOCTORAT DE L'UNIVERSITÉ DE TOULOUSE

Délivré par : *l'Université de Toulouse III - Paul Sabatier*
Discipline : *Génie mécanique et microsystème*

Présentée et soutenue par *Hikmat ACHKAR*
Le *17 juillet 2009*

TITRE : *MODELISATION ET CONCEPTION DES MICRO COMMUTATEURS RF MEMS A ACTIONNEMENT ELECTROSTATIQUE ET/OU PIEZOELECTRIQUE.*

JURY

Jean GRILHE, *Professeur, université de Poitiers (President)*
Lionel BUCHAILLOT, *Directeur de recherche, IEMN, Lille (Rapporteur)*
Pierre BLONDY, *Professeur, université de Limoge, Xlim (Rapporteur)*
Robert PLANA, *Professeur, université de Toulouse, LAAS-CNRS (Examinateur)*
Marc SARTOR, *Professeur d'université, INSA-Toulouse, LGMT (Directeur de thèse)*
Patrick PONS, *Chargé de recherche, LAAS-CNRS (Directeur de thèse)*
Emmanuel DEFAY, *Ingénieur-recherche HDR, Léti, Grenoble (Invité)*
Xavier LAFONTAN, *President NOVAMEMS, Toulouse (Invité)*
David PEYROU, *Docteur - Professeur de Chaire Supérieure, Saint-Maur des Fossés (Invité)*

Ecole doctorale : *Mécanique, Energétique, Génie civil et Procédés (MEGeP)*

Unité de recherche : *LAAS-CNRS*

Directeur de Thèse : *Marc SARTOR (INSA-Toulouse), Patrick PONS (LAAS-CNRS)*

Abstract

MEMS are electromechanical system that have a micrometric scale including sensors as well as actuators (micro motor, micro mirrors, micro switches...) manufactured using the conventional micro-electronics techniques (growth of oxide, material deposition, lithography). The majority of RF MEMS switches are actuated using the electrostatic forces to vary the distance between the two electrodes to cut or transmit the signal. This type of actuation, despite its advantages, has a major drawback which is the dielectric charging which leads to the failure of the switch. To solve this problem, we worked in parallel in two directions. The first direction consists of changing the type of actuation, which is the main reason for charging and failure, to piezoelectric while the second consists of keeping the electrostatic actuation while improving the behavior of the structures by increasing the restoring force used to overcome this charging phenomenon without increasing the actuation voltage. This work has succeeded a major step which is the numeric platform validation before using it to simulate the structure.

Acknowledgement

Le travail présenté dans ce mémoire a été effectué au Laboratoire d'Analyse et d'Architecture des Systèmes (LAAS) du Centre National de la Recherche Scientifique (CNRS) de Toulouse, au sein du groupe MINC (MIcro et Nanosystèmes pour les Communications sans fils). Je tiens tout d'abord à remercier Monsieur Raja CHATILA, Directeur du LAAS pour m'avoir accueilli dans le laboratoire et également pour la bienveillance qu'il m'a manifestée. Je remercie également Monsieur Robert PLANA, Directeur de recherche, professeur des universités à Toulouse, examinateur de mes travaux de thèse et responsable du groupe MINC.

Je remercie vivement Monsieur Lionel BUCHAILLOT, Directeur de recherche à l'IEMN-CNRS Lille, et Monsieur Pierre BLONDY, Professeur à l'Université de Limoges XLIM, pour l'intérêt qu'ils ont porté à ce mémoire en acceptant d'être les rapporteurs de mes travaux.

J'exprime également ma reconnaissance à Messieurs Emmanuel DEFAY, ingénieur-chercheur HDR au Léti, Xavier LAFONTAN, Président de NOVAMEMS et David PEYROU, Docteur - Professeur de Chaire Supérieure, Saint-Maur des Fossés, pour avoir accepté d'examiner mes travaux de thèse et de participer au jury de thèse. J'exprime ma gratitude à Monsieur Jean GRILHE, Professeur émérite de l'université de Poitiers, pour l'honneur qu'il a bien voulu nous faire en acceptant à la fois de juger mes travaux et de présider notre jury.

Je tiens à exprimer ma profonde reconnaissance à Monsieur Patrick PONS, Chargé de recherche au CNRS et à Monsieur Marc SARTOR, Professeur à l'Institut National des Sciences Appliquées de Toulouse, pour la confiance qu'ils m'ont témoignée en acceptant la direction de mes travaux ainsi que pour leurs soutiens, leurs conseils, leurs disponibilités et les échanges scientifiques que nous avons eu.

Je remercie également l'ensemble du personnel du LAAS pour son aide et plus spécialement les membres du groupe MINC, les membres du service TEAM, les membres du service Sysadmin, Madame Brigitte DUCROCQ, Monsieur Christian BERTY, Monsieur Daniel DAURAT et Monsieur Yves CROUZET pour leur sympathie et leur disponibilité.

Je n'oublie pas également mes amis et collègues du travail qui m'ont aidé en créant une ambiance agréable et amicale tout au long de ces années de thèse : Mohamed

SAADAOUI (momo), Younes LAMRANI (Jonas), Mohamed LAMHAMDI (Goldo), Fabienne PENNEC, Michal OLSZACKI, Cesary MAJ, Jean François LE NEAL, Christine MOLLIET, Mohamed Mehdi JATLAOUI, Fabio COCCETTI, Gustavo Adolfo ARDILA RODRIGUEZ, Jinyu RUAN, Tonio IDDA, Fadi KHALIL, Karim YACINE, Euloge , Dimitri LERAY, Christina VILLENEUVE, Ahmed ALI, Heba, Badreddine OUAGAGUE, Hicham YOUSSEF, André FERRAND, Antoine GHOSN,...

List of Figures

2.1. Scale giving an idea about the Microsystem size 6
2.2. Comparing the size of MEMS to a macro object 7
2.3. Gold resonating MOS gate structure, the first MEMS [1] 8
2.4. Applications of MEMS sorted by type and by domain 9
2.5. Example of medical application of MEMS [2] 11
2.6. Forecast for MEMS market [3][4] 12
2.7. Shunt and series configuration for resistive and capacitive switch 13
2.8. A RF MEMS switch scheme in both states, on and off 14
2.9. A RF MEMS resistive switch schemes. 15
2.10. Forecast for the usage of RF MEMS switches in mobile phones technology [5] 16

3.1. Actuation methods divided into molecular forces and field forces. 23
3.2. Different ways to use the electrostatic actuation 23
3.3. The electrostatic force in the case of out-of-plane actuation. 24
3.4. The electrostatic force in the case of lateral (or in-plane) actuation. . . . 25
3.5. Electromagnetic actuation. 26
3.6. The piezoelectric actuation mechanism [6][7]. 28
3.7. The in-plane modes of thermal actuation.[8][9] 29
3.8. The out-of-plane thermal actuation mode [6][10]. 30
3.9. The bipolar actuation method to reduce charging. 32
3.10. Lifetime measured at 85°C for different actuation signal methods[11]. . . 32
3.11. The contact state for solid-solid and solid-liquid contact. 33
3.12. Actuation using electrostatic force for liquid contact. 34
3.13. Actuating the Mercury drop by heating [12]. 34
3.14. Dielectric switch in both states up and down with a schematic view of substrate charging (XLIM laboratory) [13] [14] [15]. 36
3.15. RF MEMS switch with dimples on the contact area of the membrane (IMEC laboratory) [16]. 37
3.16. Electrostatic actuation with the actuation pads different than the contact electrode. 38
3.17. Résumé de la capacité des différents logiciels à résoudre des problèmes multiphysiques. 40

4.1. Contact model description 42

4.2. Finite element model for the contact between a cylinder and a plane . . . 43
4.3. Contact pressure using COMSOL 3.4. 44
4.4. Finite element model, as built on ANSYS10, for the contact between a cylinder and a plane 44
4.5. Contact pressure as simulated using ANSYS10. 45
4.6. Contact pressure as a function of the arc distance for COMSOL, ANSYS and analytical results. 47
4.7. Contact model description 48
4.8. Material properties of the piezoelectric stack in the actuator model. . . . 48
4.9. Mechanical and electrical Boundary Conditions (B.C) for Piezoelectric model. 49
4.10. Finite element simulation results 50
4.11. Deflection along the cantilever for simulated and analytical results. . . . 51
4.12. The geometrical parameters of the switch model, windmill design, used to compare COMSOL to ANSYS. 53
4.13. Finite element simulation results for windmill design, for ANSYS and COMSOL comparision 54
4.14. The electrostatic model geometry. 55
4.15. Summary of different software capacities for multiphysics problems. . . . 58

5.1. Geometrical description of Model I and its material properties. 63
5.2. Finite element simulation results for model I 64
5.3. Cut along the actuator (Model I). 64
5.4. Simulated vibration modes for model I. 65
5.5. Geometrical description of Model II. 66
5.6. Finite element simulation results for model II 66
5.7. Cut along the actuator of the windmill design (Model II). 67
5.8. Simulated vibration modes for model II. 67
5.9. Geometrical description of Model III. 68
5.10. Finite element simulation results for model III 69
5.11. Simulated vibration modes for model III. 70
5.12. Geometrical description of Model IV. 70
5.13. Finite element simulation results for model IV 71
5.14. Cut along the actuator of the cross design (Model IV). 72
5.15. Simulated vibration modes for model IV. 72
5.16. Geometrical description of the stack with platinum as compensation layer. 75
5.17. Deflection of the stack described in 5.16 as a function of platinum thickness and the initial stress in SiN, for SiN thickness 500nm. 75
5.18. Deflection of the stack described in 5.16 as a function of platinum thickness and the initial stress in SiN, for SiN thickness 1000nm. 76
5.19. Deflection of the stack described in 5.16 as a function of platinum thickness and the initial stress in SiN, for SiN thickness 2000nm. 76

5.20. Geometrical description of the stack for stress and thermal compensation. 77
5.21. Deflection of the actuator for Pt initial stress of 500 and 1100MPa. . . . 78
5.22. The actuator initial deflection due to thermal mismatch. 79
5.23. Deflection of the actuator for temperture variation from -40°C to 85°C with a reference temperature of 20°C. 80
5.24. Experimental measurments of the cantilever deflection with the stack of figure 5.20 as a function of the annealing temperature of Pt. 81
5.25. The membrane flatness of model II. 81
5.26. The membrane flatness of model III. 82
5.27. The membrane flatness of model IV. 82
5.28. The membrane flatness for model II after contact. 83
5.29. The membrane flatness for model IV after contact. 83

6.1. The shift in the C-V curve of an electrostatic switch. 87
6.2. The geometrical parameters of an electrostatic switch. 88
6.3. Graph of the applied forces on the beam as a function of the distance between the bridge and the electrode. 89
6.4. Graph of the applied forces on the beam showing a nonlinear stiffness. . . 90
6.5. Representaion of the concept to have non linear stiffness. 90
6.6. Representaion of the concept after contact. 91
6.7. The geometry of the stopper and different dimensions. 91
6.8. Geometry of the model used for simulation. 93
6.9. Simulation of the straight fixed-fixed beam on COMSOL3.4. 93
6.10. Graph of the displacement at the center of the beam as a function of the element size. 94
6.11. The regenerated geometry for a switch without stoppers. 95
6.12. The regenerated geometry for a switch with stoppers. 95
6.13. Photos showing the direction of the stress direction. 96
6.14. Model simulated to find new coordinate systems following the topology. . 97
6.15. the X-axis direction shown by arrows for the geometry with stoppers in order to validate the method. 97
6.16. The deflection of the beam due to 10MPa initial stress as simulated in the global coordinate system. 98
6.17. The deflection of the beam due to 10MPa initial stress as simulated in the local coordinate system. 98
6.18. The Deflection due to initial stress of the real geometry for a switch without stoppers. 99
6.19. The Deflection due to initial stress of the real geometry for a switch with stoppers. 100
6.20. The cut view of the deflection of the real geometry without stoppers due to initial stress. 101

6.21. The cut view of the deflection of the real geometry with stoppers due to initial stress. 101
6.22. The deflection of a straight beam under the action of 10MPa initial stress due to the anchor. 102
6.23. isolated parts of the structure with the forces acting on them. 103
6.24. The deflection of a beam with 5μm wide stoppers and 500μm inter-distance, under the action of 10MPa initial stress. 104
6.25. The deflection of a beam with 10μm wide stoppers and 500μm inter-distance, under the action of 10MPa initial stress. 105
6.26. The deflection of a beam with 20μm wide stoppers and 500μm inter-distance, under the action of 10MPa initial stress. 105
6.27. The deflection of a beam with 5μm wide stoppers and 800μm inter-distance, under the action of 10MPa initial stress. 106
6.28. The deflection of a beam with 5μm wide stoppers and 200μm inter-distance, under the action of 10MPa initial stress. 106
6.29. A cut view of the deflection due to initial stress along the beam for different stoppers width with respect to a flat beam. 107
6.30. A zoom in the stoppers zone for cut view presented in figure 6.29. 108
6.31. A cut view of the deflection due to initial stress along the beam for different stoppers position with respect to a flat beam. 108
6.32. Modeling of a straight beam to calculate its mechanical stiffness. 109
6.33. Simulation of the beam with 5μm wide stopper and inter-distance of 500μm 110
6.34. Simulation of the beam with 10μm wide stopper and inter-distance of 500μm 110
6.35. Simulation of the beam with 20μm wide stopper and inter-distance of 500μm 110
6.36. Simulation of the beam with 5μm wide stopper and inter-distance of 200μm 111
6.37. Simulation of the beam with 5μm wide stopper and inter-distance of 800μm 112
6.38. Graph of the displacement at the center of the beam as a function of the applied force for different stopper width and an inter-distance between the stoppers Ls=500μm. 114
6.39. Graph of the displacement at the center of the beam as a function of the applied force for different stoppers inter-distance. 115
6.40. Contact model 116
6.41. Simulation results for the contact model at different stages. 117
6.42. Graph of the load-displacement curve of the beam for contact model. . . 118
6.43. Constraint model 119
6.44. Graph of the load-displacement curve comparing the two studied models. 120
6.45. The model used to simulate stoppers on coventor. 123
6.46. The hysteresis behavior for the design with and without stoppers. 123
6.47. Scheme of the stopper design parameter shown on a deformed bridge. . . 126
6.48. Graph showing the different points used for the design. 127
6.49. Flow chart of the stopper design parameters. 134
6.50. Scheme of the design parameters. 135

6.51. First choice, depositing stoppers on the fixed part. 135
6.52. Second choice, creating the stoppers in the bridge using two sacrificial layers. 136
6.53. Third choice, creating the stoppers in the bridge using partial screening. 136
6.54. Profile of the etched hole in the photoresist for stopper deposition. 137

A.1. Forces diagram acting on the beam with stoppers 143
A.2. The two load cases used for superposition. 143
A.3. Scheme of the concentrated load. 144
A.4. Scheme of the two symetrical concentrated loads. 145
A.5. Superposition of two groupes of forces. 146
A.6. Modele of a beam like stretched wire with a concentrated load. 149
A.7. Model of a beam as a stretched wire with stoppers and two symetric concentrated loads. 150

List of Tables

3.1. Summary of the actuation methods characteristics.[17][18] 31

4.1. Material properties and dimensions for the piezoelectric stack layers. . . . 47
4.2. Material properties of the piezoelectric stack layers for the windmill design. 52
4.3. Simulation results of the windmill design for different element size. 53
4.4. Geometrical dimensions of the bridge material. 54
4.5. Material properties of the bridge material. 54

5.1. Dimensions of the piezoelectric stack of the actuator model I. 62
5.2. Summary of the studied criteria for the different models. 74

6.1. Simulation parameters for mesh size tunning. 92
6.2. Simulation parameters for real geometry simulation. 94
6.3. Summary of the initial deflection for different stopper size and positions. 107
6.4. Summary of the relative shift for different stopper width with respect to a straight beam. 113
6.5. Summary of the relative error for different inter-distance between the stoppers with respect to a straight beam. 114
6.6. Simulation parameters for stiffness extraction by constraint method. . . . 116
6.7. Mechanical boundary conditions for the constraints model to extract the stiffnessK_s after contact. 118
6.8. Results summary for both methods. 119
6.9. Comparing analytical to numerical values of stiffness (K) before contact and (K_s) after contact. 121
6.10. Pull-in voltage calculated by analytical formula. 124
6.11. Pull-in voltage obtained for real geometry and for perfectly straight geometry. 124
6.12. The fixed parameters for the design. 128
6.13. The calculated design parameters. 128
6.14. The MEMS switch process (LAAS). 131
6.15. Measured geometrical parameters versus targetted value 132

Contents

1. General introduction **1**

2. Overview on MEMS **6**
2.1. Introduction to MEMS 6
2.1.1. Definition of MEMS 6
2.1.2. History 7
2.1.3. Interest and applications 8
2.1.4. RF MEMS and RF MEMS switches 12
2.2. Challenges facing RF MEMS switches and solutions 14
2.2.1. Will RF MEMS switches find their way to the market? 15
2.2.2. Reliability 16
2.2.3. Packaging 17
2.2.4. Manufacturing 17
2.2.5. Material characterisation 17
2.2.6. Modelling and simulation 17

3. Approaches for solution **21**
3.1. Introduction 21
3.2. Actuation methods 22
3.2.1. Electrostatic actuation 22
3.2.2. ElectroMagnetic actuation 26
3.2.3. Piezoelectric actuation 26
3.2.4. Electrothermal actuation 27
3.2.5. Magnetostrictive actuation 29
3.2.6. Shape memory alloys (SMA) 29
3.2.7. Comparision of actuation methods 30
3.3. Solutions for charging problem in electrostatic actuation 31
3.3.1. Bipolar actuation and HOLD-ON voltage 31
3.3.2. Liquid contact 32
3.3.3. Dielectricless switch 34
3.3.4. Side actuation 35
3.4. Conclusion 35

4. Numerical platform validation **41**
4.1. Introduction 41

4.2. Contact models . . . 42
4.2.1. Model description . . . 42
4.2.2. COMSOL . . . 42
4.2.3. ANSYS . . . 43
4.2.4. Analytical results . . . 45
4.2.5. Comparison . . . 46
4.3. Piezoelectric models . . . 46
4.3.1. Actuator . . . 46
4.3.2. Switch . . . 51
4.4. Electrostatic models . . . 53
4.4.1. Model description . . . 53
4.4.2. COMSOL . . . 54
4.4.3. Coventor . . . 55
4.4.4. Analytical results . . . 55
4.4.5. Comparison . . . 55
4.5. Conclusion . . . 56

5. Piezoelectric actuation 61
5.1. Introduction . . . 61
5.2. Design study . . . 61
5.2.1. Introduction . . . 61
5.2.2. Simple actuator design (Model I) . . . 62
5.2.3. Windmill design (Model II) . . . 63
5.2.4. Circular design (Model III) . . . 67
5.2.5. Cross design (Model IV) . . . 69
5.2.6. Comparision of different designs and conclusion . . . 71
5.3. Initial deflection problem . . . 73
5.3.1. Initial stress disequilibrium . . . 73
5.3.2. Thermomechanical disequilibrium . . . 77
5.4. Membrane flatness problem . . . 78
5.5. Conclusion . . . 79

6. Electrostatic actuation 86
6.1. Introduction . . . 86
6.2. Finite element modeling . . . 89
6.2.1. Introduction . . . 89
6.2.2. Tuning the mesh size . . . 92
6.2.3. Real geometry simulations . . . 92
6.2.4. Effect of initial stress on initial deformation. . . . 92
6.2.5. Effect of stoppers size and position on the initial stiffness . . . 107
6.2.6. Simulation of the force-displacement curve . . . 114
6.2.7. Analytic validation . . . 119

6.3. Design 125
6.4. Fabrication 128
6.4.1. Stopper developement 128
6.4.2. Switch process 130
6.4.3. Geometrical measurments 132

7. General conclusion and perspective 140

A. Analytical model 142
A.1. Introduction 142
A.2. Stiffness due to bending 142
A.3. Stiffness due to initial stress 149

1. General introduction

The widest domain of application foreseen for RF MEMS switches is the mobile phones, also known by the "cell phone billion unit market". This explains the news about ramping-up its production and the interest of big companies existing on the cell phone market to develop a reliable RF-MEMS switch [19]. In this orientation, our group decided to work in the direction to obtain a reliable RF MEMS switch and capable to fulfill certain criteria.

The interest of using RF-MEMS switches is their high linearity, low loss, high Q factor and especially for mobile phones their negligible power consumption. In addition to these characteristics, The design of any RF-MEMS switch for mobile phones should lead to a component with low actuation voltage and less sensitive to temperature variations with the simplest process for mass production. An actuation voltage of less than 5V is needed, so we chose to fix it to 3V in this study, while the temperature conditions vary from -40°C to 85°C.

Most RF MEMS switches use electrostatic force to actuate the structure, as to create the variable capacitor needed. Despite the negligible power consumption and the high contact force of electrostatic RF MEMS switches, this type of actuation has a major drawback which is the dielectric charging causing stiction. Stiction now is the main reliability issue in order for RF MEMS to hit the market. For this reason, our study will be done on two axes to solve the stiction problem; the first is changing the actuation method in order to reduce charging while the second consists of keeping the electrostatic actuation but proposing a design to overcome stiction.

The thesis is organized as follows; The first chapter of this PhD thesis gives a general overview about the MEMS. It shows the historical backgroung about the MEMS and how it developed to become interesting to almost all the industriel domaines. We will then talk about the interest of using RF MEMS held by a market study. In the last part of the same chapter, we present briefly the challenges facing the MEMS which will introduce us to the work presented in this thesis.

As already stated, the two axes that we will follow in order to solve the stiction issue are, either changing the actuation type or propose a design to reduce stiction in electrostatic switches. For this purpose, chapter II is devoted to the state of the art of the actuation methodes existing for MEMS as well as some solutions used to reduce the stic-

tion in electrostatic switches. The first part of the chapter describes different actuation methodes with their advantages and drawbacks with respect to our application and our specifications. A second part presents the solutions to reduce stiction either by controlling the actuation signal (Bipolar actuation), a dielectricless switch or actuating a liquid drop.

Before begining our study, we shall validate the numerical platform and test the capacity of different softwares, which is what will be presented in chapter III. Specific models are used to test the contact problem due to its importance when used to simulate the contact of the deformable membrane with the electrode. For this reason, a contact model built on COMSOL is compared to analytical results and to numerical results simulated using ANSYS. Piezoelectric actuation are also validated using two different models, a simple model for validation with analytical results and a more complicated one to compare with ANSYS. Finally, we validated the electrostatic actuation using a bridge model on COMSOL and Coventor.

We are interested in studying capacitive switches. An initial gap of 1.5μm is needed to respect the list of specifications. The value of the down state capacitance will define the dimensions of the moving membrane forming the capacitance.

Once the softwares are chosen, chapter IV deals with the study of feasibility of a switch with piezoelectric actuation. First, we study the simple actuator which will consist the common part of the three designs. Three different designs of piezoelectric switch are then presented. A study is realized on the deflection of each structure under a bias of 3V in order to compare between the designs for a better performance. The time response as well as the Eigen frequencies are calculated and serve only for comparison between designs because the damping parameters we have are not precise. In a later part of this chapter, we verified some important points relative to capacitive switches, like the flatness of the membrane after actuation, the initial deflection (due to initial stress gradient and temperature variations) and the way to solve them.

On the other hand, we carried a study of a new concept for the reduction of the stiction effect on the reliability of the electrostatic RF MEMS switch. In this part we didnt respect the design specifications of the capacitance and actuation voltage, we focuse on the validation of the new concept. The actuation voltage that we tolerate is 10V to stay in low voltages. Chapter V deals with this new concept consisting of a variable stiffness through the actuation. Firstly, we explain the principle and the interest of having the double stiffness state obtained by adding stoppers. An analytical mechanical model of the switch is presented, which is used for predesign of the stoppers position. Finite element simulations are then done to complete the design phase and fixe the final parameters, as well as, verifying the effect of the initial stress on the deflection. Finally we present the design of the test structure and the fabrication process permitting us to obtain the switch with stoppers.

The softwares are validated, and were classified as a function of application. The feasibility study of a piezoelectric actuator shows a good results but with a significant complexity in fabrication. The study of the electrostatic switch with the stopper design is promising, especially that we decoupled the pull-in from the pull-out.

Vu d'ensemble sur les MEMS

Le nom de MEMS est une abréviation pour Systèmes Micro Electro-Mécaniques (Micro Electro Mechanical Systems). Comme leur nom indique, ils sont des machines ou des structures mécaniques ayant de très petites dimensions, allant de 0.1μm jusqu'à l'ordre quelques millimètres. Ces systèmes électromécaniques comprennent des capteurs ainsi que des actionneurs (micro moteurs, micro miroirs, micro relais...) fabriqués avec les techniques de la micro-électronique conventionnelle (croissance d'oxyde, dépôt de matériaux, lithographie).

Feynman, pendant son discours le 29 décembre à CALTECH, il a tiré l'attention des chercheurs sur la petite échelle quand il a écrit sa phrase célèbre " il y a assez d'espace au fond ". Il était le premier à parler des micro-machines et à comprendre leur intérêt et les problèmes reliés à la physique aux très petites dimensions. Au mois de Mars 1967 citeNATHANSON67, le premier papier sur un composant MEMS a été publié concernant la structure de port de MOS en or résonnant (figure 2.3). Pourtant le terme de MEMS n'existait pas à l'époque. De nos jours, MEMS est devenu un terme largement utilisé et résume une grande variété de composants variant des microcapteurs aux microactionneurs. Les européens préfèrent le terme Microsystems alors que les Japonais préfèrent le terme micromachines. [20]

L'intérêt d'utilisation des MEMS réside principalement dans leur poids, leur taille, et leur coût. S'ajoute à cela le fait que ces systèmes peuvent avoir des applications spécifiques comme RF-MEMS dont l'intérêt est le suivant :

- Leur faible masse fait d'eux un bon candidat pour plusieurs d'applications surtout dans le domaine spatial. Ceci a été confirmé par les discours de multiples participants Pendant l'atelier de CANEUS qui a pris lieu au CNES (Centre National Spatial) au mois de mai 2008, cet intérêt lié à la masse a été confirmé par multiples participants comme ASC (Agence Spatiale Canadienne), DGA (Délégation Générale verse l'Armement), Airbus, ThalesAlenia space et autres.

- Leur miniaturisation (volume réduit) permet leur intégration et augmente la fiabilité d'un système via la redondance de microsystèmes multiples. Par exemple, pendant l'atelier de CANEUS (Toulouse, mai 2008), ThalesAlenia space a montré l'intérêt d'utilisation de technologie MEMS grâce à son rôle de réduction de la taille de l'antenne par satellite frontale.

- La réduction de coût, en lançant la fabrication en chaine ou en masse. Cette qualité est intéressante pour toutes les applications industrielles et constitue la clef de la commercialisation des MEMS.

Les avantages énumérés ci-dessus ont donné au MEMS leur billet pour beaucoup d'applications. Le RF-MEMS utilisés dans différents domaines comme la communication sans fil (la télécommunication et l'industrie mobile), les systèmes de radar, les satellites et la radio militaire. Le commutateur de RF-MEMS est à la base des fonctions complexes comme les antennes reconfigurables, les capacités variables et le "signal rerouting".

RF-MEMS sont des Micro structures mécaniques conçues pour réaliser les fonctions électriques dans les systèmes de radiofréquence. L'objectif d'utilisation de RF-MEMS est de remplacer les composants électroniques et quelques fonctions réalisées par les circuits intégrés par un composant de MEMS offrant un meilleur fonctionnement (moins de perte, facteur Q élevé, faible consommation et haute linéarité). Ils sont fabriqués par l'utilisation de 5 à 8 étapes de photolithography (5 à 8 masques), ce qui leur confère un avantage technologique par rapport au MMIC (Circuits intégrés de Micro-onde Monolithiques) qui a besoin de 13 à 25 étapes de lithographie citewikipediarfmems.

Les commutateurs RF-MEMS sont des microstructures mobiles actionnées par accouplement électromécanique afin de créer un court-circuit utilisé pour le traitement de signal (filtrant et/ou déviant le signal). Les structures les plus communes utilisées sont des ponts et des poutres. Ces structures remplissent la tâche souhaitée et sont faciles à modéliser. Elles sont divisées en deux types : capacitif et résistif.

- Le type capacitif, surtout utilisé en configuration shunt, sont des structures actionnées pour former un condensateur variable entre la ligne de signal et la masse. Contrairement au commutateur résistif, la structure actionnée forme la première électrode en ayant alors un contact métal avec le diélectrique (voit la figure 2.8(a)). Quand elle est actionnée, la valeur de capacitance formée entre la structure et le signal revêt des changements pour court circuiter le signal ou lui permettre de passer (voir la figure 2.8(b)). Le rapport de la capacitance entre les positions finale et initiale est une propriété importante du commutateur ainsi que sa tension d'actionnement. Ce type de commutateur est utilisé pour changer des signaux dans une gamme de fréquence entre 6 et 120 GHz citeRebeiz1.

- Le commutateur résistif, utilisé en configuration série, aussi connu par le commutateur à contact métal-métal et fonctionne selon le même principe que le commutateur capacitif. Quand la structure est actionnée le signal est laissé passer reflété. Ce type de commutateur est utilisé surtout pour changer le signal de basse fréquence variante de DC à 60 GHz citeRebeiz1 (voir la figure 2.9).

2. Overview on MEMS

2.1. Introduction to MEMS

2.1.1. Definition of MEMS

MEMS is the abbreviation for Micro Electro Mechanical Systems. As their name indicates, they are mechanical machines or structures having very small dimensions ranging from sub micron level (0.1μm) up to few millimetres (figure 2.1). The understanding of this definition for Europeans differs from that of the Americans. Starting by the American definition, the MEMS is an electro mechanical system in the micrometric scale containing sensors as well as actuators fabricated using the conventional techniques of micro-electronics (growth of oxides or dielectrics, metal deposition, lithography, wet or dry etching).

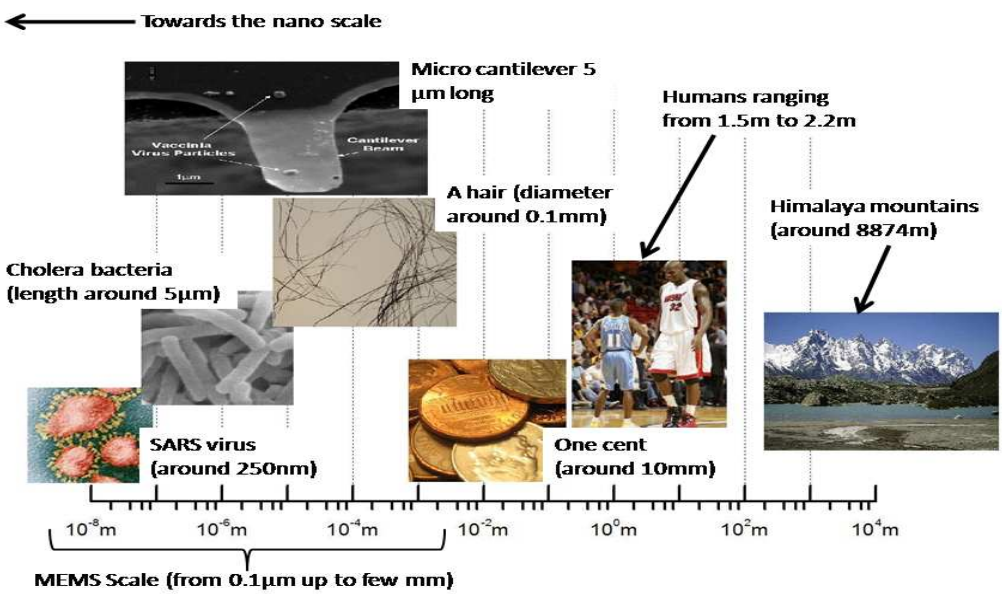

Figure 2.1.: Scale giving an idea about the Microsystem size

Concerning the European definition, microsystems are intelligent miniaturized systems combining sensors and actuators to some functions of signal treatment.

As already cited, these systems use the fabrication techniques developed for integrated circuit industry in order to combine electrical components with mechanical elements

such as beams, bridges, diaphragms, gears and springs. It is a combination of material deposition at controlled thickness, with selective etching in specific regions using masks and photolithography finishing by sacrificial layers removal in order to built a three dimensional micro structure.

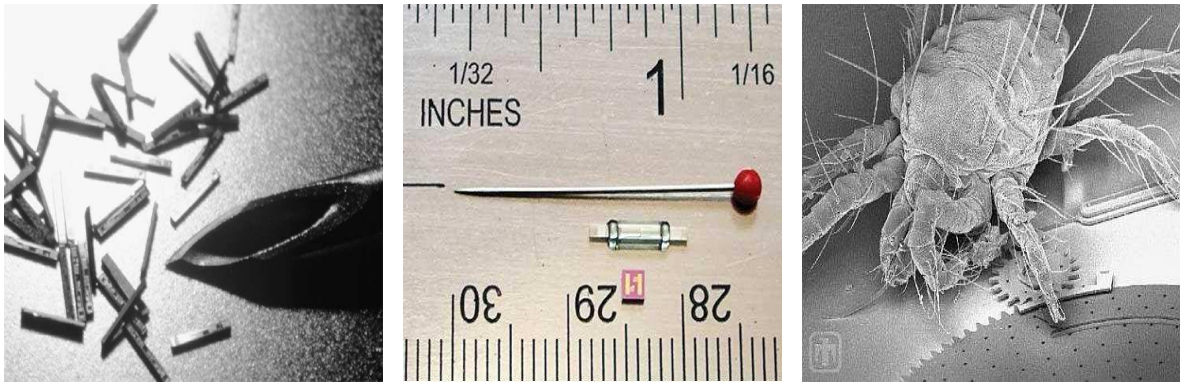

(a) Pressure sensors versus a thin needle [2]

(b) A MEMS switch developed by MEMSCAP

(c) The smallest mite on the top of micro gears developed by Courtesy Sandia National Laboratories

Figure 2.2.: Comparing the size of MEMS to a macro object

2.1.2. History

Each year, after the meeting of the American Physical Society, new ideas come out and new axis for research is opened. Year 1959 was different. Feynman, during his talk on the 29th of December at CALTECH, opened the eyes of researchers on the small scale when he spelled his famous sentence "There's plenty of room at the bottom". He was the first to talk about micro machines and understood their interest and the problems rose by the physics and mechanics of very small dimensions. This talk took some time before it began giving its effect. Maybe it stayed for some people a crazy idea that might be good for science fiction movies specially when he asked "Why cannot we write the entire 24 volumes of the Encyclopedia Britannica on the head of a pin?" until the late sixties. In March 1967 [1], the first paper on MEMS device was published and it was a gold resonating MOS gate structure (figure 2.3), in that period the term MEMS didn't exist yet. This very first use of mechanical structures in an electronic device showed the possibility to use the microelectronic fabrication techniques to build micromechanical structure. The use of such micro structures began after the mentioned paper in a very shy way and people used a sacrificial layer to separate the microstructure from the substrate which is then removed in the release etch step to free the structural layer to move relative to the substrate but these structures were limited in motion. What pushed people more to develop micro mechanics was the excellent mechanical properties that the micro electronics material possess for their application. In fact, poly silicon

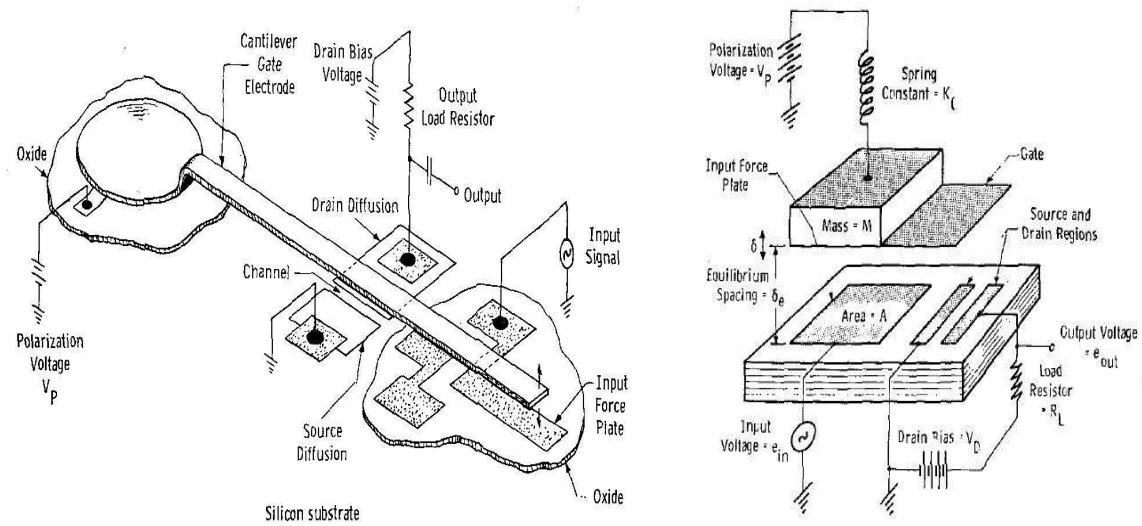

(a) The first MEMS geometry (b) The first MEMS equivalent model

Figure 2.3.: Gold resonating MOS gate structure, the first MEMS [1]

and silicon have a very high Young modulus (160 and 190 GPa respectively) and they work mostly in the elastic domain that is no plasticity and by consequence no mechanical hysteresis. In 1987 a turning point was reached in micromachining demonstrating, for the first time, techniques for integrated fabrication of mechanisms using volume and surface micromachining which is the selective etching of different materials. This turning point was the spark for the development of research on MEMS and after three workshops on microdynamics in 1987, the term MEMS saw the light. It's only in the year 1990 that MEMS began to find industrial application with the appearance of multi-users fabrication which gave access to this technology at a cheaper rate. Nowadays, MEMS became a term widely used and summarizing a wide variety of components from microsensors arriving to microactuators even though European people prefer the term Microsystems and Japanese prefer micromachines.[20]

2.1.3. Interest and applications

Why to use MEMS and develop a new technology if electronics works well? This is a question that is posed by many people specially those who are not involved in the domain. Sure if everybody is investing there and pushing this technology to advance, that means it has a lot of advantages and can solve many problems faced with electronics.

The interests of using MEMS are mainly weight, size, and cost. In addition to that, there are some interests for specific applications such as RF-MEMS.

- Their low mass makes them a good candidate for many applications, especially interesting for space applications. This was confirmed through the talks of multiple

participants during the CANEUS workshop held at the CNES (Centre National d'Etudes Spatial) in May 2008 for example the Canadian space agency as well as the DGA (Délégation Générale pour l'Armement), Airbus, ThalesAlenia Space and many others for whom mass plays an important role.

- Miniaturization, that is their reduced volume, permits their integration and increase the reliability or capability of a system via redundancy of multiple microsystems. For example, ThalesAlenia Space during the CANEUS workshop (Toulouse, May 2008), showed an interest of using MEMS technology for its role in reducing the size of the satellite antenna front-end.

- Cost reduction, by running batch fabrication. This quality is interesting for all industrial applications and is a very important key to commercialization of MEMS.

The advantages and interests listed above gave MEMS their way to many applications. The definition of MEMS applications is not as simple as it seems. In published papers, some lists the application of MEMS following its type, for example MEMS sensors, while others define their application following the domain of use or in better words following their market for example MEMS in automotive industry. Figure 2.4 lists different applications of MEMS sorted by type and by domain of application.

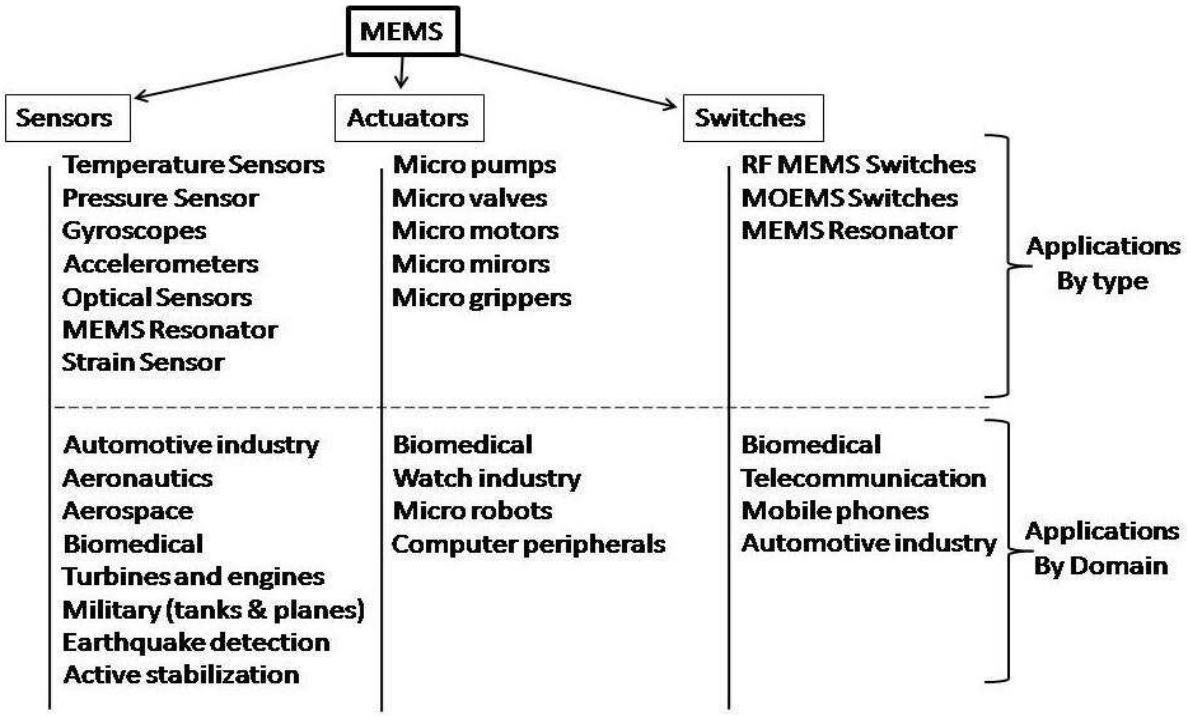

Figure 2.4.: Applications of MEMS sorted by type and by domain

Since their appearance to date, sensors are the major domain applying MEMS technology. These sensors are used in different domains or applications in order to monitor and control difficult access spaces.

Sensors, with all their varieties, find an important court of application in automotive engineering ranging from the system of security to the efficiency and pollution control. For example for real time monitoring of the pressure in the tires, pressure sensor with a wireless system to communicate data can be used. Accelerometers and gyroscopes are used to monitor the movement and stability of the car in order to know when to deploy the airbag or the anti slip braking system. Concerning pollution reduction and efficiency amelioration, chemical sensors (artificial nose) are used to measure the quantity of gazes (CO2, CO, NOx ...) at the exhaust in order to step in on the fuel-air mixture. For sure in cars, we will not forget the application of temperature sensors used for the protection of the motor and the material. Moreover, vibration sensors are used for active suspension.

Biomedical application is another important and promising market that uses almost all types of MEMS. Sensors are used to monitor blood pressure in the vessels, urine pressure in the bladder, etc... While strain gauges can be used to control the movement of the scalpel through the tissue (Figure 2.5). MEMS DNA analysers also exist and are a practical application of MEMS in medicine. Actuators such as micro pumps are useful to inject drugs or pump out unfavourable liquids. A micro actuator could be as well the cutting element for surgery, a micro gripper or a micro positioner. When integrating these different functions it becomes a micro robot, in other words a micro surgeon. It can walk inside our body and repair what is deficient for example the scalpel fabricated by Verimetra, Inc.[2] which classifies the tissue touched using the combination of pressure sensor together with a force sensor and an electrical properties analyser. With all these functions integrated in a micro surgeon (Figure 2.5(a)), we might need a way to command the tool and read the feedback from the sensors without bringing inside the body a bunch of wires (Figure 2.5(b)).

Then, we will call for the wireless communicating systems and RF MEMS will find their way into medicine. Aeronautics is also concerned with the technology of MEMS since they search for low mass and cost components and products that are easy to integrate. This is another domain where the sensors RF MEMS switches are widely used. In planes for example we can find sensors that are used for inertial sensing such as accelerometers and gyroscopes, also pressure sensors are widely applied there. RF MEMS play a role in communication and navigation systems. This giant domain makes room for new potential research, like those developed by the research program on micro and nano satellite, by finding for example a new micro system of propulsion (micro propulsion).

MEMS are not only limited to the above mentioned application, but they are promising to have a very open market. In addition to what was mentioned, MEMS find their

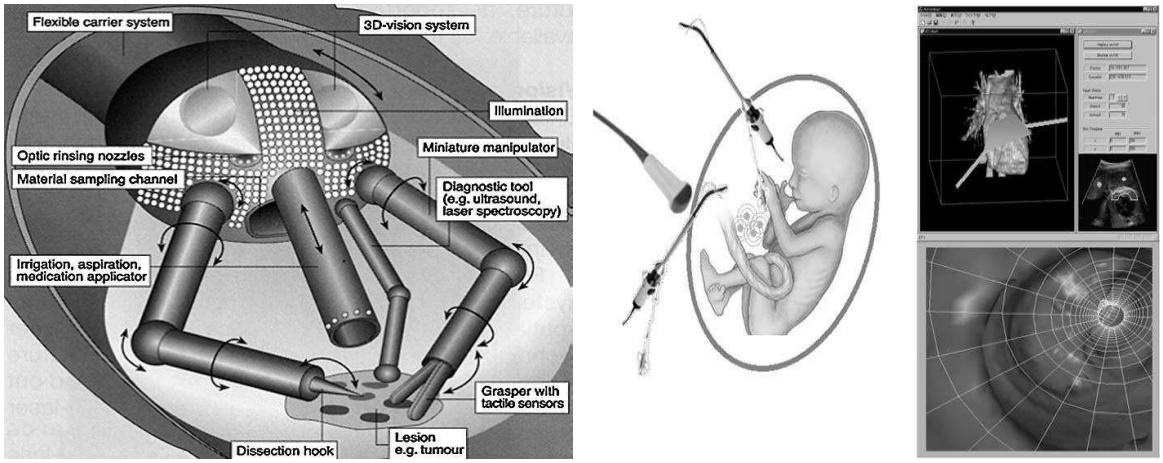

(a) A micro surgeon as expeted to be (b) MEMS applied to fetal heart surgery

Figure 2.5.: Example of medical application of MEMS [2]

way to military applications such as tanks, planes, detection systems, radars... Some other civil applications are the earthquake detectors. Concerning the applications of RF MEMS switches, we will detail it in paragraph "About RF MEMS switch".

The more the applications for MEMS, the wider the market becomes. This pumps more money in the field and leads to mass production which reduces the fabrication cost. For this reason, we are living nowadays a very dynamic period for MEMS where each day a new application is found and we have a potential to apply MEMS to all the domains that uses electronics. With this growth of the market, especially when it touches to human's life, we have bigger challenges to solve and more requirements concerning precision and reliability.

The first serious program for research on MEMS was funded by the DARPA (Defense Advanced Research Projects Agency) in the USA in order to develop an RF MEMS switch for defense and military applications. Now MEMS is targeting a wider market in biomedical and telecommunication applications. The MEMS manufacturers revenue has evolved from 100M$ in 2004 to 430M$ in 2008 [3][21] as we can see in figure 2.6. This growth could be explained by three reasons, the continuous increase in the activities of the companies, increase of the Asiatic MEMS foundry activities mainly linked to Asiatic market and the most important is the entrance of new players to the market targeting the high volume applications like silicon microphones[21], inertial sensors... and the MEMS market forecast expects an increase of this market once reliability issues of RF MEMS switches is solved in order to enter the mobile phones applications.

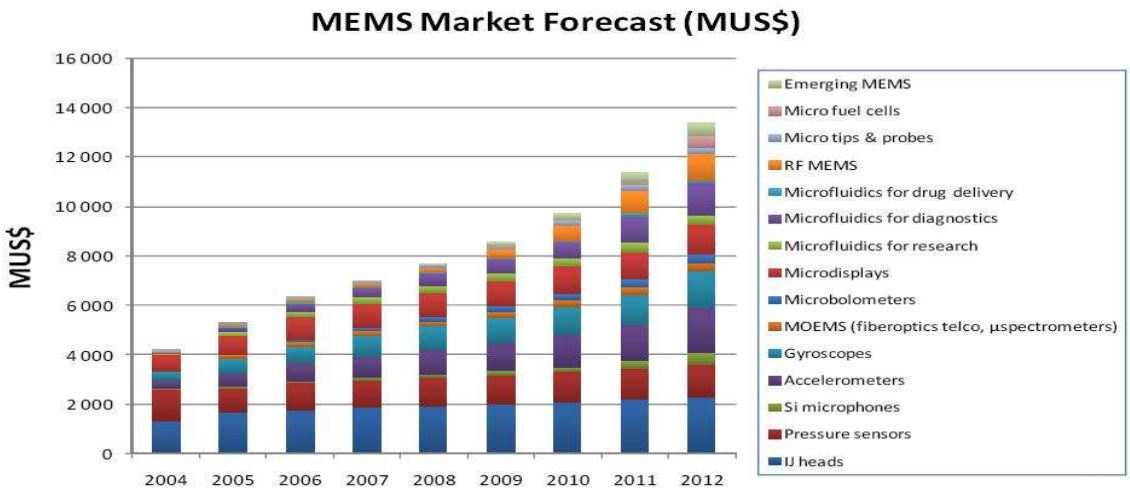

(a) MEMS market forecast

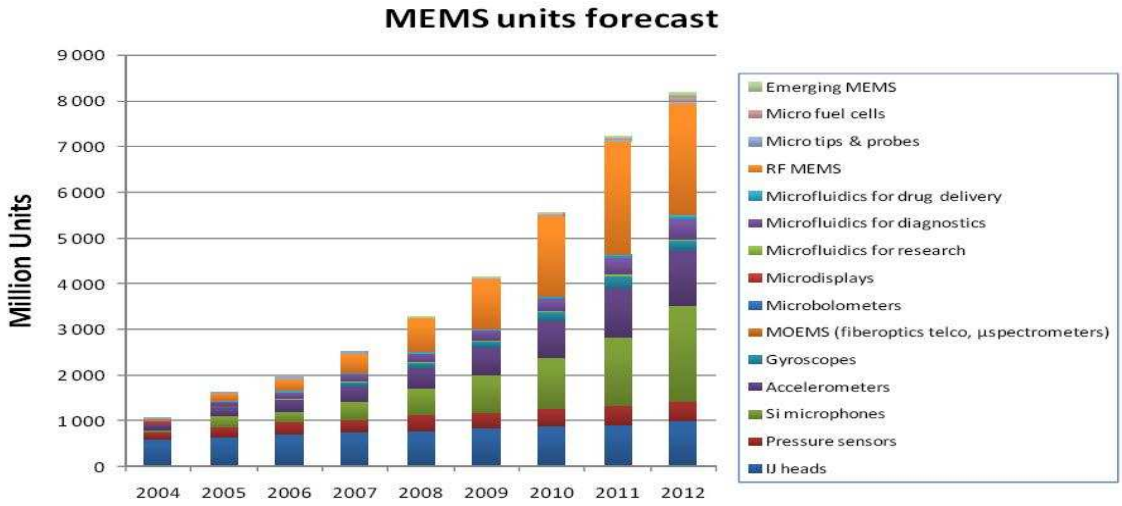

(b) MEMS forecast per units

Figure 2.6.: Forecast for MEMS market [3][4]

2.1.4. RF MEMS and RF MEMS switches

RF MEMS are Micro mechanical structures designed to do an electrical function in the radiofrequency systems. The goal of using RF MEMS is to replace the electronic components and some functions realized by integrated circuits by a MEMS component offering a better performance (Less loss, high linearity, high Q factor and less power consumption). They are fabricated using 5 to 8 photolithography steps (5 to 8 masks) giving them the technological advantage over the MMIC (Monolithic Microwave Integrated Circuits) that needs 13 to 25 lithography steps [22]. RF MEMS consists of switches, varactors, inductors, resonators, filters and phase shifters. They found their way between the micro-

electronics after the development in the telecommunication technology that resulted in the jamming of the frequency spectrum and by consequence favoured systems functioning at higher frequencies. The RF MEMS are applied to different domains such as wireless communication (telecommunication and mobile industry), radar systems, satellites and military radio. The RF MEMS switch is the corner stone to realise complex functions such as reconfigurable antennas, variable capacitors and signal rerouting.

The RF MEMS switches are movable microstructures actuated using electromechanical coupling in order to create a short circuit used for signal processing (filtering and/or rerouting). The most common structures used are bridges and cantilevers, since they are easy to model and they do the work very well. They function over a wide range of frequencies going from DC to tens of GHz. They are now competing with microelectronics since the later is increasing in frequency as Gabriel REBEIZ said during his talk at the "9th international symposium on RF MEMS and RF Microsystems"(MEMSWAVE 2008). There are two designs under which RF MEMS switches exists, depending on the contact type to deal with the signal, a capacitive switch and an Ohmic switch each of which can be used in a shunt configuration and a series configuration (see figure 2.7).

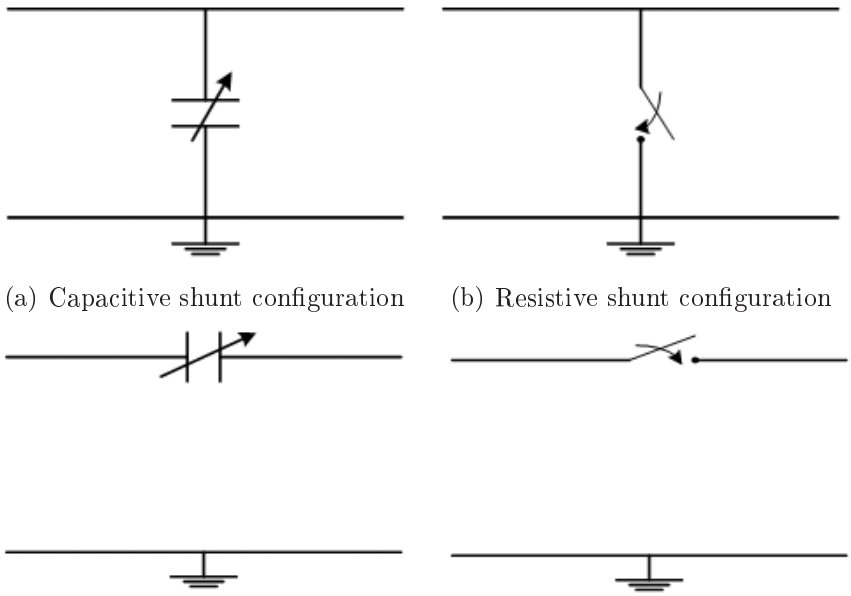

(a) Capacitive shunt configuration (b) Resistive shunt configuration

(c) Capacitive series configuration (d) Resistive series configuration

Figure 2.7.: Shunt and series configuration for resistive and capacitive switch

Capacitive switch

The capacitive switches, mostly used for shunt configuration, are structures actuated to form a variable capacitor between the signal line and the ground. Unlike the resistive

switch, the actuated structure itself forms the top electrode and having then a metal to dielectric contact (see figure 2.8(a)). When actuated, the capacitance value formed between the structure and the signal line changes in order to ground the signal or let it pass (see figure 2.8(b)). The ratio of the capacitance between the final and initial position is an important property of the switch as well as its actuation voltage. This type of switches are used to switch signals with a frequency range between 6 and 120GHz [23].

Resistive switch

Resistive switch, used in both shunt and series configuration, also known by the metal to metal contact switch and work by the same principal as the capacitive switch. When the structure is actuated it either reflects the signal or let it pass. They are mostly used in series with the signal line to cut it then link it, and are used to switch low frequency signal varying from DC to 60GHz [23] (see figure 2.9).

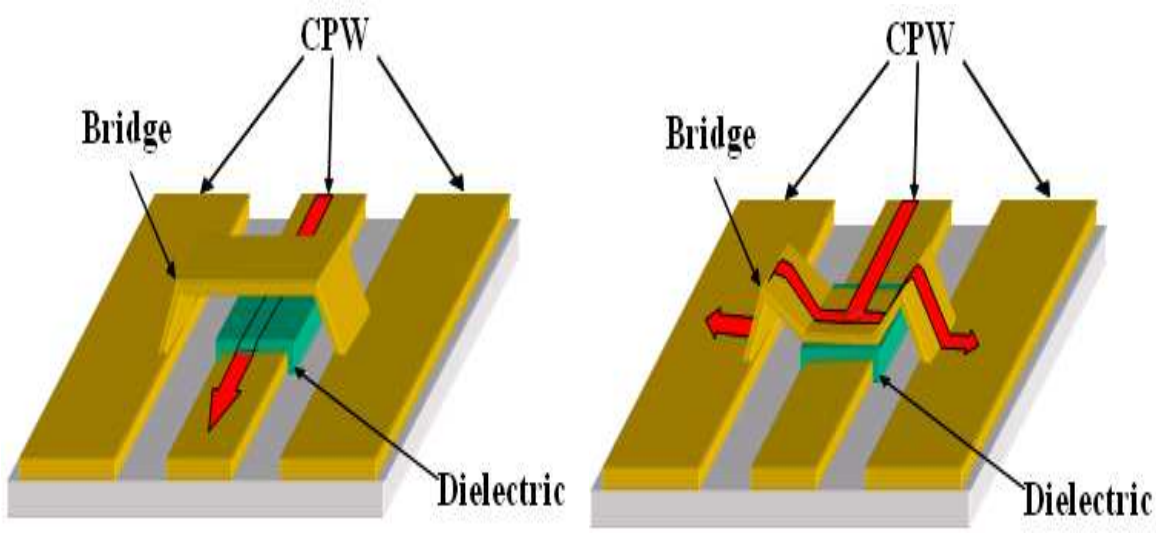

(a) RF MEMS switch in the up state (b) RF MEMS switch in the down (actuated) state

Figure 2.8.: A RF MEMS switch scheme in both states, on and off

2.2. Challenges facing RF MEMS switches and solutions

The challenges facing RF MEMS are very diverse and of different levels. On the reliability level, as was discussed during MEMSWAVE 2008, it is a wide issue especially for European researchers who are willing to fabricate not only a functioning switch, but

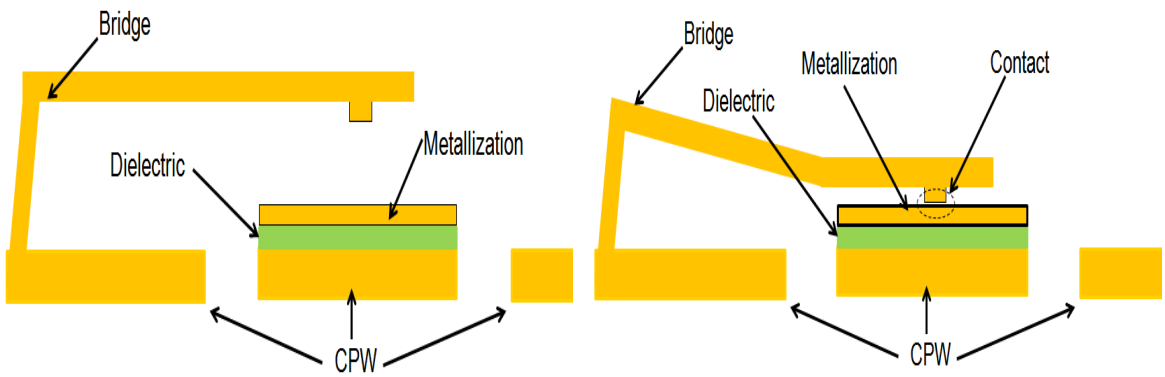

(a) RF MEMS resistive switch in the up state (b) RF MEMS resistive switch in the down state

Figure 2.9.: A RF MEMS resistive switch schemes.

also a switch with a long life time. On the packaging level, the high cost, the good hermitic package and the losses are in optimization phase so that MEMS can attack the harsh environment market. Manufacturing is a major domain for the development of MEMS, with all the uncertainties and difficulties to control the process. The two linked key points helping in the development of MEMS and for efficient MEMS modelling are material characterisation and simulation tools.

2.2.1. Will RF MEMS switches find their way to the market?

The first commercialized RF MEMS switch, outside DOD (Department Of Defence) programs, was when Teravicta and Magfusion announced their samples in 2003 but very soon they failed to supply all the demands that poured from all around the world. Fortunately, after the down that RF MEMS switches went through in 2003, it gave MEMS companies a good lesson to reach in 2006 to the enlightening phase with the new management team and good funding rounds at Teravicta. These achievements by Teravicta and some competitors (MEMSTRONICs, Advantest,MEW)[24][19] show that MEMS is gaining momentum specially that meanwhile Radant and MEMtronics have done important advances on reliability and they attained the 100 Billion cycle switch. The issue of reliability is very important in this period. After the success of obtaining a functioning switch it is fundamental to understand the causes of failure and design switches to overcome it. The question of reliability is the centre of attention since its commercialization is dependent on that point precisely to find applications in the mobile phones and in defence the thing that all the MEMS consumers (EADS, DGA, AIRBUS, Astrium, CNES, FREESCALE, TRONICS, THALES ALENIA SPACE) showed in the CANEUS workshop.

Until nowadays, RF MEMS switches are used for defence applications in the United States and their sales is restricted to the US market [19]. Their prices vary from 6 to 60 Euros depending on the specifications and volume. The widest domain of application for

RF MEMS switches will be the mobile phones, also known by the "cell phone billion unit market" which explains the news about NXP ramping-up its production [19]. NXP have a clear roadmap to the success of its capacitive switch and worked a lot on the reliability of RF MEMS in a view to invade the cell phone market.

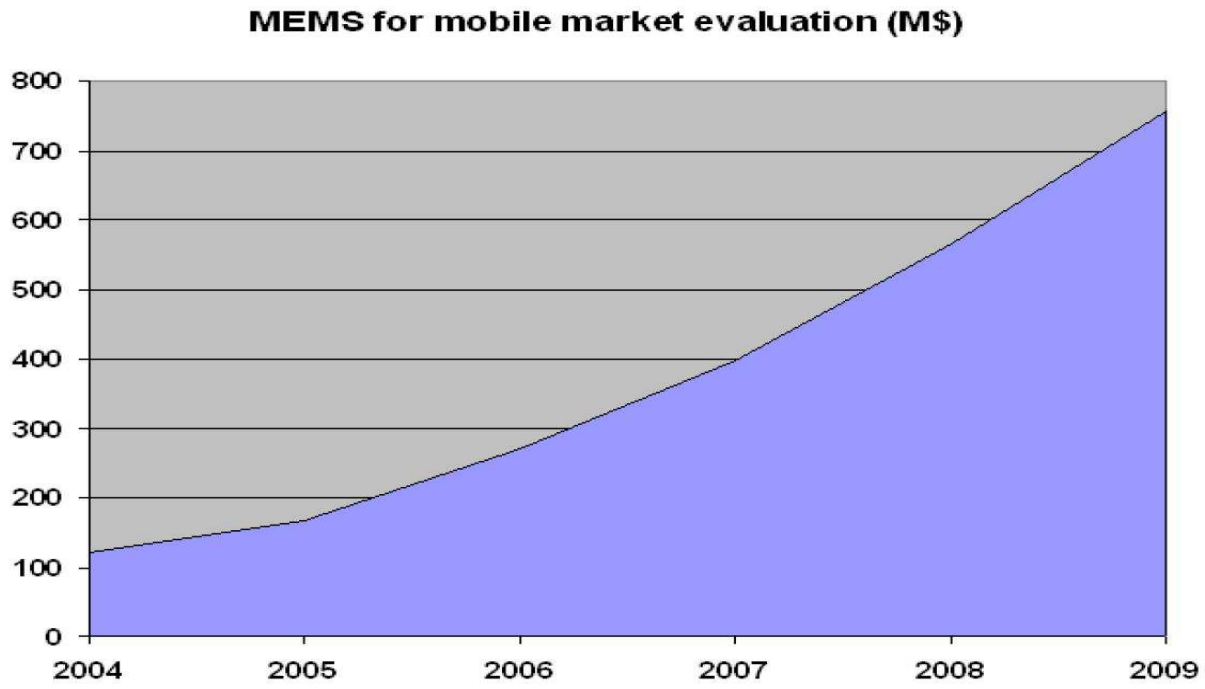

Figure 2.10.: Forecast for the usage of RF MEMS switches in mobile phones technology [5]

2.2.2. Reliability

The reliability is the ability to rely on a component before failure. This issue is discussed widely and is a key for the entrance of MEMS in the market. Many failure modes are defined for which scientists are trying to find a mathematical model. Some of these failure modes appears at low cycles (example: stiction) and others related to the high number of cycles (example: mechanical fatigue). In what follows a list of the failure mechanisms that researchers defined:

- Dielectric charging and stiction
- Temperature effect and induced deformation
- Metal pitting
- Hardening of metal

- Plasticity
- Stiction due to adhesive surface forces
- Auto actuation
- Electrical breakdown
- Mechanical fatigue and crack propagation
- Aging
- Creep

2.2.3. Packaging

Since MEMS switch moves in small cavities and because of their fragile nature, it is necessary to be packaged. Humidity, corrosive liquids and dust must be isolated from the MEMS component in order to find application in harsh environments. Although the packaging techniques are in continuous development, the cost per package is still very high in the order of 5 times the components cost. Many efforts are done to reduce the package cost in order to reduce the global MEMS components cost to be ready for the market.

2.2.4. Manufacturing

Many efforts are to be done in this direction. Until nowadays, we are still facing problems on the process stability and repeatability. As an example, the piezoelectric materials show different piezoelectric coefficients for the same process flow. Moreover, the step of sacrificial layer removal is very critical even with super critical drying.

2.2.5. Material characterisation

Understanding the material is necessary to understand the behaviour of any system. Concerning MEMS, special methods for material characterisation are still under development due to difficulties to fabricate the test structures. The existing methods lead to a high uncertainty level due to the dependence of the parameters on each others.

2.2.6. Modelling and simulation

Modelling is of great importance for designing MEMS and for developing it. It participates in the understanding of some problems, the understanding of the structures behaviour and will participate in the cost reduction. Developing simulation and modelling techniques, permits us to model for example the effect of the geometrical parameters on

the initial deflection. A good simulator will help obtaining a precise model of our component which will be used for virtual prototyping in order to optimize a certain function without passing through fabrication.

Etat de l'art

Un des majeurs problèmes de fiabilité dans les micro systèmes électromécaniques (MEMS) est la stiction, l'adhérence des deux surfaces en contact dû aux forces de surface. Ces forces apparaissent quand la distance entre deux surfaces devient, accidentellement ou intentionnellement, très faible. La stiction a lieu quand la force de rappel de la structure n'est pas suffisante pour surmonter les forces d'adhérence.

Le papier [25] présente un modèle pour prédire quantitativement l'énergie d'interaction de deux surfaces en contact en tenant compte de la rugosité des surfaces et les conditions ambiantes (humidité et température). L'énergie d'interaction de surface est décrite comme fonction de la distance entre les surfaces qui est en réalité une distribution de distances. Il est montré que, si nous savons cette distribution, nous pouvons calculer l'énergie d'interaction de surface. Ces forces ou énergies d'interaction sont compliquées à évaluer parce qu'elles sont d'origines différentes mais la modélisation nous aidera à comprendre sur quels paramètres nous avons besoin d'agir pour réduire le phénomène de collage.

Les forces jouant un rôle important dans l'interaction entre deux surfaces est la condensation capillaire, les forces moléculaires de Van der Waals, les forces électrostatiques, le " H-bridging " et " solid-bridging " [26]. Bien que les scientifiques essaient d'utiliser la stiction comme un avantage pour l'auto assemblage des microstructures [27], la stiction reste un inconvénient majeur contre la fiabilité des commutateurs RF-MEMS. Il y a deux types de stiction : le premier apparait après la libération des structures dû au liquide piégé dans les écarts et la seconde a lieu pendant l'usage des MEMS appelé IN USE STICTION fondamentalement en raison du chargement du diélectrique.

La problématique principale est d'améliorer la fiabilité de PENDANT-USAGE (IN-USE) et de réduire le collage. La source de stiction la plus importante dans les commutateurs RF-MEMS électrostatiquement actionnés est le chargement du diélectrique. Les charges prises au piège dans le diélectrique, créent une force de surface attrayante qui tiendra le commutateur dans son état actionné si l'énergie d'interaction de surface est suffisante pour surmonter l'énergie élastique emmagasinée dans la structure déformée. Pour réduire la stiction liée au chargement du diélectrique, on doit réduire le chargement du diélectrique ou augmenter la force de rappel de la structure. De ce point de vue, l'étude a été menée sur deux axes: la première porte sur la réduction du chargement du diélectrique et la seconde porte sur l'augmentation de la force de rappel.

Réduire le chargement du diélectrique peut être fait soit en réduisant la zone de contact entre les deux électrodes, soit en réduisant le champ électrique à travers le diélectrique. La réduction de la zone de contact est faite en ajoutant des plots dans la zone de contact. Ceci mène à la diminution de la surface chargée et à la réduction du champ électrique. Le champ électrique élevé à travers le diélectrique est principalement dû à la tension d'actionnement du commutateur électrostatique. La réduction de ce champ pourrait être faite en changeant la méthode d'actionnement. Ce chapitre est dédié à la description des méthodes d'actionnement et de quelques concept pour réduire le chargement du diélectrique.

Pour augmenter la force de rappel on pourrait augmenter la raideur. La raideur affecte en même temps la tension d'actionnement et la tension de relâchement. Par conséquent, si on augmente la raideur pour améliorer la force de rappel, on augmente automatiquement la tension d'actionnement, ce qui n'est pas souhaitable. Ce concept sera discuté dans le chapitre 6 avec plus de détails.

Résoudre le problème de stiction doit respecter les spécifications gardant les commutateurs de MEMS intéressant pour l'application de téléphone mobile. Le choix de n'importe quelle solution doit prendre en considération les critères suivants : une faible tension d'actionnement, une haute déflexion, un faible temps de réponse, une faible consommation et une faible sensibilité aux variations de température.

Dans ce chapitre, on présente les différentes méthodes d'actionnement possibles comme alternatives de l'actionnement électrostatique. Ensuite, le choix d'une méthode d'actionnement convenable à l'application est fait. D'une autre part, les solutions utilisées pour réduire l'effet du collage (stiction) sont présentées. Finalement on introduit un nouveau concept pour réduire le collage.

3. Approaches for solution

3.1. Introduction

One of the most important reliability problems in micro-electromechanical systems (MEMS) is stiction, the adhesion of contacting surfaces due to surface forces. These forces shows up when two surfaces come into contact intentionally or accidentally, forming a very low interdistance between them. Stiction occurs when the restoring force of the structure is not enough to overcome the adhesion forces.

Paper [25] present a model to predict quantitatively the surface interaction energy of surfaces in contact including the roughness of the contacting surfaces and the environmental conditions (humidity and temperature). The surface interaction energy is described as a function of the distance between the surfaces which are actually a distribution of distances. It is shown that, if we know this distribution, we can calculate the surface interaction energy. These interaction forces or interaction energies are complicated to evaluate because they are of different origins but the models will help us understand on which parameters we need to act in order to reduce the stiction phenomena.

The forces playing an important role in the interaction between two surfaces are capillary condensation, molecular van der Waals forces, electrostatic forces, H-bridging and solid bridging [26]. Although scientists are trying to use stiction as an advantage for self assembling microstructures [27], stiction remains a major drawback on the reliability of MEMS switches. There are two types of stiction, first one occurring after the release etch due to liquid stuck in the gaps and the second occurring during the use of MEMS so called IN-USE stiction basically due to dielectric charging.

Our main concern is to ameliorate the IN-USE reliability that is reduce the IN-USE stiction. The most important stiction source in electrostatically actuated RF-MEMS switches is the dielectric charging. The trapped charges in the dielectric, create a surface attractive force which will hold the switch in its actuated state if the surface interaction energy was enough to overcome the elastic energy stored in the deformed structure. To reduce stiction due to charging, one should either reduce the dielectric charging or increase the restoring force of the structure. From this point of view, the study went in two axes: The first is to reduce the dielectric charging and the second is to increase the restoring force.

Reduce the dielectric charging can be done either by reducing the contact area between the two electrodes, or by reducing the electric field across the dielectric. Reducing the contact area is done by adding bumps in the contact zone, this leads to less charged surface and also will reduce the electric field. The high electric field across the dielectric is majorly due to the actuation voltage of the electrostatic switch. The reduction of this field could be done by changing the actuation method. This chapter is dedicated to the state of the art on the actuation methods and on some ways to reduce the dielectric charging.

Concerning the increase of the restoring force, this can be done by increasing the stiffness. The stiffness affects at the same time the pull-in and the pull-out voltage, that's why increasing the stiffness to ameliorate the restoring force will increase the pull-in voltage which is unfavorable. This concept will be discussed further in chapter 6.

Solving the stiction problem must respect the specifications keeping MEMS switches interesting for the mobile phone application. The criteria for the choice of any solution must take into consideration to have: A low actuation voltage, a high deflection (high deflection for capacitive switch while we need high contact force or low resistance for resistive switch), a high speed of response, a low power consumption and, last but not least, a low sensitivity to temperature variations.

3.2. Actuation methods

To get reduce the stiction problem, we will study the possibility to replace the electrostatic actuation by another actuation method. The deflection of the micro structures in order to vary the capacitance or to contact the metal pads, is obtained using an external force coming from an electromechanical coupling. Different methods of actuation exist varying from field forces to molecular forces [18] as shown in figure 3.1 and are described in this section.

3.2.1. Electrostatic actuation

One of the most used way for actuating MEMS is the electrostatic actuation, specially where the gap is very small. It is a mode of actuation using the attraction force between opposite charges following Coulomb's law, so called electrostatic force or Lorentz force. This attraction force is the most used for actuating micro switches for its high contact force, nearly zero consumption power, their high speed of actuation and their simplicity of use. There are two ways to use electrostatic actuation, parallel plate actuation (as in figure3.2(a)) resulting in a more compact component or lateral actuation (as in figure 3.2(b)) resulting in a large size component.

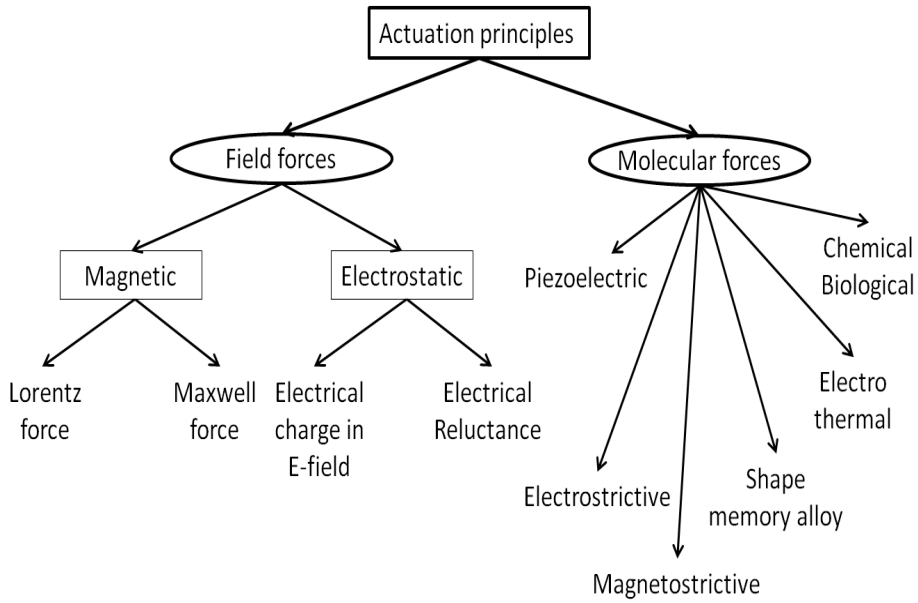

Figure 3.1.: Actuation methods divided into molecular forces and field forces.

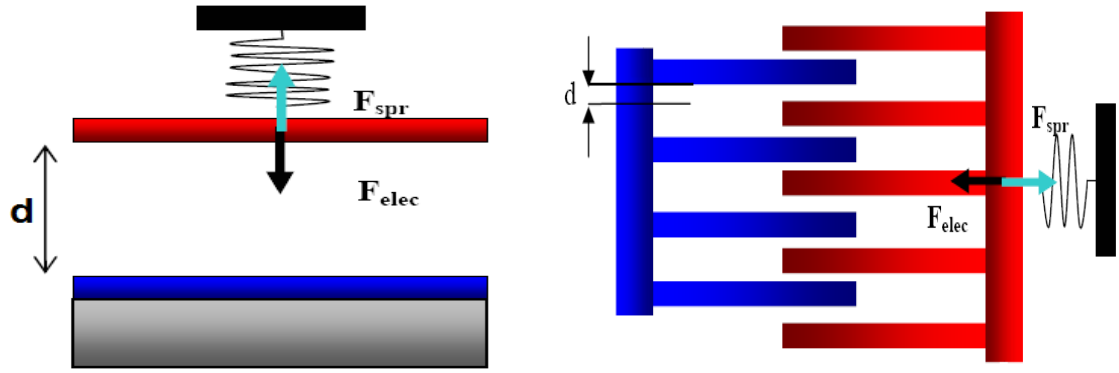

(a) RF MEMS out of plane actuation or parallel plate.[6][28]

(b) RF MEMS in plane actuation or comb drive.[6][29]

Figure 3.2.: Different ways to use the electrostatic actuation

Parralel plate actuation

For the parralel plate actuation (also known by out of plane actuation), the electrostatic force between the electrodes is proportional to the applied voltage and inversly proportional to the square of the gap between them. A restoring force, due to the structure stiffness acts on the structure so for a given bias we can find an equilibrium position for the two forces. Increasing the voltage will decrease the gap and the electrostatic force will increase quadratically while the restoring force increases but linearly. At a certain bias, we reach a point of unstability between the forces where the electrostatic force over-

comes the restoring force and the mobile electrode will be pulled down to the bottom electrode. This mode of actuation is used for out of plane displacement as shown in figure 3.2(a). Figure 3.3 shows the electrostatic forces acting from one electrode to another. Figure 3.3(a) shows the forces acting by the charges of the bottom electrode on one point charge of the top electrode. The forces are then projected on the horizontal and vertical axis showing an equilibrium in the horizontal forces due to symmetry as shown in figure 3.3(b). The total resulting force is vertical as described in figure 3.3(c).

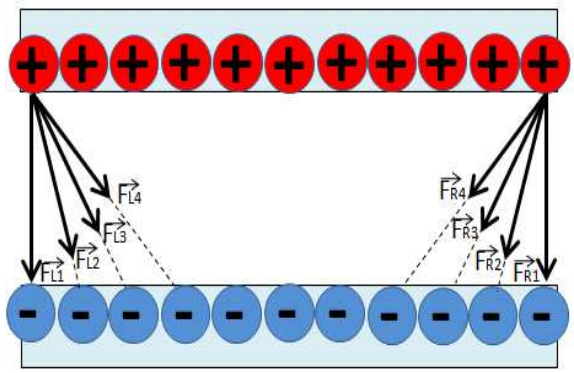

(a) Electrostatic forces acting by one electrode on the other.

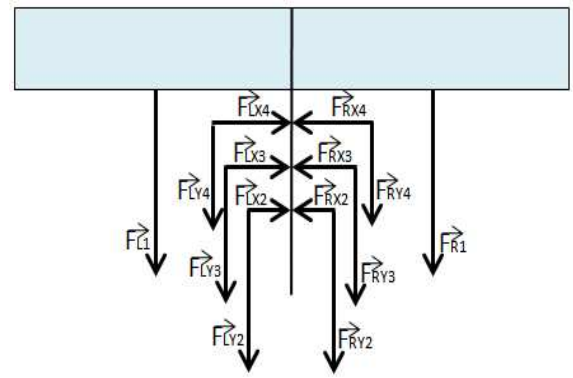

(b) Projection of the electrostatic forces along X and Y axis.

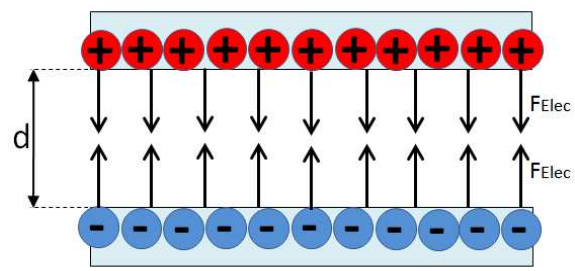

$$F_{Elec} = \frac{\varepsilon . A . V^2}{2 . d^2}$$

(c) The resultant electrostatic force acting on both electrodes.

Figure 3.3.: The electrostatic force in the case of out-of-plane actuation.

In-plane actuation

Lateral actuation is another way to use the electrostatic force, in this case the movement is parallel to the surface of the electrodes. It is called combe-drives and used for in plane movements but due to technological constraints (thickness of the material, and inter fingers distance...) a large number of fingers is needed to obtain an important electrostatic force resulting in a large size component. The lateral force is proportional

to the number of fingers, on the actuation voltage and the inter fingers gap but it is constant all through its displacement. This actuation mode is very used to actuate MEMS in-plane resonators as shown in figure 3.2(b). Figure 3.4 shows the electrostatic forces acting from one electrode to another. Figure 3.4(a) shows the forces acting by the charges of the bottom left electrode on one point charge of the top right electrode. The forces are then projected on the horizontal and verticcal axis showing a resultant non zero horizontal forces as shown in figure 3.4(b). The total resulting force is horizontal and vertical. If the fingers of actuation are symetrical from both sides of the electrode, a vertical equilibrium will be acheived and we will finish by a pure horizontal force as described in figure 3.4(c). One of the applications of in-plane actuation is shown in the paper [30].

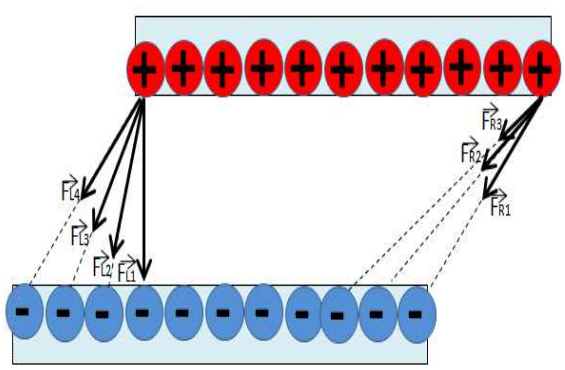

(a) Electrostatic forces acting by one electrode on the other.

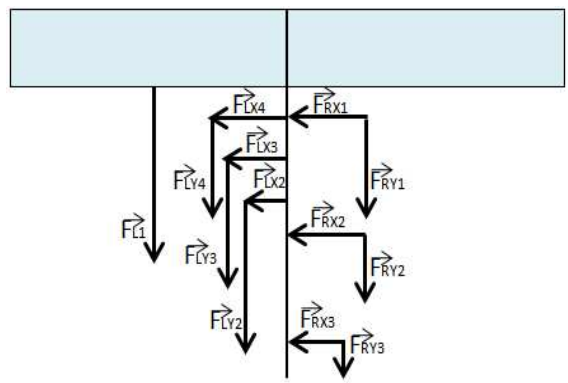

(b) Projection of the electrostatic forces along X and Y axis.

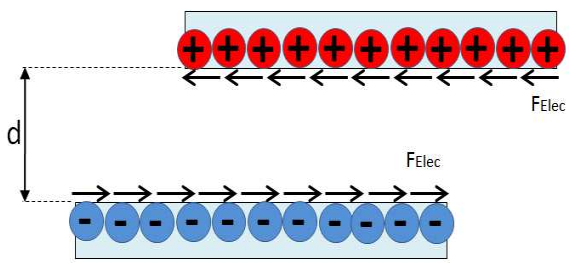

$$F_{Elec} = \frac{\varepsilon . W . V^2}{2 . d}$$

(c) The resultant electrostatic force acting on both electrodes.

Figure 3.4.: The electrostatic force in the case of lateral (or in-plane) actuation.

3.2.2. ElectroMagnetic actuation

This actuation method is classified as field actuation or contactless actuation. Bringing an ferromagnetic material into a magnetic field will creat an attraction force between them. The same if we deposit a permanent magnetic material on the structure to be actuated and put it inside an electromagnetic field obtained from a solenoid, the attraction or repulsion can be obtained by controlling the sense of the curent in the solenoid (see figure 3.5(a))[31][32][33]. This method needs a small distance for actuation as any field force actuation (Electrostatic). Eventhough this method offers a high force and low response time, it stays limitted in MEMS actuation because of its complicated fabrication process. The high curent for actuation leads to high disipation and finally the heating of the system which is tolerated but to a certain limit.

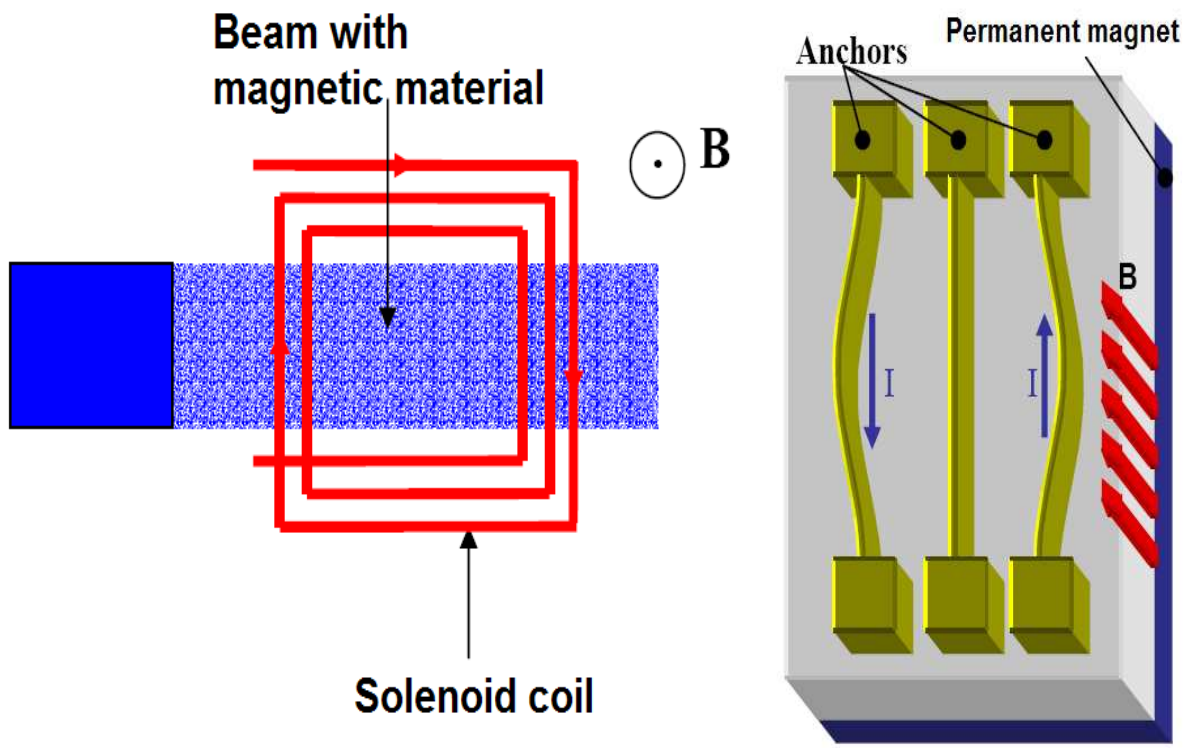

(a) Electromagnetic coil to atract the permanent magnet[6].

(b) Magnetic actuation by passing a curent in a magnetic field[17].

Figure 3.5.: Electromagnetic actuation.

3.2.3. Piezoelectric actuation

Piezoelectricity is a property that is found in some cristaline materials. These materials have a certain cristal orientation which gloably shows a neutral charge. When a force

is applied, the orientation of these crystals changes with the strain induced and charges appear on the surface of the film in the form of potential difference. Using the reverse effect, by applying an electric field (electric potential) across the film a deformation in the piezoelectric film is obtained. For each piezoelectric material, we can measure the electromechanical coupling coefficients which gives us the relation linking the component of the electric field applied across the film and the deformation in each direction of the film.

If we consider that our piezoelectric film is polarized in the thickness direction and that the applied electric field E is in the same direction we obtain a deformation (contraction or elongation) in the plane. The in-plane deformation is linked to the electric field by the coefficient d_{31} as shown in figure 3.6. If the piezoelectric film is sandwished between two electrods on the top of an elastic layer, the deformation in the active film will induce a bending moment due to the deformation gradient and an out-of-plane deflection is obtained. The piezoelectric actuator functions in the same principal as the thermal and magnetostrictive methods. A piezoelectric material can be neutralized if the applied field in combination with temperature where high enough to modify the crystal orientation and though loose its piezoelectric property. The advantage of this type of actuation is the fast response of the material and its high force [34]. The major disadvantage is being a multilayered actuator which makes it very sensitive to temperature changes. Another disadvantage is the degradation of the piezoelectric properties with time beside some technological difficulties in elaborating PZT thin films.

3.2.4. Electrothermal actuation

The electrothermal actuation also widely used in MEMS actuation because for small volumes, the temperature variations are faster. This actuation is much less used in RF MEMS due to its sensitivity to temperature and its slow response time with respect to other actuation methods as well as their high energy disipated during actuation. It is used for appications that needs large displacements and permits to obtain relatively huge force in the order of mN. From the principle of thermal expansion, when any material heated to a certain temperature it needs to react to absorb this energy and therefor their atoms are excited and the intermolecular distance increases consequently inducing the expansion of the object. A beam having originaly a length L at a temperature T, after being heated to a temperature T+ΔT, it will undergo an expansion of a value ΔL=α.L.ΔT. Where α is the coefficient of thermal expansion. By the means of a controlled heat source for heating the structure, we can obtain an actuator using thermal expansion phenomena to generate displacement. A word should be said on the repeatability of the thermal actuation which is not stable because material changes their behaviour when cycles under high temperatures. More applications of thermal actuation to micro switches can be found in [35][36][37].

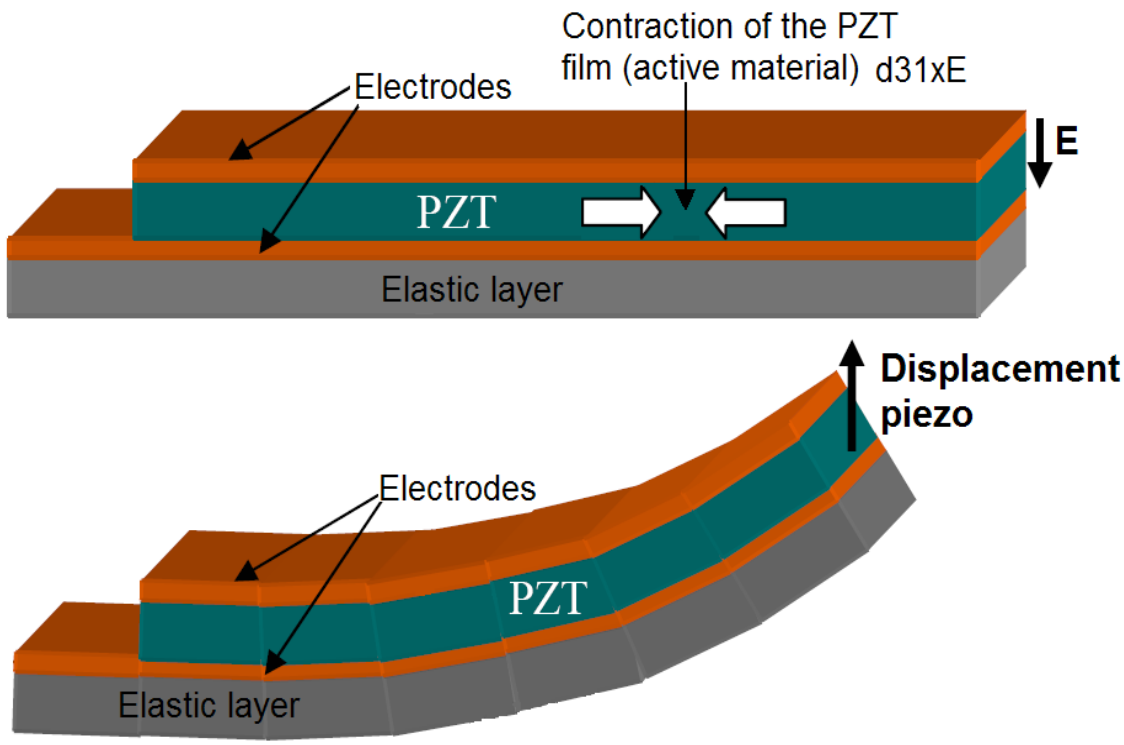

Figure 3.6.: The piezoelectric actuation mechanism [6][7].

Like electrostatic actuation, we can have thermal actuators either working in plane using directly the elongation of the actuator or out of plane by using a multilayered actuator.

In-plane actuation

The in-plane actuation is obtained using two basic geometries, either a V-shaped structure as in figure 3.7(a) or a U-shaped as in figure 3.7(b). For the V-shaped structure [38], this specific geometry is used to amplify the thermal expansion into large deflection. Passing a current in the structure material, it will heat up and the opposite sides of the actuator pushes in one direction.

The U-shape actuator functions in a different way but always in-plane. A thermal expansion gradient is needed in order for one side of the U structure to push the other (see figure 3.7(b)), that's why we need to have one hot arm and one cold arm [39]. The hot and cold arms could be obtained either by changing the resistivity of each arm so that the current passing in the U heat a side more than the other or by modifying the geometry leading to a smaller current density and a higher cooling coefficient which creates the temperature gradient (consequently expansion gradient).

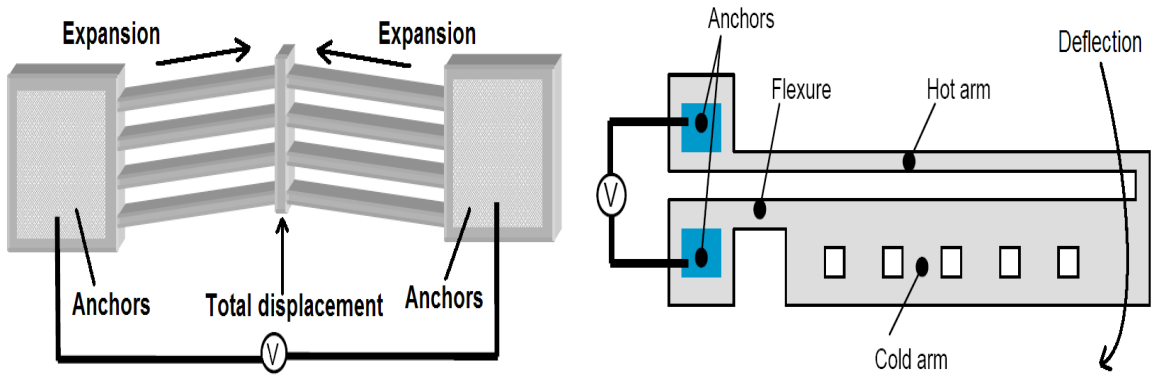

(a) The V-shaped design also known as Chevron-shape design[17].

(b) The U-shaped design[17].

Figure 3.7.: The in-plane modes of thermal actuation.[8][9]

Out-of-plane actuation

For the out-of-plane actuation, a multilayered beam is the most used. A similar principle as the in-plane actuation but this time the expansion gradient is in the thickness direction. The multilayer is composed of layers with different coefficient of thermal expansion (CTE). When the structure is heated, each layer will expand proportionaly to its respective CTE. For a bilayered beam, as the one showed in figure 3.8, the top layer having a CTE greater than the bottom one will undergo an expansion ΔL_1 ΔL_2. This mismatch in the deformation of each layer will generate a bending moment due to the continuity at the interface, causing the beam to deflect downwards.

3.2.5. Magnetostrictive actuation

The magnetostrictive actuation is very similar to the piezoelectric phenomena. In piezoelectricity, a deformation is obtained by subjecting the film to an electric field while in magnetostrictive the crystals direction are sensitive to a magnetic field. The magnetostrictive material is deposited on the top of an elastic passive layer. When the electromagnet is activated a magnetic field causes the contraction or expansion of the active film leading to a deformation gradient (equivalent to a stress gradient)[40]. Every time we have a magnetic coil, we have high energy dissipation for actuation and a certain complexity of fabrication.

3.2.6. Shape memory alloys (SMA)

As all the molecular force actuation methods, the shape memory alloy is sensitive to a physical field which is the temperature. These type of alloys changes their deformation, resistance and flexibility after a certain temperature limit. The deformation obtained

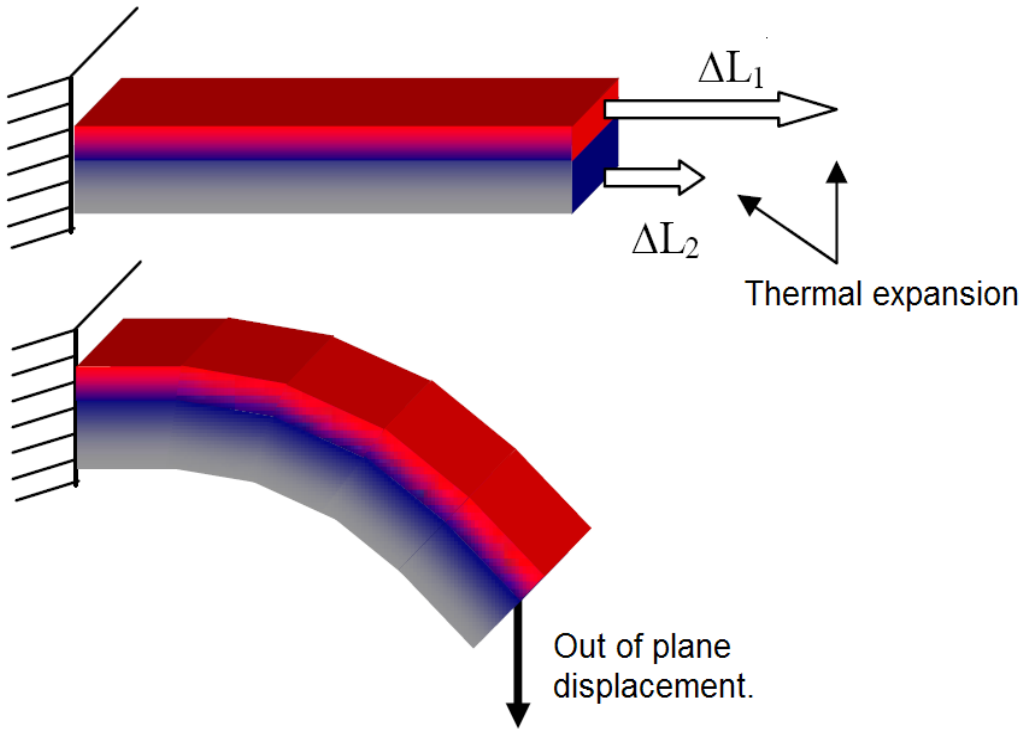

Figure 3.8.: The out-of-plane thermal actuation mode [6][10].

from this phenomena is much more important than the classical thermal expansion. We use the two way effect where the material remembers two different shapes, one at low temperatures and one at high temperatures [41]. We can make use of the reversibility of this phenomena in order to control the movement and form an actuator [42][43][44]. Thin film shape memory alloy mico actuators exists an can cycle at a frequency up to 100 Hz due to the rapid heat transfer rates associated with thin film devices [45]. These actuators are very dependent on the conductivity of the material, it depends a lot on the ambient temperature and like electrothermal actuators it dissipate a lot of energy.

3.2.7. Comparision of actuation methods

In our application, a low actuation energy dissipation is needed, a fast response and if possible high forces for Ohmic switches. Table 3.1 below summarizes the list of characteristics for different actuation methods. The conclusion drawn from this table is to focus our research on the electrostatic and piezoelectric actuation which are the most convenient for our application.

	Electrostatic	Electromagnetic	Piezo	Thermal	SMA	Mag stric
Contact force	High	Low (initially)	Low	High	Low	High
Consumption	$\simeq 0$	High	$\simeq 0$	High	High	High
Deflection	Low	Low	High	High	High	High
Speed	High	High	High	Low	Low	High

Table 3.1.: Summary of the actuation methods characteristics.[17][18]

3.3. Solutions for charging problem in electrostatic actuation

The thin dielectric layers causes a high electric field in the down position of the switch. These high fields causes the injection of the charges in the dielectric layer. There are many mechanisms of charging like charges transfer due to the contact of the bridge with the dielectric, contactless charging [46], charges trapped in voids etc...

The charge quantity and the charging time depends on the applied voltage, the type of material, the time of application of the voltage (time in the down state) and of course the temperature. When the charge density trapped in the dielectric reaches a certain critical value where the electrostatic force is enough to keep the switch down, we obtain stiction or in other words failure of the switch.

3.3.1. Bipolar actuation and HOLD-ON voltage

The charges sign depends on the electric field direction. A method to reduce the induced charges, is by injecting opposite charges by reversing the electric field. The actuation is then made on the pull-in voltage but one actuation cycle in the positive and the next on the negative as shown on the diagram in figure 3.9(a). Since the value of the applied voltage plays a role in charging, another method of actuation is used. The switch is actuated with the pull-in voltage then it is decreased to a value higher than pull-out, so called HOLD-ON voltage, but signaficantly lower than the pull-in [11]. Figure 3.9(b) shows the diagram of actuation as a function of time.

The charge injection rate depends on many factors and specially on material of the dielectric [47][11]. The rate of injection is not the same for all field directions or when the dielectric is already charged [48] therefore the supression of induced charges is incomplete[49][50][51]. A new method called the "Intelligent bipolar actuation" is developed in 2008 at the university of Pennsylvania [51] a little bit complicated but efficient. It consist of measuring the residual field in the charged dielectric and as a function of the field direction they apply a positive or a negative voltage. The comparision between all actuation methods

is presented in figure 3.10 showing that bipolar actuation gives a longer life time wit hrespect to unipolar but failure is postponed with the intelligent bipolar actuation.

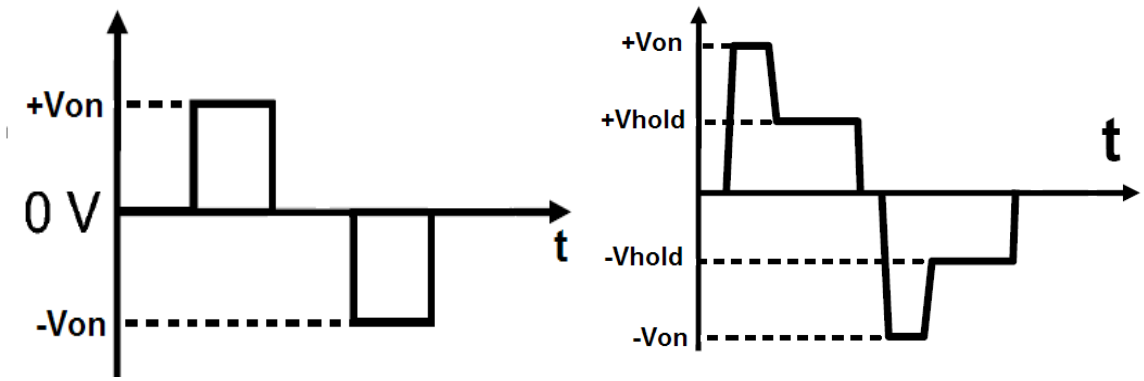

(a) Simple bipolar actuation. (b) Bipolar actuation with HOLD-ON voltage.

Figure 3.9.: The bipolar actuation method to reduce charging.

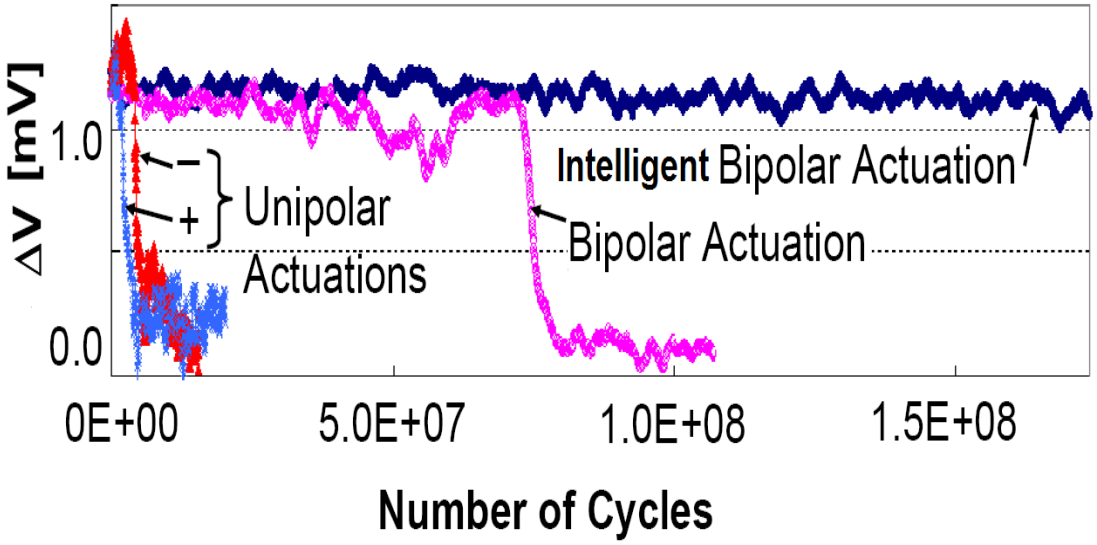

Figure 3.10.: Lifetime measured at 85°C for different actuation signal methods[11].

3.3.2. Liquid contact

The liquid contact is a solution for resistive RF-MEMS switches where the high contact resistance is a major drawback. Usually in contact switches (solid to solid contact) a high contact force is needed in order to increase the contact surface and by that decreasing

the contact resistance. The high contact force will need a high actuation voltage and as a consequence we obtain dielectric charging and stiction problem. The high resistance is due to airgap created between two rough contacting surfaces as shown in figure 3.11(a). The liquid to solid contact offers a package of advantages such as:

-Low contact resistance (less than 0.1Ω [52]) due to higher contact surface generated from intimate contact between the liquid droplet and the rough surface (see figure 3.11(b)).

-Naturally bistable operation due to surface tension forces dominating the inertial force (only in micro scale) facilitating the comutation between lines.

-The wear and friction degradation is eliminated unlike the solid to solid contact which degrades the performance of the switch.

Unlike the classical resistive switches, the contact to connect the inlet and the outlet of the signal line is done through a liquid metal, Mercury. The actuation of the Mercury micro drop, in order to establish the connection or cut it, is done by different methodes. Thermally, either we heat the layer on which the Mercury drop is deposited and by this changing the surface tension pushing the drop to move or we heat locally a closed reservoir filled with DI water forming a vapor bubble and generating a flow which forces the Mercury drop to creat a conductive path for the signal [12](figure 3.13). Electrosatically we have also two methods to attain contact, either by actuating the cantilever to contact a fixed mercury drop on the signal line [53] (figure 3.12(b)) or actuate directly the drop [52] as shown in figure 3.12(a) which reduces the charging effect. The Mercury drop is deposited on the line by condensation of the Mercury vapor on a seed point of gold.

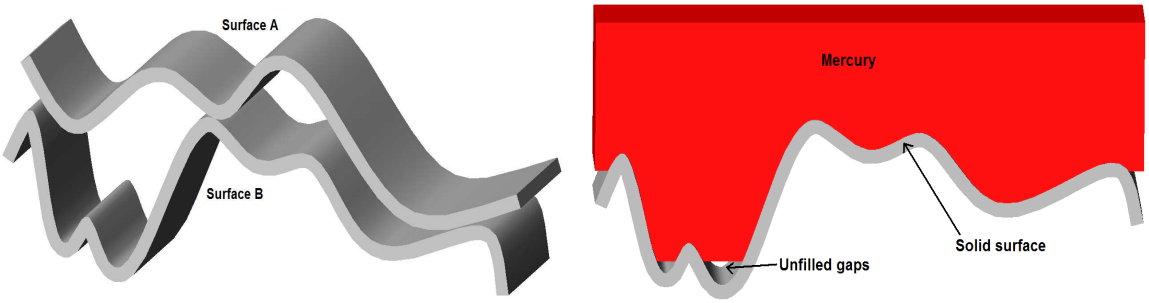

(a) Contact between two rough surfaces.

(b) Contact between a rough surface and a liquid drop.

Figure 3.11.: The contact state for solid-solid and solid-liquid contact.

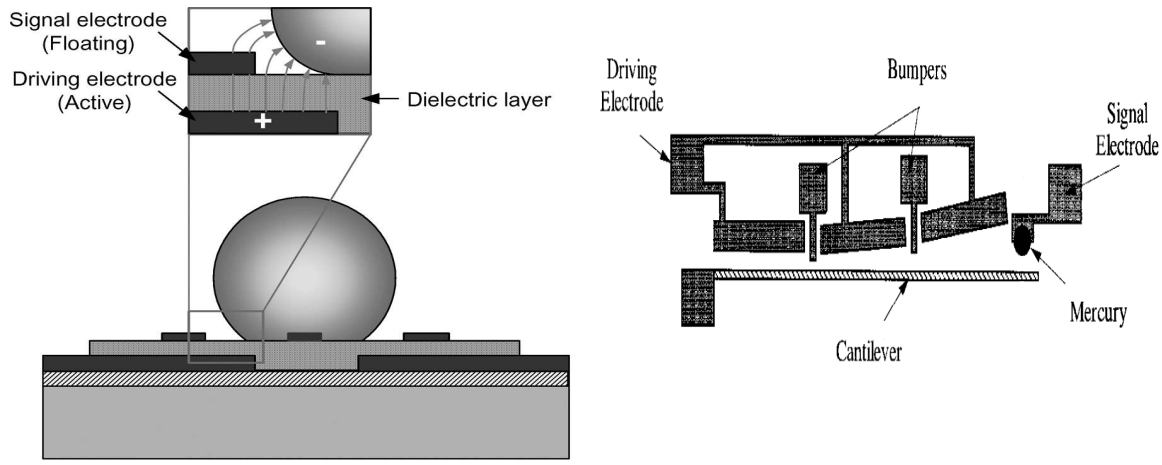

(a) Actuation of the Mercury drop by electrostatic force [52].

(b) Electrostatic actuation of the cantilever to contact the fixed Mercury drop [53].

Figure 3.12.: Actuation using electrostatic force for liquid contact.

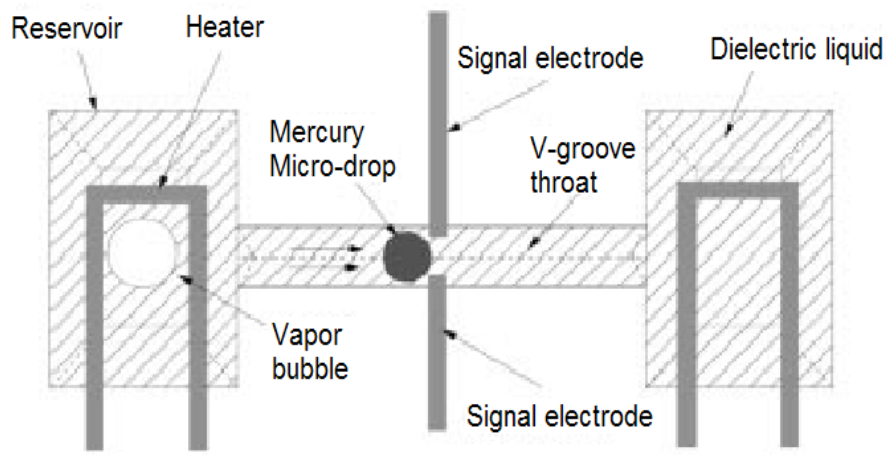

Figure 3.13.: Actuating the Mercury drop by heating [12].

3.3.3. Dielectricless switch

As we already presented on stiction, its main reason comes from the dielectric charging. To reduce charging occuring in the dielectric, scientists tried to reduce the contact between the membrane and the actuation electrode, or by fabricating a dielectric less switch. For dielectric less switches the only dielectric used is air. The bridge is fabricated with dimples which will stop it from touching the bottom electrode and short circuiting the actuation circuit. Figure 3.14 shows the up and down state of a dielectric less switch design with the actuation electrodes at the center [13]. When the bridge is pulled down, the dimples touches the substrate keeping an air gap td=0.3μm between the electrode

and the bridge. The membrane is 7.86μm thick to keep it flat after actuation, while the bridge is thinned to a thickness t=360nm along a distance L=300μm near the anchorage so that the stiffness of this thin part of the bridge will dominate on the overall stiffness. The switch with an electrode width Wf=20μm and a dimple interdistance W=40μm needs around 60 to 80V to actuate it.

Figure 3.15 presents a design with the dimples on the active zone (zone forming the capacitance) and they touches the actuation electrode. In this case, we either deposit locally dielectric to avoid the short circuit or we deposit what is called islands in the contact region to seperate it from the actuation electrode [16]. The up and bottom states of this design is shown in figure 3.15 for the global view and for a zoom on the membrane. These designs can reach the 100 millions of cycles under unipolar actuation.

Even with dielectric less switch, studies and experiments showed that we have charging in the substrate under the contact zone [14] [15] as we can see in figure 3.14. These switches have a drawback which is a small capacitance ratio because of the air gap. The air gap also affects the behavior by increasing its hold down voltage (Voltage slightly higher than the pull-out).

3.3.4. Side actuation

This method consists of actuating the bridge outside the contact zone as shown in figure 3.16. Basically, this design reduces charging because there is no contact at the actuation pads. Despite this advantage, there is an air gap created between the bridge and the signal line where the capacitance is formed due to the absence of the electrostatic force in this zone. This air gap reduces the capacitance in the down state that is decreases the performance.

3.4. Conclusion

This litterature review permitted us to summarize in table 3.1 the advantages and drawbacks of each of the actuation method. Table 3.1 classifies the actuation method with respect to our criteria defined in the introduction of this chapter. The selection of our actuation method is done by elimination. Electromagnetic actuation was rejected for two reasons, the first is due to the complexity of the process to fabricate the actuation solenoid and the second is due to the high power consumption due to the current passing in the solenoid. The high power consumption to heat the actuator together with the low actuation speed makes from thermal actuation a weak candidate in front of the other types so it is rejected as well. The shape memory alloy similar to the thermal actuation and the magnetostrictive method similar to electromagnetic actuation consumes a lot of power for actuation. The actuation methods must offer a high contact force to be

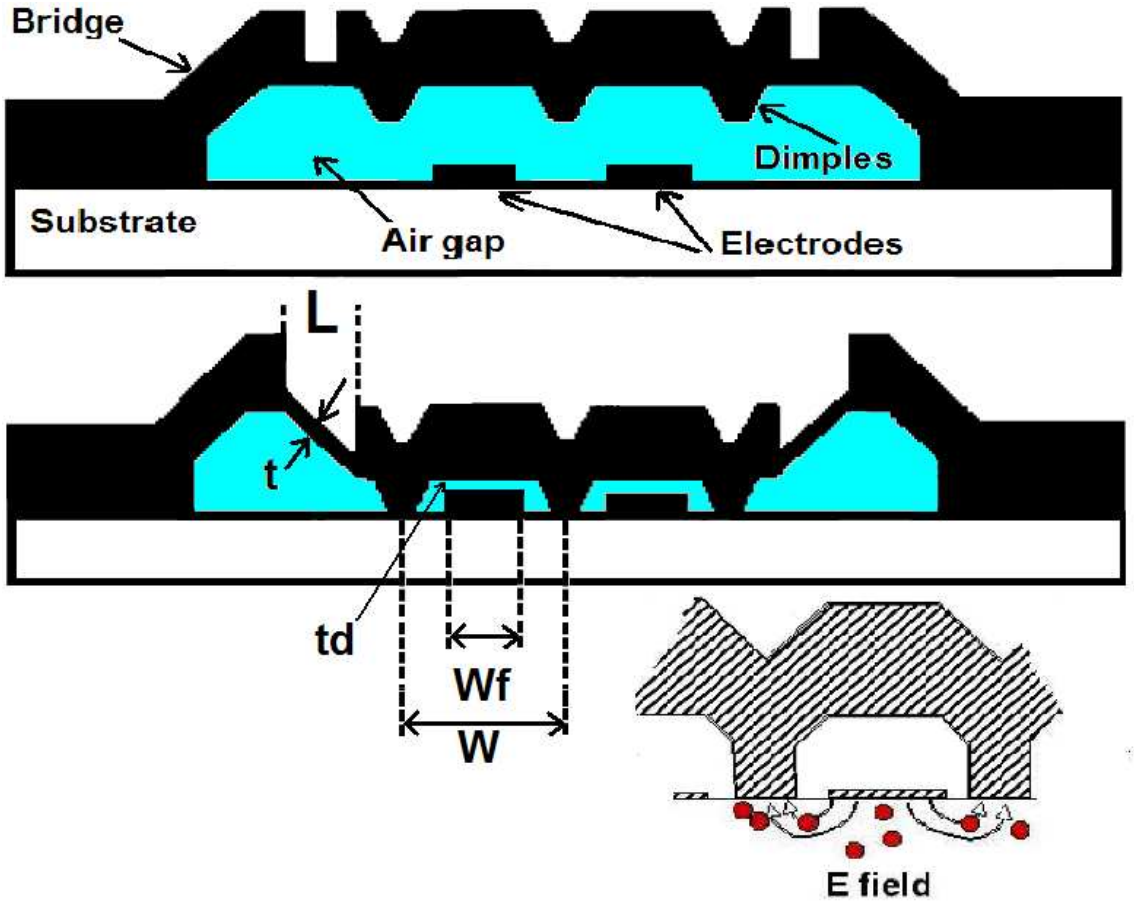

Figure 3.14.: Dielectric switch in both states up and down with a schematic view of substrate charging (XLIM laboratory) [13] [14] [15].

interesting for resistive switches and/or they must undergo a high deflection in order to be interesting for the capacitive switch application.

Concerning the reduction of the dielectric charging, the proposed designs have a common drawback which is the air gap in the contact zone. This air gap is responsible for the low capacitance value at the down state. The liquid contact design offers a very low contact resistance with almost no charging in the actuation region but stays complicated to process and works for low frequencies as all resistive switches. This was at the design level, now on the actuation level, the bipolar actuation with HOLD-ON voltage can be interesting but since the pull-out voltage shifts with time due to charging it will be difficult to choose the value of the HOLD-ON voltage. In addition to that, the different charging laws for different dielectrics make it difficult for scientists to define the parameters for the bipolar actuation.

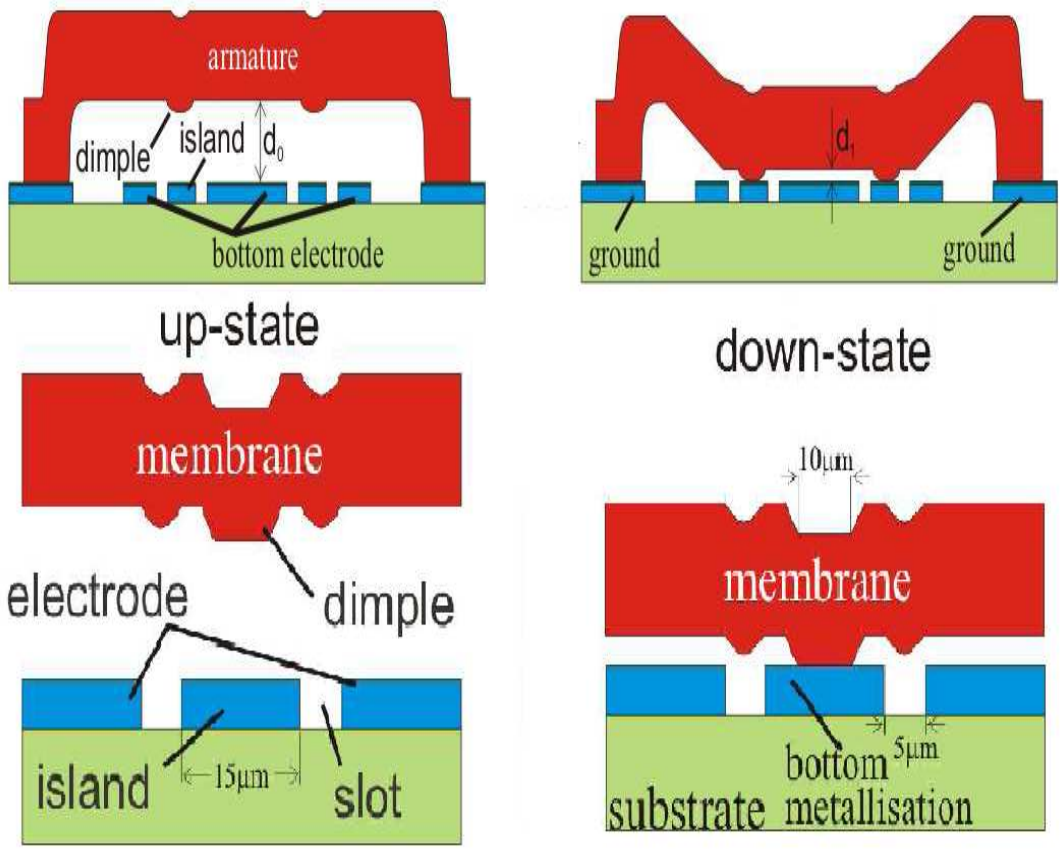

Figure 3.15.: RF MEMS switch with dimples on the contact area of the membrane (IMEC laboratory) [16].

We choose the piezoelectric actuation as an alternative actuation method due to its low consumption, high speed of response and the high deflection for a small actuation voltage. We keep the option of electrostatic actuation and designing a switch with a higher restoring force without increasing the actuation voltage.

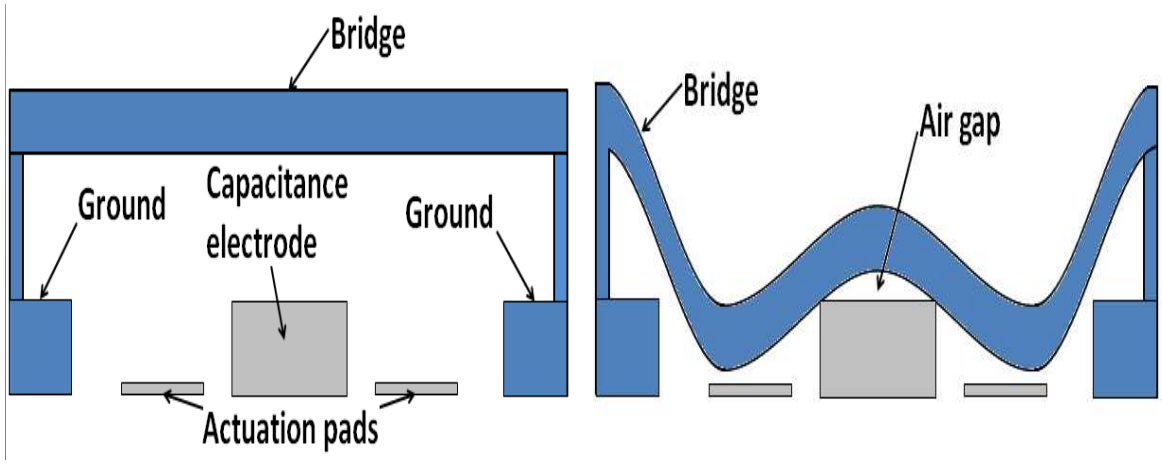

(a) Before actuation. (b) After actuation.

Figure 3.16.: Electrostatic actuation with the actuation pads different than the contact electrode.

Validation du plateforme numérique

MEMS, comme affirmé dans sa définition, sont des systèmes un grand facteur d'échèle où les différents physique interfère faisant la modélisation un peu difficile. Les logiciels multiphysique d'élément finis de nos jours trouvés dans le marché sont limités à seulement deux, COMSOL et ANSYS. Coventor peut être placé dans un mi-chemin entre les logiciels de multiphysique et les logiciels classiques puisque il est limité à seulement quelques applications de multiphysique. Les autres logiciels, comme IDEAS et ABAQUS, dédié aux problèmes non linéaires mécaniques sont utilisé pour un problème mécanique spécifique dans le champ de MEMS surtout dans la caractérisation. Même avec les logiciels de multiphysique, touts problèmes ne sont pas complètement résolu. Quelques codes sont plus commodes pour résoudre un certain type de problèmes que d'autres peuvent pas. Avec le développement des outils de modélisation globaux, les chercheurs préfère maintenant avoir des modèles comportementaux pour l'intégrer dans VHDL-AMS, Matlab simulink ou AMESIM pour obtenir une simulation de système, mais la méthode des éléments finie sera toujours nécessaire pour étudier chaque partie du système.

Pour les raisons énumérées ci-dessus et puisque les codes ne sont pas dédié aux simulations de MEMS avec leur haute facteur d'échèle, bien qu'ils offrent un outil de multiphysique, une étape de validation de logiciel et de capacité de logiciel est essentielle d'être fait avant de modéliser nos composants. Les structures utilisées dans la validation sont déformé en fonction d'un phénomène physique que nous rencontrerons dans notre application. Ces effets peuvent être des forces électrostatiques, l'effet piézoélectrique, l'effet de température ou la contrainte initiale. Le logiciel que nous cherchons doit offrir un temps de calcul rapide et nous permet de construire des modèles paramétriques pour les buts d'optimisation.

Le mécanisme d'actionnement piézoélectrique sera étudié pour l'appliquer aux microcommutateurs ou les condensateurs variables. La simulation de la déflexion en fonction de la tension appliquée est un problème principal pour la simulation de l'ensemble c'est pour ca qu'une validation de ce phénomène physique doit être faite. Pour commencer, un modèle d'actionneur piézoélectrique simple est construit sur COMSOL pour être comparé à un modèle analytique. Pour valider COMSOL avec ANSYS, un modèle plus compliqué d'un commutateur, consistant d'un actionneur connecté à une membrane, est choisis pour que nous puissions être le plus proches possible au cas de notre application.

Continuer dans le voyage de validation des modules qui sont utilisés pour notre étude

est notre prochain arrêt. Le contact est d'une grande importance dans nos applications puisque il définira l'état de planéité entre deux surface échangeant des paramètres physiques (ex : la qualité de capacitance, la résistance de contact...). Pour ces raisons, un problème de contact d'HERTZ a été simulé sur COMSOL et donc comparé à ANSYS et au modèle analytique.

Pour finir, nous avons validé l'actionnement électrostatique résolu sur Coventor, avec COMSOL et les valeurs analytiques. A la fin, une synthèse est faite sur la capacité des trois logiciels pour résoudre chaque type de problème voire figure ci après.

Software	Application	Static	Modal analysis	Time dependent	Harmonic response	Parametric	Transatory quasi-static	Large deformation	Linear bukling	Elastoplasticity	Multiphysics	Electrostatic	Piezoelectric	Thermal	Mean stress σ_0	$\sigma_0(x,y,z)$	Initial deformation ε_0	Thermal deformation ε_{th}
COMSOL	Solid	☺	☺	☺	☺	☺	☺	☺	☺	☺	☺	☺	☺	☺	☺	☺	☺	☺
	Shell	☺	☺	☺	☺	☺	☺	☺		☺	☺	☺	☺	☺	☺		☺	☺
ANSYS	Solid	☺	☺	☺	☺	☺	☺	☺	☺	☺	☺	☺	☺	☺	☺			☺
	Shell	☺	☺	☺	☺	☺	☺	☺	☺		☺	☺	☺	☺	☺			☺
COVENTOR	Solid	☺	☺		☺	☺	☺	☺	☺			☺	☺	☺	☺	☺		☺
	Shell											☺			☺			☺

Figure 3.17.: Résumé de la capacité des différents logiciels à résoudre des problèmes multiphysiques.

4. Numerical platform validation

4.1. Introduction

MEMS, as stated in its definition, are systems with high aspect ratio where different physics interfere making the modeling a bit difficult. The real multiphysics finite element softwares found in the market nowadays are limited to only two, COMSOL and ANSYS. Coventor can be placed in midway between multiphysics softwares and classical softwares since it is limited to some multiphysics applications. Other softwares, such as IDEAS and ABAQUS, dedicated to mechanical nonlinear problems are used from time to time for a specific mechanical problem in the MEMS field especially in characterization. Even with multiphysics softwares, all problems are not solved completely. Some codes are more convenient to solve a certain type of problems that others cannot. With the development of the global modeling tools people prefer now to have behavioral models in order to integrate it in VHDL-AMS, Matlab simulink or AMESIM to obtain a system simulation, but finite element method will be always necessary to study each part of the system.

For the reasons listed above and since the codes are not dedicated to MEMS simulations with their high aspect ratio, even though they offer a multiphysics tool, a step of software validation and software capacity is essential to be done before modeling our components. The structures used in validation are deformed due to the physical phenomenon that we are going to meet in our application. These effects can be electrostatic forces, piezoelectric effect, temperature effect or initial stress. The software we are searching for must offer a fast calculation time and permits us to build parametric models for optimization purposes.

Piezoelectric actuator will be studied in order to apply it for micro switches or variable capacitors. The simulation of the deflection as a function of the applied voltage is a main issue for the simulation of the whole switch thus a validation of this physical phenomenon has to be done. To begin, a simple piezoelectric actuator model is built on COMSOL in order to be compared to an analytical model. To validate COMSOL with ANSYS, a more complicated model of a capacitor plate switch, consisting of actuators connected to a membrane, is chosen so that we can be nearer to the case of our application.

Continuing in the trip of validation of the modules that are used for our study contact is our next stop. Contact is of a big importance in our applications since it will define the state of flatness between two surface exchanging physical parameters (ex: capacitance

quality, contact resistance...). For these reasons, a HERTZ contact problem was tested on COMSOL and then compared to ANSYS and its analytical model.

To finish, we validated the electrostatic actuation solved on Coventor, with COMSOL and the analytical values. At the end a synthesis is done on the capacity of the three softwares to solve each type of problem.

4.2. Contact models

4.2.1. Model description

The model under investigation consists of a cylinder in contact with a plane surface. The plane surface can be considered as an arc of radius infinity. For this model, Hertz has already written the equations describing the contact length and the contact pressure distribution. The cylinder is made of Gold while the block is made of steel with the geometrical and material properties as described in figures 4.1(a) and 4.1(b)respectively.

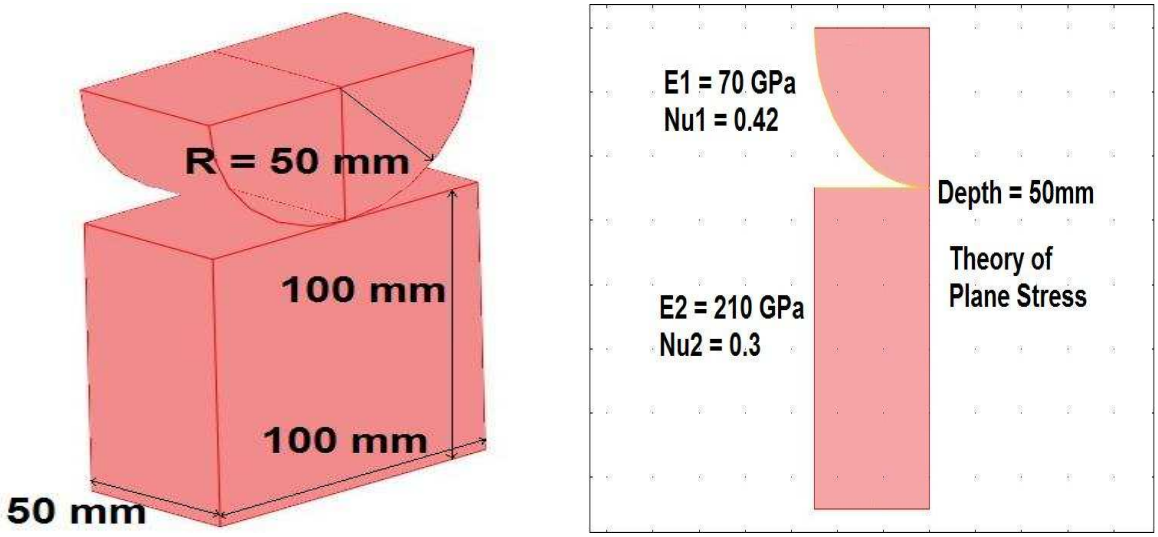

(a) Geometrical details and dimensions (b) Material properties of the contact model

Figure 4.1.: Contact model description

4.2.2. COMSOL

We used a 2D model to define the problem using the PLANE STRAIN hypothesis and friction was neglected between the two surfaces. Due to geometrical and load symmetry, we modeled the half of the geometry (figure 4.1(b)) with symmetry boundary conditions (figure 4.2(a)) to reduce the calculation time. The load is a vertical pressure of 500MPa,

applied on the longitudinal half section of the cylinder, squeezing the two solids on each others. The geometry was meshed using free triangular linear mesh with an element size of 10 mm while the mesh in the contact zone was refined to an element size of 0.2 mm as shown in figure (figure 4.2(b)). We faced some difficulties with COMSOL's contact solver due to convergence problems. The parameters that affected the convergence were the load step size and the mesh size near the contact zone as well as some contact parameters that had to be tracked manualy to find the right value. The results of the simulation are shown in figure 4.3 displaying the the contact pressure distribution in the cylinder and the block.

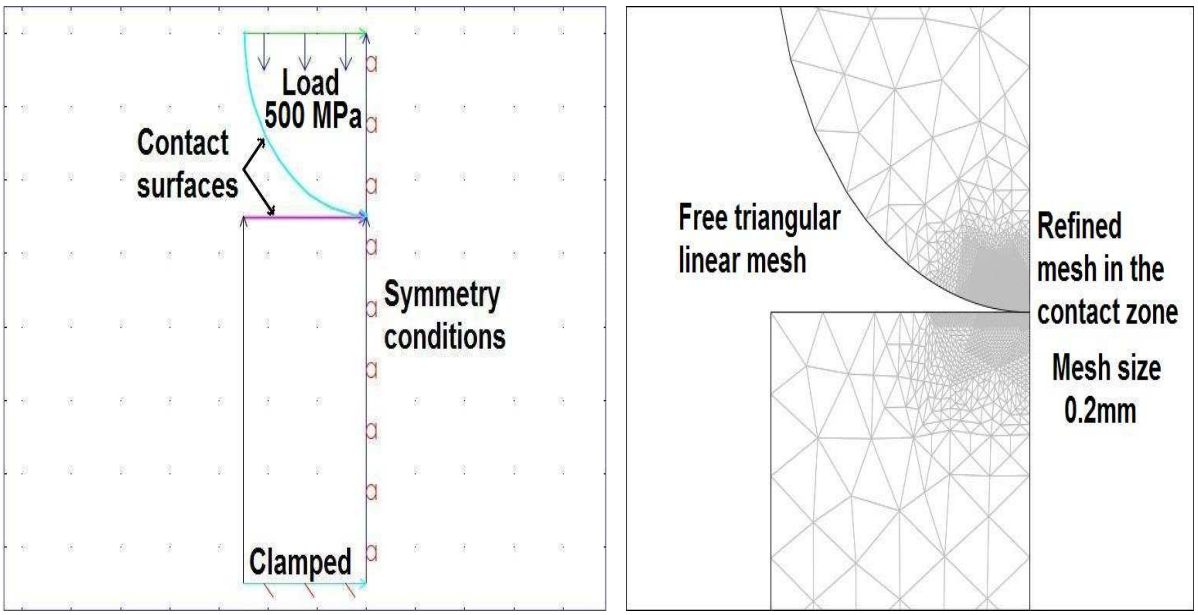

(a) Boundary conditions for contact model (b) Mesh distribution near the contact zone

Figure 4.2.: Finite element model for the contact between a cylinder and a plane

4.2.3. ANSYS

A 2D model was built on ANSYS10. The element used is PLANE182 with the option PLANE STRAIN hypothesis and friction was neglected between the two surfaces. Due to geometrical and load symmetry, half of the geometry was considered with symmetry boundary conditions (figure 4.4(a)). The geometry was meshed using free triangular linear mesh with a mesh concentration in the contact zone as shown in figure 4.4(b). The convergence difficulties faced with COMSOL was solved using ANSYS10 with the different contact routines that are propose. The Results are displayed in figure 4.5 showing the contact pressure distribution along the contact length.

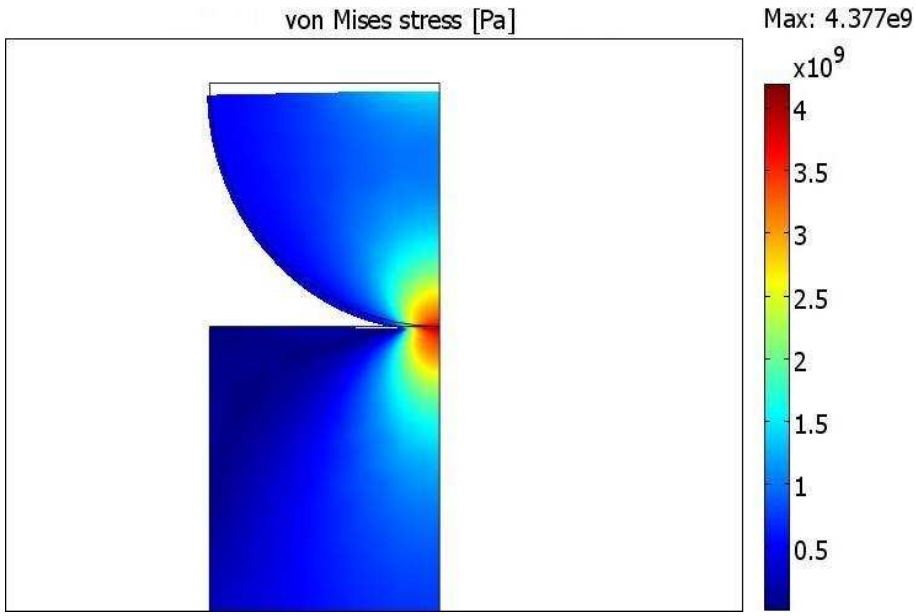

Figure 4.3.: Contact pressure using COMSOL 3.4.

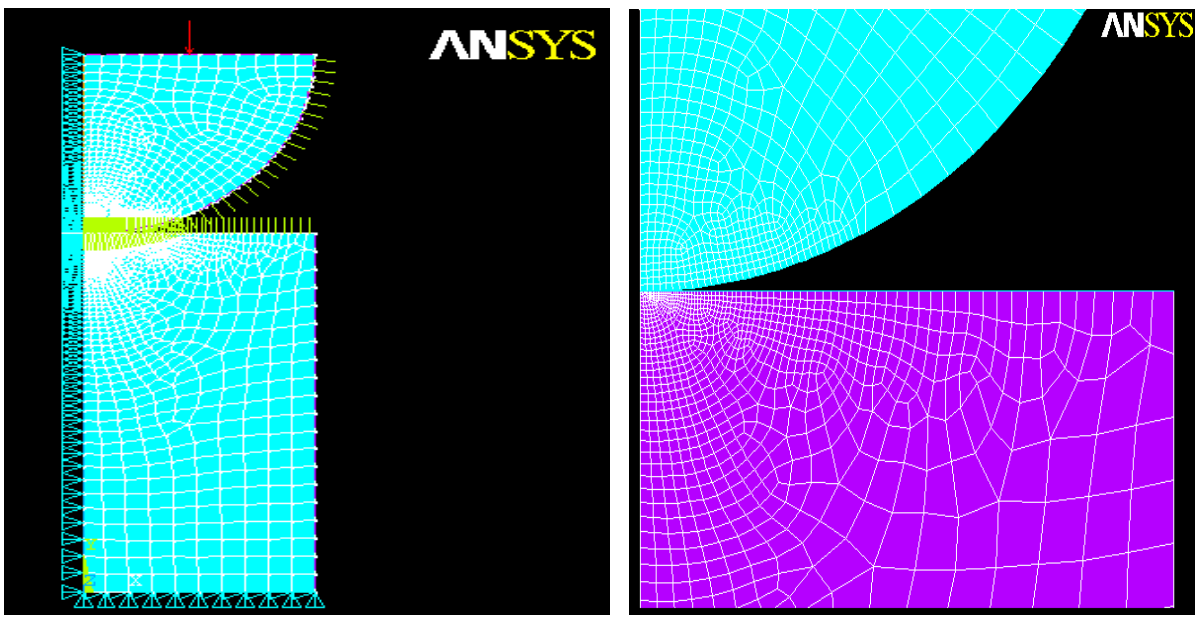

(a) Boundary conditions for contact model on ANSYS10

(b) Mesh distribution near the contact zone in ANSYS10

Figure 4.4.: Finite element model, as built on ANSYS10, for the contact between a cylinder and a plane

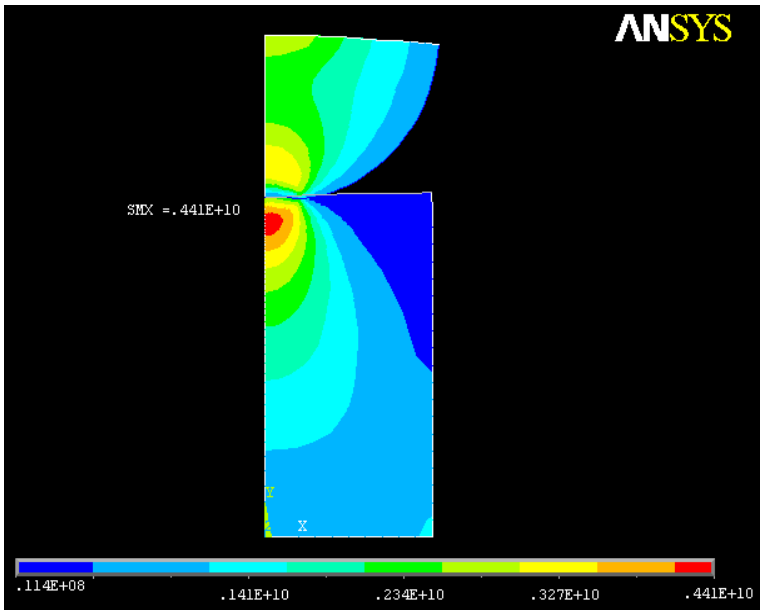

Figure 4.5.: Contact pressure as simulated using ANSYS10.

4.2.4. Analytical results

Hertz analytical formulation for this problem gives the expression of the contact pressure distribution as a function of the contact length b and the maximum contact pressure P_{max}. The expressions are given by:

$$b = \sqrt{\frac{4F.R}{\pi.l}\left(\frac{1-\nu_1^2}{E_1} + \frac{1-\nu_2^2}{E_2}\right)} \tag{4.1}$$

$$P_{max} = \sqrt{\frac{F}{\pi.R.l\left(\frac{1-\nu_1^2}{E_1} + \frac{1-\nu_2^2}{E_2}\right)}} \tag{4.2}$$

Where F is the total applied vertical load which in our case is $F = 2.R.l.500.10^6$

R the cylinder radius (the block is considered as a cylinder with radius infinity)

E_1, E_2 the Young modulii of the cylinder and the block respectively

ν_1, ν_2 the poisson's ratio of the cylinder and the block respectively

and finally l is the length of the cylinder and the block (the length of the cylinder and the block is equal).

and the contact pressure distribution P_r along the contact length is given by,

$$Pr(b) = P_{max}\sqrt{1-\left(\frac{x}{b}\right)^2} \tag{4.3}$$

Where x is the distance from the center of the contact length (on the plane of symmetry) to any point on the contact arc.

4.2.5. Comparison

In order to have efficient validation, we compare the critical values of the parameters describing the contact which are the maximum contact pressure and the contact length. The analytical maximum contact pressure has a value of 4446 MPa with a difference of 2% from the 4380 MPa obtained by simulation on COMSOL. The contact length showed 1% difference between the 7.3 mm obtained from COMSOL simulation and the 7.2 mm calculated analytically. The contact pressure distributions for the three cases, COMSOL simulation, ANSYS simulation and analytical results, are compared in graph 4.6.

Comparing the maximum contact pressure of 4410 MPa obtained on ANSYS10 and the 4380 MPa obtained on COMSOL, presented an offset of about 0.5% which is negligible.

4.3. Piezoelectric models

For Piezoelectric models validation, we will first validate an analytical model of the actuator with COMSOL simulation, then a switch model will be used to compare COMSOL to ANSYS.

4.3.1. Actuator

Model description

An actuator consisting of a 500 μm long cantilever, multilayered to compose the piezoelectric stack is our case study for this physics validation. The multilayer is composed of 4 layers: A thick elastic layer made of polysilicon,an isolation layer of Silicon nitride (SiN), a piezoelectric (active) layer of Zinc oxide (ZnO) and a top electrode made of Platinum. The geometrical details are shown in figures 4.7(a) and 4.7(b) while the material properties and the electromechanical coupling coefficient of ZnO are as shown in figure 4.8. In reality, the elastic layer is wider than the rest of the layers due to fabrication concerns. For this reason, two geometries were simulated to check the effect of the different widths on the deflection of the beam. The first one considers that the elastic layer is wider than the rest of the stack while the second model considers that all the layers have the same width. The mechanical material properties as well as the geometrical parameters for each layer of the piezoelectric stack are summarized in table 4.1.

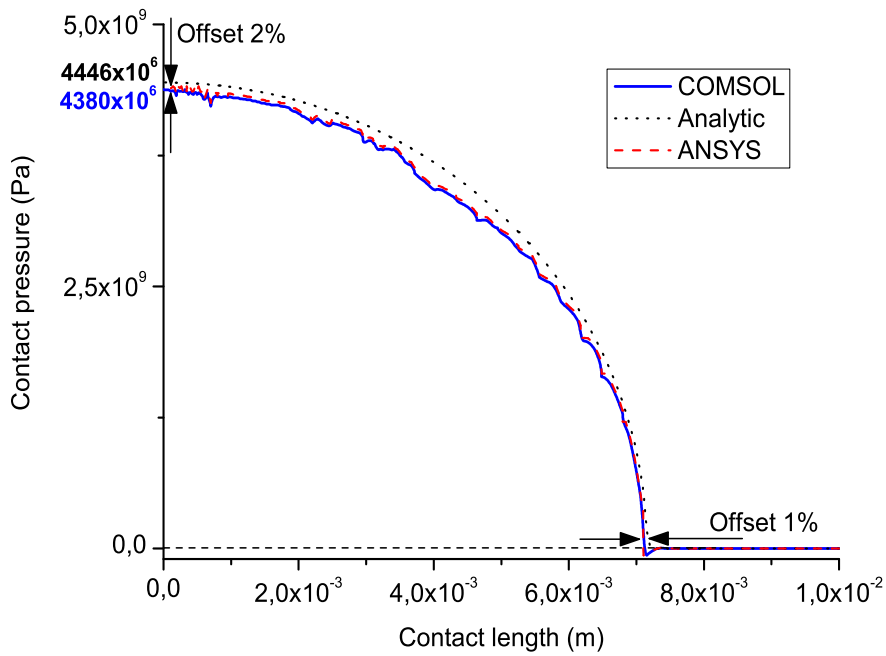

Figure 4.6.: Contact pressure as a function of the arc distance for COMSOL, ANSYS and analytical results.

Material	Width	Thickness	Yound modulus (GPa)	Poisson's ratio	d_{31}
Pt	26μm	0.2μm	250	0.25	
ZnO	26μm	1μm	161	0.36	$2.3pC/N$
SiN	26μm	0.2μm	290	0.28	
Poly Si	30μm	1.7μm	162	0.23	

Table 4.1.: Material properties and dimensions for the piezoelectric stack layers.

COMSOL

We used a 2D model to define the problem using the PLANE STRESS hypothesis. In COMSOL, we combined the structural mechanics PLANE STRESS stress with PIEZOELECTRICITY. The cantilever is clamped at the first end and kept free on the other end. The source of deformation comes from the stress induced by the piezoelectric layer under the effect of an electric field. The piezoelectric layer is polarized between two electrodes subjected to a potential diffrence of 3V. The boundary conditions are presented on figure 4.9. The geometry was meshed with quadrilateral elements of 4 μm in size. The initial stress in all layers is set to zero. Two simulations were run for the same model but

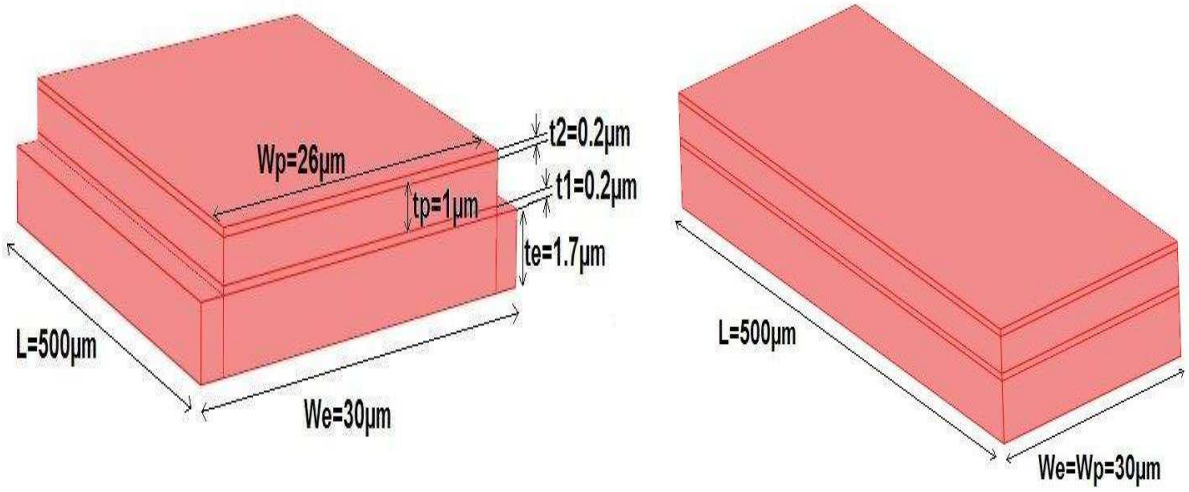

(a) Geometrical dimensions of a piezo actuator, first model

(b) Geometrical dimensions of a piezo actuator, second model

Figure 4.7.: Contact model description

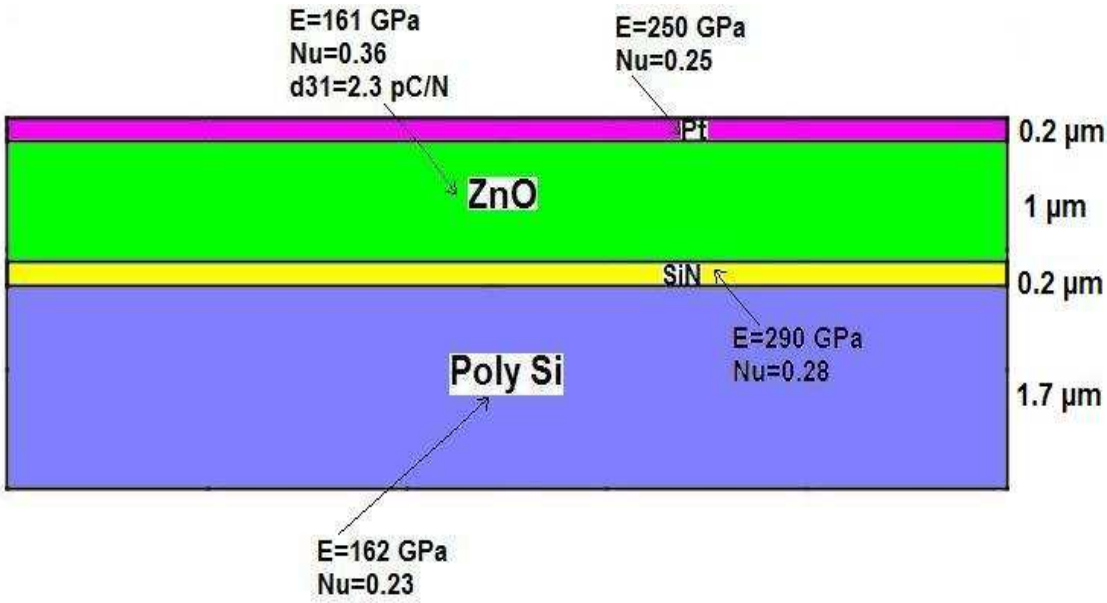

Figure 4.8.: Material properties of the piezoelectric stack in the actuator model.

different geometrical parameters.

Different width The first model have an elastic layer width of 30 μm and the rest of the layers 26 μm. This model represents the real dimensions as the structure should be

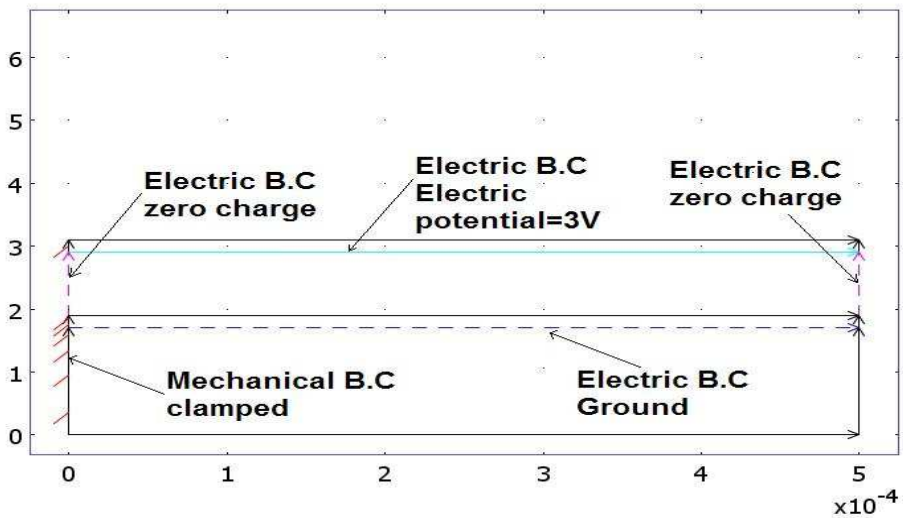

Figure 4.9.: Mechanical and electrical Boundary Conditions (B.C) for Piezoelectric model.

fabricated with the piezoelectric stack thinner that the elastic layer. The Results of the simulation is shown in figure 4.10(a) displaying the vertical displacement of the cantilever with a maximum of 223 nm.

Same width The second model simplifies the modeling and considers all the layers of the same thickness with a value of 30 μm. Figure 4.10(b) shows the vertical deflection obtained by finite element simulation, with a maximum of 224 nm at the tip.

Comparison for width effect The error that we might commit by simplifying the model and considering the whole stack with the same width is 0.5%. This negligible error permits us to simplify our models in all our studies.

Analytical results

The analytical formulation given by Smits [54] for the deflection of a piezoelectric heterogeneous bimorph as a function of the cantilever length is of the forme below:

$$\delta(x) = \frac{x^2 d_{31} E_F (t_e + t_p) A_e E_e A_p E_p}{(t_e + t_p)^2 A_e E_e A_p E_p + 4(A_e E_e + A_p E_p)(I_e E_e + I_p E_p)} \tag{4.4}$$

Where:

- x is the distance of the point of interest from the clamp of the cantilever.

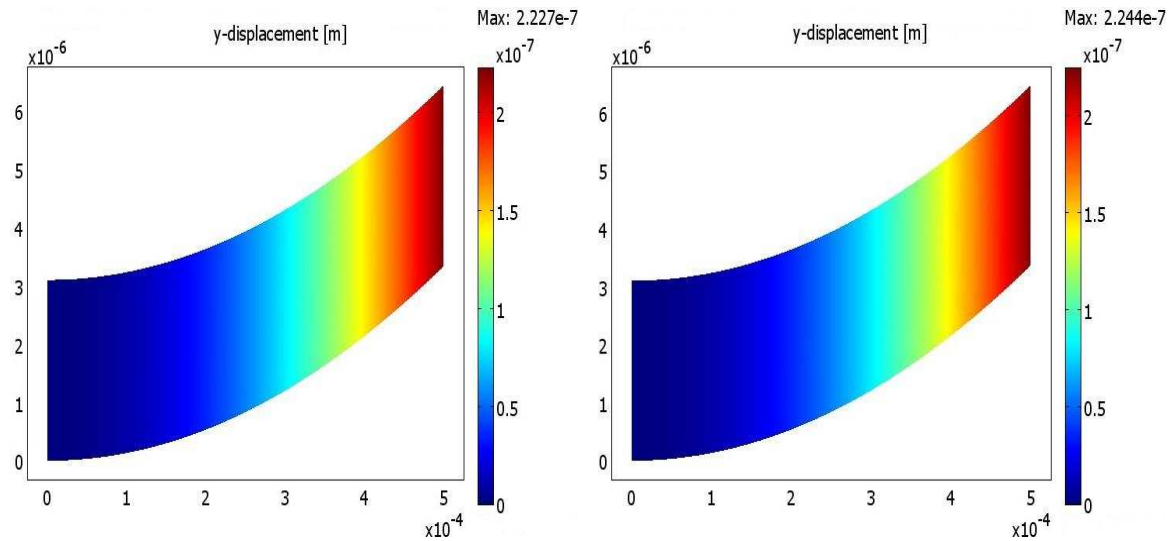

(a) Simulation results for the model with different widths

(b) Simulation results for the model with the same width

Figure 4.10.: Finite element simulation results

- E_F is the electric field (in the thickness direction) in the piezoelectric layer given by $E_F = \frac{V}{t_p}$.
- d_{31} the electromechanical coupling coefficient for the piezoelectric material used.
- E_e, E_p the Young modulus of the elastic layer and the piezoelectric layer respectively.
- t_e, t_p the thickness of the elastic layer and the piezoelectric layer respectively.
- A_e, A_p the cross section surface of the elastic layer and the piezoelectric layer respectively.
- I_e, I_p the cross section moment of inertia of the elastic layer and the piezoelectric layer respectively.

To simplify our model to a bimorph, the thickness of the Platinum and that of SiN was added to the thickness of the elastic layer. The negligible effect of the layers width on the actuation results, as presented in paragraph 4.3.1, permits us to simplify and consider that the elastic layer as well as the piezoelectric stack, has the same width $W_e = W_p = W$. A_e, A_p, I_e, I_p and E_F can be then replaced by their values as a function of t_e, t_p and W.

The expression of the deflection becomes:

$$\delta(x) = \frac{3t_e d_{31} V (t_e + t_p) E_e E_p x^2}{E_e^2 t_e^4 + E_e E_p (4t_e^3 t_p + 6t_e^2 t_p^2 + 4t_e t_p^3) + E_p^2 t_p^4} \tag{4.5}$$

If L is the length of the cantilever, the deflection on the tip is then given by:

$$\delta(L) = \frac{3t_e d_{31} V (t_e + t_p) E_e E_p L^2}{E_e^2 t_e^4 + E_e E_p (4t_e^3 t_p + 6t_e^2 t_p^2 + 4t_e t_p^3) + E_p^2 t_p^4} \tag{4.6}$$

Comparison

To validate the simulations with the analytical results, we compared the deflection at the tip of the actuated cantilever. At the tip, the offset between the two deflections is 5%, 0.22 μm obtained from simulation and the 0.23 μm calculated analytically. The deflection along the cantilever length for both cases (simulated and analytical) are illustrated in figure 4.11.

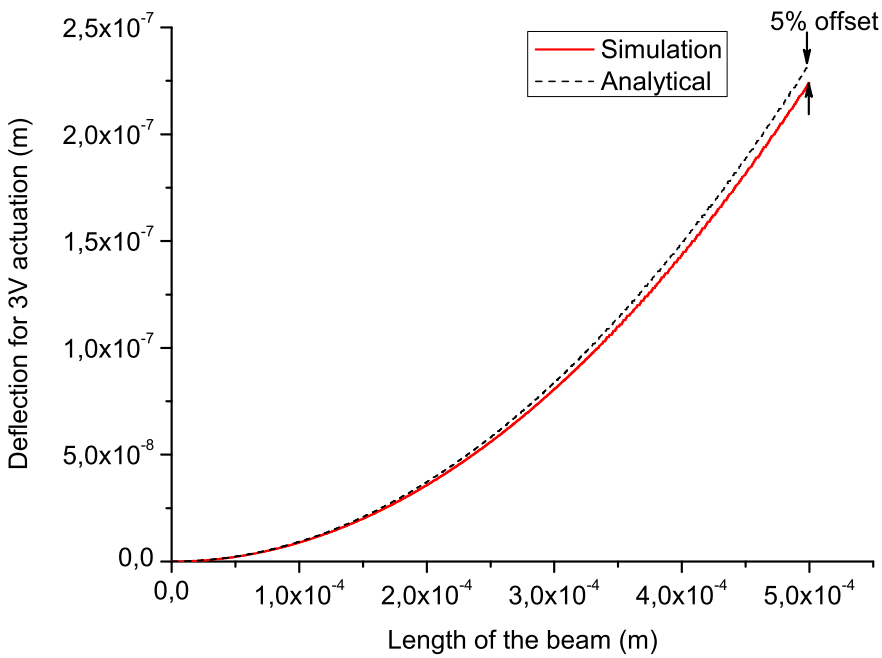

Figure 4.11.: Deflection along the cantilever for simulated and analytical results.

4.3.2. Switch

Model description

To compare the two softwares, COMSOL to ANSYS, we can choose a complicated structure, near to the reality unlike the analytical models which exists only for simple actuator. The deformation of a piezoelectric switch with four actuators linked to a membrane is

now considered. The dimensions of the model used, windmill design, are as presented in figure 4.12.

The actuator is composed of a bilayer, an elastic layer and a layer of piezoelectric material whose properties are presented in table 4.2. This model serves only to study the deflection of such a switch under the piezoelectric actuation, the effect of the top and bottom electrode is neglected. The membrane and its connectors to the actuator is formed of one layer and of the same material as the elastic layer. Each actuator is clamped from one end and connected to the membrane from the other end. The piezoelectric material is actuated under 3V.

Material	Yound modulus (GPa)	Poisson's ratio	$d_{31}(pC/N)$
ZnO	70	0.25	274
Poly Si	162	0.23	

Table 4.2.: Material properties of the piezoelectric stack layers for the windmill design.

COMSOL

The element size used in COMSOL simulation is 10μm. Figure 4.13(a) shows the deflection of the windmill design obtained by simulation on COMSOL.

ANSYS

The elements type used in ANSYS simulations is SOLIDE5 in order to induce the piezoelectric effect with the mechanical effect. A mapped meshing has been used with elements size varying from 1.6μm to 10μm. The deflection obtained by simulation on ANSYS for an element size of 1.6μm is presented in figure 4.13(b).

Comparison of COMSOL to ANSYS

For an element size of 10μm on COMSOL, we needed to refine the mesh until 1.6μm in ANSYS to obtain a fit of results in terms of deflection and Von-Mises stress. Table 4.3 summarizes the simulation results obtained on COMSOL and ANSYS for different element sizes. From the table we can see that in order to obtain the same results on ANSYS and COMSOL, we need to refine the mesh in ANSYS 6 times more than COMSOL inducing an increase in the time of calculation 30 times more.

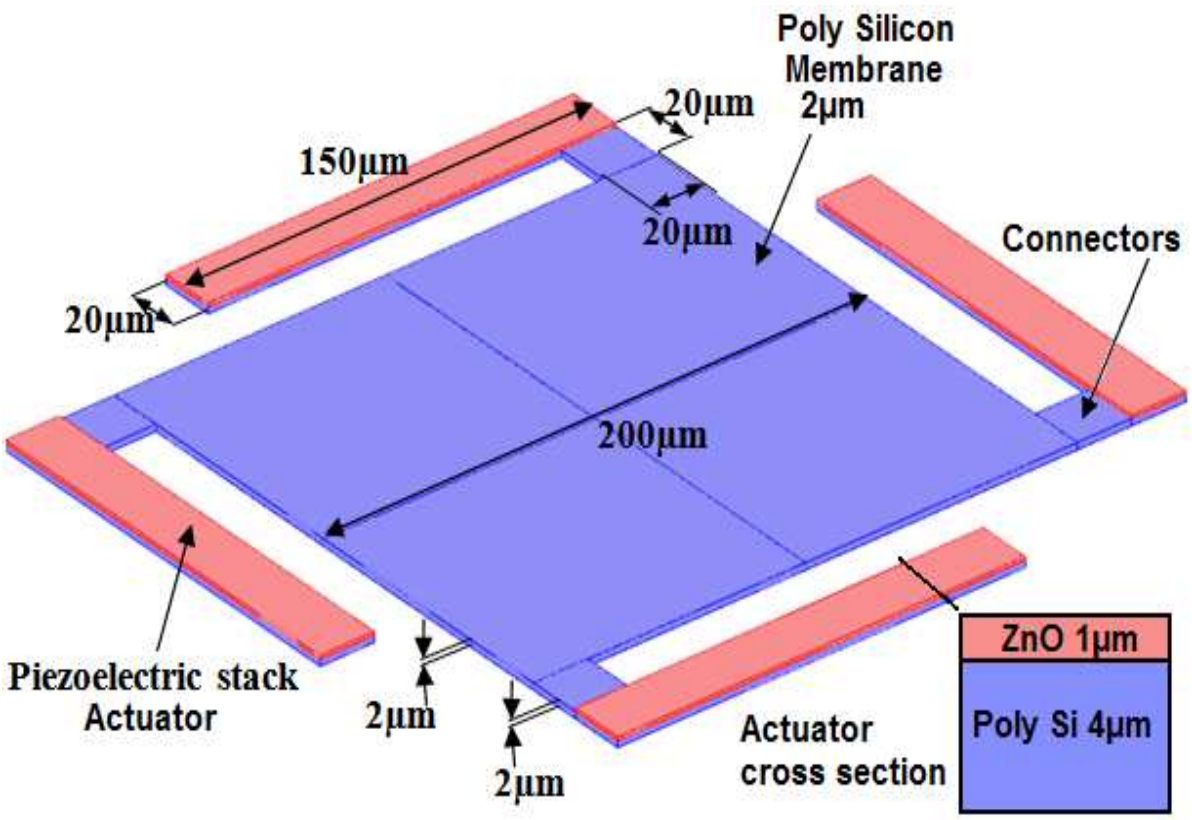

Figure 4.12.: The geometrical parameters of the switch model, windmill design, used to compare COMSOL to ANSYS.

Software	Mesh size	Max deflection	Max Von-mises stress	Calculation time
ANSYS10	5 μm	0.793 μm	73 MPa	33 sec
ANSYS10	1.6 μm	0.821 μm	123 MPa	690 sec
COMSOL	10 μm	0.817 μm	129 MPa	22 sec

Table 4.3.: Simulation results of the windmill design for different element size.

4.4. Electrostatic models

4.4.1. Model description

To validate the electrostatic actuation, we took a simple bridge whose geometrical and material properties are given in table 4.4 and 4.5 respectively. The bridge is clamped at both ends and actuated at its center with an electrode 100μm wide as shown in figure 4.14. The model is not done on ANSYS due to the complexity to apply the electrostatic force on the structure. A transducer element should be created between each node of the

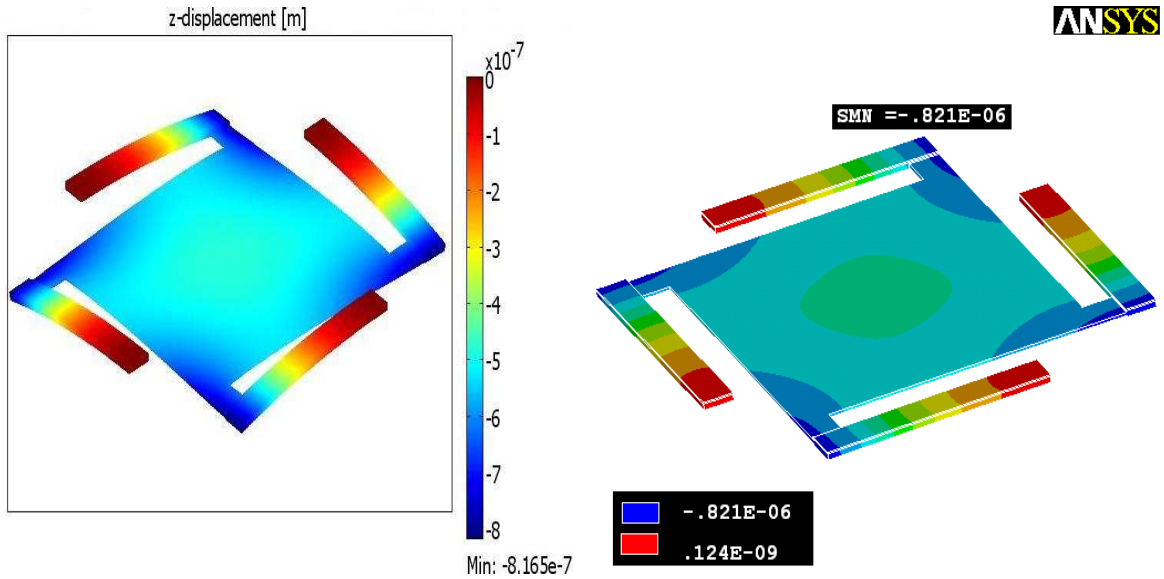

(a) Results of simulation on COMSOL for element size 10μm

(b) Results of simulation on ANSYS10 for element size 1.6μm

Figure 4.13.: Finite element simulation results for windmill design, for ANSYS and COMSOL comparision

bridge surface with the nodes of the electrode surface.

Length	Width	Thickness	Gap
1000 μm	60 μm	3 μm	2.5 μm

Table 4.4.: Geometrical dimensions of the bridge material.

Material	Initial stress	Young modulus	Poisson's ratio
Gold	10 MPa	70 GPa	0.23

Table 4.5.: Material properties of the bridge material.

4.4.2. COMSOL

When simulating the electrostatic problem on COMSOL, we needed to mesh the air gap between the bridge and the electrodes. This additional meshing increases the degrees of freedom and the memory needed to run the simulation. No hysterisis can be obtained, the pull-in can be deduced from the value of the applied voltage at the step where the calculation diverge. The pull-in was found to be 34V.

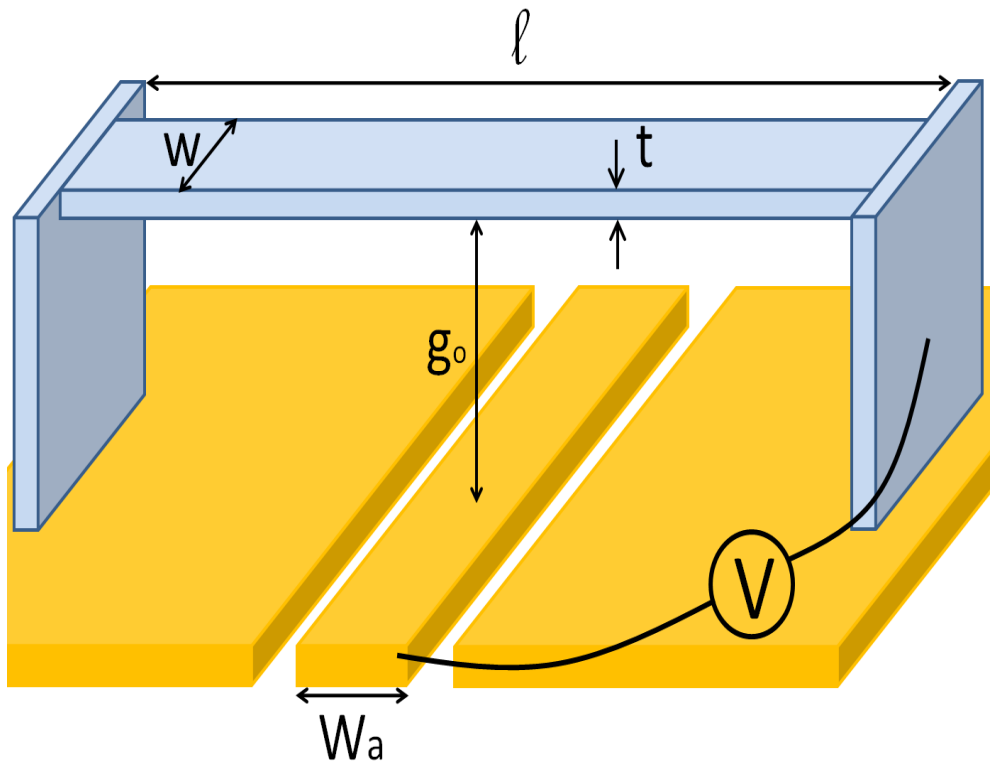

Figure 4.14.: The electrostatic model geometry.

4.4.3. Coventor

On Coventor, the simulation of electrostatic problem is easier to define. No meshing is needed in the gap, and we can use the GDS file to construct our model by defining the convenient process. The pull-in detection is done automatically and the software stays stable even when pull-in is detected. The hysterisis cycle can be detected in the form of capacitance as a function of voltage or displacement as a function of voltage. The simulated pull-in is 36V and the pull-out 2V.

4.4.4. Analytical results

The analytic equations of the simple bridge are described in the appendix A. The pull-in voltage was calculated to be 31.5V and the pull-out was found to be 1.7V.

4.4.5. Comparison

The difference in the actuation voltage between the analytical result and Coventor is around 14% while it is only 8% between the analytical value and COMSOL. The difference in the results between the two softwares is 5% which is acceptable but keeps Coventor

in advantage on COSMOL for the facility to build the model and for the hysterisis cycle that COMSOL can't simulate.

4.5. Conclusion

Figure 4.15 summarizes the capacities of ANSYS and COMSOL as well as COVENTOR. The smiley face signifies that the software is capable to do this and the empty case is to say that it is difficult or impossible to do. In the following lines, we will list briefly the advantages and inconvenience that we have faced on each of COMSOL, ANSYS and COVENTOR during our application.

COMSOL COMSOL offers a wide palette of advantages summarized in:

- Unlimited coupling of any physics.

- Reduced computing time.

- Any simulation parameter (Material properties, initial stress, forces ...) can be written as a function of simulation variables or exterior variables.

- We can integrate initial stress gradient through the thickness of any material.

- Possibility to build a model in SCRIPT format, communicate with matlab and add loops for optimization or for parametric study.

- Possibility to import STL files which are useful for the reverse engineering studies.

While COMSOL's major drawbacks are:

- The out of memory error, when modeling large models with many couplings. This can be ameliorated by using larger memory or a 64 bits computer.

- Drawing complicated geometries (circular geometries) is not simple. This issue was solved by drawing the geometry on AutoCAD and exported as DXF file which is then read by COMSOL.

- Difficulties to build contact models, and to find the appropriate parameters for the solver convergence.

- Simulation of electrostatic actuation could be run until pull-in. No hysteresis curves can be obtained.

ANSYS ANSYS also knows many advantages even if the simulation is time consuming, these are summarized in:

- Very efficient in solving contact problems and in the convergence of the solver.

- Possibility to build a model in a text file format, and add loops for optimization or parametric study.

- Possibility to import STL files which are useful for the reverse engineering studies.

The drawbacks of ANSYS are:

- Simulations are time consuming.

- Some complications for electrostatic actuation modeling. We need to create a force as a function of displacement between the nodes of two opposite surfaces.

COVENTOR Coventor is a software dedicated to MEMS and circuit simulation, it has many advantages that are listed below:

- Very efficient for the electrostatic actuation simulation, specially the pull-in and pull-out voltages (hysteresis simulation).

- Use of the Mask file (GDS or CIF files) in order to build the geometry of the model.

- Possibility to export the geometry from ANSYS under the IGES format or DXF format.

Being very dedicated to a specific domain, Coventor has many drawbacks with respect to our application that can be summarized in:

- Simulations are time consuming.

- No 2D models can be simulated. The 2D mesh is only used in order to extrude the mesh into a 3D structure.

- Flat surfaces are only simulated, since it functions in layers to build the model. This drawback can be solved by exporting any geometry from ANSYS under a IGES format.

- No script file for the model, making it very difficult for multi parametric simulations, optimization or reverse engineering studies. (For reverse engineering, we need to build the geometry in ANSYS, export it into IGES format, and then import it into COVENTOR)

Software	Application	Static	Modal analysis	Time dependent	Harmonic response	Parametric	Transatory quasi-static	Large deformation	Linear bukling	Elastoplasticity	Multiphysics	Electrostatic	Piezoelectric	Thermal	Mean stress σ_0	$\sigma_0(x,y,z)$	Initial deformation ε_0	Thermal deformation ε_{th}
COMSOL	Solid	☺	☺	☺	☺	☺	☺	☺	☺	☺	☺	☺	☺	☺	☺	☺	☺	☺
	Shell	☺	☺	☺	☺	☺	☺	☺		☺	☺	☺	☺	☺	☺		☺	☺
ANSYS	Solid	☺	☺	☺	☺	☺	☺	☺	☺	☺	☺	☺	☺	☺	☺			☺
	Shell	☺	☺	☺	☺	☺	☺	☺	☺		☺	☺	☺	☺	☺			☺
COVENTOR	Solid	☺	☺		☺	☺	☺	☺	☺			☺	☺	☺	☺	☺		☺
	Shell											☺			☺			☺

Figure 4.15.: Summary of different software capacities for multiphysics problems.

In this study, we validated the results of simulation for the physics that we are going to use for modeling and solving our problems. COMSOL showed a good agreement with the analytical values which gives a first degree of certainty on the results. The comparison of COMSOL with ANSYS had a double goal, the first was to validate the results with well known reliable software and the second was to compare their performances and advantages with respect to each others. In paragraph 4.3.2, we can see that ANSYS needs about 30 times more time for calculation. Nevertheless, ANSYS offers a wider option of routines than in COMSOL for the contact problem solving which make of ANSYS excellent software for contact problems convergence. As a result, we used COMSOL for piezoelectric, initial stress and thermal problems as well as for the pull-in simulation to validate the analytical design. ANSYS is used for the contact models, where the membrane contacts the electrode in the piezoelectric switch. Coventor was used finally to simulate the hysteresis curve of our electrostatic switch design.

Actionnement piezoelectrique

Pour résoudre le problème de stiction lié à l'actionnement électrostatique, nous étudierons d'autres méthodes d'actionnement. La méthode d'actionnement piézoélectrique semble être un bon alternatif, surtout qu'il est promettant d'une grande déflection et faible consommation d'énergie. Pour cette raison il est intéressant pour nous de faire une étude de faisabilité d'un commutateur piézoélectrique. Des différents topologies du commutateur ont été étudié et les différents modes de connections de la membrane a l'actionneur ont été simulée.

Tout d'abord, l'actionnement était sous l'investigation. La déflexion et le temps de réponse des différents modèles ont été étudiés pour avoir une idée de la meilleur mode de connecter l'actionneur à la membrane. Les fréquences propres ont été calculées mais ils servent seulement pour comparaison. La membrane a montré une déformation importante suite à l'actionnement, donc sa planéité après qu'elle touche l'électrode a été vérifié.

Quelques problèmes ont fait face a notre étude quand il s'agit de la déflection initiale de l'actionneur a cause du déséquilibre dans les contraintes initiales de chaque couche. Le même problème est confronté pour la variation de la température ambiante. Les coefficients de dilatation thermiques des différentes couches induisent un déséquilibre qui cause une déflexion initiale significative. Pour cette raison, nous avons essayé différentes solutions pour compenser ce déséquilibre mécanique. Dans un premier lieu nous allons équilibrer les coefficients de dilatation thermique et dans une deuxième étape nous avons compensé le gradient des contraintes mais la solution semble compliquer la fabrication. Les critères pour comparer les modèles sont la déflexion maximale sous l'actionnement, la raideur, les fréquences de résonance mécaniques et le temps de commutation.

Le concept consiste de déplacer une membrane vers une électrode fixe avec laquelle elle va créer une capacitance variable en fonction de la position de membrane. Les critères comme déjà expliqué sont d'obtenir une membrane plate quand elle vient contacter l'électrode. Une tension d'actionnement de 3V est imposée par l'application aux téléphones mobiles. Il aussi devrait résister aux variations de la température de -40°C à 85°C.

Nous sommes intéressés dans l'étude des commutateurs RF capacitive. Les valeurs de $C_{on}/C_{off} = 30$ définissent l'écart initial qui est imposé par l'application pour avoir un bon isolement. Un écart initial d'au moins 1.5μm est nécessaire pour obtenir l'isolement

nécessaire. Des valeurs de la fréquence de résonance électrique, nous concluons la valeur de C_{on} qui nous mène ensuite à calculer la surface de notre membrane (les dimensions de la membrane). Une surface de $4.10^{-8}m^2$ est nécessaire, donc la membrane carrée aura un côté de 200μm.

En premier temps, le mécanisme de positionnement est étudié (Modèle I) alors ce mécanisme de positionnement est connecté de différentes façon à une membrane. Les différentes façons de connexions mènent à 3 concepts différents (Modèle II, Modèle III et Modèle IV).

N'importe quelle force de déséquilibre ou la déformation est l'origine de déflexion. Le problème de déflection initial des structures multicouches vient du déséquilibre dans les contraintes initiales dans les différentes couches ou du déséquilibre dans la déformation induite par la dilatation thermique de chaque couche. Pour cette investigation nous avons choisi le modèle I puisque s'il est compensé ca implique la compensation de l'autre modèles.

La rotation du bout du mécanisme d'actionnement est transmise à la membrane induisant une poche d'air entre la membrane et l'électrode. Courbes 5.25, 5.26 et 5.27 montrent la distribution de déflexion sur la membrane des modèles II, III et IV respectivement. Cet écart d'air cause une perte importante dans la valeur de capacitance qui affecte la qualité de commutation. Pour étudier la planéité de ces membranes, c'est nécessaire de modéliser leur contact avec l'électrode pour vérifier si l'énergie d'actionnement est assez pour aplatir la membrane contre l'électrode.

5. Piezoelectric actuation

5.1. Introduction

To solve the problem of stiction related to electrostatic actuation, we shall study other actuation methods. Piezoelectric actuation seems to be a good alternative, specialy that piezoelectric actuators promises with a high deflection and low energy disipation. For this reason it is interesting for us to do a feasibility study of a piezoelectric switch. Different topologies for the switch were studied and different modes of connecting the membrane to the actuator was simulated.

First of all, the actuation was under investigation. The deflection and the response time of the different models were studied in order to have an idea of the better mode of connecting the actuator to the membrane. The Eigen frequencies were calculated but it will serve only for comparision. The membrane showed an important deformation due to the actuation, so its flatness after contacting the electrode was checked.

Some problems were faced when it comes to the initial flatness of the actuator due to disequilibrium in the stress of each layer. Same problem is faced with the temperature variation. Thermal expansion coefficients of different layers induces deformation disequilibrium causing a significant initial deflection. For this reason, we tried different ways to compensate this disequilibrium. In a first place we equilibrated the coefficients of thermal expansion and in a second step we compensated the stress gradient but the solution seems complicated.

The criteria to compare the models and those investigated in these models are the maximum actuation deflection, stiffness, mechanical resonance frequencies and switching time.

5.2. Design study

5.2.1. Introduction

The concept consists of moving a membrane towards a fixed electrode with which it will creates a variable capacitance as a afunction of the membrane position. The criteria as already explained is to obtain a flat membrane when it comes into contact with the

electrode. An actuation voltage of 3V imposed by the application to mobile phones. It should also withstand the temperature variations from -40°C to 85°C.

We are interested in studying capacitive switches. The values of $C_{on}/C_{off} = 30$ defining the initial gap is imposed by the application in order to have a good isolation. An initial gap of at least 1.5μm is needed to get the needed isolation. From the values of the electric resonance frequency, we deduce the C_{on} value leading to calculate the surface area of our membrane (the dimensions of the membrane). An area of $4.10^{-8}m^2$ is needed, so the square membrane will have a side of 200μm.

First, the actuator is studied (Model I) then this actuator is connected in different ways to a membrane. The different ways of connections leads to 3 different designs (Model II, Model III and Model IV).

5.2.2. Simple actuator design (Model I)

Model I description

First, the isolated actuator is studied (Model I) since it is the only source of deflection and is common for all the designs. It consist of a cantilever formed of four layers composing the piezoelectric stack: an elastic layer of silicon nitride, two platinium electrodes, and a PZT piezoelectric layer. The layers thickness of the actuator and the width are imposed by the process while the length value is a tradeoff between obtaining a high deflection at actuation and low initial deflection due to initial stress and temperature variation. The dimensions are presented in table 5.1 and the material properties are shown on the figure 5.1.

Neither initial stress effect nor temperature variation effect are considered in this paragraph and they will be treated in paragraphs 5.3.1 and 5.3.2 respectively.

Layer	Thickness (nm)	Width (μm)	Length (μm)
Pt	100	20	275
PZT-5H	100	20	275
Pt	100	20	275
SiN	500	20	275

Table 5.1.: Dimensions of the piezoelectric stack of the actuator model I.

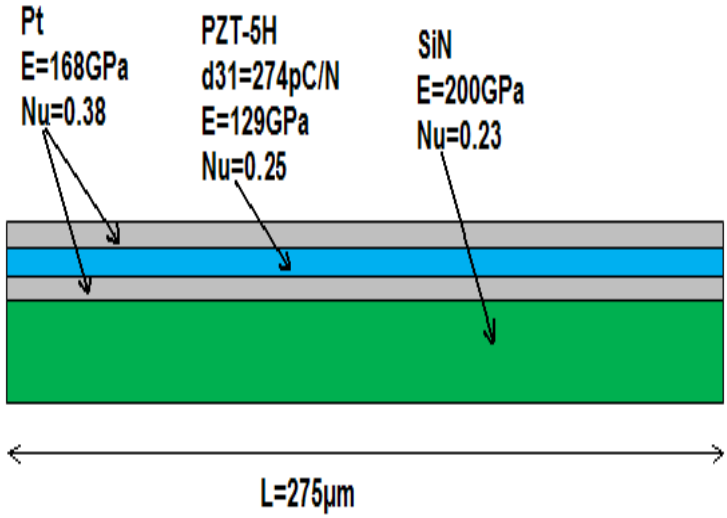

Figure 5.1.: Geometrical description of Model I and its material properties.

Model I simulation

For 3V actuation voltage we obtained a very high deflection which is normal because the actuator is not connected to any structure absorbing the deformation or blocking it. The maximum deflection obtained at the tip is 72μm as shown in figure 5.2(a).

The stabilization time for the cantilever to run the 72μm is from 4 to 6 mSec obtained from the graph in figure 5.2(b). A cut along the actuator is shown in figure 5.3.

The eigen frequencies starts from 8KHz and stays in the range of hundreds of KHz. Figures 5.4(a), 5.4(b) and 5.4(c) shows the 4th, 5th and the 6th vibration modes obtained in simulation for 207.3, 218.1 and 281.4KHz as a representation of the important modes we can meet.

5.2.3. Windmill design (Model II)

This model consist of the actuator presented in paragraph 5.2.2, attached to a membrane with torsion arms. The material properties of the stack are already presented in paragraph 5.2.2 and we consider that the membrane is made of the same material as the elastic layer of the actuator.

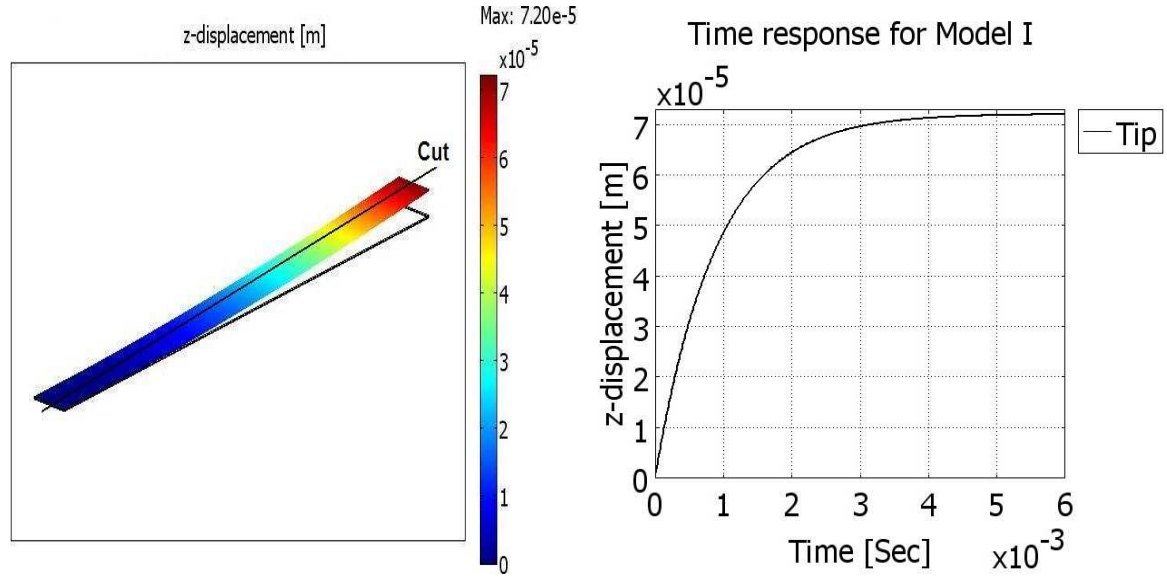

(a) The deflection simulation of Model I due to piezoelectric actuation.

(b) The time response of the tip of Model I.

Figure 5.2.: Finite element simulation results for model I

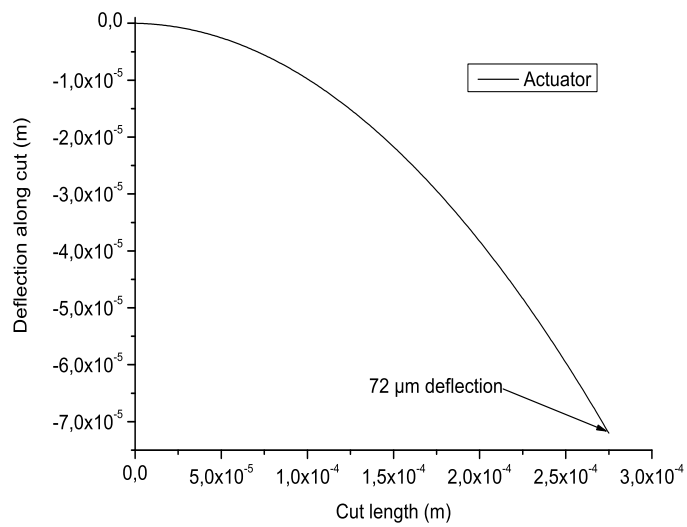

Figure 5.3.: Cut along the actuator (Model I).

Model II description

Model II is a cantilever as the one described in model I, and connected to the membrane with what we call torsion arms. The silicon nitride forming the elastic layer is 500nm

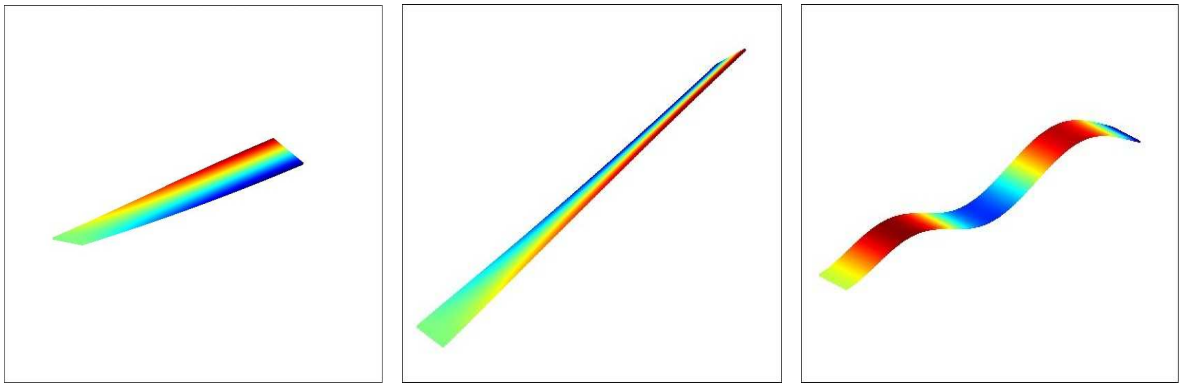

(a) Simulated vibration mode at 207.3 KHz for model I (b) Simulated vibration mode at 218.1 KHz for model I (c) Simulated vibration mode at 281.4 KHz for model I

Figure 5.4.: Simulated vibration modes for model I.

thick and forms at the same time the membrane as well as the connections (torsion arm) between the actuator and the membrane. The connectors dimension affects the torsion at the corner of the membrane and the total deflection. A stress study on the connectors showed that the minimum value for the connectors width $W_{tor} = 5\mu m$. The length of the connectors affects the transmission of the actuator rotation at the tip as a bending moment to the membrane. It is then chosen to be $L_{tor} = 20\mu m$ a compromise between the surface occupied by the switch and the flatness of the membrane. The membrane dimensions is a square of side L_m=200μm. The design parameters L_m, $L_{tor}$and W_{tor} are shown on figure 5.5.

Model II simulation

Actuated under 3V, we obtained a deflection which is smaller than what was obtained from the cantilever since the actuator is connected to a structure absorbing the deformation.

The maximum deflection obtained at the tip of the actuator is 36.7μm as shown in figure 5.6(a), while at the center of the membrane 32.7μm. The center of the membrane is deflected less than the tip which creates an air gap between the membrane and the electrode translated to a loss in the capacitance value. This deformation in the membrane is due to the rotation of the section at the tip inducing a torsion moment at the corners of the membrane leading it to bend.

The stabilization time for the membrane and cantilever to run the 36.7μm is between 4 to 6 mSec obtained from the graph in figure 5.6(b) showing the deflection of the tip and the center of the membrane as a function of time. The cut along the actuator is presented in figure 5.7.

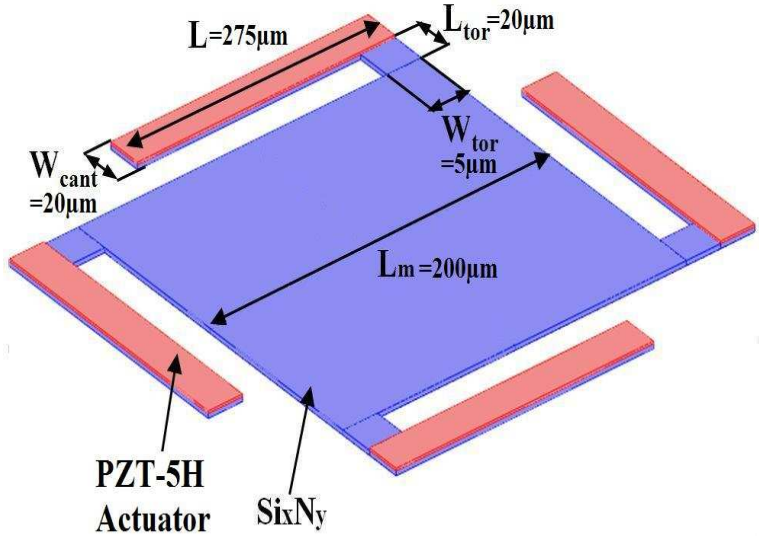

Figure 5.5.: Geometrical description of Model II.

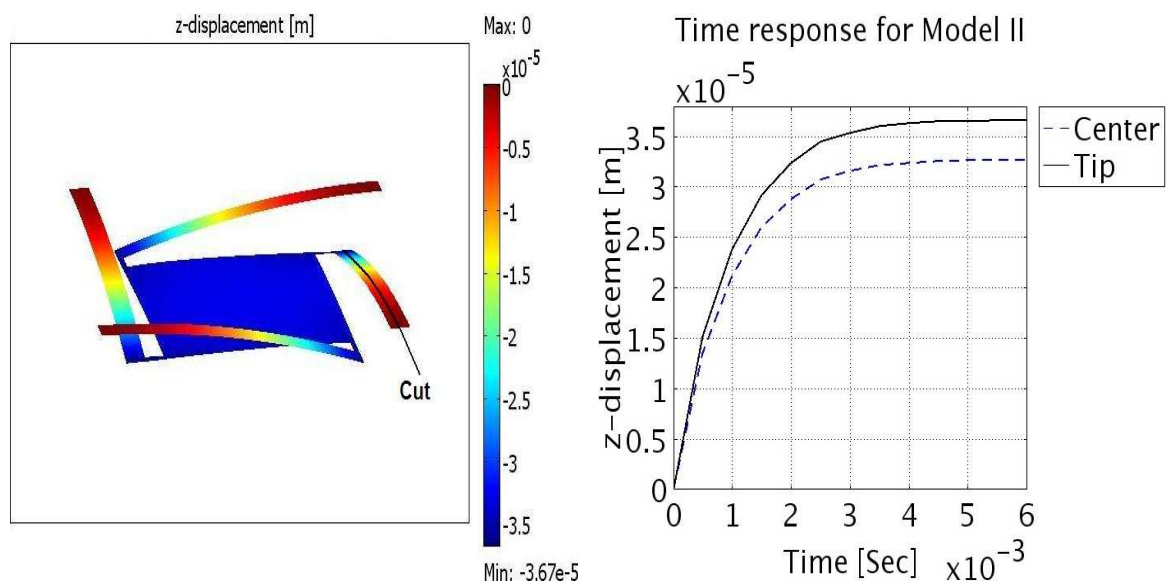

(a) The deflection simulation of Model II due to piezoelectric actuation.

(b) The time response of the tip of Model II.

Figure 5.6.: Finite element simulation results for model II

The eigen frequencies starts from 5KHz and stays in the range of few KHz. Figures 5.8(a), 5.8(b) and 5.8(c) shows the 4th, 5th and the 6th vibration modes obtained in

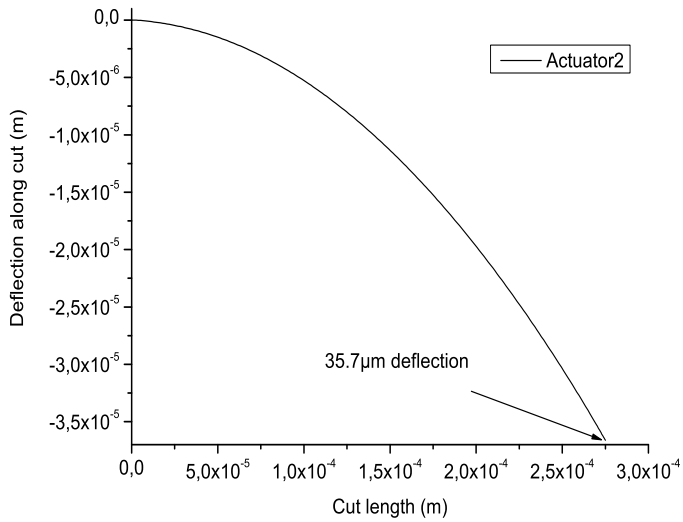

Figure 5.7.: Cut along the actuator of the windmill design (Model II).

simulation for 23.3, 34.5 and 42.6KHz as a representation of the important modes we can meet. The stiffness of the stack was simulated to be 0.131 N/m, relatively high with respect to model I.

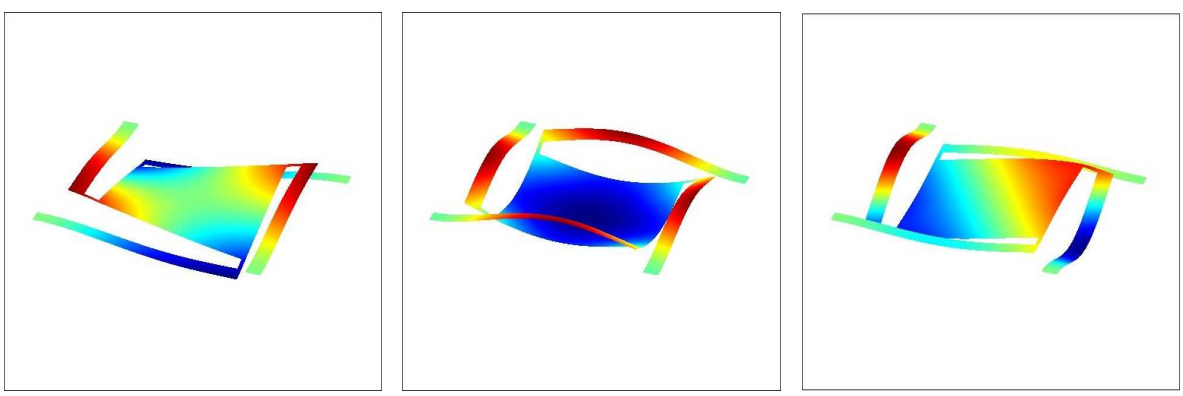

(a) Simulated vibration mode at 23.3 KHz for model II (b) Simulated vibration mode at 34.5 KHz for model II (c) Simulated vibration mode at 42.6 KHz for model II

Figure 5.8.: Simulated vibration modes for model II.

5.2.4. Circular design (Model III)

A circular model was tested consisting of a curved geometry of the actuator presented in paragraph 5.2.2, attached to a membrane with torsion arms. An equivalence of the area

and the actuator length between this model and model II was done in order to obtain the same functioning specifications.

Model III description

Model III is a curved cantilever of average perimeter L=275μm and width W_{cant}=20μm in order to keep the equivalence with a straight actuator for comparison reasons. The piezoelectric stack of the actuator is the same as for model I. The actuator is connected to the membrane with the torsion arm of length L_{tor}=20μm and width W_{tor}=5μm. Similar to model II, the silicon nitride forming the elastic layer is 500nm thick and forms at the same time the circular membrane and the connections (torsion arm). The membrane is a circular of radius R=113μm, to have an equivalence on the surface area as the previous model. The geometric details are shown in figure 5.9.

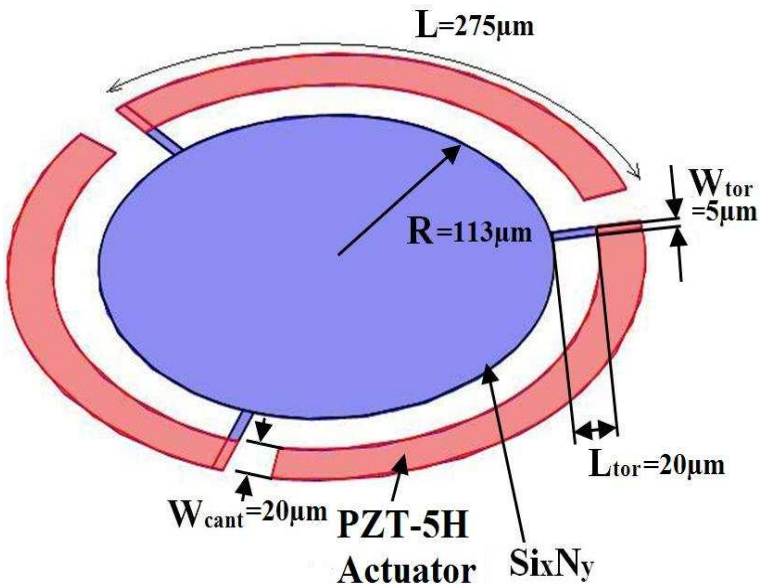

Figure 5.9.: Geometrical description of Model III.

Model III simulation

Actuated under 3V, we obtained a deflection which is the smallest among the three other models.

The maximum deflection obtained at the tip of the actuator is 20.6μm as shown in figure 5.10(a), while at the center of the membrane 14.7μm. The center of the membrane is deflected less than the tip which creates an air gap as for the case of model II.

The stabilization time for the membrane and the cantilever to run the 20.6μm is between 4 to 6 mSec obtained from the graph in figure 5.10(b) showing the deflection of the tip and the center of the membrane as a function of time.

The eigen frequencies are in the same range as for model II. Figures 5.11(a), 5.11(b) and 5.11(c) shows the 4th, 5th and the 6th vibration modes obtained in simulation for 34.3, 40.6 and 40.7KHz as a representation of the important modes we can meet for this model. The stiffness of the stack was simulated to be 0.206 N/m, relatively the highest with respect to the other models listed here.

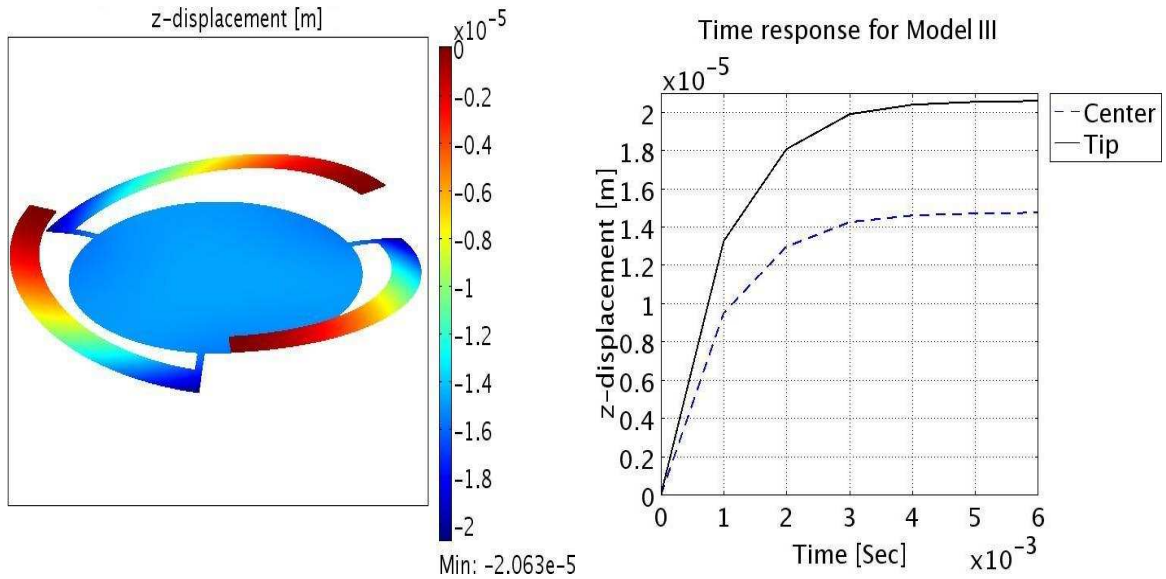

(a) The deflection simulation of Model III due to piezoelectric actuation.

(b) The time response of the tip of Model III.

Figure 5.10.: Finite element simulation results for model III

5.2.5. Cross design (Model IV)

The cross design was studied in order to check different connection methods. In this model, the actuator of length $L = 275\mu m$ presented in paragraph 5.2.2, is connected to the membrane in a flexion mode. The material properties of the stack are already presented in paragraph 5.2.2.

Model IV description

Model IV is the cantilever already described in model I, and connected to the membrane with flexion arm. Here also, the elastic layer forms at the same time the membrane as well as the connections (flexion arm) between the actuator and the membrane. The

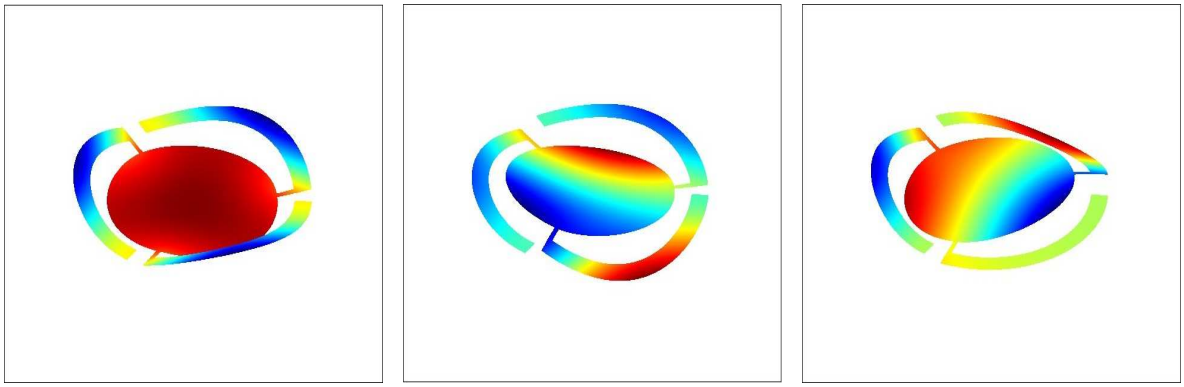

(a) Simulated vibration mode at 34.3 KHz for model III (b) Simulated vibration mode at 40.6 KHz for model III (c) Simulated vibration mode at 40.7 KHz for model III

Figure 5.11.: Simulated vibration modes for model III.

membrane is a square of side L_m=200μm, the flexion arm has a length L_{con}=20μm and width W_{con}=5μm as shown in figure 5.12.

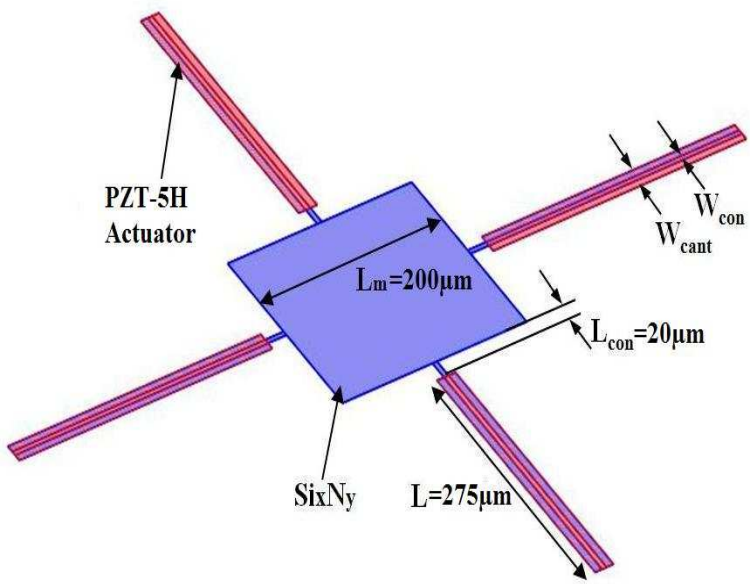

Figure 5.12.: Geometrical description of Model IV.

Model IV simulation

Actuated in flexion mode, the 3V actuation voltage gives the highest deflection among the models with moving membranes. The maximum deflection obtained at the tip of the actuator is 46.4μm as shown in figure 5.13(a), while 52.3μm at the center of the

membrane. The center of the membrane in this model is deflected more than the tip which leads to a better flatness after the contact of the membrane with the electrode. The stabilization time for the membrane and the cantilever to run the 52.3μm is between 4 and 6 mSec obtained from the graph in figure 5.13(b) showing the deflection of the tip and the center of the membrane as a function of time.

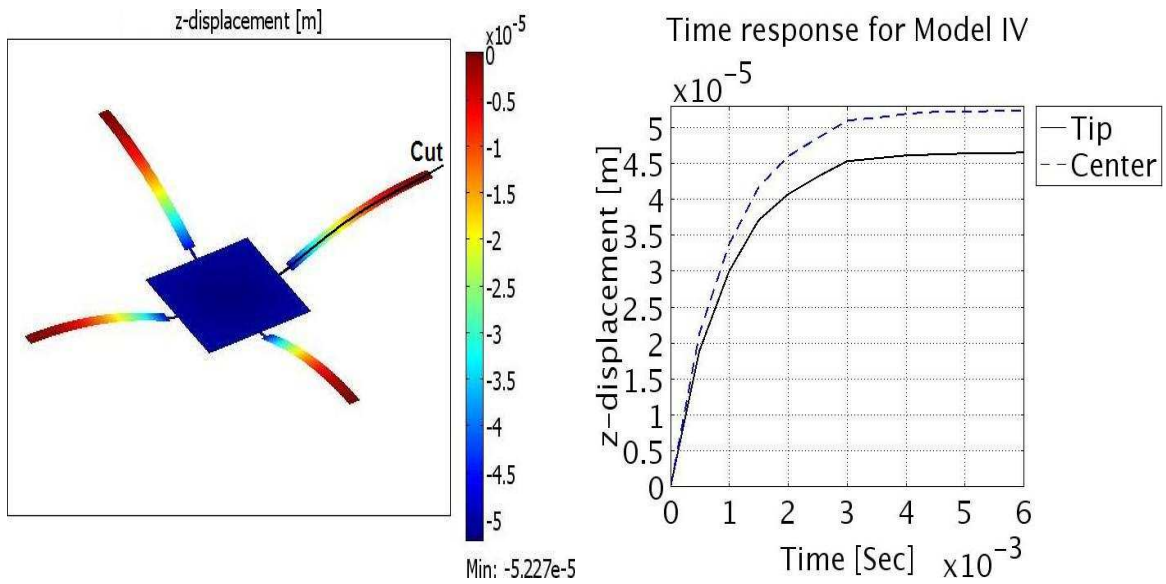

(a) The deflection simulation of Model IV due to piezoelectric actuation.

(b) The time response of the tip of Model IV.

Figure 5.13.: Finite element simulation results for model IV

The eigen frequencies are in the same range as for model II. Figures 5.15(a), 5.15(b) and 5.15(c) shows the 4th, 5th and the 6th vibration modes obtained in simulation for 27.5, 35.3 and 39.8KHz as a representation of the important modes we can meet for this model. The stiffness of the stack was simulated to be 0.11 N/m, higher than the cantilever model but keeping the high deflection property.

5.2.6. Comparision of different designs and conclusion

A summary of the studied criteria for different models is shown in table 5.2.

The simple actuator presents the highest deflection which is very appreciable but this deflection decreases when the actuator is connected to the membrane and very significantly in model III. Model IV shows very interesting results at all levels, good deflection, good stiffness and a deflection at the center of the membrane larger than that of the actuator tip. Having a deflection at the center more important that the actuators tip implies that the center of the membrane touches the electrode before the actuator which

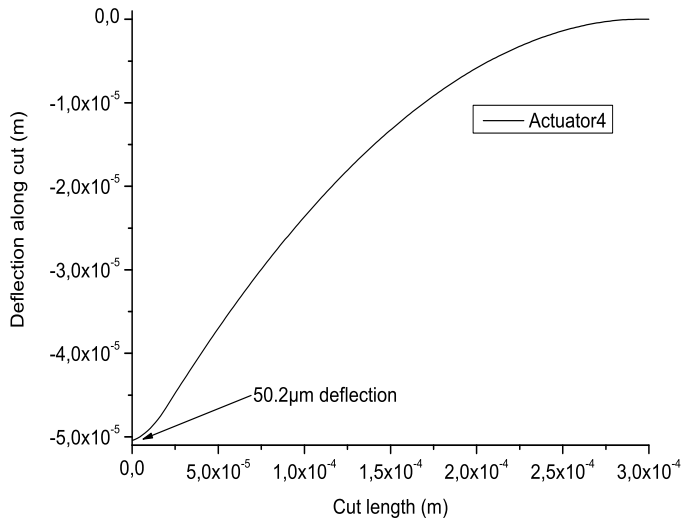

Figure 5.14.: Cut along the actuator of the cross design (Model IV).

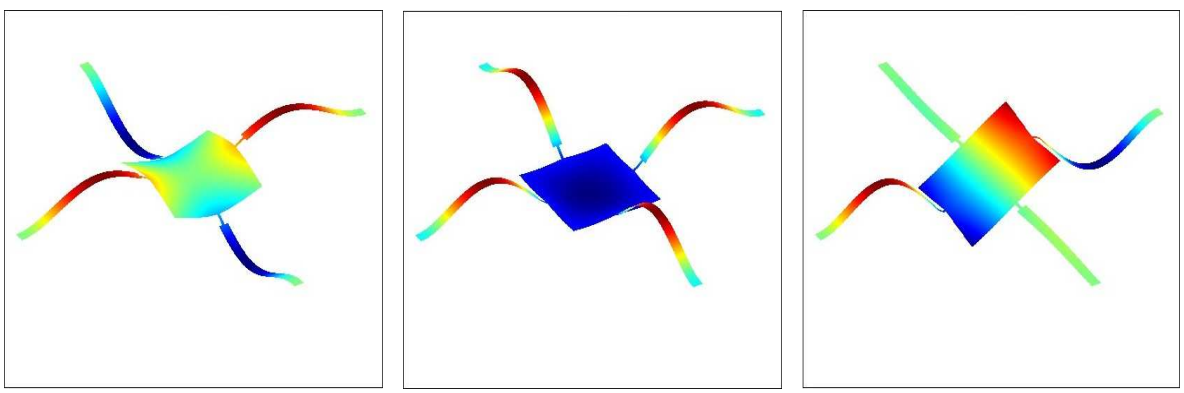

(a) Simulated vibration mode at 27.5 KHz for model IV (b) Simulated vibration mode at 35.3 KHz for model IV (c) Simulated vibration mode at 39.8 KHz for model IV

Figure 5.15.: Simulated vibration modes for model IV.

is interesting for the contact quality in order to obtain a flat surface. The percentage difference of deflection between the center and the tip for models II and IV are of 11% while it is 29% for model III, thats why a further study on the flatness of the membrane will be done only for models II and IV. The flatness problem will be treated in the next paragraph.

The eigen frequency of the moving sructure must be far from the functioning frequency in order to prevent it from autoactuation. The models shows approximately the same

order of eigen frequencies far from the GHz level. The damping effect being difficult to characterize and very dependent on the packaging cavity, we used approximative parameters for modeling.

The response time is the same for the 4 models but this doesn't mean that they have the same response. All models are responding with the same time but to cover different deflections which implies that the cantilever has the fastest response time.

5.3. Initial deflection problem

Any disequilibrated force or deformation is the origin of deflection. Initial deflection problem in multilayered structures comes from the disequilibrium of initial stress in the different layers or from the disequilibrium in the deformation induced by the thermal expansion of each layer. For this investigation we chose model I since if it is compensated and straight will implies the compensation of the other models.

5.3.1. Initial stress disequilibrium

The initial deflection due to the initial stress gradient is in the order of 9μm upwards. To compensate this gradient in the layers, a layer with variable stress should be induced. Two solutions was proposed, either add a Pt layer underneath the SiN or study another combination of layers with variable initial stress state. In the case of compensation with platinum, the stack has the properties shown in figure 5.16, where Γ_i is the initial stress in the layer. A study was done on the sensitivity of the actuator deflection to the platinum and nitride thicknesses. Figures 5.17, 5.18 and 5.19 show the initial deflection of the compensated stack described in 5.16 as a function of the platinum compensation layer thickness and the initial stress in the layers.

In figures 5.17, 5.18 and 5.19, the Y-axis is limited to 1μm deflection (upwards or downwards) as a criteria for compensation.

The sensitivity to the platinum thickness is high when the slope of the curves is high, while the sensitivity to the stress value in SiN is high when the distance between the curves is high. We can see from figure 5.17 that the initial deflection, in the case where SiN thickness is 500nm, is very sensitive to the uncertainties on the platinum thickness and on the initial stress in SiN. The sensitivity decreases when the thickness of SiN increases to 1000nm and it reaches a good value for a SiN thickness of 2000nm. The values of the deflections as shown in 5.19 are limited to 0.5μm, which is acceptable, for any uncertainty obtained from fabrication.

Studied Criteria / Concept #	Deflection (µm)	Occupied surface (µm^2)	Eigen frequencies (KHz)	Spring constant (N/m)	Switching Time (mSec)
I	72	5500	207.3 218.1 281.4	0.020	4 to 6
II	Center 32.7 Tip 36.7	78400	23.3 34.5 42.6	0.131	4 to 6
III	Center 14.7 Tip 20.6	93600	34.3 40.6 40.7	0.206	4 to 6
IV	Center 52.3 Tip 46.4	624000	27.5 35.3 39.8	0.110	4 to 6

Table 5.2.: Summary of the studied criteria for the different models.

The 2000nm of SiN is very big and it affects the deflection under the piezoelectric actuation while the 1000nm makes the stack sensitive to fabrication uncertainties. In addition to that, the stack is not at thermal equilibrium so an alternative was chosen.

The alternative for this stack will be the the one presented in 5.20, which compensates the thermal and the initial stress disequilibrium at the same time. The advantage in this

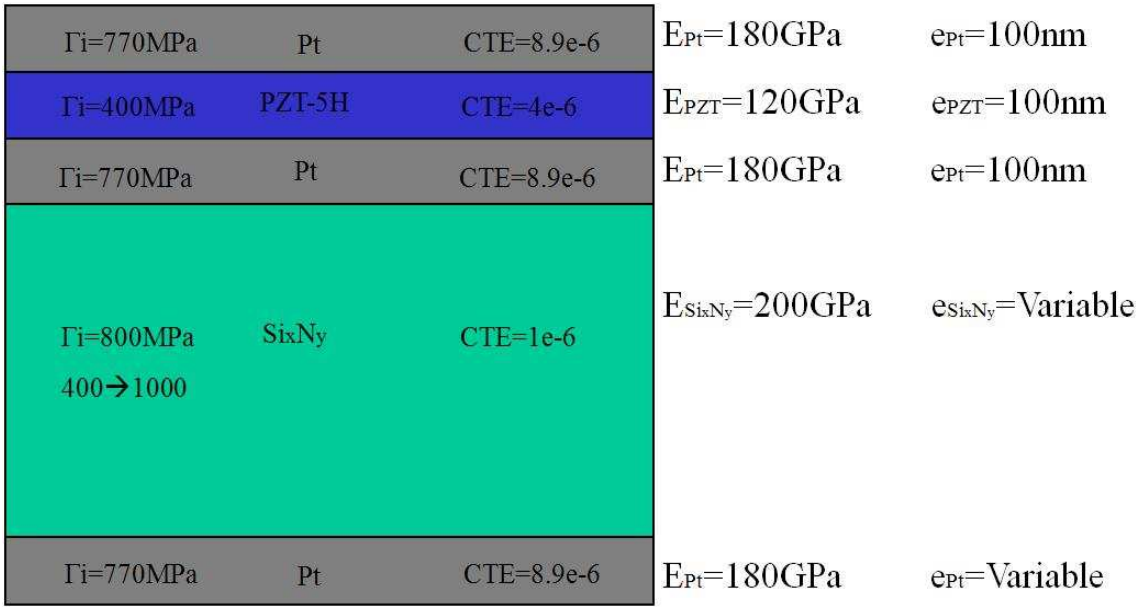

Figure 5.16.: Geometrical description of the stack with platinum as compensation layer.

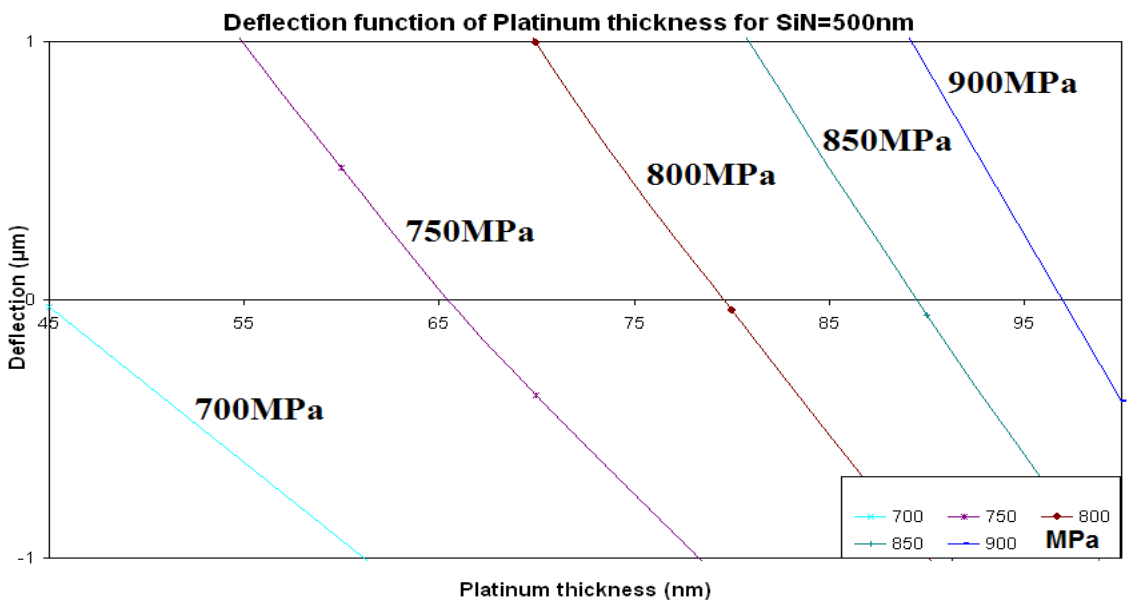

Figure 5.17.: Deflection of the stack described in 5.16 as a function of platinum thickness and the initial stress in SiN, for SiN thickness 500nm.

configuration, is that we can deposite two layers of SiN with two different and variable stress states. The initial stress in the top platinum layer is dependent on the annealing temperature and can vary from 500MPa to 1100MPa. Figure 5.21 shows that the deflec-

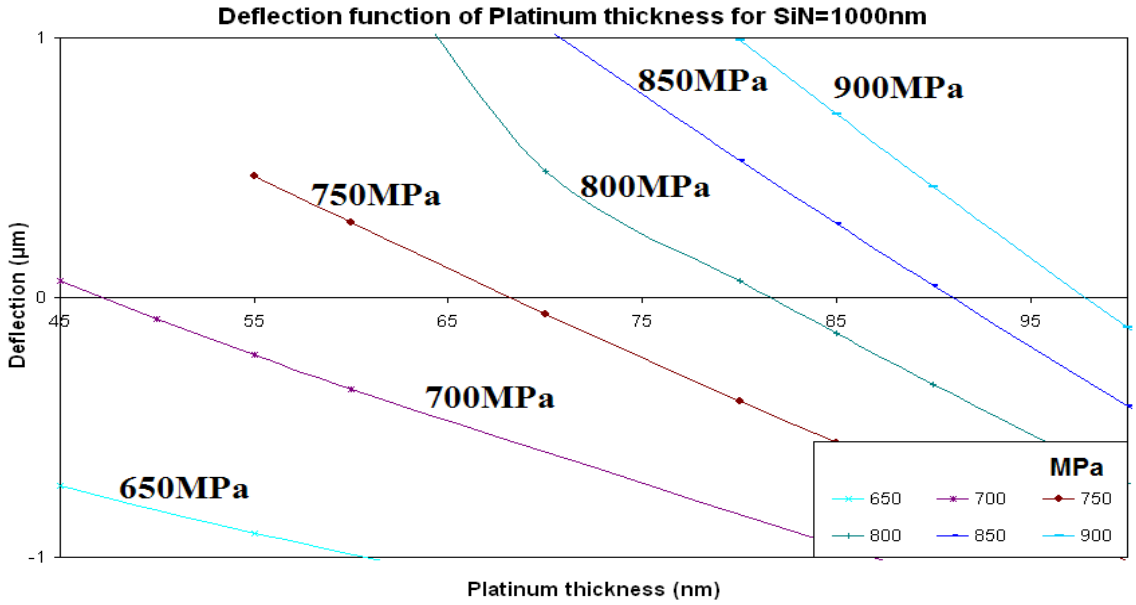

Figure 5.18.: Deflection of the stack described in 5.16 as a function of platinum thickness and the initial stress in SiN, for SiN thickness 1000nm.

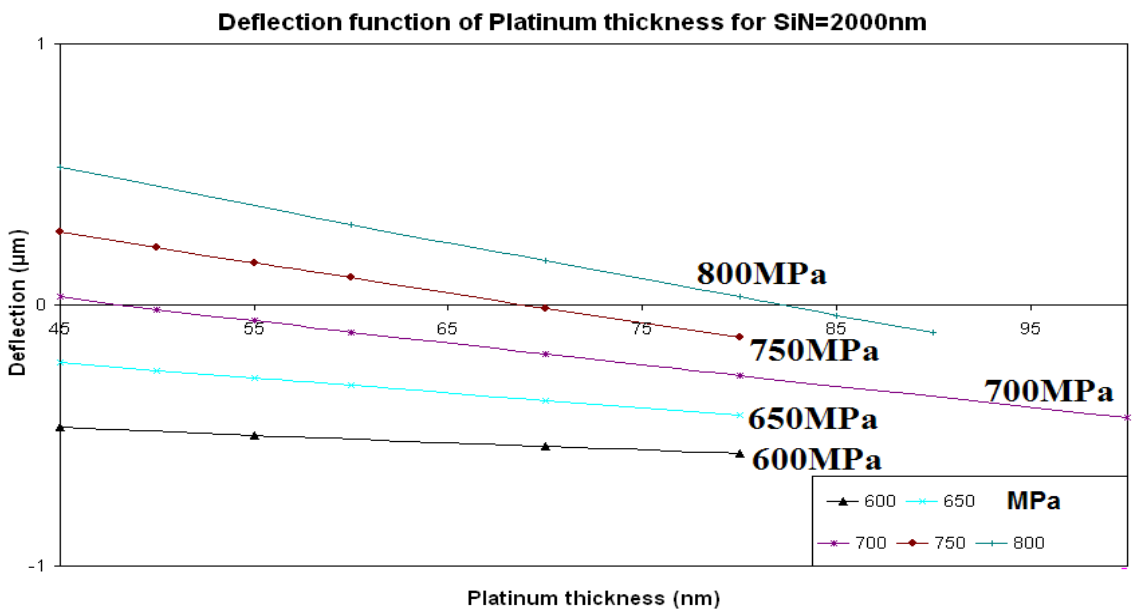

Figure 5.19.: Deflection of the stack described in 5.16 as a function of platinum thickness and the initial stress in SiN, for SiN thickness 2000nm.

tion changes from downward to upward when varying the Platinum initial stress from 500 to 1100MPa. This means we can control the initial deflection due to intial stress by controling the curing temperature in order to obtain a flat actuator.

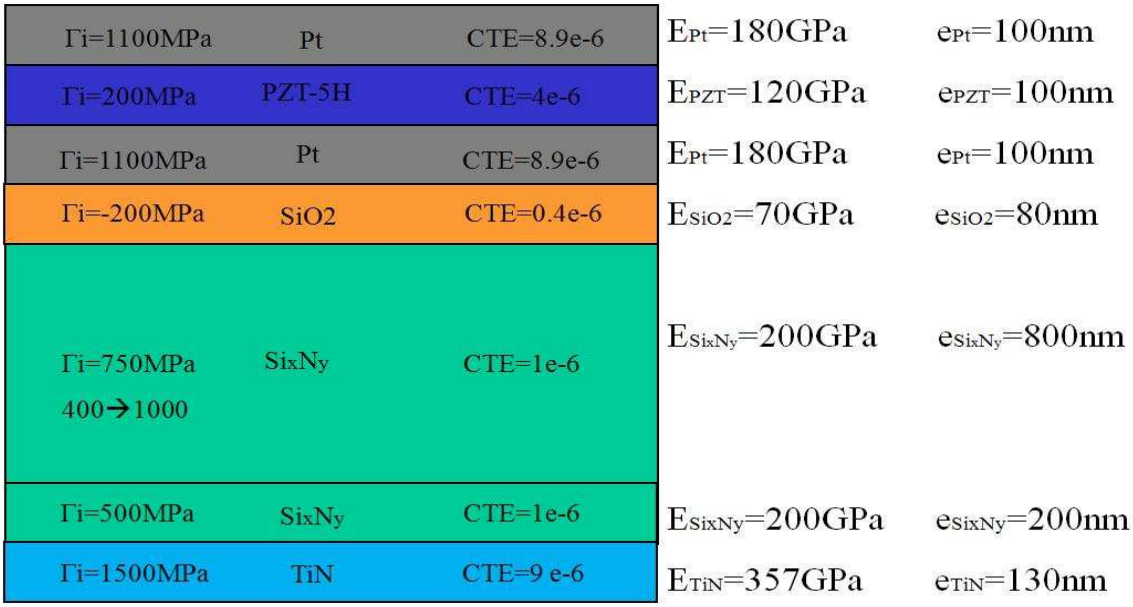

Figure 5.20.: Geometrical description of the stack for stress and thermal compensation.

5.3.2. Thermomechanical disequilibrium

The ISO for a certified RF switch to be marketed is to pass the reliability test and to function in a range of temperature between -40°C and +85°C. Simulations done on the stack of figure 5.1 showed deflections 3 times higher than the gap as figure 5.22 shows. The reference temperature taken 20°C, the increase in temperature till 85°C leads to a deflection of 9.2μm downwards and the decrease to -40°C leads to 8.5μm deflection upwards.

Using the alternative stack presented in figure 5.20, the structure will be compensated thermally. Figure 5.23 illustrates the deflection, after thermal compensation, of the beam under the temperature variation from -40°C to 85°C with a reference temperature of 20°C. The total deflection for the temperature variation moves from -550nm to +600nm which is acceptable.

The measurments of the deflection of the test cantilever tip as a function of the annealing temperature is shown in figure 5.24. We can see that the deflection goes from negative values to positive values as a function of the annealing temperature, that is we can find a value of annealing temperature giving a Pt stress value convenient to compensate the initial stress disequilibrium.

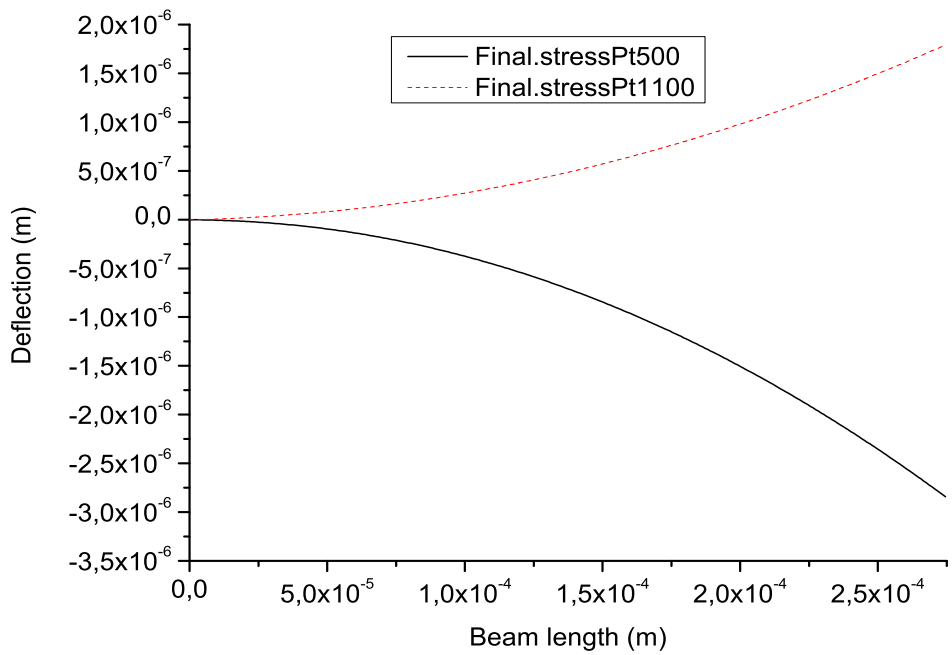

Figure 5.21.: Deflection of the actuator for Pt initial stress of 500 and 1100MPa.

5.4. Membrane flatness problem

The rotation of the actuator tip is transmitted to the membrane inducing an air gap between the membrane and the electrode. Figures 5.25, 5.26 and 5.27 shows the deflection distribution on the membrane of models II, III and IV respectively. This air gap causes an important loss in the capacitance value which in its turn affects the switching quality.

To study the flatness of these membranes, it is necessary to model their contact with the top electrode in order to verify if the actuation energy is enough to flatten the membrane on the electrode. Contact simulation was run for models II and IV using ANSYS. The contact zone is the membrane and the electrode seperated by 3μm gap. The simulations showed that the actuation energy is sufficient to obtain a good flatness. The flatness is obtained after a voltage equivalent to a deflection of 20μm of the switches. As displayed in figures 5.28 and 5.28, the cut view after contact of the membranes shows a complete flatness face to the electrode at 3μm from the initial position. The friction coefficient between the two surfaces was varied from 0 to 0.5 to check their effect on the flatness, and no effect was observed.

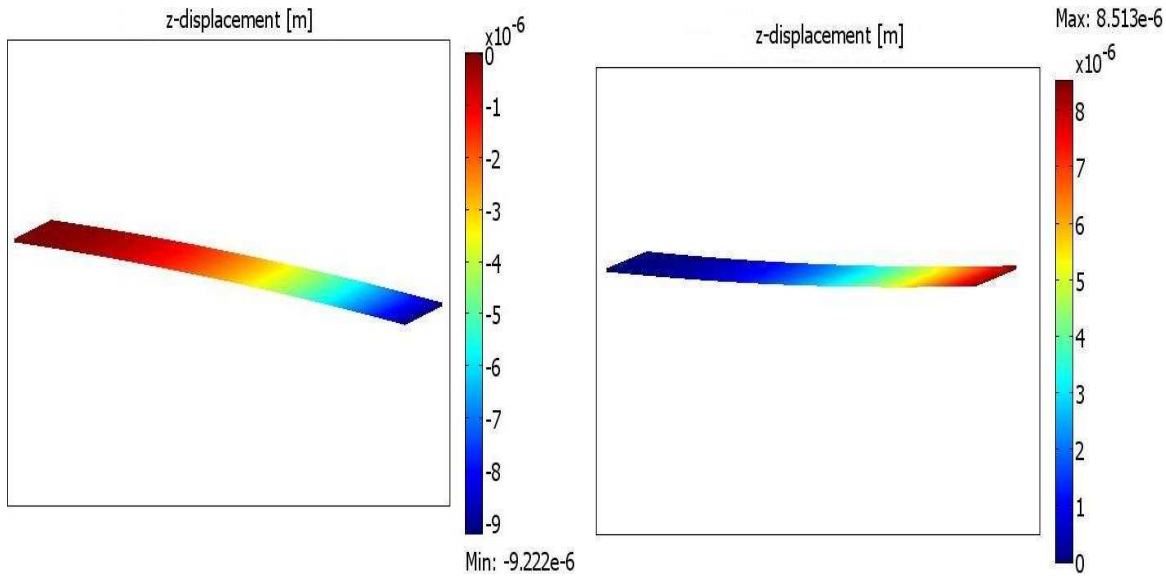

(a) The initial deflection due to an increase in temperature to 85°C with respect to 20°C.

(b) The initial deflection due to a decrease in temperature to -40°C with respect to 20°C.

Figure 5.22.: The actuator initial deflection due to thermal mismatch.

5.5. Conclusion

Piezoelectric actuation was under investigation in order to study if it can replace the electrostatic actuation and get rid of its drawbacks. Different models were simulated in static, transient (time dependent) and Eigen frequency analysis in order to have a table of criteria for our choice.

Model I showed the highest deflection among all the models but it had a very low stiffness. All other models consisting of a membrane connected to the actuator, showed a lower deflection but it was enough to fill the gap and cause the flatness of the membrane.

The high initial deflection problem due to stress and thermal disequilibrium was treated in two ways. The first solutions, where Platinum layer was added under the elastic, can compensate the stress in the stack but not the thermal mismatch. In addition to that the first solution, presented in figure 5.16, needs a high thickness of the elastic layer which reduces also the deflection due of the actuation. For that reason a second solution was considered consisting of adding Titanium layer with SiO_2 as presented in figure 5.20. The second solution is more interested since it compensates the thermal mismatch and the initial stress, though it is more complicated in terms of fabrication.

The contact simulation, of designs model II and model IV with the final compensated stack, of the contact between the membrane and the electrode demonstrate a flat mem-

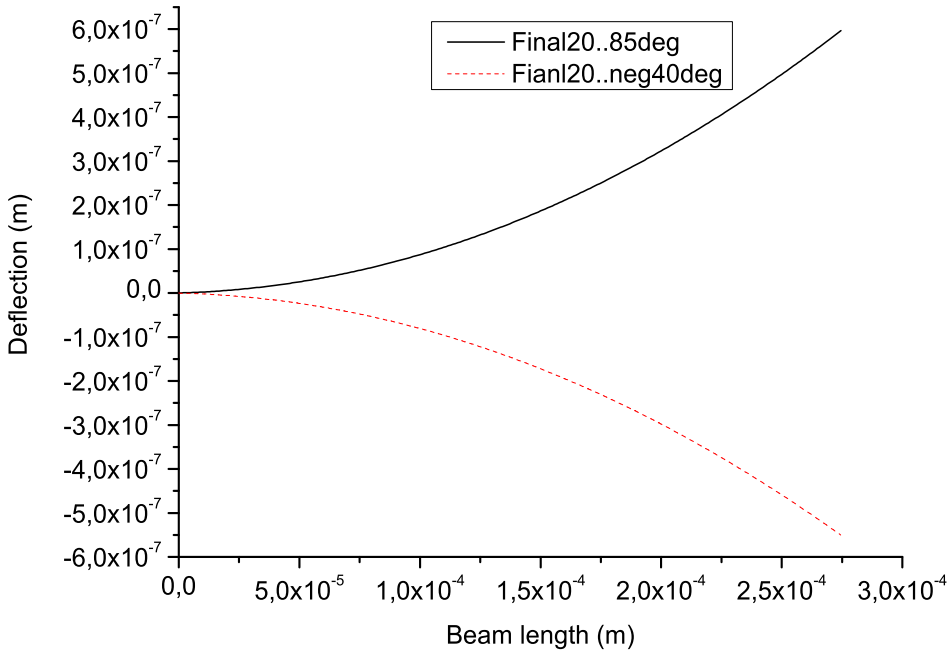

Figure 5.23.: Deflection of the actuator for temperture variation from -40°C to 85°C with a reference temperature of 20°C.

brane. Even for high values of the coefficient of friction the flatness is not affected.

The present study showed that it is feasible to obtain a piezoelectric switch functioning with the defined specifications but it needs a complicated process. Searching for a simpler process will motivate us to go back to electrostatic switches and try solving the stiction problem.

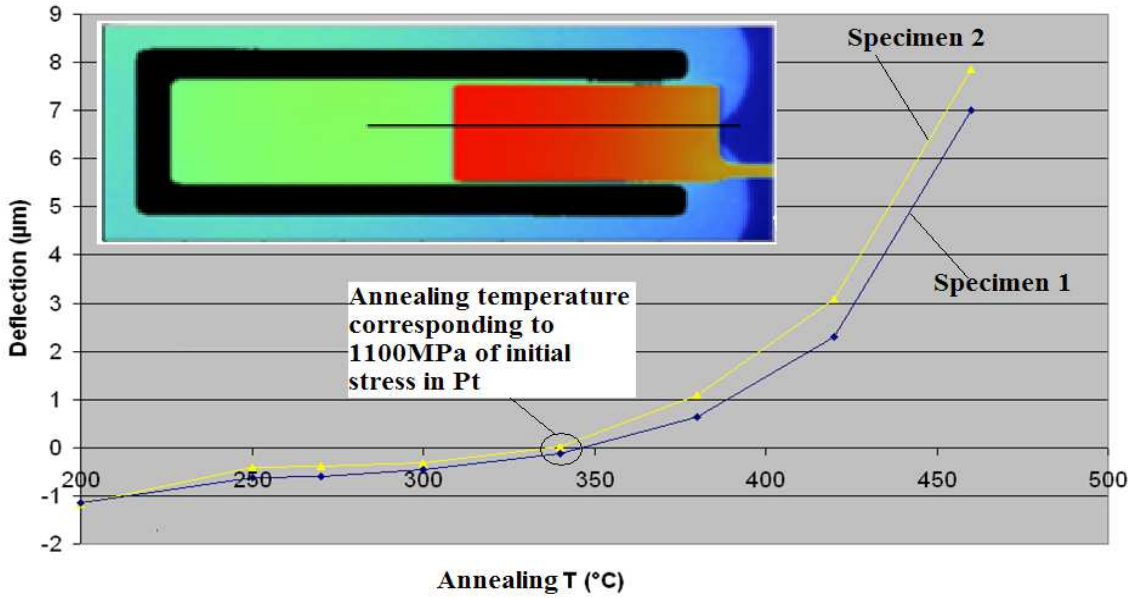

Figure 5.24.: Experimental measurments of the cantilever deflection with the stack of figure 5.20 as a function of the annealing temperature of Pt.

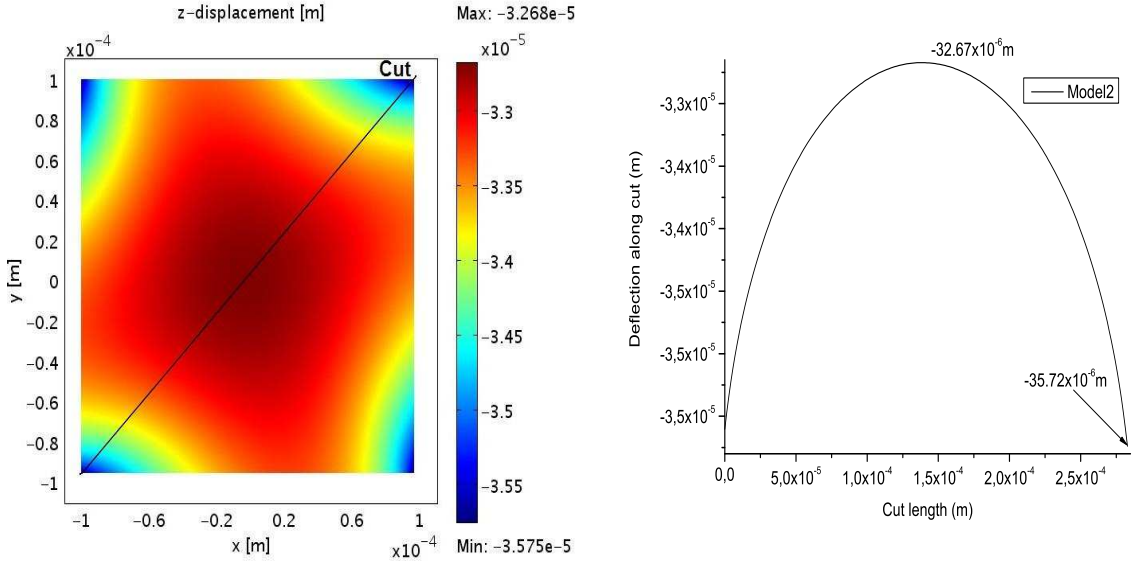

(a) The local flatness of model II.

(b) A cut of the local flatness of model II.

Figure 5.25.: The membrane flatness of model II.

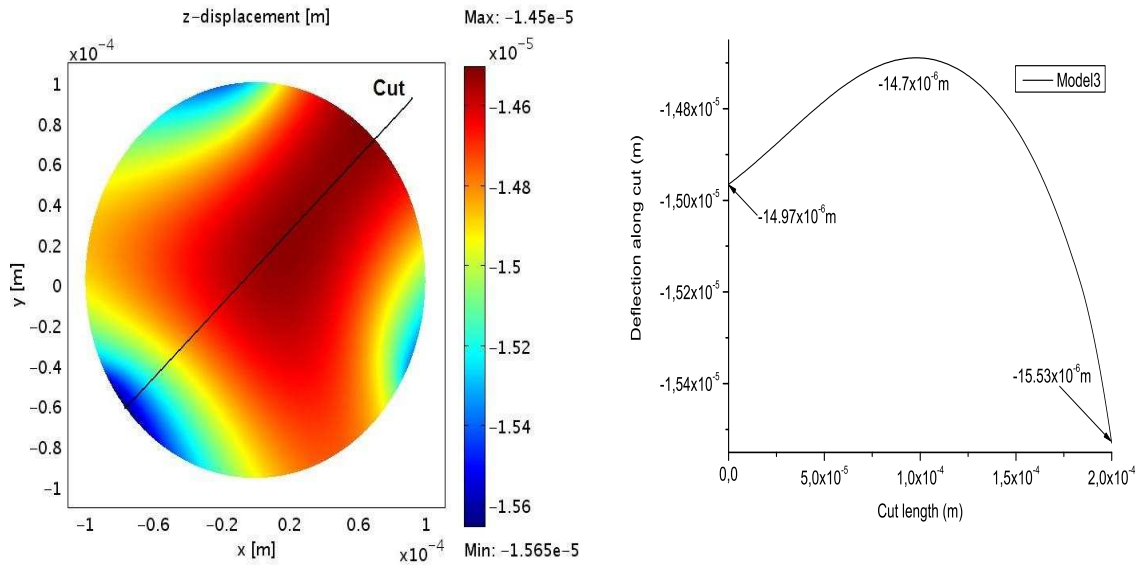

(a) The local flatness of model III. (b) A cut of the local flatness of model III.

Figure 5.26.: The membrane flatness of model III.

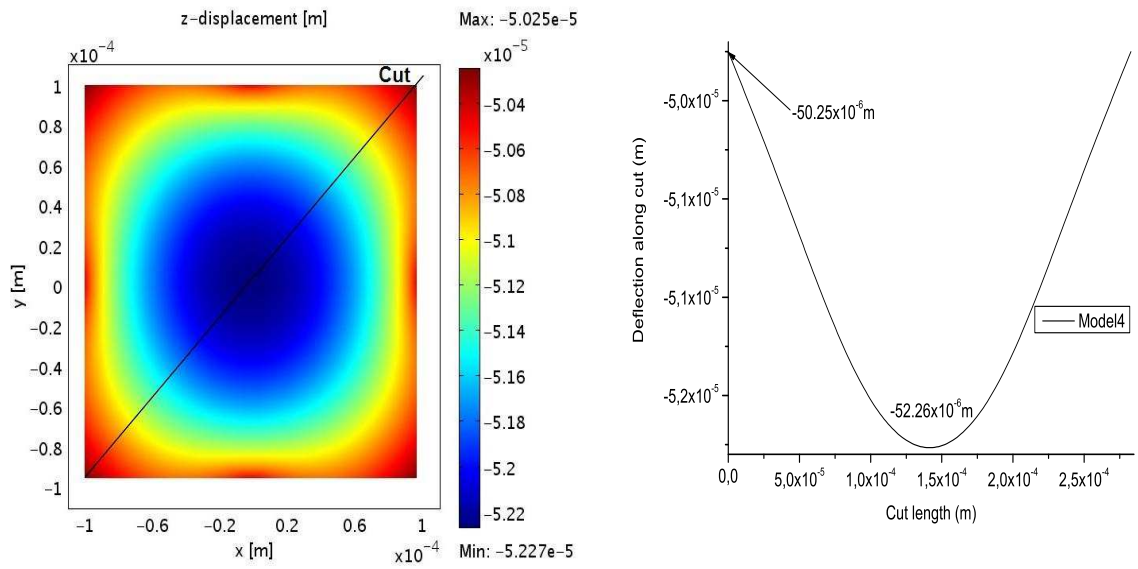

(a) The local flatness of model IV. (b) A cut of the local flatness of model IV.

Figure 5.27.: The membrane flatness of model IV.

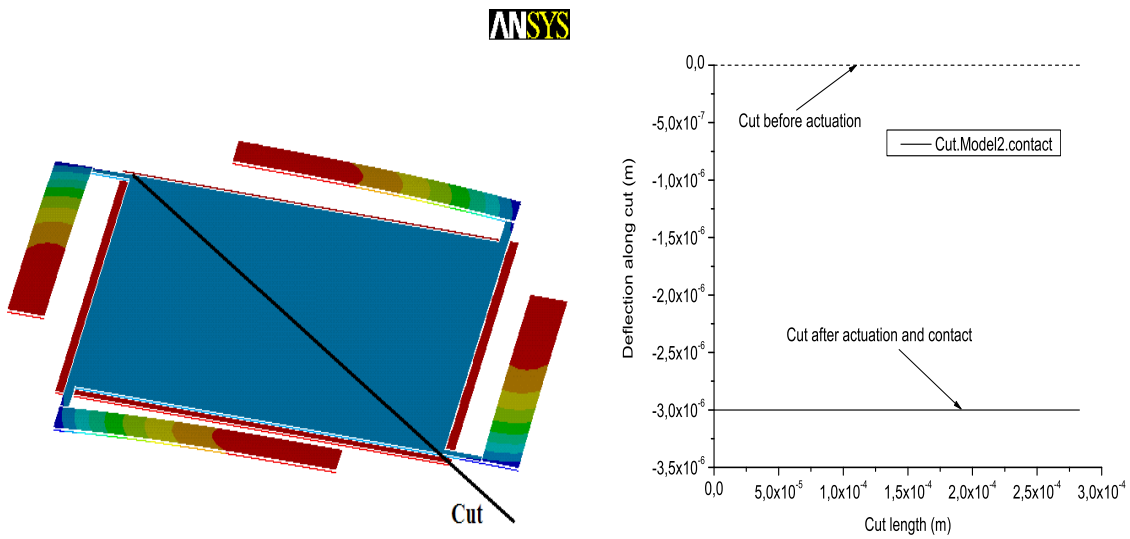

(a) The membrane flatness of model II after contact.

(b) The cut view of figure 5.28(a) after contact.

Figure 5.28.: The membrane flatness for model II after contact.

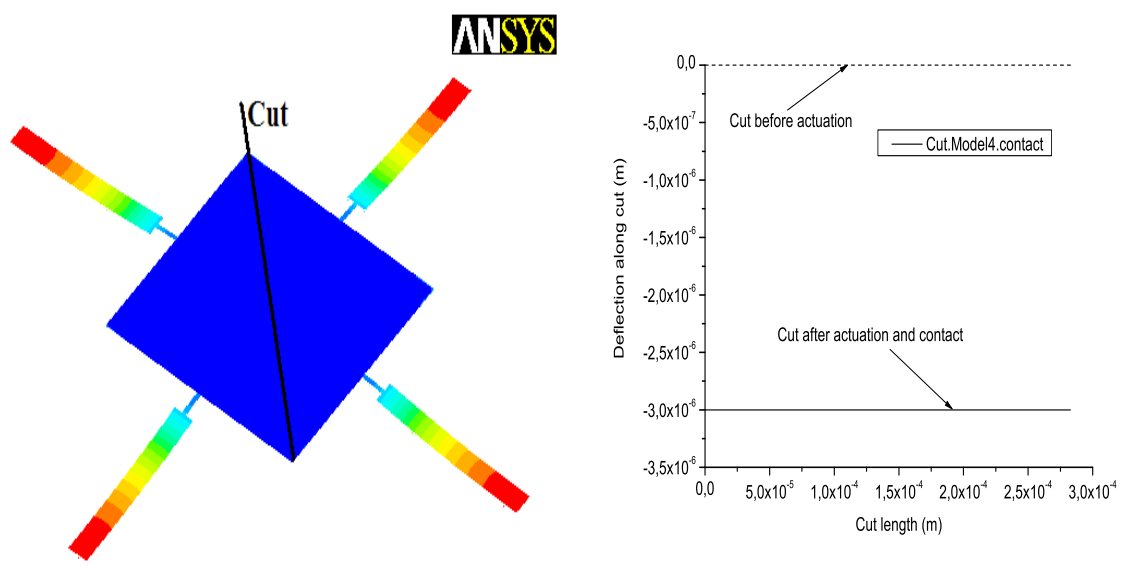

(a) The membrane flatness of model II after contact.

(b) The cut view of figure 5.29(a) after contact.

Figure 5.29.: The membrane flatness for model IV after contact.

Actionnement electrostatique

Le processus compliqué pour obtenir un commutateur piézoélectrique, ainsi que le processus relativement simple du commutateur électrostatique nous a poussés à étudier une solution pour le problème de stiction dans les commutateurs électrostatique.
Pour réduire la stiction, les chercheurs essaient de réduire le chargement du diélectrique utilisant des méthodes différentes énumérées ci dessous :

- Actionnement bipolaire.
- Actionnement sur les cotés pour séparer l'actionnement de la zone du contact.
- Commutateur sans diélectrique.

Toutes les solutions énumérées sont discutés dans chapitre 3 et ils présentent beaucoup d'inconvénients surtout sur le niveau de la qualité de capacitance dans l'état actionné. Notre solution s'agit donc d'augmenter la force de rappel.

Une grande raideur implique directement une grande tension d'actionnement pendant qu'une faible tension d'actionnement implique une faible raideur équivalente à dire une faible force de rappel. La faible raideur est traduite par une faible tension de relâchement qui est la tension minimal pour maintenir le commutateur à l'état actionné. Si nous vérifions le mécanisme d'échec d'un commutateur à actionnement électrostatique sous cyclage, nous voyons un décalage de la tension de relâchement vers zéro en raison de chargement. L'échec du commutateur est quand la tension de relâchement atteint zéro, cela signifie que le commutateur est plaqué d'une façon permanente en bas dû à la force électrostatique produite par les charges prises au piège dans le diélectrique.

Un exemple du décalage de la tension de relâchement en fonction du cyclage est trouvé dans figure 6.1. Il montre la courbe d'hystérises C-V d'un commutateur testé montrant le glissement dans cette courbe vers l'axe Y. Ceci explique le besoin d'une haute tension de relâchement pour éloigner de zéro le point d'échec et par cela l'augmentation de la durée de vie.
Examiner l'expression de la tension d'actionnement (donné par équation (6.1)) et la tension de relâchement (donné par équation (6.2)) pour un pont simple (montré dans la figure 6.2). Nous nous rendons compte que quand nous diminuons l'écart initial, nous pouvons

augmenter la raideur tout en gardant la même valeur de la tension d'actionnement.

L'écart est réduit en fonction de la déflection du pont, nous avons trouvé que c'est intéressant si nous pouvons augmenter la raideur aussi en fonction de l'actionnement. Le défi est maintenant de trouver une structure ayant une raideur variable, augmentant en fonction de la déflection (en fonction du déplacement). Pour garder la même tension d'actionnement, la raideur doit respect la condition que la force de rappel soit toujours au dessous de la force électrostatique.

En traçant les forces qui s'applique au pont (la force et rappel et la force électrostatique) en fonction de la distance entre le pont et l'électrode, nous pouvons conclure la tension d'actionnement en trouvant la courbe de la force électrostatique tangent à la force de rappel selon la figure 6.3. Figure 6.4 montre la force de rappel qui s'applique au pont avec un comportement non linéaire où la raideur de structure change en fonction de l'actionnement.
Le comportement non linéaire d'une structure est obtenu par contacte ou flambement. Un papier publié déjà dans MEMS 2008 parle d'une processus de fabrication d'un commutateur a actionnement électrostatique avec un comportement non linéaire utilisant le flambement [55]. La fabrication est compliqué à établir puisque ils utilisent l'actionnement dans le plan et donc des électrodes verticales.

Une autre façon pour obtenir une raideur non linéaire est d'avoir le contact mécanique entre la structure qui se déforme et une partie fixe. Pour avoir un changement spécifique de la raideur, nous ajouterons deux plots que nous appellerons des bouchons pour permettre ce contact. Le concept est de permettre au pont un certain déplacement avant qu'il atteint un certain point où nous imposons un contact à une certaine hauteur pré calculé d'une façon à respecter la condition que la force de rappel reste plus petit que la force électrostatique.

Les paramètres à étudier pour ce concept sont la hauteur des bouchons et la distance entre eux qui définira le rapport entre les deux états de raideur. Le pont aura la forme comme montré sur la figure 6.5. Figure 6.5 montre le concept, avant le contact, qui est utilisé à obtenir les deux états de raideur. Figure 6.6 montre l'état du commutateur après le contact qui permet pour nous avoir une plus haute raideur quand le gap est réduit.

6. Electrostatic actuation

6.1. Introduction

The complicated process needed to obtain a piezoelectric switch, together with the relatively simple process of the electrostatic switch made us study a solution for the stiction problem in electrostatic switches.

To reduce the stiction people try to reduce the dielectric charging using different methods listed below:

- Bipolar actuation.
- Side electrodes to seperate the actuation from the contact zone.
- Dielectricless switches

All of the listed solutions are discused in chapter 3 and they present many drawbacks especially on the level of the capacitance quality in the actuated state. Our solution is to increase the restoring force.

A large stiffness implies directly a high actuation voltage while a low actuation voltage implies a low stiffness equivalent to a low restoring force. The low stiffness is translated by a low pull-out voltage which is the minimum voltage to maintain the switch in the down state. If we check the failure mechanisim of an electrostaticaly acutated switch under cycling, we see a shift in the pull-out voltage towards zero due to charging. The failure of the switch is when the pull-out voltage reaches zero, that means the switch is permanently stuck down due to the electrostatic force generated by the traped charges in the dielectric.

An example of the shift can be found in figure 6.1. It shows the C-V hysterises curve of a tested switch showing the shift in this curve towards the Y-axis. This explains the need of a high pull-out voltage in order to move away from zero the point of failure and so gain in terms of life time.

Examining the expression of pull-in (given by equation (6.1)) and pull-out (given by equation (6.2)) voltages given for a double clamped simple bridge (shown in figure 6.2), we realize that when we decrease the initial gap we can increase in the stiffness while

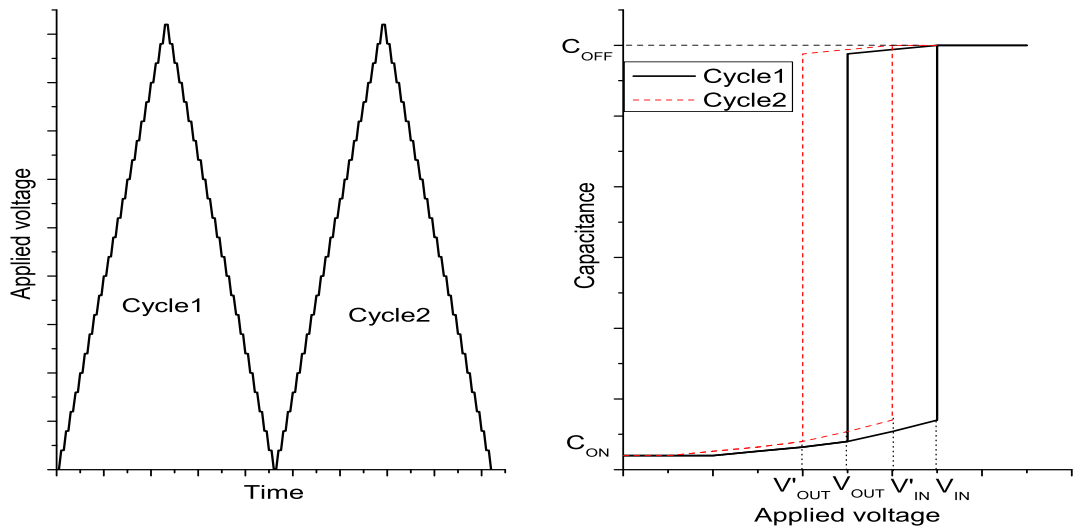

Figure 6.1.: The shift in the C-V curve of an electrostatic switch.

keeping the same value of the actuation voltage.

$$V_{in} = \sqrt{\frac{8K(g_0 + \frac{t_d}{\varepsilon_r})^3}{27\varepsilon_0 W_a W}} \tag{6.1}$$

$$V_{out} = \frac{t_d}{\varepsilon_r}\sqrt{\frac{2Kg_0}{\varepsilon_0 W_a W}} \tag{6.2}$$

where g_0 is the initial gap, K is the stiffness of the bridge. W, W_a and t_d are respectively the width of the bridge, the width of the actuation pad and the dielectric thickness. ε_0 and ε_r are the permitivity in vaccum and the relative permitivity of the dielectric respectively. With t the thickness of the bridge that affects the stiffness K.

The gap is reduced as a function of the actuation so we found it interesting if we can increase the stiffness also as a function of actuation. The challenge now is to find a structure having a variable stiffness increasing as a function of the actuation (as a function of the displacement). In order to keep the same actuation voltage, the stiffness have to respect the condition that the restoring force be always below the electrostatic force.

Plotting the forces acting on the beam (electrostatic force and restoring force) as a funtion of the distance between the bridge and the electrode, we can deduce the actuation voltage by finding the corresponding electrostatic force curve tangent to the restoring

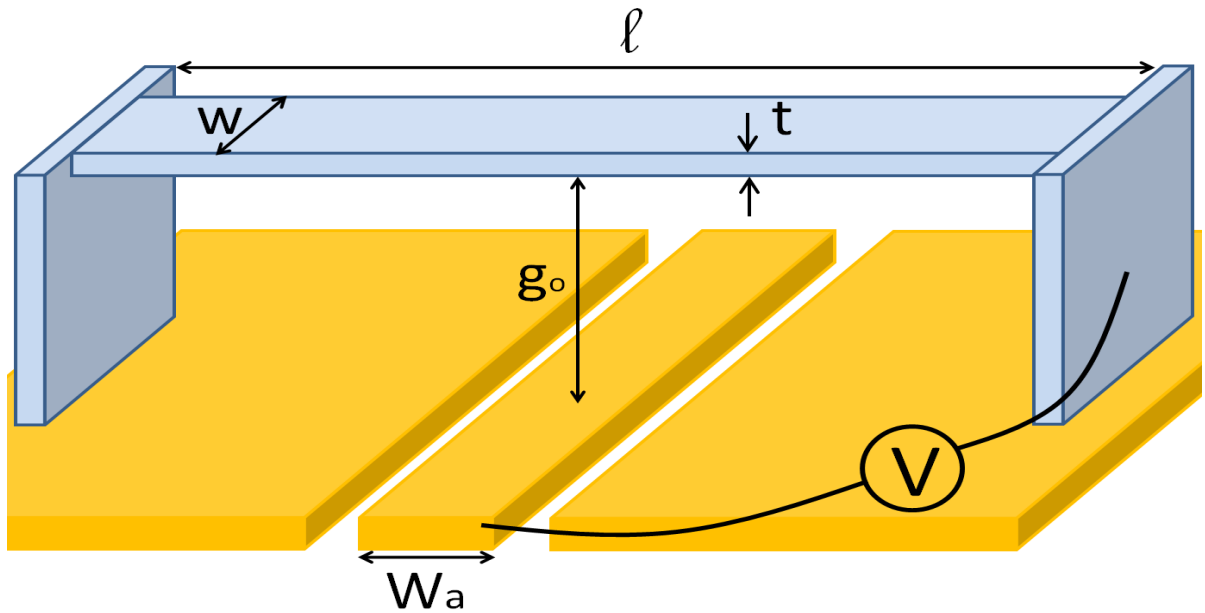

Figure 6.2.: The geometrical parameters of an electrostatic switch.

force as shown in figure 6.3. Figure 6.4 shows the restoring force of a beam with a nonlinear behaviour where the structure stiffness changes during the actuation.

The non linear behavior of a structure is obained by either contact or buckling. A paper already published in MEMS 2008 proceeding talks about fabricating an electrostaticaly actuated switch with a nonlinear behavior using buckling [55]. The process is complicated to establish since they use in plane actuation and so they use vertical electrodes.

Another way to obain a nonlinear stiffness is to have mechanical contact between the deforming structure and a fixed part. In order to have a specific stiffness change, we will add two pads that we will call stoppers in order to permit this contact. The concept is to permit for the bridge a certain displacement before reaching a certain point where we impose a contact at a certain height calculated in a way to respect the condition that the restoring force stays lower than the electrostatic force.

The parameters to be studied for this concept are the height of the stoppers and the distance between them which will define the ratio between the two states of stiffness. The bridge will have the form as shown in figure 6.5. Figure 6.5 shows the concept before contact used to obtain a two states of stiffness. Figure 6.6 shows the state of the switch after contact which permits for us to have a higher stiffness when the gap is reduced.

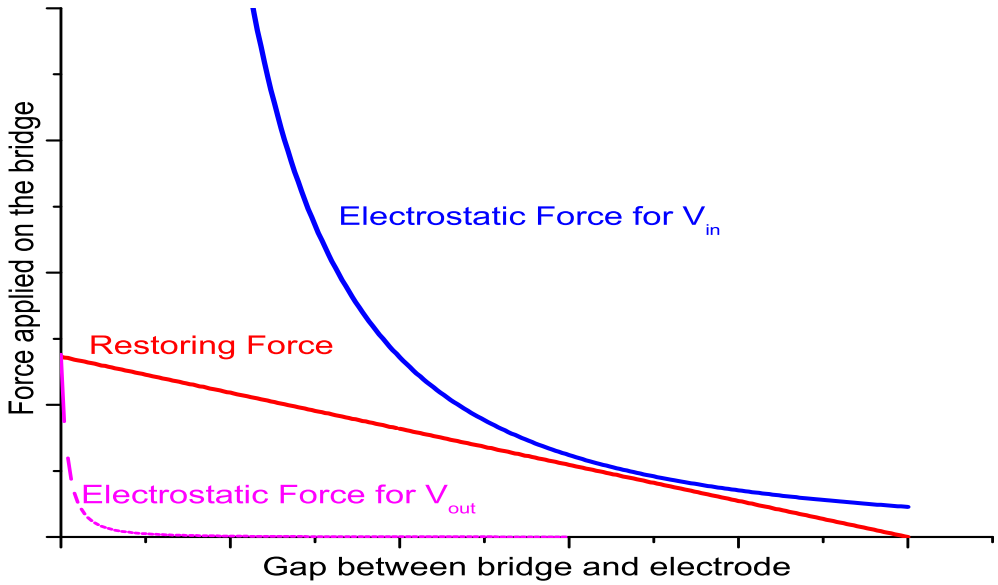

Figure 6.3.: Graph of the applied forces on the beam as a function of the distance between the bridge and the electrode.

6.2. Finite element modeling

6.2.1. Introduction

In the frame of studying the feasability of the stopper and its effect on the behavior of the switch, different mechanical simulations were run. In this paragraph, we verify some hypothesis taken in the analytical model, like the effect of the stopper on the initial stiffness. Then we present a study on the initial deflection due to initial stress and geometrical discontinuities.

The stopper is molded into a hole, etched into the photoresist so it will take the shape of this later. The photoresist will be annealed after development in order to relax the stresses and give it its final shape. The walls after relaxation will be inclined and the measurements showed that they will form an inclination of 12° with the horizontal as shown in figure 6.7.

The nonuniformity must be added to the studied geometry, with different stopper width. We fixed the stoppers interdistance l_s to 500μm and studied three different width possibilities 5, 10 and 20μm and their impact on the initial stiffness. The goal is to see if the stopper size has any influence on the stiffness before touching the ground plane.

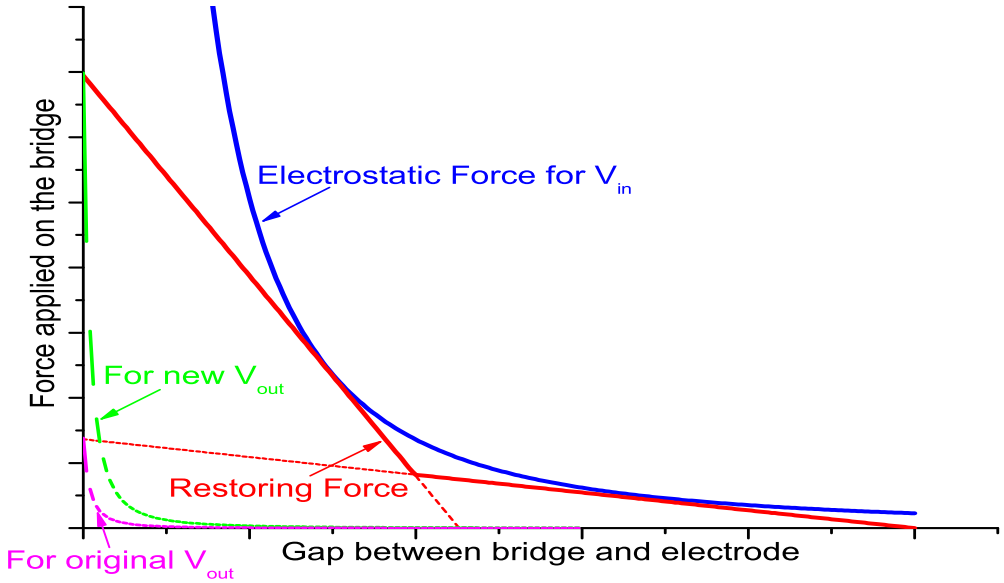

Figure 6.4.: Graph of the applied forces on the beam showing a nonlinear stiffness.

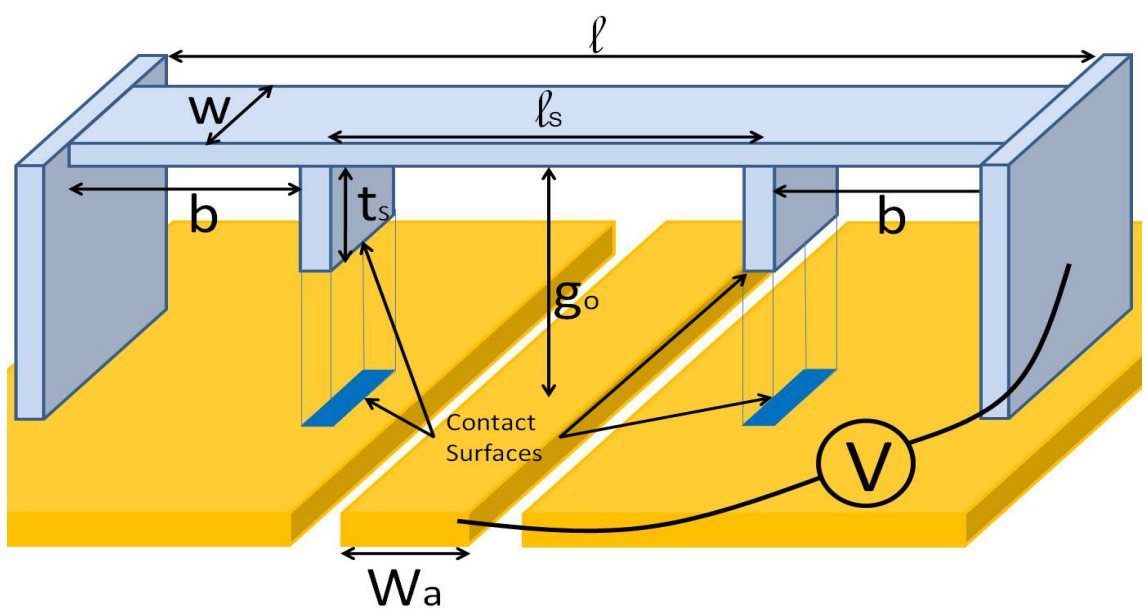

Figure 6.5.: Representaion of the concept to have non linear stiffness.

What we need for our application is a sharp stopper just to make the contact possible and increase the stiffness after contact. The values of the stopper width comes from

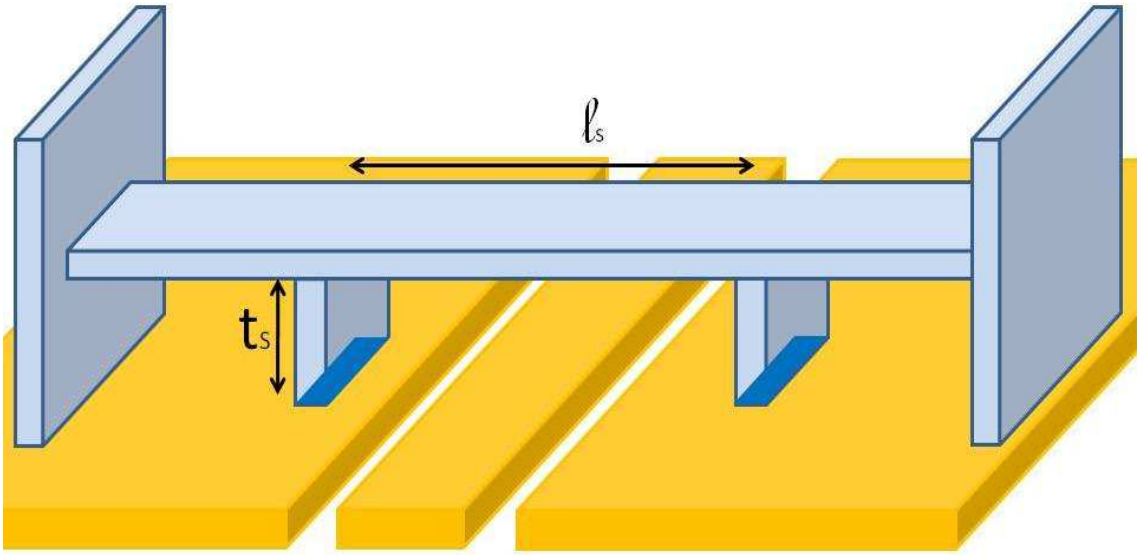

Figure 6.6.: Representaion of the concept after contact.

technological constraints since we can't go below 5μm and we would like to verify if its feasible with 20μm. The geometries are drawn on AutoCad and then imported into COMSOL3.4.

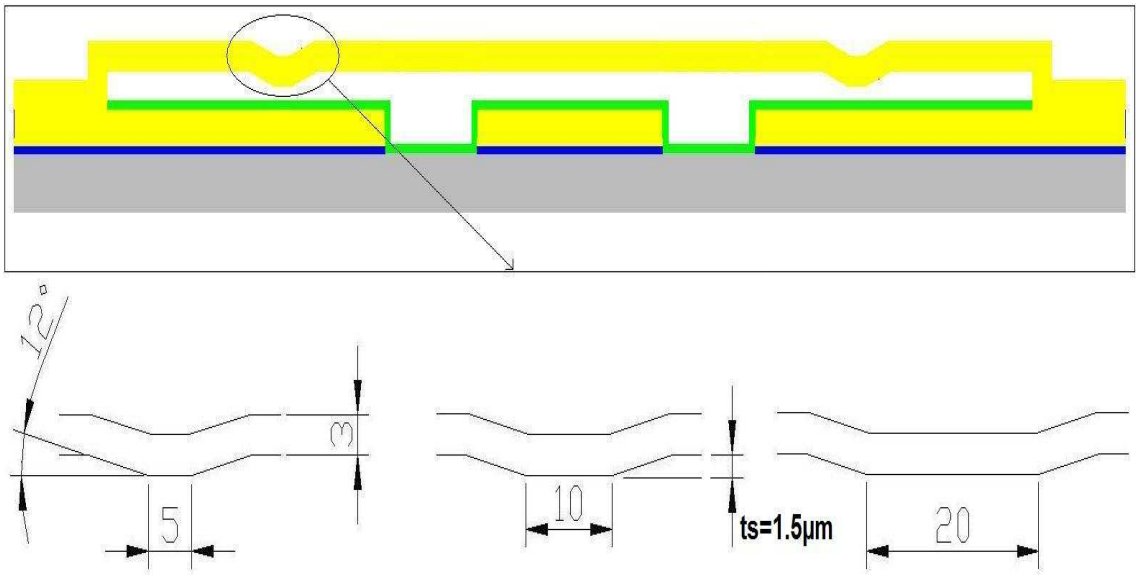

Figure 6.7.: The geometry of the stopper and different dimensions.

6.2.2. Tuning the mesh size

Before starting simulations, a sensitivity study of the effect of the element size on the results is necessary. COMSOL3.4 is the software used for the finite element analysis. Since the length of the beam is much greater than the width, a simplified 2D model is used using the hypothesis of plan stress. The model consists of a fixed-fixed straight beam loaded at its center along 100μm as in figure 6.8. The load is uniformly distributed along the actuation distance in a way to be equivalent to the electrostatic force that is used in our application. The result of the simulation is presented in figure 6.9.

The deflection of different models with different element size is calculated and the results are shown in figure 6.10. On the right of the vertical reference line, the effect of the element size becomes important so we manage to mesh our models in a way to stay inferior to this value.

Parameter	Value	Description
l	1330μm	Beam length
W_a	100μm	Distance of actuation
W	80μm	Beam width
t	3μm	Beam thickness
E	70GPa	Young modulus
ν	0.23	Poisson's ratio
σ	no	Initial stress

Table 6.1.: Simulation parameters for mesh size tunning.

6.2.3. Real geometry simulations

During the fabrication phase, we did topography measurments after each step in order to control the structure growth. The reverse engineering method described in Part I. permitted us to regenerate the real topography obtained by measurments. This real geometry will help us understand the importance of the non-uniformities on the behavior of the switch. We used two geometries, the first without stoppers and the other with stoppers. The simulation parameters used are listed in table 6.2. The Regenerated geometries are shown in figures 6.11 and 6.12.

6.2.4. Effect of initial stress on initial deformation.

Initial deformation are induced from initial stress which impacts the functionning of the switch. This initial deformation may tend to either reduce the gap between the bridge and the electrode or increase it. In both cases there are inconvenients, if the gap is

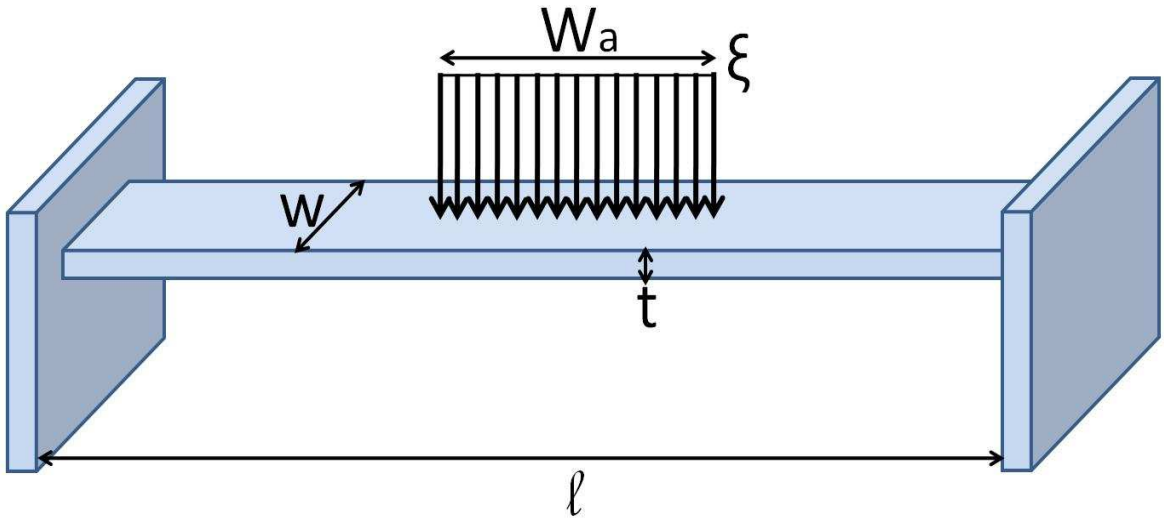

Figure 6.8.: Geometry of the model used for simulation.

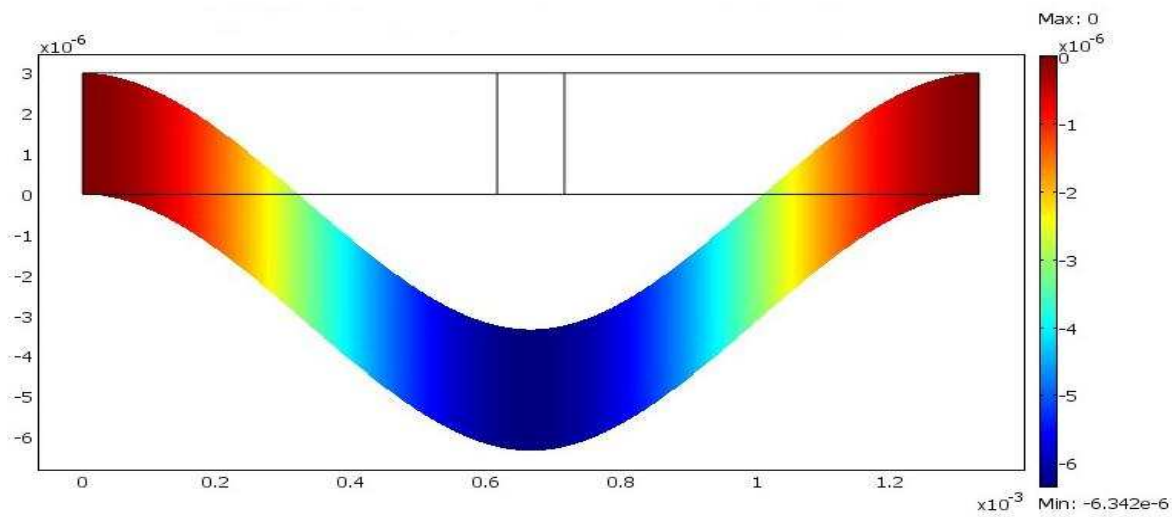

Figure 6.9.: Simulation of the straight fixed-fixed beam on COMSOL3.4.

reduced we will loose in terms of capacitance ratio while if the gap is increased the actuation voltage will increase.

The initial stress is a result of depositing different layers at different temperature and from the induction of dislocations. The value of this initial stress is linked to the process parameters and to the material used.

In this section we will deal with two main problems. The first is the effect of the

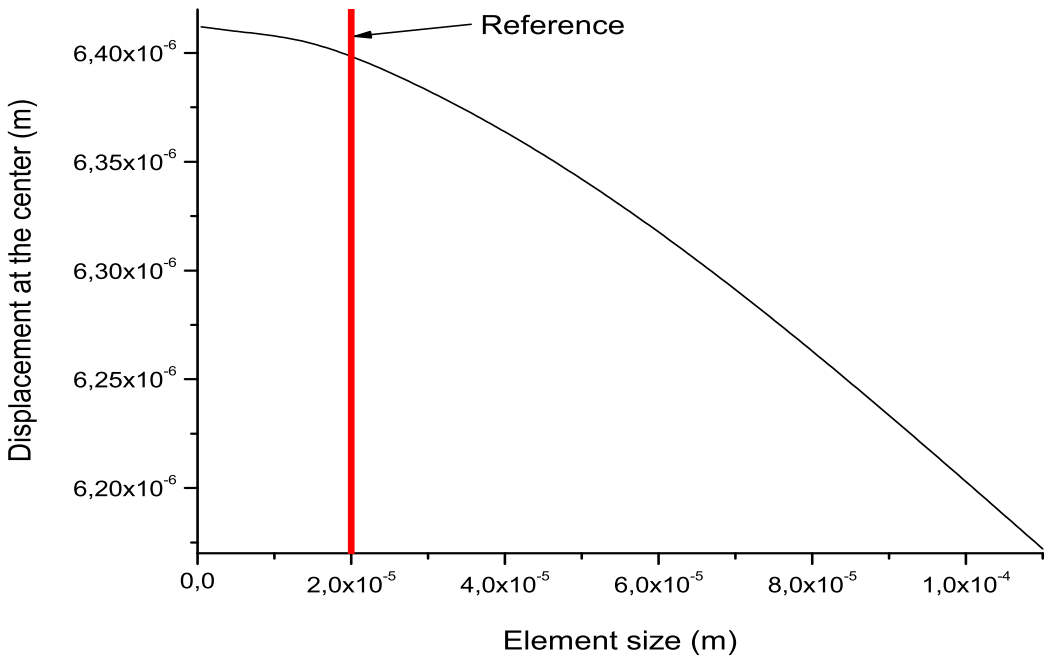

Figure 6.10.: Graph of the displacement at the center of the beam as a function of the element size.

Parameter	Value	Description
W_a	100μm	Distance of actuation
W	80μm	Beam width
E	70GPa	Young modulus
ν	0.23	Poisson's ratio

Table 6.2.: Simulation parameters for real geometry simulation.

direction of the initial stress in the non uniform geometry on the initial deformation. The second is the effect of the position and size of the non uniformity on the initial deformation. Most non uniformities are unvoluntary and they come as a result of the topology underneath the sacrificial layer while some are voluntary and are fabricated to do a certain function for example the stoppers. Usually the large deformation are due to stress gradient in the structures but in our case, since we are working on fixed-fixed cantilever and since we reduced a lot the gradient, we will be interested in the mean stress.

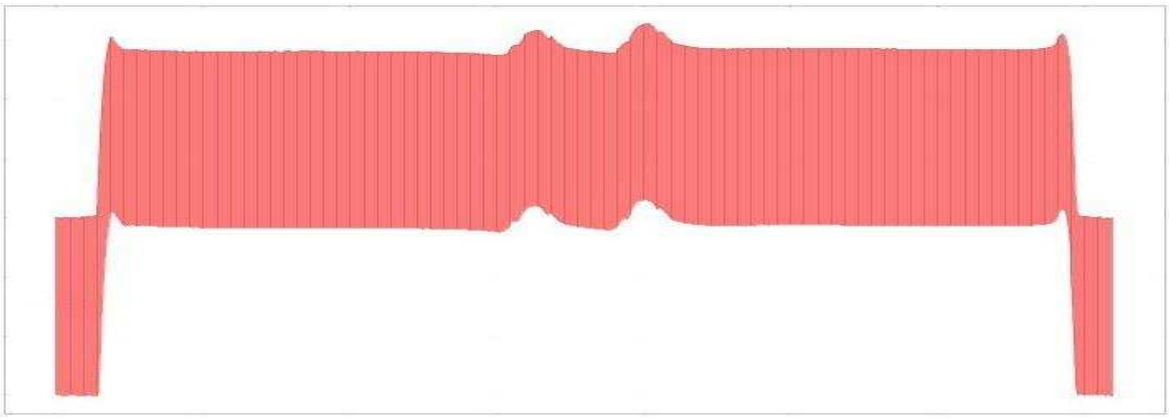

Figure 6.11.: The regenerated geometry for a switch without stoppers.

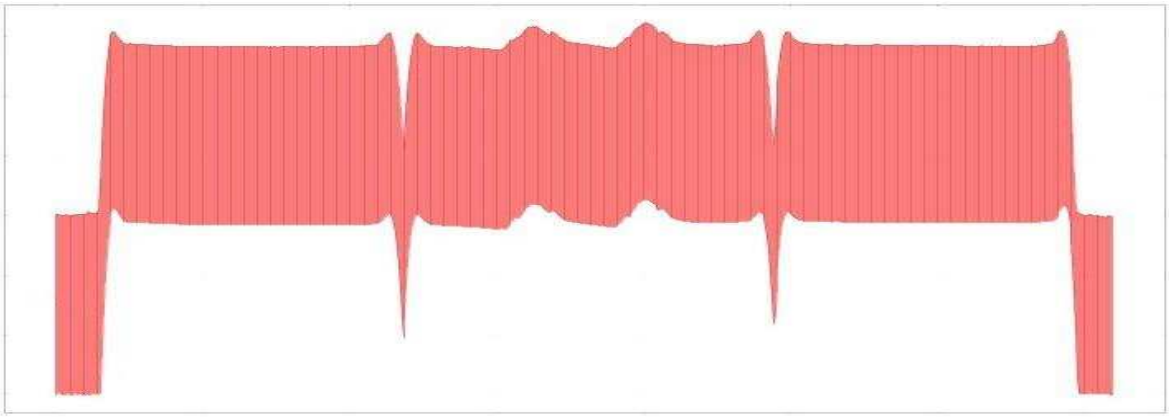

Figure 6.12.: The regenerated geometry for a switch with stoppers.

Creat a local coordinate system for initial stress inplantation

All the finite element analysis softwares, specially those dedicated to solve mechanical problems, can deal with the initial stress and include it in their simulation. This is good when we have a straight geometry with no non-uniformities and no curvature because the initial stress is applied in the global coordinate system (as in figure 6.13(a)). In reallity, the initial stress direction follows the topology of the structure so we have to change the coordinate system as a function of the topology (as in figure 6.13(b)).

If the structure is simple, that is it is formed of only few subdomains, we can create coordinate systems manually and apply it to each case. This is not the case for us, since the structure that we want to simulate has a random shape and with unpredictable curvatures. For this reason, we need a universal and automatic method to creat the corresponding coordinate system coherent with any structure at each point of it. To solve this problem, we use COMSOL3.4 with the multiphysics option and adding a problem of

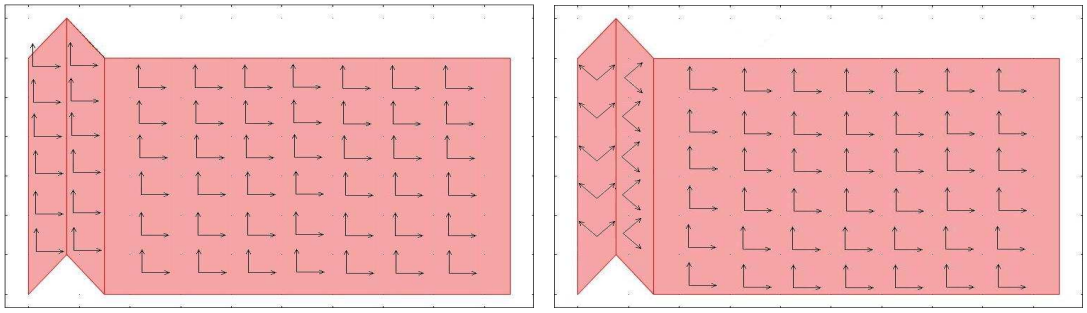

(a) A non uniform geometry with the global axis representation

(b) A non uniform geometry with the global axis representation

Figure 6.13.: Photos showing the direction of the stress direction.

diffusion to the mechanical problem.

The diffusion problem added to our analysis is only used to obtain at each point a vector perpendicular to the surface. In figure 6.14(a) we show the boundary conditions for the diffusion problem. Since we insulate the sides of the geometry, we impose the diffusion to happen in one direction perpendicular to the surfaces. Applying a concentration of 1 mol/m^3 on the first face and 0 mol/m^3 on the opposite face, we will obtain the gradient of concentration between the two faces which will define the Y-axis direction. The components of the concentration gradient are used to define the X-axis and the Y-axis direction as displayed in figure 6.14(b).

We verified this method on the geometry of the beam with stoppers, and the X-axis direction obtained can be seen on figure 6.15. Now we can define a new local coordinate system in the mechanical design coupled to the diffusion simulation in order to define the appropriate coordinate system following the topology. The new X-axis will have as coordinates (cy,-cx) where cx and cy are the concentration gradient component along the x and y direction respectively in the global coordinate system. This will permit us now to define the initial stress in a non uniform geometry in a correct way following the topology of the surface.

With and without changing the coordinate system

In this paragraph, we will check if it is necessary to do the changement of the coordinate system. We took the model of the beam with a 5μm stopper and an inter-distance of 500μm. Figure 6.15 shows the X-axis direction in the stopper model as simulated using the method described to generate a local coordinate system. The simulation was run for 10 MPa initial stress and the results are shown in figures 6.16 and 6.17. In figure 6.17 we display the deflection of the beam as well as the lines showing the direction of the new coordinate system. The relative difference in the deflection between a simulation with

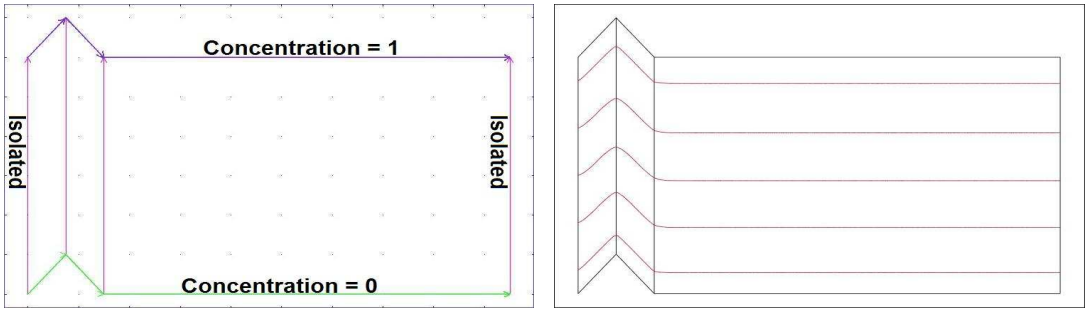

(a) Boundary conditions for the diffusion simulation

(b) the results of the simulation showing the direction of the X-axis as simulated

Figure 6.14.: Model simulated to find new coordinate systems following the topology.

initial stress in the global coordinate system and initial stress in local coordinate system is only 1%. The effect of changing the coordinate system is negligible but it will be tested later on the real geometry obtained from the measurments.

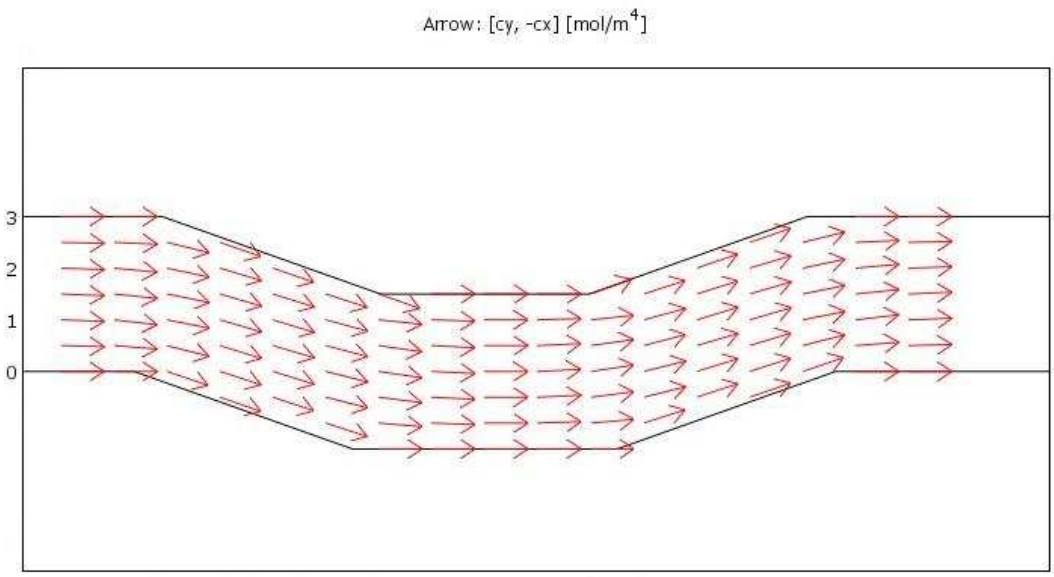

Figure 6.15.: the X-axis direction shown by arrows for the geometry with stoppers in order to validate the method.

Deflection of real geometry due to initial stress

The initial deformation is an important issue and impacts also the pull-in voltage since the deformation can increase or decrease the gap. Evaluating the initial deformation of the real geometry will help understand if it is mandatory to fabricate a flat beam, and

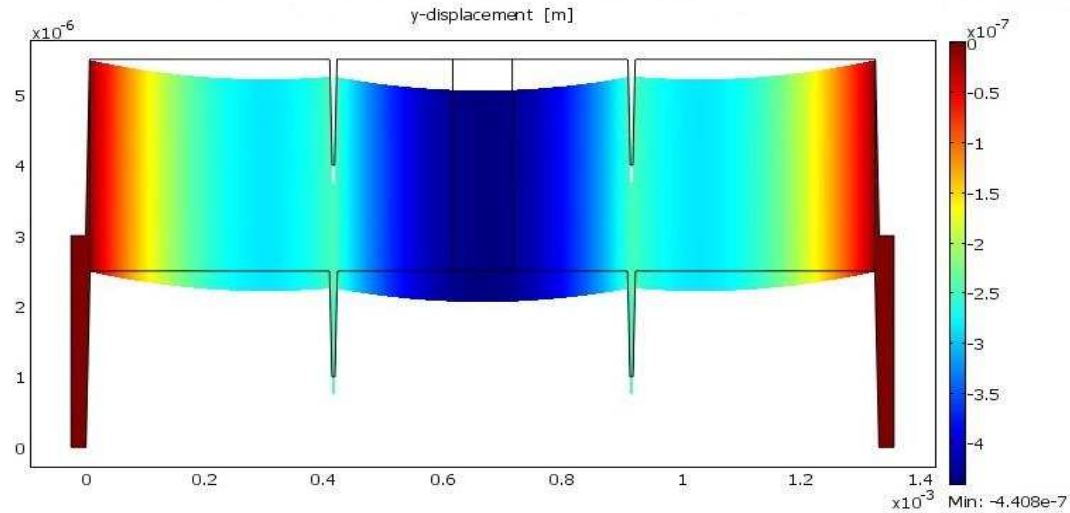

Figure 6.16.: The deflection of the beam due to 10MPa initial stress as simulated in the global coordinate system.

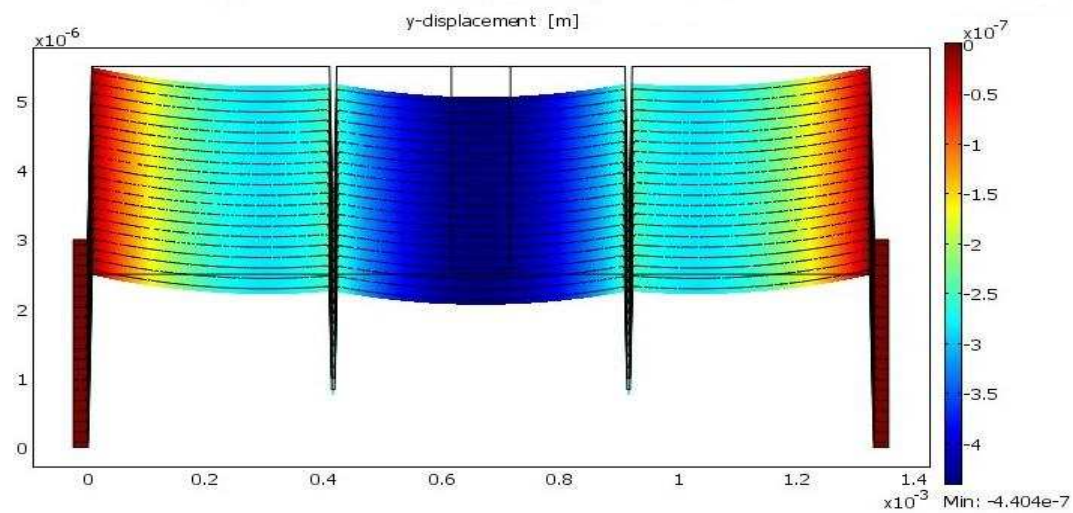

Figure 6.17.: The deflection of the beam due to 10MPa initial stress as simulated in the local coordinate system.

to understand if there are ameleorations that should be done to the process.

Figure 6.18 shows the simulated initial deflection of the beam without stoppers under an initial stress of 10MPa. The maximum deflection at the center is about 209nm for a 3μm thickness of gold beam and 195nm for a 3.4μm and a cut view comparing both cases is presented in figure 6.20.

The simulated deflection of the real geometry with stoppers is presented in Figure 6.19 showing a deflection of 261nm for a 3μm thickness of gold beam and 235nm for a 3.4μm. The cut view of the real geometry with stoppers for both thicknesses is presented in figure 6.21 with respect to the non deformed reference geometry. The real geometry with stoppers deformes more with respect to the one without stoppers which is expected.

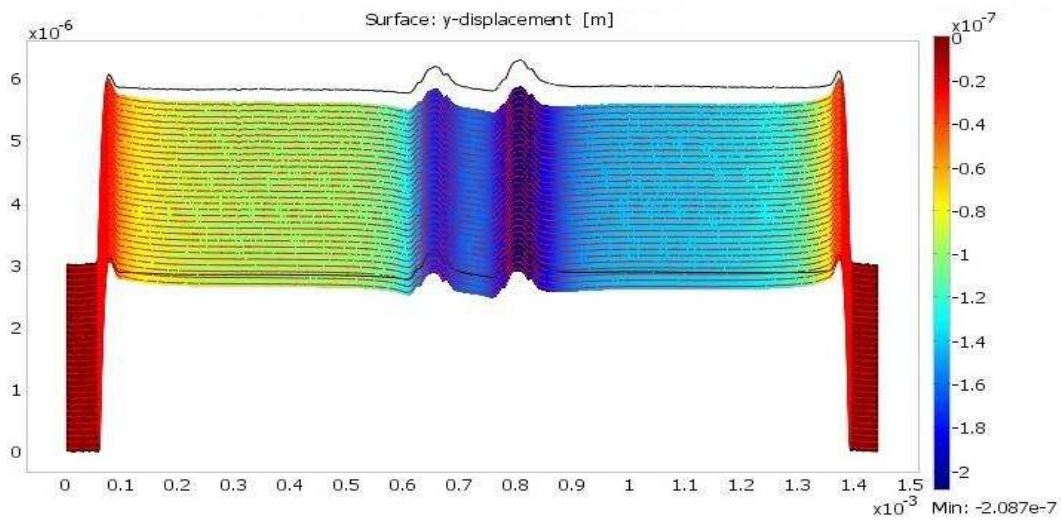

(a) The initial deflection for a 3μm gold beam without stoppers.

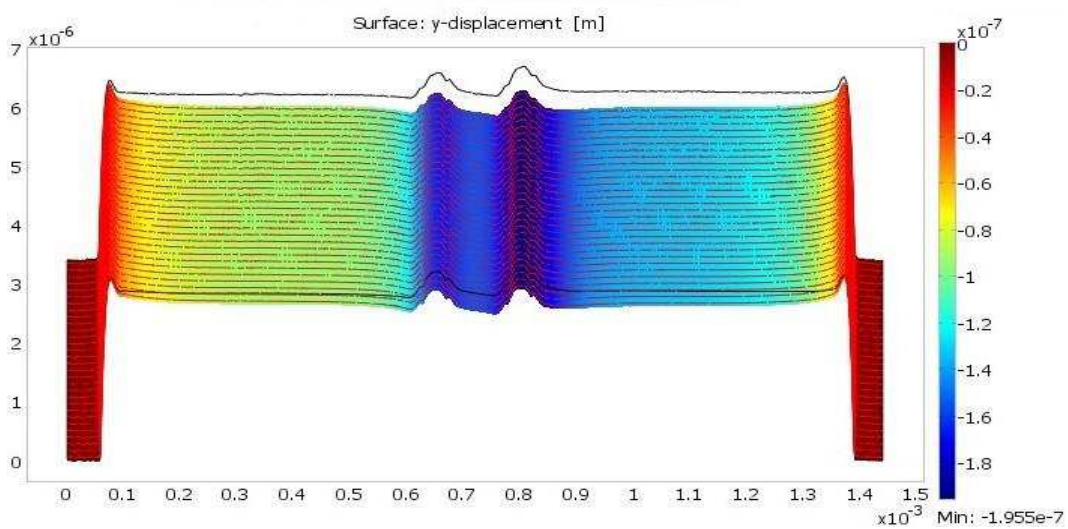

(b) The initial deflection for a 3.4μm gold beam without stoppers.

Figure 6.18.: The Deflection due to initial stress of the real geometry for a switch without stoppers.

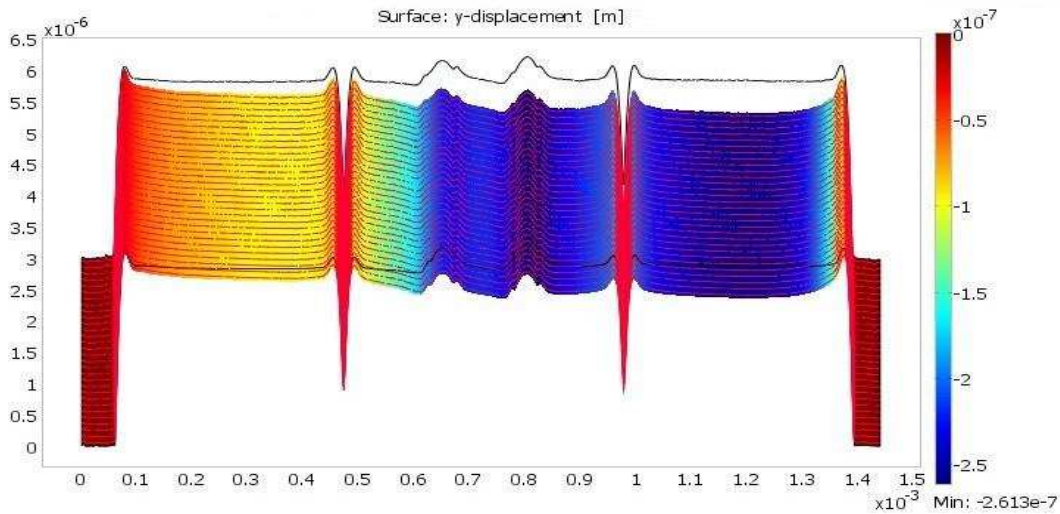

(a) The initial deflection for a 3μm gold beam with stoppers.

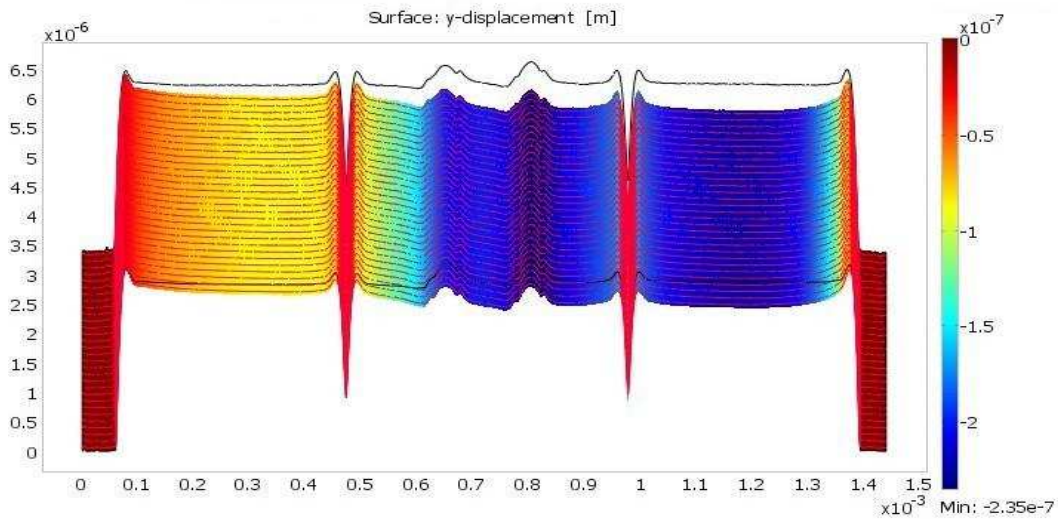

(b) The initial deflection for a 3.4μm gold beam with stoppers.

Figure 6.19.: The Deflection due to initial stress of the real geometry for a switch with stoppers.

Straight beam

For most of the people, a perfectly straight beam will stay straight even if there are initial stress. The reality is different, even if we succeed to obtain a straight beam, there will be the effect of the anchor which will exist always. Figure 6.22 shows the simulation of a perfectly straight beam with the effect of the anchor and for an initial stress of 10MPa. The deflection is 142nm downward which is 6% of the initial gap. The anchor can then be considered as a non uniformity in the upward direction.

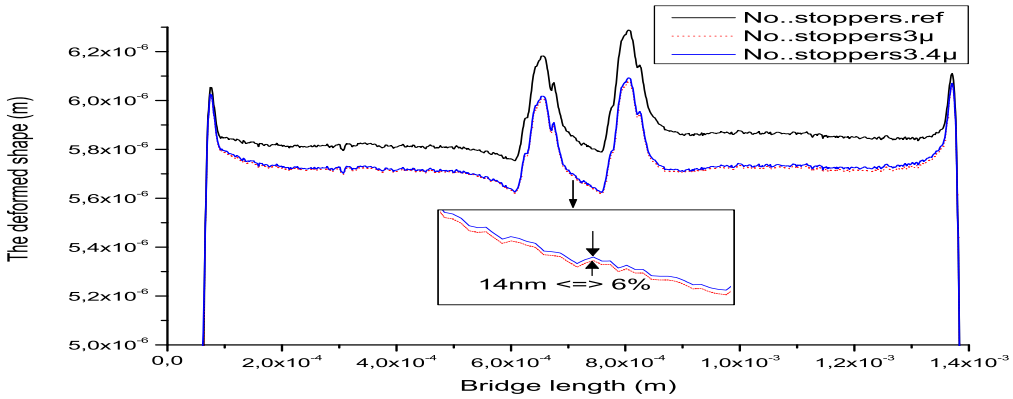

Figure 6.20.: The cut view of the deflection of the real geometry without stoppers due to initial stress.

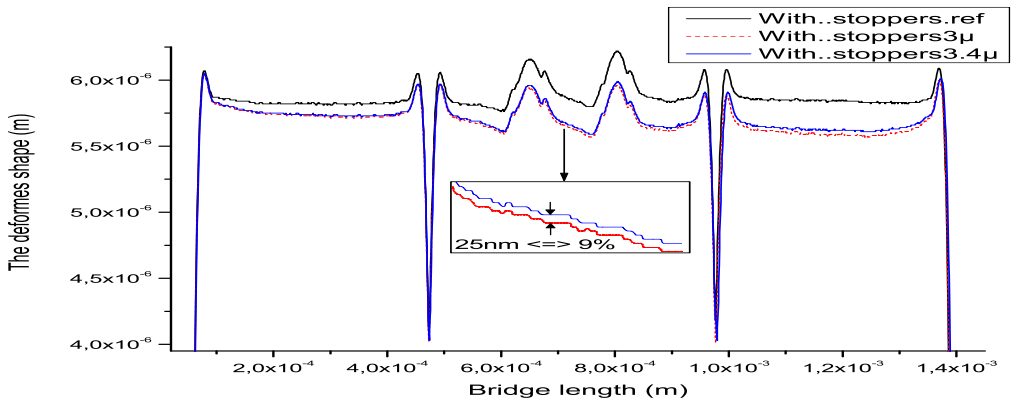

Figure 6.21.: The cut view of the deflection of the real geometry with stoppers due to initial stress.

The deflection is due to a bending moment generated from the tensile force. Figure 6.23(a) presents the anchor isolated with the forces applied on it due to the initial stress. The equivalence of this force is a bending moment dependent on the height of the anchor and causing its deflection as shown in figure 6.23(b). The stopper or any non uniformity induces in the structure a moment. Figure 6.23(c) is the isolated stopper (non uniformity) with the applied tensile force on both ends. The forces are at equilibrium but the moment at the tip of the stopper will not be zero, it will have a value dependent on the height of the non uniformity as shown in figure 6.23(d). The deformation due to the non uniformity must be local since the moment acts only in the non uniform zone and is zero in the rest

of the structure.

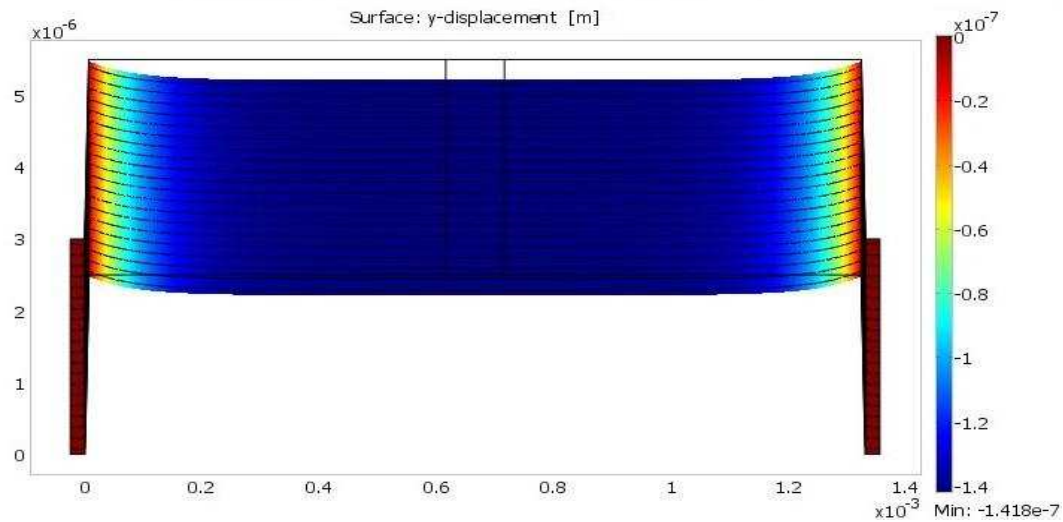

Figure 6.22.: The deflection of a straight beam under the action of 10MPa initial stress due to the anchor.

Effect of the stoppers size on the initial deformation

The non uniformity in the geometry due to the stopper fabrication, as any other non uniformity, amplifies the initial deflection caused by the initial stress. In this part we will study the effect of the stopper size on the initial deformation. The stoppers interdistance is fixed to 500μm and the subjected initial stress is 10 MPa. The width of these stoppers is the only parameter studied in this paragraph.

- Deflection for 5μm wide stopper In this paragraph we show the simulated deflection of a switch with 5μm wide stopper. We will give the results for a model with anchor and another without in order to validate the necessity of adding the anchor to models studying the initial stress effect. Figure 6.24(a) displays the simulated deflection obtained on COMSOL3.4 for the model without anchor while figure 6.24(b) shows a deflection of 134nm for the model with anchor. An important difference in the result can be seen, which means that the model cannot be simplified by neglecting the anchor effect.

- Deflection for 10μm wide stopper For the rest of this section, we will always add the anchor on the models used to study the initial deflection due to initial stress. The stoppers interdistance and the initial stress values being fixed, this simulation is for a stoppers width of 10μm. Figure 6.25 displays the deflection as well as the lines defining the direction of the initial stress for the beam. The deflection is found to be 129nm downward.

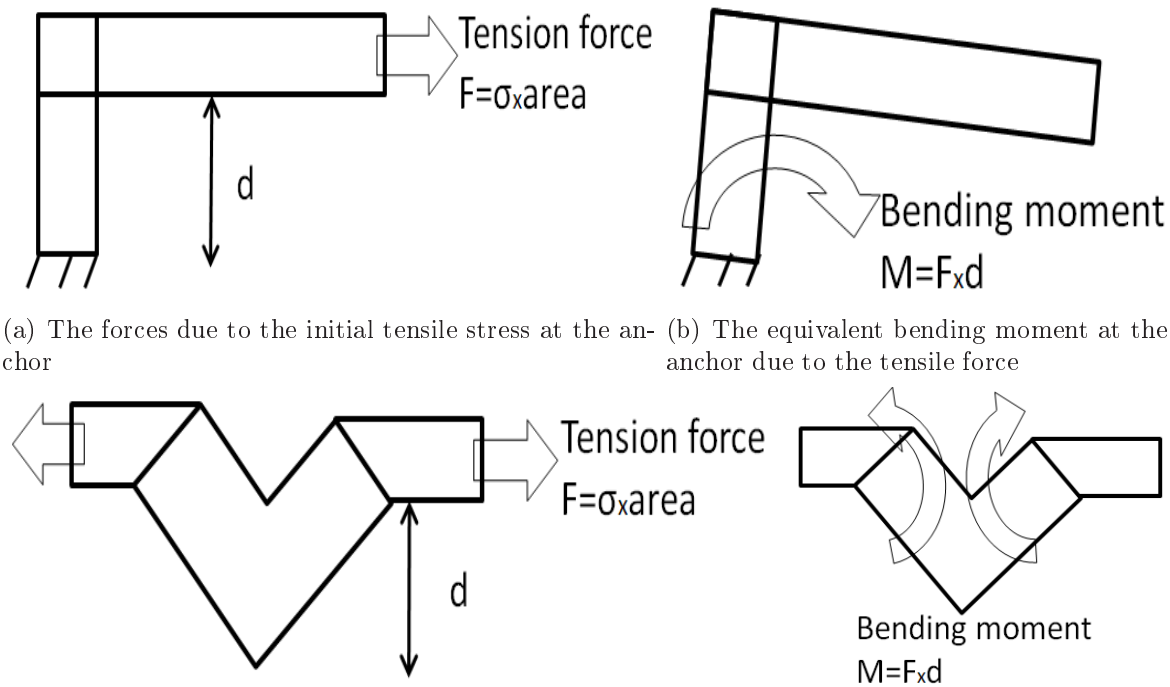

(a) The forces due to the initial tensile stress at the anchor

(b) The equivalent bending moment at the anchor due to the tensile force

(c) The forces due to the initial tensile stress at the stopper

(d) The equivalent bending moment at the bottom of the stopper due to the tensile force

Figure 6.23.: isolated parts of the structure with the forces acting on them.

- Deflection for 20μm wide stopper The simulation results of a 20μm wide stopper are presented here. The display of the deformation as well as the lines defining the direction of the initial stress are presented in figure 6.26. The deflection was found to be 120nm downward.

Effect of the stoppers position on the initial deformation

This part deals with the effect of the stoppers position on the initial deformation due to initial stress. The stoppers interdistance beacame now our variable, the width is fixed to 5μm and always subjected to an initial stress of 10 MPa.

- Deflection for stoppers with 800μm inter-distance This part presents the deflection of a switch with an inter-distance of 800μm. The display of the deformation as well as the lines defining the direction of the initial stress are presented in figure 6.27. The deflection is 142nm downward.

- Deflection for stoppers with 200μm inter-distance The inter-distance is now 200μm, the simulation results showed 134nm deflection downward as displayed in figure 6.28.

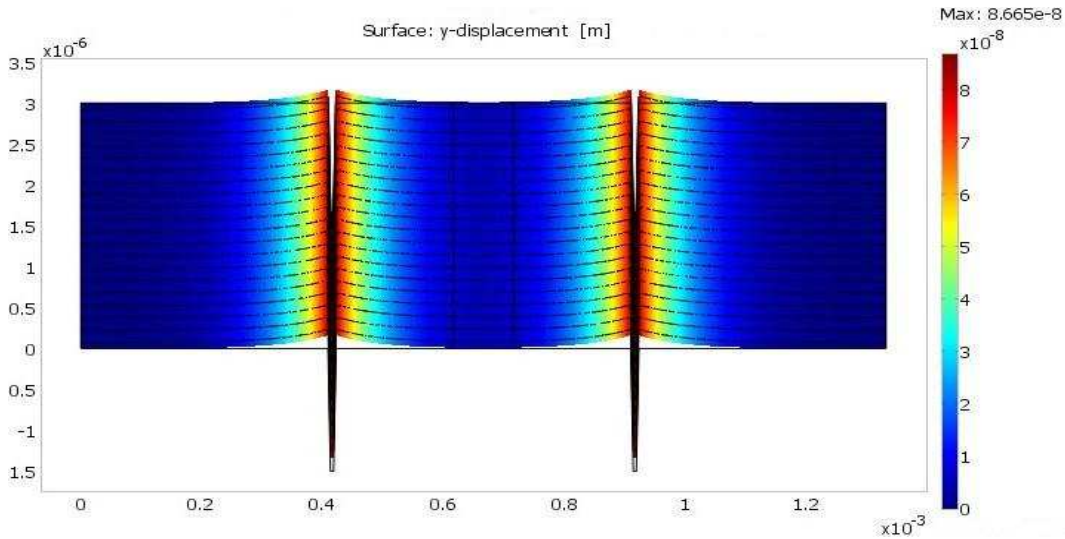

(a) The deflection of the model neglecting the anchor.

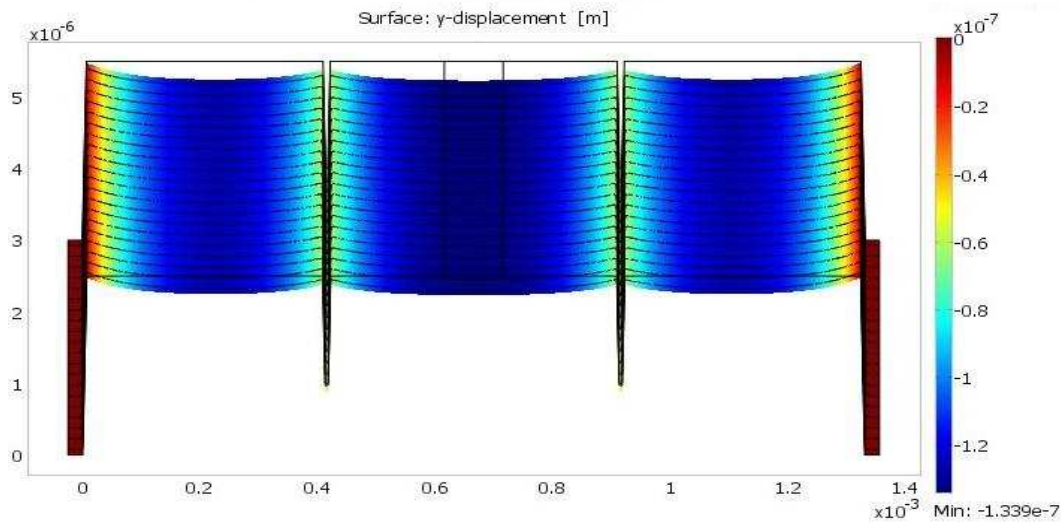

(b) The deflection of the model with anchor.

Figure 6.24.: The deflection of a beam with 5μm wide stoppers and 500μm inter-distance, under the action of 10MPa initial stress.

Summary on initial deformation and conclusion

From this study we can conclude that any non uniformity in the beam will cause a deflection in the opposite direction of this non uniformity. This means, since the stopper is a non uniformity downwards, it will induce a deflection upwards. The deflection due to the anchor affects the whole beam, since the moment will rotate the whole structure leading to a global deflection as figures 6.29 and 6.31 shows. Figures 6.29 and 6.31 presents only half of the structure since it is symmetrical with respect to the center. A zoom on the

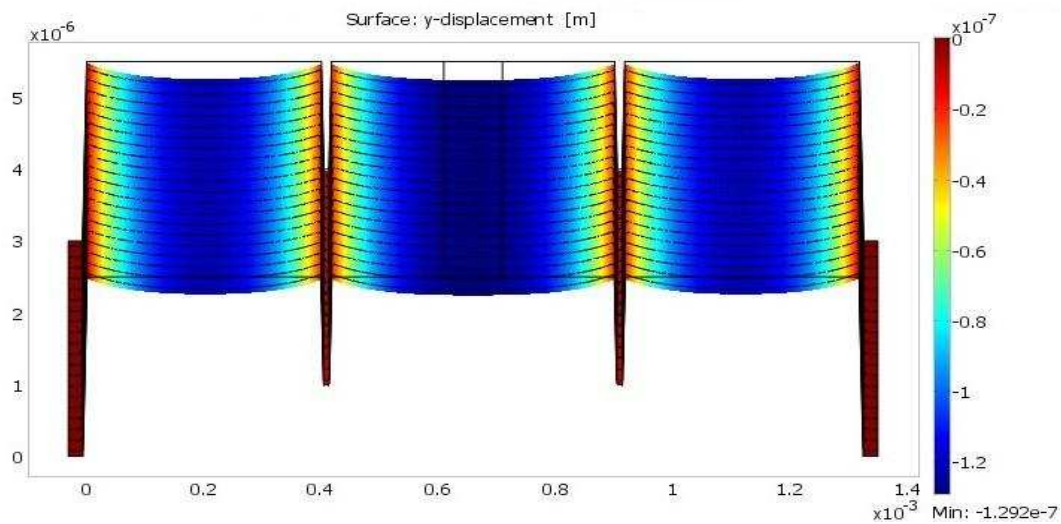

Figure 6.25.: The deflection of a beam with 10μm wide stoppers and 500μm inter-distance, under the action of 10MPa initial stress.

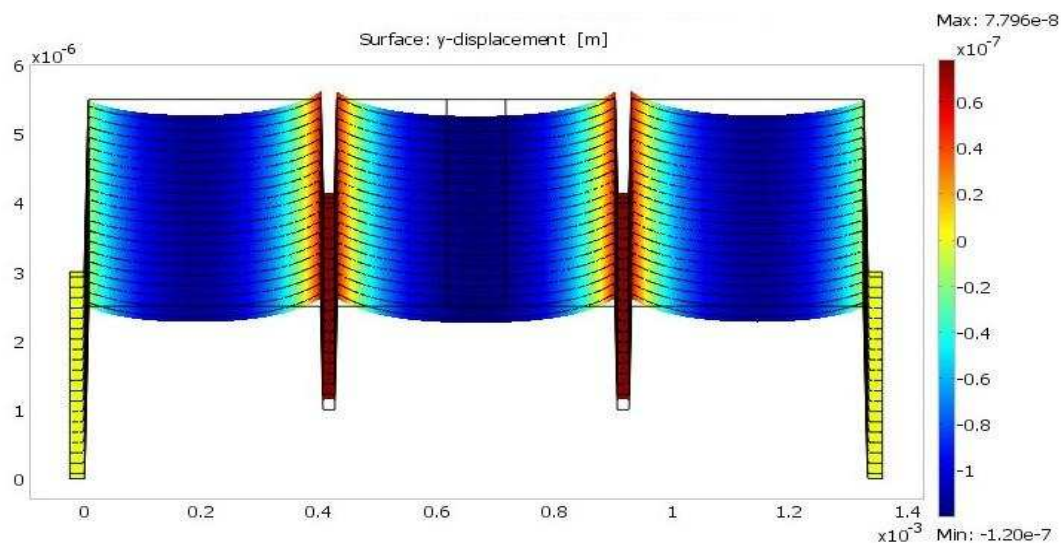

Figure 6.26.: The deflection of a beam with 20μm wide stoppers and 500μm inter-distance, under the action of 10MPa initial stress.

stoppers zone of figure 6.29 is presented in figure 6.30 showing that the stoppers or any non uniformity induces a local deformation around it and nothing elsewhere since the profile tends to fit the straight beam deflection. The deflection of the beam far from the non uniformity zone only depends on the deflection induced by the anchors.

Moreover, we know that to study the initial deformation due to initial stress, it is

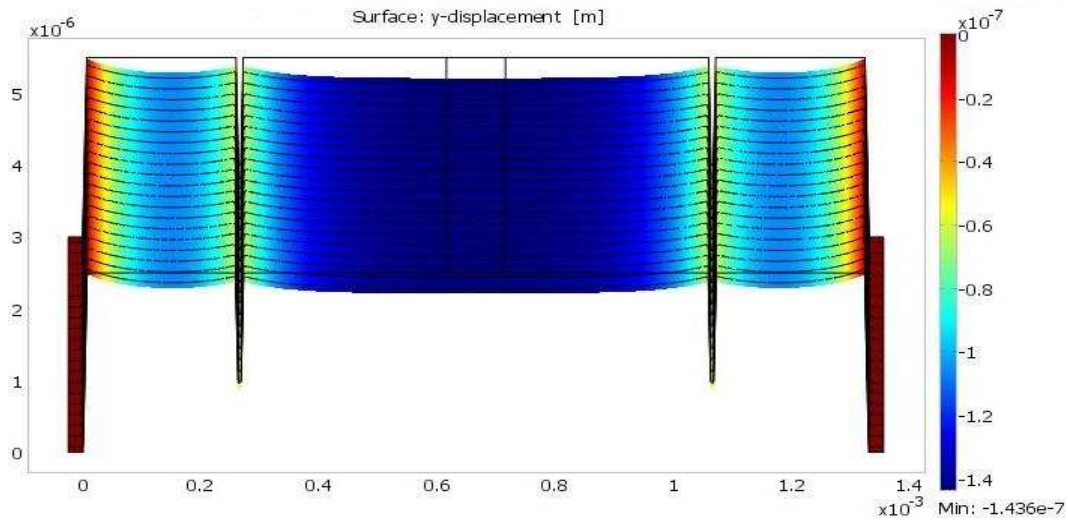

Figure 6.27.: The deflection of a beam with 5μm wide stoppers and 800μm inter-distance, under the action of 10MPa initial stress.

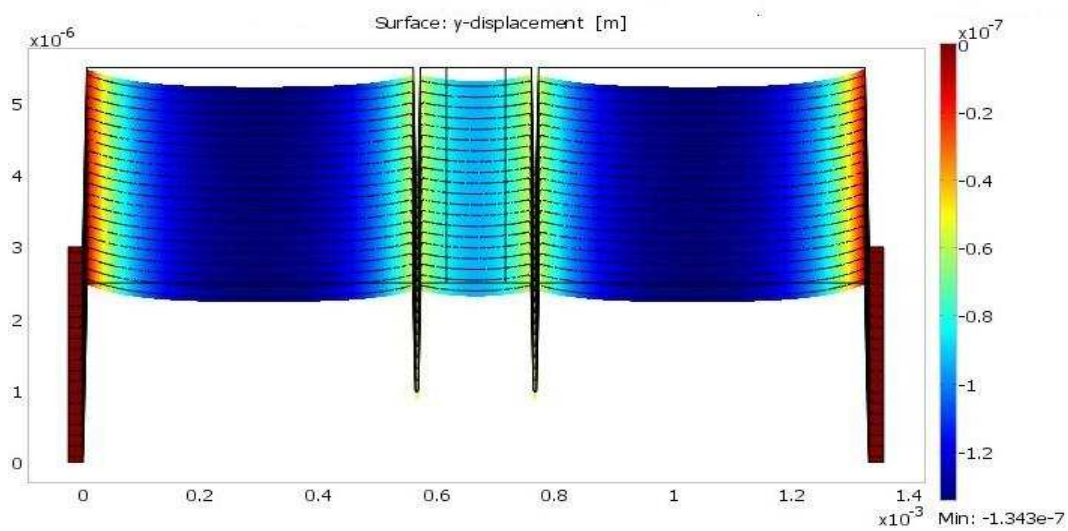

Figure 6.28.: The deflection of a beam with 5μm wide stoppers and 200μm inter-distance, under the action of 10MPa initial stress.

obligatory to include the anchor in the model since it is a major and dominant source of deflection. Table 6.3 below summarizes the deflections obtained by simulation for the different positions and different widths for the stoppers.

The 35% difference in deflection, between the 134nm deflection presented for ideal geometry in table 6.3 and the 209nm found for real geometry, is due to the non uniformities

Stopper width	Stopper inter-distance	anchor included	Initial deflection (nm)
No stopper	No	yes	142 downwards
5μm	200μm	yes	134 downwards
5μm	500μm	No	87 upwards
5μm	500μm	yes	134 downwards
5μm	800μm	yes	142 downwards
10μm	500μm	yes	129 downwards
20μm	500μm	yes	120 downwards

Table 6.3.: Summary of the initial deflection for different stopper size and positions.

size and quantity which add a deflection downwards that were not considered in the previous model.

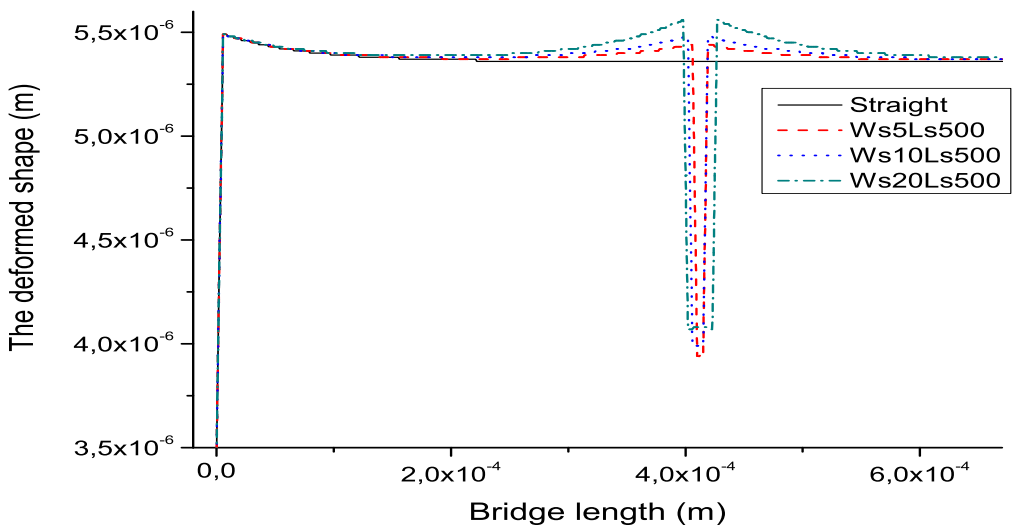

Figure 6.29.: A cut view of the deflection due to initial stress along the beam for different stoppers width with respect to a flat beam.

6.2.5. Effect of stoppers size and position on the initial stiffness

The stoppers will induce discontinuities in the geometry as shown in figure 6.53 in paragraph 6.4.1 on fabrication study. In this objective, we ran simulations to compare the stiffness of a beam with a stopper and a perfectly straight one. Different forms and size of the stoppers were considered in order to have an idea on the sensitivity of this parameter

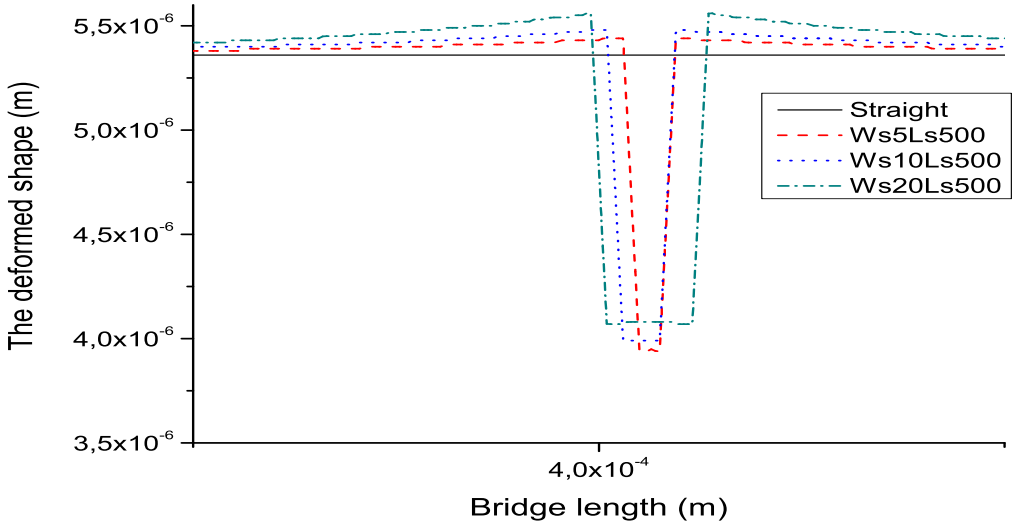

Figure 6.30.: A zoom in the stoppers zone for cut view presented in figure 6.29.

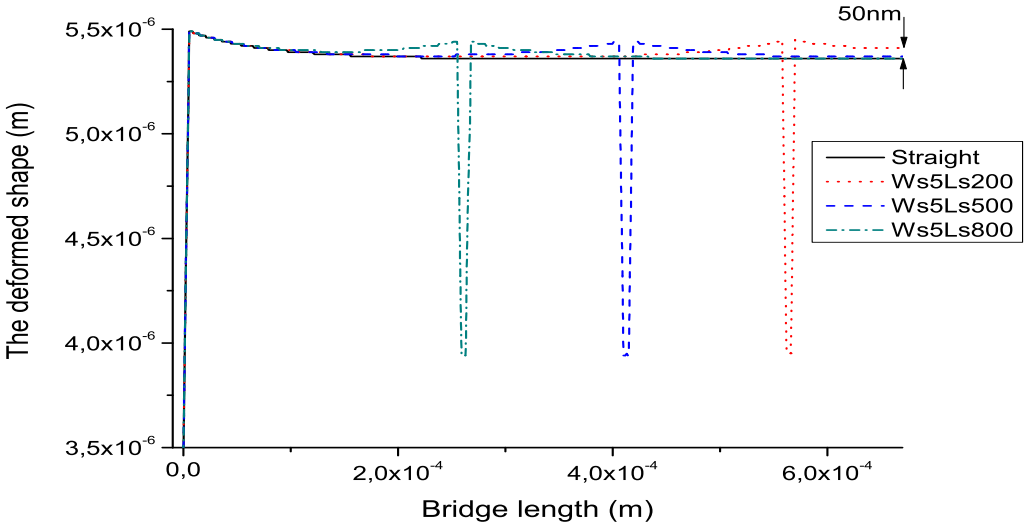

Figure 6.31.: A cut view of the deflection due to initial stress along the beam for different stoppers position with respect to a flat beam.

on the stiffness. The method consists of loading the beam at its center with a uniformly distributed load (equivalent to the electrostatic force). From the Force-displacement curve we deduce the stiffness for different models.

Straight beam

We begin with a simplified finite element model, always using COMSOL 3.4, of a straight beam fixed at both ends, loaded at the middle and with the same parameters as the modele treated before in figure 6.8. This simplified geometry will be our reference model.

Figure 6.32(a) shows the geometry of our simplified reference model while figure 6.32(b) shows the results obtained by finite element simulation of the beam and displaying the displacement under a force of 10 μN. Since there are no nonlinearities, the stiffness of the reference model is deduced to be 1.0344 N/m calculated from the value of the force and deflection simulated.

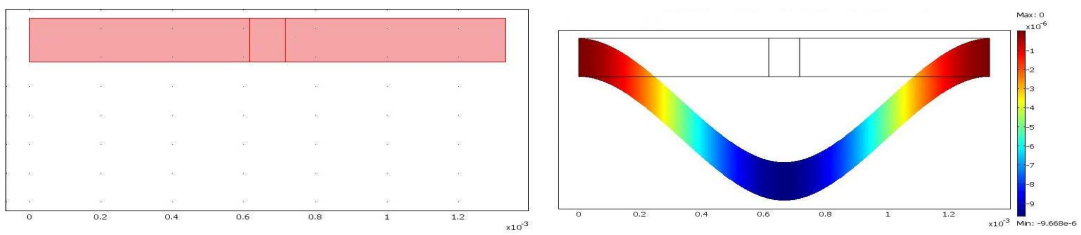

(a) The geometry of the straight beam

(b) The Finite element model of the straight beam

Figure 6.32.: Modeling of a straight beam to calculate its mechanical stiffness.

Effect of stoppers size

- Stiffness for 5μm wide stopper

  In this paragraph, the 5μm wide stopper is modeled with an inter-distance 500μm between them. It is reasonable that the stiffness here be lower than that of a straight beam, due to non uniformity, and this is what we see in figure 6.38. In figure 6.33(a) we can find the geometry of the model while in figure 6.33(b) the simulated displacement is displayed. The difference between this model and the reference model is only 0.003%. This is the minimum width of the stopper that we can obtain due to technological constraints.

- Stiffness for 10μm wide stopper

  The stoppers height are well controlled and the process is developed for a stopper width of 10μm so we need to check what will be the beam behaviour at this stoppers width. This model simulates the mechanical behavior of the beam with a 10μm wide stopper and a distance of 500μm between them. The geometry is shown in figure 6.34(a) and the simulation results can be seen in figure 6.34(b) in an unequal axis frame.

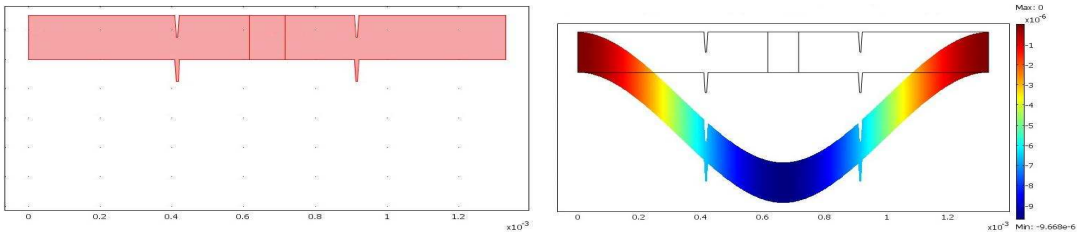

(a) The geometry of the beam with 5μm wide stopper

(b) The Finite element model of the beam with 5μm wide stopper

Figure 6.33.: Simulation of the beam with 5μm wide stopper and inter-distance of 500μm

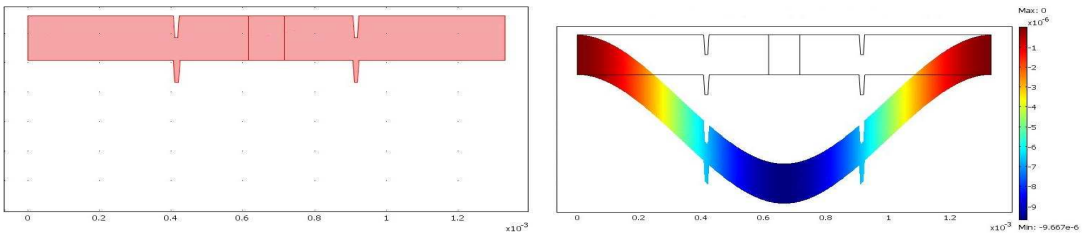

(a) The geometry of the beam with 10μm wide stopper

(b) The Finite element model of the beam with 10μm wide stopper

Figure 6.34.: Simulation of the beam with 10μm wide stopper and inter-distance of 500μm

- Stiffness for 20μm wide stopper

  In order to test the flexibility of the design, we are interested to study the case of a 20μm wide stopper. In this paragraph we present the geometry of a beam 20μm wide stopper and an inter-distance of 500μm as shown in figure 6.35(a). The mechanical simulation results are presented in figure 6.35(b).

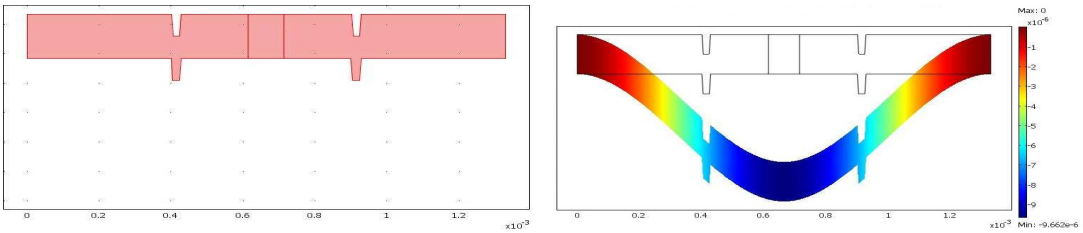

(a) The geometry of the beam with 20μm wide stopper

(b) The Finite element model of the beam with 20μm wide stopper

Figure 6.35.: Simulation of the beam with 20μm wide stopper and inter-distance of 500μm

Effect of stoppers position

In this part we have the objective to check the effect of the stoppers position on the initial stiffness value. Since we have found negligible effect of the stoppers size on the results, we fixed for this study the width to 5μm and varied the inter-distance.

- Stiffness for 200μm stopper inter-distance

  After we have studied the effect of the stopper width on the initial stiffness, we have to verify that the design of the initial stiffness is independent of the position of these stoppers. The minimum distance we can have used between the stoppers is 200μm since the signal line width (100μm) and the (50μm) gap between the line and the ground plane imposes it. Figure 6.36(a) shows the geometry of the model with 5μm wide stopper and an inter-distance between them of 200μm. Figure 6.36(b) shows the displacement of the switch as simulated on COMSOL3.4.

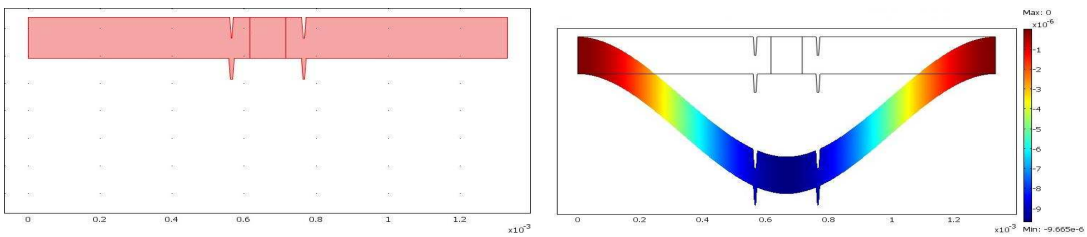

(a) The geometry of the beam with 5μm wide stopper inter-distance of 200μm

(b) The Finite element model of the beam with 5μm wide stopper inter-distance of 200μm

Figure 6.36.: Simulation of the beam with 5μm wide stopper and inter-distance of 200μm

- Stiffness for 800μm stopper inter-distance

  The maximum inter-distance we may have in order for the stopper design to be efficient is 800μm. Figure 6.37(a) shows the geometry of the model with 800μm inter-distance between the stoppers and keeping their width 5μm. Figure 6.37(b) shows the displacement results as simulated on COMSOL3.4 and displayed on unequal axis.

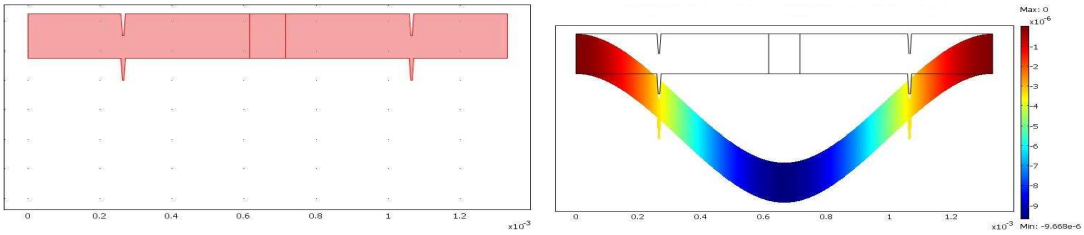

(a) The geometry of the beam with 5μm wide stopper inter-distance of 800μm

(b) The Finite element model of the beam with 5μm wide stopper inter-distance of 800μm

Figure 6.37.: Simulation of the beam with 5μm wide stopper and inter-distance of 800μm

Initial stress effect on the stiffness.

It is usual in MEMS domain that the initial tensile stress have an important impact on the stiffness of non relaxed structures. We mean by non relaxed structures, the double clamped structures (bridges, membranes...) that are not free to move in the stress direction to relax the axial tensile stress. It is mandatory for us to evaluate the effect of the initial stress on the stiffness before and after contact. The initial stress measured on the wafer for the gold layer is 10MPa. The corresponding model presented previously gave an initial stiffness K of 7.7 N/m and a stiffness after contact K_s of 29.6 N/m. The model used to calculate the stiffness after contact K_s is the "Constraint model".

The ratio K_s/K decreased to 3.85 while it was 10.4 for the model without initial stress. From these results we can deduce that our concept of double stiffness state works better for cantilevers where the initial stress have no impact on the stiffness. When designing our switch, we will take the critical value of the ratio K_s/K which is the highest one. The stoppers designed for a high ratio will work for smaller value of K_s/K but the gain in the restoring force will not be optimal.

Comparision of the stiffnesses and conclusion

Figure 6.38 compares the Force-Displacement curves for the models of the stoppers with different widths. The max relative error between the two extreem curves is 0.06% meaning the effect of this parameter on the initial stiffness are negligible. Table summarizes the offset of the initial stiffness for different stoppers width with respect to the straight beam model.

Stopper width	Stopper inter-distance	Shift
5μm	500μm	0.003%
10μm	500μm	0.02%
20μm	500μm	0.06%

Table 6.4.: Summary of the relative shift for different stopper width with respect to a straight beam.

Figure 6.39 compares the Force-Displacement curves for the models of the stoppers at different positions on the beam. The max shift between the two extreem curves with respect to the straight beam model is 0.03% meaning there are negligible effect of this parameter on the initial stiffness. Table 6.5 summarizes the relative offset of the initial stiffness obtained for different stopper inter-distance with respect to the straight beam model. The design become simpler since the initial stiffness is independent of the stoppers width and its position so the stiffness can be calculated from a simple straight beam model.

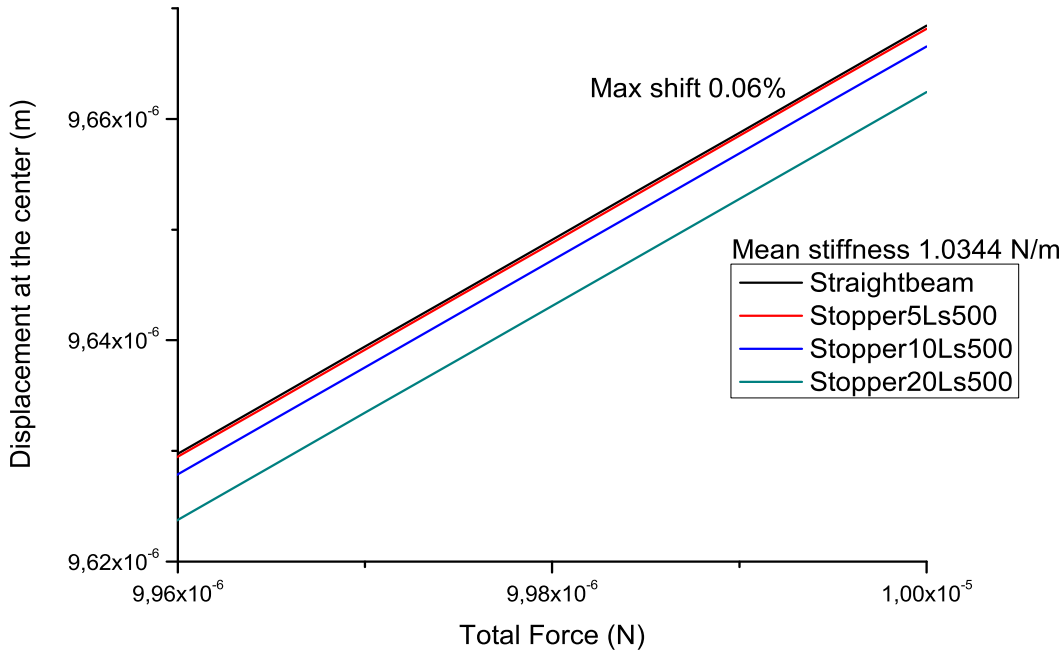

Figure 6.38.: Graph of the displacement at the center of the beam as a function of the applied force for different stopper width and an inter-distance between the stoppers Ls=500μm.

Stopper width	Stopper inter-distance	Relative error
5μm	200μm	0.03%
5μm	500μm	0.003%
5μm	800μm	0.006%

Table 6.5.: Summary of the relative error for different inter-distance between the stoppers with respect to a straight beam.

6.2.6. Simulation of the force-displacement curve

As shown in paragraph 6.3, the key for the design is to know the stiffness state before the stoppers touche the wafer and after touching. For this purpose, we need a rapid way to simulate the beam behavior to obtain the load-displacement curve (to deduce stiffness). The initial stiffness, before the contact, can be easily obtained by a fast simulation of the structure double clamped with a distributed load at the center. A model on COMSOL will be used to simulate the stiffness with initial stress befor and after contact. Any contact simulation is heavy and time consuming so the goal is to simplify the model the

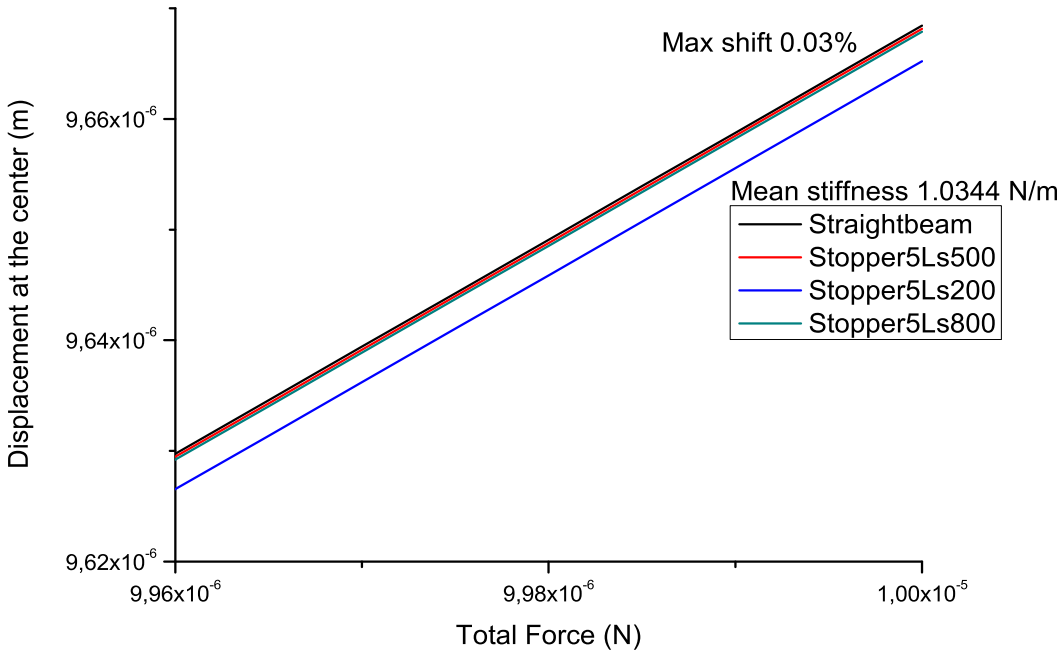

Figure 6.39.: Graph of the displacement at the center of the beam as a function of the applied force for different stoppers inter-distance.

most possible. For this reason, two models for simulating the stiffness after contact are considered. First model is using the classical method by defining a contact area between the stopper and the wafer. The second model consist of applying a constraint on the point of contact.

Contact model

As a basic model, no simplification will be done. A beam with stoppers is modeled and a contact problem is defined between the two surfaces, the bottom of the stoppers and the top of the ground lines. The structure is loaded at its center with a distributed load along a distance W_a and no mechanical constraints are applied at the contact point, only the contact definition is applied. The beam will initially deflect with an initial stiffness and this state will change after the detection of a contact between the stoppers and the wafer in order to pass to a new stiffness state. The model parameters are shown in table 6.2.6, the model geometry is displayed in figure 6.40 showing how the contact surfaces are defined while the simulation results are shown in figure 6.41. The load-displacement curve for the two stiffness states obtained from the same simulation is as shown in figure 6.42.

Parameter	Value	Description
l	1330μm	Beam length
W_a	100μm	Distance of actuation
W	80μm	Beam width
t	3μm	Beam thickness
E	70GPa	Young modulus
ν	0.23	Poisson's ratio
σ	no	Initial stress
g_0	2.5μm	Initial gap
t_s	1.5μm	Stopper height
L_s	500μm	Distance between stoppers

Table 6.6.: Simulation parameters for stiffness extraction by constraint method.

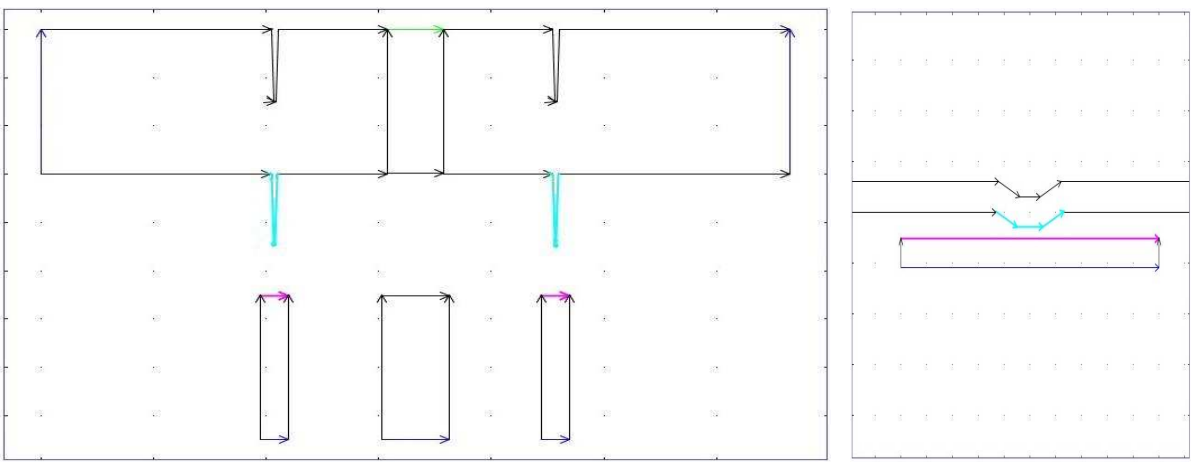

(a) The model used to simulate the stiffness state by contact method. (b) A zoom showing the defined surfaces of contact.

Figure 6.40.: Contact model

Constraint model

This model consits of a beam with stoppers by simplifying the contact between the stopper and the wafer as a point contact. The model parameters are similar to those of the contact model that are listed in table while the constraints at the contact zone are listed in table 6.7. The contact can then be reduced by a constraint in the deflection direction leaving a free rotation at this point. Considering the beam presented in figure 6.40 and by blocking the displacement in the vertical direction as shown in figure 6.43 we obtain the stiffness after contact K_s to be 10.306N/m. This model considers that the stoppers are initialy in contact and the beam will not undergo any displacement before

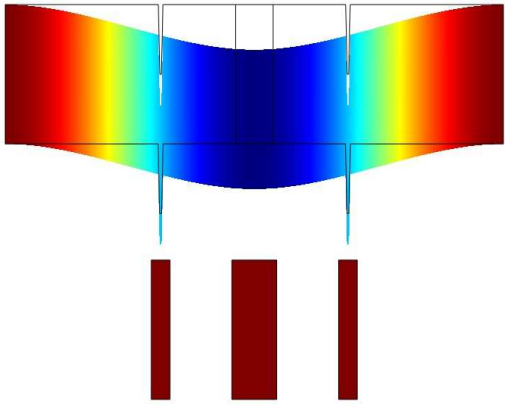

(a) Deformation before contact.

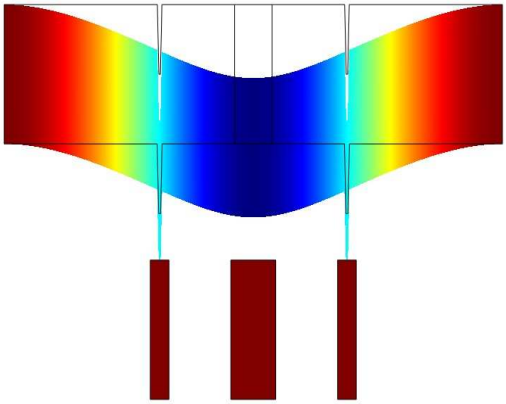

(b) Simulation results when the stoppers touche.

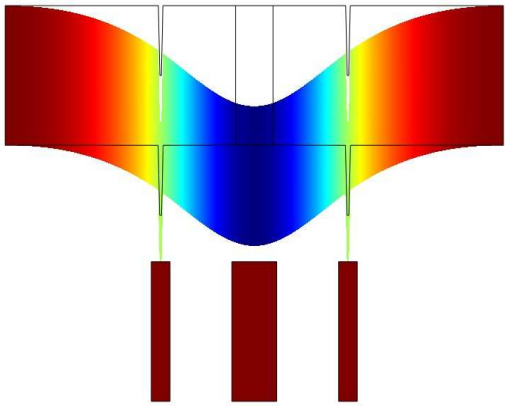

(c) Deformation in the second stiffness state (after stopper contact).

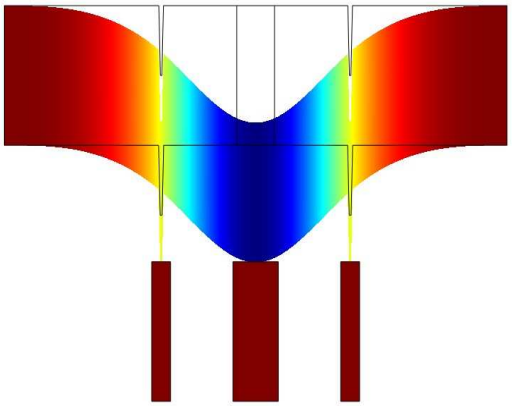

(d) When the beam touches the electrode.

Figure 6.41.: Simulation results for the contact model at different stages.

passing to the second stiffness state. The model gives only the stiffness for the state after contact. To obtain the load-displacement curve for both stiffness states this simulation needs to be run two times, first for a double clamped beam and second for the same beam with a constraint in the deflection direction.

Comparison of models

Comparing the two models studied above, we conclude that they give very close results. Even though the constraint model needs two simulation to obtain the needed results. The calculation time for the constraint model is 8 seconds that means for two simulations the calculation time stays inferior to that of the contact model which takes 704 seconds. The results for both models are also summarized in table 6.8. Figure 6.44 presents the

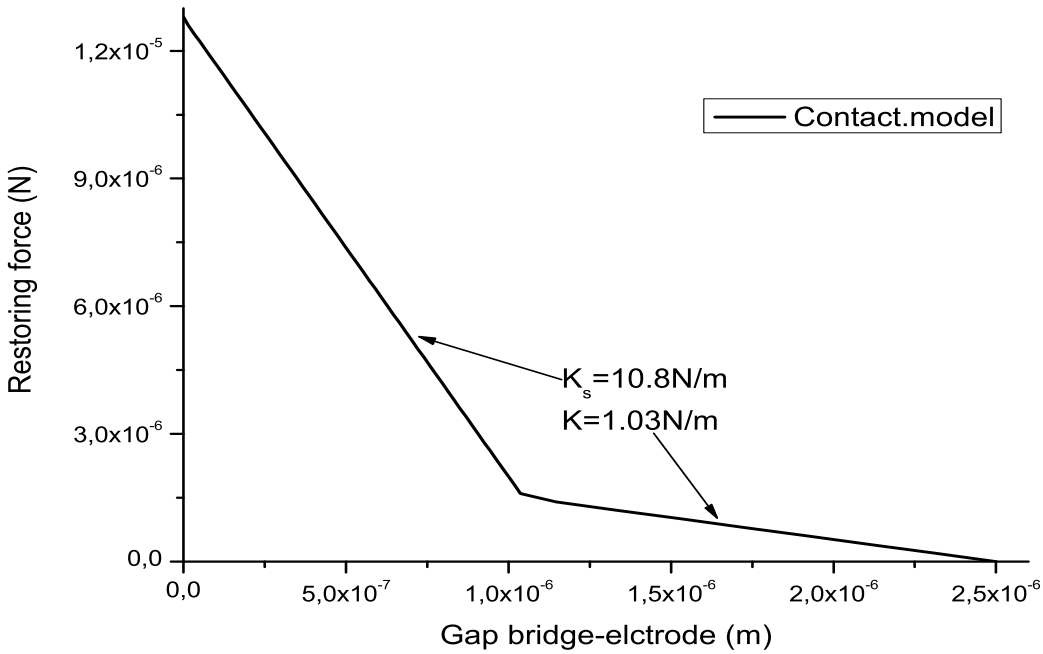

Figure 6.42.: Graph of the load-displacement curve of the beam for contact model.

Parameter	Value	Description
U_x	Free	Displacement constraint along X
U_y	Fixed to 0	Displacement constraint along Y
R_x	Free	Rotation constraint about X
R_y	Free	Rotation constraint about Y
R_z	Free	Rotation constraint about Z

Table 6.7.: Mechanical boundary conditions for the constraints model to extract the stiffnessK_s after contact.

load displacement curve for both models showing a difference at the largest shift of 4%. From this study, we deduce that we can simplify our contact model to a constraint model without loosing precision on the stiffness value.

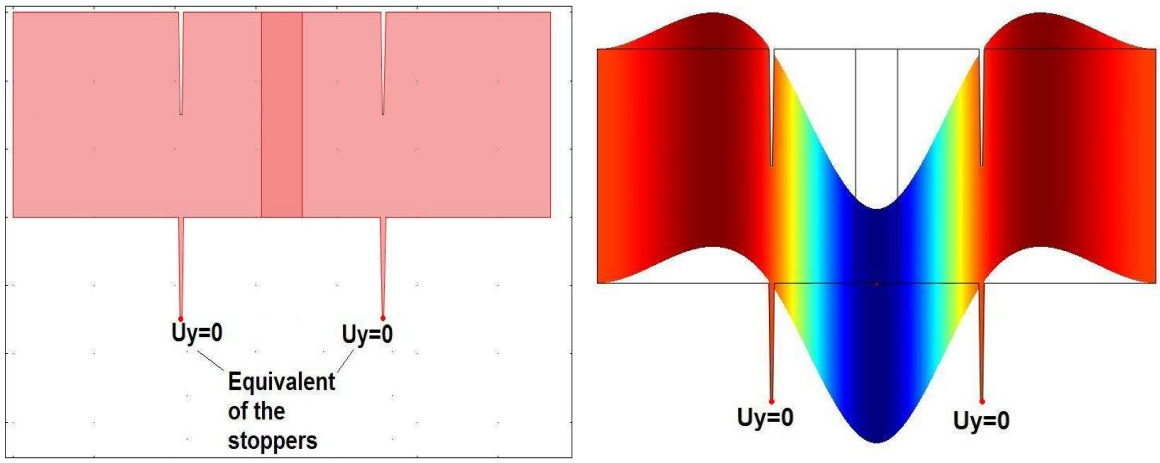

(a) The model used to simulate the stiffness state after contact using the costraint method

(b) The simulation results.

Figure 6.43.: Constraint model

Result	Description	Contact model	Constrains model	offset
K	Stiffness before contact	1.0343N/m	1.0343N/m	0%
K_s	Stiffness after contact	10.767N/m	10.306N/m	4%
t	Calculation time	704 sec	8 sec	

Table 6.8.: Results summary for both methods.

6.2.7. Analytic validation

Analytical stiffness validation

We used equation (A.36) to calculate analytically the stiffness due to bending of the beam developed in paragraph A.2 which excludes the initial stress effect. For the initial stiffness we should consider that the distance between the stoppers equal to the length of the beam (the stoppers are considered at the anchor) so the equation gives K_B=1.03N/m. The analytical stiffness after the contact is calculated using equation (A.35) giving K_{sB}=10.6N/m.

If we add the initial stress effect, using equation (A.56) we obtain the initial stiffness K_{IS}=5.8N/m and the stiffness after contact K_{sIS}=16.4N/m. The total stiffness will be then the summation of the two stiffnesses (Due to bending and due to initial stress) $K = K_B + K_{IS}$=6.8N/m before contact and $K_s = K_{sB} + K_{sIS}$=27N/m after contact.

Table 6.9 below summarizes the results of the stiffness for analytical and numerical models. We can see that when the initial stress is zero, the analytical model before and after contact, fits well with the simulation while the two models have a more significant

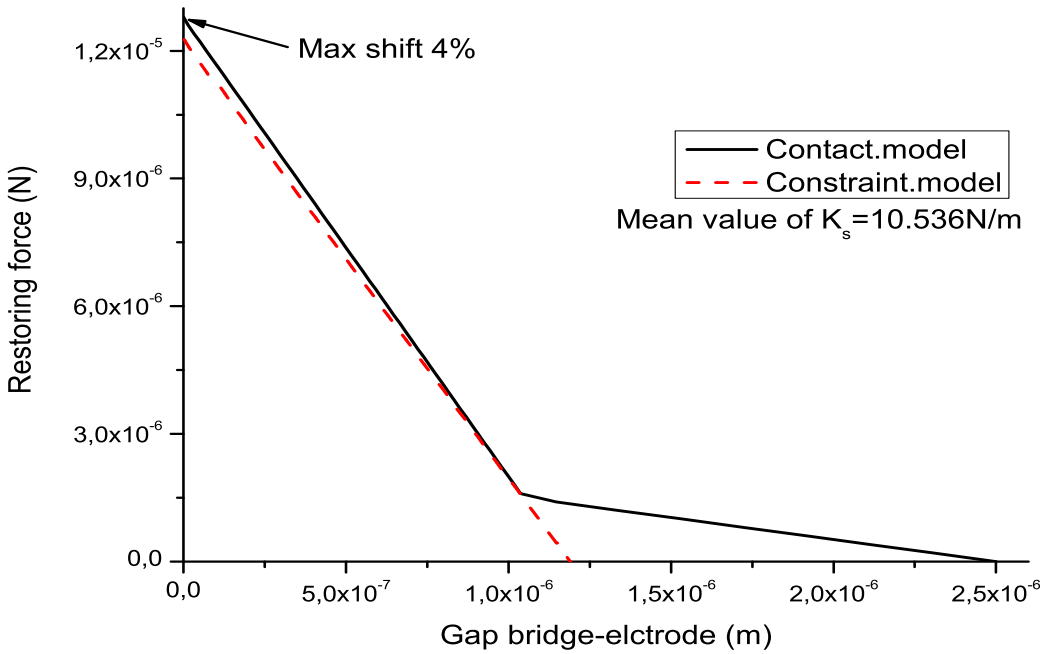

Figure 6.44.: Graph of the load-displacement curve comparing the two studied models.

offset when the initial stress is included. The difference obtained when we add the initial stress effect may be due to the hypothesis that the bridge behaves as a string. The bridge actually undergoes bending which induces some uncertainties due to the estimation of the angle formed between the tension force with the vertical. This explains why the shift is smaller after contact, since the bending is reduced and we are nearer to the conditions of the string theory. The difference between the analytical values and the simulated values are reasonable and then analytical model can be used for stiffness calculation.

Actuation voltage of real geometry

In the frame of study of the real geometry effect on the actuation voltage, the pull-in voltage simulation was run on the regenerated geometry. The material properties being presented at the begining of this paragraph in table 6.2.

- Without initial stress, 2.5μm gap and 3μm gold This section presents the pull-in voltage for the real geometry, without initial stress. This will help us compare the effect of the non uniformities near the actuation region, on the pull-in value. The real geometry is regenerated with a thickness of 3μm gold and and initial gap of 2.5μm. The simulated pull-in is 8.69V with an offset of 1.5% with respect to the flat beam model.

Stiffness	Stress	Model	Value (N/m)	Difference (%)
K	No stress	Numerical	1.03	0
		Analytical	1.03	
	10MPa	Numerical	7.7	11
		Analytical	6.8	
K_s	No stress	Numerical	10.8	2
		Analytical	10.6	
	10MPa	Numerical	29.6	8
		Analytical	27	

Table 6.9.: Comparing analytical to numerical values of stiffness (K) before contact and (K_s) after contact.

- 10MPa initial stress, 2.5μm gap and 3μm gold In this simulation, we added the 10MPa initial stress on the previous model, while keeping a gap of 2.5μm and a gold thickness of 3μm. The pull-in voltage was found to be 20.1V, with an offset of 12% with respect to the flat beam.
- 10MPa initial stress, 2.8μm gap and 3μm gold This model aproaches more from the reality since we used a gap of 2.8μm as measured on the real process. The initial stress is set to 10MPa as the previous models and the gold thickness to 3μm. The pull-in voltage increased to 23.8V due to the increase of the initial gap. We obtained 16.5% error on the pull-in due to the 11% fabrication uncertainty on the gap. The offset between this model and its corresponding model of a straight beam is 12%.
- 10MPa initial stress, 2.8μm gap and 3.4μm gold Simulating the reality can be the title of this section, since all the parameters entered to the simulation are as measured. The real geometry, with 2.8μm gap, 3.4μm gold thickness and an initial stress of 10MPa was fed to the simulator to give a pull-in voltage of 27.9V. We obtained the same offset of 11% from the straight beam model.

Pull-in voltage for the ideal geometry

In this section, we will study, by simulation, the pull in voltage of an ideal beam (uniform beam) for different model parameters. This parametric study permits us to evaluated the impact of each parameter on the actuation voltage. The measured parameters used in the simulation will be presented in paragraph 6.4.3. The varied parameters are the initial stress, gold thickness and the initial gap while the rest of the parameters are fixed and are the same used in paragraph 6.3.

- Pull-in voltage without initial stress, 2.5μm gap and 3μm thick gold In these numerical models, we use the geometrical parameters calculated previously in the

design. This model simulates ideal case of a switch, without any initial stress and with the designed parameters. A 3μm thick gold beam with an initial gap of 2.5μm is modeled. Due to the geometrical and load symmetry, we will consider half of the geometry with symmetry boundary conditions. The simulated pull-in voltage is 8.6V with an offset of 4% with respect to the analytical value.

- Pull-in voltage with 10MPa initial stress, 2.5μm gap and 3μm thick gold In this section, we added only the stiffenning due to initial stress. This gave a pull-in voltage of 22.9V with an offset of 6% from the analytical value. To be noted here is that the stiffness was calculated using the numerical models and only the pull-in is calculated using the analytical formula. This huge effect of the initial stress on the stiffness (pull-in voltage), leaded the scientists to use cantilevers instead of bridges. We didnt use cantilevers in our design because there will be a problem of initial deflection to be controlled. Once the concept will be validated, the study will be applied to cantilevers in the same way as for the bridge.

- Pull-in voltage with 10MPa initial stress, 2.8μm gap and 3μm thick gold The measurments done during the fabrication showed an offset with respect to the designed values. One of the measured parameters that affects the pull-in and that has an important offset is the initial gap. The initial gap g_0 was measured to be 2.8μm instead of 2.5μm, that is 11%. Simulating this effect, the pull-in voltage was found to increase to 27V and an offset of 5.5% with respect to the analytical value. The sensitivity of the pull-in voltage on this parameter is 17% which is near to what is obtained by equation (6.9) that is $\frac{\Delta V_{in}}{V_{in}} = \frac{3}{2}\frac{\Delta g_0}{g_0} = 16.5\%$.

- Pull-in voltage with 10MPa initial stress, 2.8μm gap and 3.4μm thick gold Another parameter affecting the pull-in voltage by affecting the stiffness is the thickness of the gold layer forming the bridge. It is measured to be 3.4μm instead of 3μm. This last model includes in it all the measured parameter in order to be the nearest possible to the real case. A 10MPa initial stress, 2.8μm gap and a 3.4μm beam thickness as measured. The pull-in voltage is now 31.7V showing a huge offset between what we designed and what we obtain due to fabrication uncertainties.

Hysteresis behavior of the design and 10 MPa initial stress

The designed switch with stoppers is simulated using Coventor in order to obtain the hysterisis curve. To make it simple for simulation, the stoppers were placed on the lines and not on the bridge as shown in figure 6.45. We are aware that the pull-out voltage will be lower than designed because the initial stress stiffness is included here. Figure 6.46 shows the hysteresis curve for both cases of a switch with stoppers and without stoppers. The ameleoration in the pull-out voltage is significant while keeping the same pull-in value. The pull-in value of 21.5 V is only 6% different than the 22.9 V simulated on COMSOL. The degradation of 10% in the capacitance value is acceptable and is due

to the higher restoring force which reduces the contact quality between the bridge and the electrode.

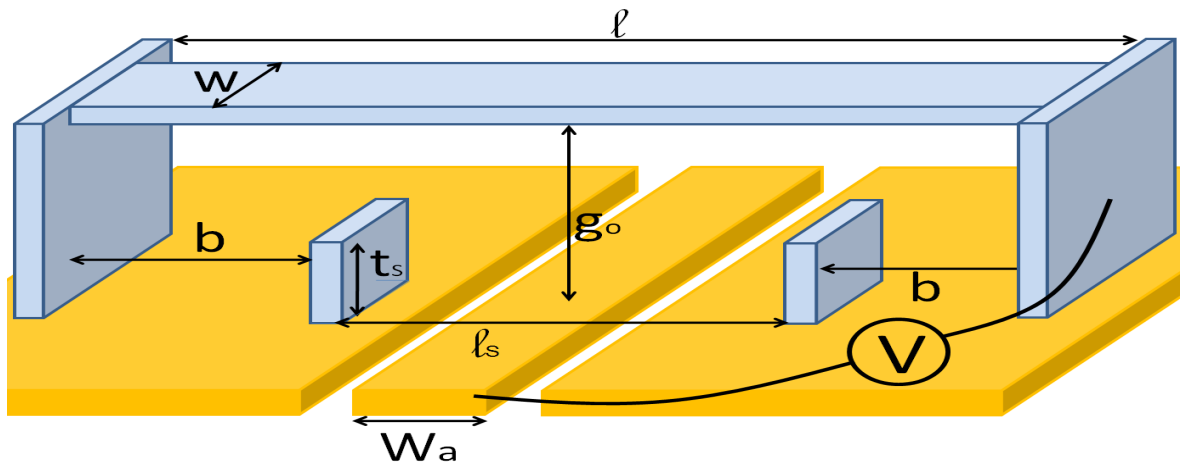

Figure 6.45.: The model used to simulate stoppers on coventor.

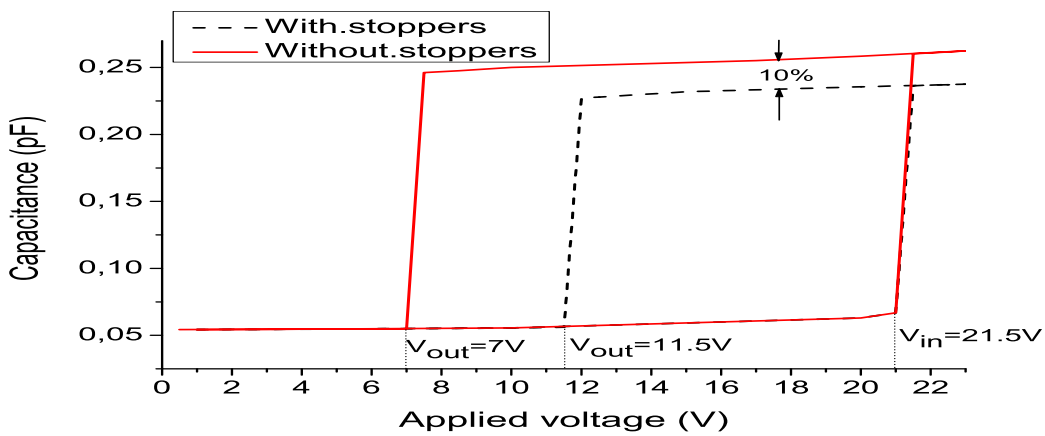

Figure 6.46.: The hysteresis behavior for the design with and without stoppers.

Analytical values of pull-in voltage

From the stiffness calculated by analytical model, we calculate analytically the pull-in voltages using equation (6.1). The results are summarized in the table 6.10 as a function of the used parameters.

Pull-in voltage (V)	Stress (MPa)	stiffness (N/m)	Gap (μm)
8.4	No stress	1.03	2.5
21.7	10	6.8	2.5
25.6	10	6.8	2.8

Table 6.10.: Pull-in voltage calculated by analytical formula.

Comparision ideal geometry with real geometry

The models shown above helped us to understand the effect of each parameter on the pull-in voltage and the results are coherent with previous analysis. The models we have run without including the initial stress effect was to understand the effect of the deformation near the actuation zone on the pull-in voltage. We found that the flatness in the actuation zone has 1.5% effect on the pull-in voltage while its impact on the down state capacitance is important but not yet quantified. We can see clearly that the pull-in voltage for the real geometry, in all the cases, is lower than that of the ideal straight geometry except for the case without initial stress. This is explained by the initial downward deflection due to initial stress (not existing for the flat geometry) which reduces the gap and by that reduces the pull-in voltage. The 12% offset between the real model and the straight model is not due to the deformation in the actuation zone. This is validated by a simple calculation of uncertainties. The downward deflection due to initial stress for the real geometry is 9% of the gap value, which reduces the pull-in voltage by a percentage of $\frac{\Delta V_{in}}{V_{in}} = \frac{3}{2}\frac{\Delta g_0}{g_0} = 13.5\%$. If we consider the 1.5% increase in the pull-in value due to the non flat actuation zone we will finish by obtaining the 12% offset between the models. The table below summarizes the pull-in voltages obtained for the real geometry and the straight beam geometry.

Initial stress	Initial gap	Gold thickness	V_{in}(real geom)	V_{in}(ideal geom)	Offset
No stress	2.5 μm	3 μm	8.69	8.6	1%
10 MPa	2.5 μm	3 μm	20.1	22.9	12%
10 MPa	2.8 μm	3 μm	23.8	27	12%
10 MPa	2.8 μm	3.4 μm	27.9	31.7	11%

Table 6.11.: Pull-in voltage obtained for real geometry and for perfectly straight geometry.

6.3. Design

To design the concept, we combine certain equations describing the behavior of the switch.

From the list of specifications we have the values of V_{in} and V_{out} and some other parameters fixed from the process like the initial gap g_0, the dielectric thickness t_d, the relative permittivity of the dielectric ε_r, the bridge width W and the actuation pad width W_a. From V_{in} we can deduce the value of the initial stiffness K using equation (6.1). From the equality of pull-in voltages for both cases, (K and g_0) for the first case and (K_s and g_{0s}) for the second case, we can deduce the equation (6.3). Equation (6.3) together with the expression of the pull-out shown in equation (6.2) we deduce the values of K_s and g_{0s}. With g_{0s} being the equivalent initial gap of a switch with a stiffness of K_s and having the same pull-in voltage as the switch with a stiffness K and an initial gap g_0. The stiffness K_s will be used to deduce the value of l_s, the distance between the stoppers, by applying equation (6.4) calculated analytically in appendix A.

$$g_{0s} = g_0 \sqrt[3]{\frac{K}{K_s}} + \frac{t_d}{\varepsilon_r}\left(\sqrt[3]{\frac{K}{K_s}} - 1\right) \tag{6.3}$$

$$K_s = K_{sB} + K_{sIS} \tag{6.4}$$

With K_{sB} and K_{sIS} are the stiffness after contact due to bending and initial stress respectively, given by the expressions (refer to appendix A):

$$K_{sB} = \frac{-32EWt^3(2l-3b)}{W_a^3(3b-2l) + W_a^2(4l^2 - 12bl + 8b^2) + l(-4l^3 + 24l^2b - 48lb^2 + 32b^3)} \tag{6.5}$$

$$K_{sIS} = \frac{8\sigma(1-\nu)tw}{2l - 4b - W_a} \tag{6.6}$$

We will call g_s the intersection point of the force-displacement curves for stiffness K with stiffness K_s. Physically, it is the gap at the center of the beam when the stoppers touch the ground as shown in figure 6.47. This parameter is basic to define the height of the stopper and its expression is given by equation (6.7) below.

$$g_s = \frac{K.g_0 - K_s.g_{0s}}{K - K_s} \tag{6.7}$$

Once g_s is known, we now know at which point we need to have contact in order to change the stiffness state. When the gap at the center of the beam reaches g_s, the gap at the position of the stoppers will define the stoppers height. To formulate this step, considering the origin of a coordinate system at the left anchor we can say that the gap between the bridge and the lines is a function of X, g(X). We can then write

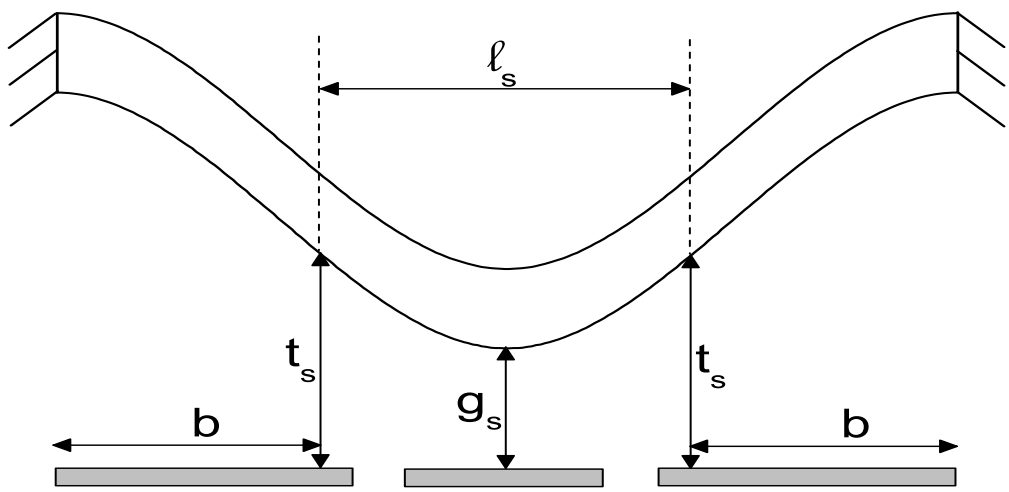

Figure 6.47.: Scheme of the stopper design parameter shown on a deformed bridge.

when $g(\frac{l}{2}) = g_s$ then we obtain the height of the bridge $t_s = g(\frac{l-l_s}{2})$ or $t_s = g(b)$ where b is the distance of the stoppers from the anchor and l_s is the distance separating the stoppers as shown in figure 6.47. Figure 6.48 shows the different points of the actuation curves corresponding to g_0, g_{0s}, g_s and the restoring forces. This design procedure is also described in a flow chart presented in figure 6.49.

As already said, we will need to know the value of the initial stiffness K and the stiffness after contact K_s for the predesign of the stoppers position. The values of K and K_s can be calculated analytically and numerically (by simulation). For the predesign, we use the analytical expression of K and K_s as a function of l_s. These values of the stiffness are then validated with finite element models.

This paragraph describes the design of the test structures. After studying the process and its limitations to fabricate the switch, test structures have to be designed in order to validate the concept that we have studied. Some design parameters are fixed such as $V_{in}, V_{out}, g_0, t_d, \varepsilon_r, W, W_a$ representing the actuation voltage, the pull-out voltage, the initial gap, the dielectric thickness, the relative permittivity of the dielectric, the beam width and the actuation pad width respectively. Table 6.12 gives the values of these parameters.

Since the Ratio K_s/K is a critical parameter for the design which impacts the calculation of the stoppers height, we will design our switches for the worst case which is the highest ratio. As seen in section 6.2.5 about the stiffness due to initial stress, the initial stress increases the stiffness which becomes more linear as a function of the length of the

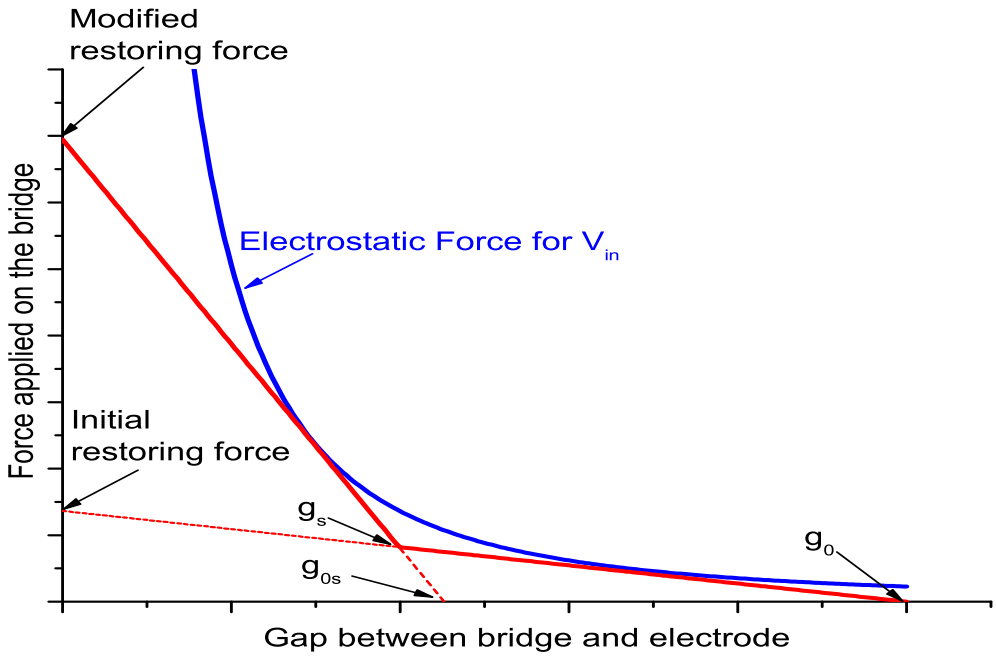

Figure 6.48.: Graph showing the different points used for the design.

beam and by that decreasing the stiffness ratio. We design the switch without initial stress (For the higher value of stiffness ratio) which assures the functioning of the switch for any stress value.

The pull-in voltage of the electrostatic switch was chosen to be 10 V in order to stay in the low acuation voltages limits. The pull-out voltages is fixed to 0.67 V designed in a way to get double the pull-out voltage of the switch without stoppers. For design conditions, we will ameleorate the voltages choice by 20% in order to foresee the calculation errors and be safe. Ameleorating the voltage consists of decreasing the pull-in voltage and increasing the pull-out voltage of 20% leaving an uncertainty interval. For the design, the pull-in voltage becomes 8 V and pull-out 0.75 V.

The design parameters are summarized in table 6.12 and the scheme in figure 6.50 shows the corresponding parameters.

From the pull-in voltage of 8 V we deduce an initial stiffness $K = 1N/m$ from which we calculate analytically the length of the beam $l = 1330\mu m$. We use the two equations (6.2) and (6.3) in order to calculate g_{0s} and K_s. The value of $g_{0s} = 1.12\mu m$ and that of $K_s = 10.6N/m$. Using the analytical equation (6.5) permits to deduce the stoppers interdistance $l_s = 500\mu m$. Applying equation (6.7) we deduce $g_s = 0.97\mu m$ leading to

Parameter	Value	Description
V_{in}	8V	Actuation voltage
V_{out}	0.75V	Release voltage
W_a	100μm	Distance of actuation
W	80μm	Beam width
t	3μm	Beam thickness
E	70GPa	Young modulus
ν	0.23	Poisson's ratio
σ	no	Initial stress
g_0	2.5μm	Initial gap

Table 6.12.: The fixed parameters for the design.

the stopper height $t_s = 1.47\mu m$. Table 6.13 lists the calculated design parameters.

Parameter	Value	Description
l	1330μm	Beam length
l_s	500μm	Stoppers inter distance
t_s	1.5μm	Stoppers height

Table 6.13.: The calculated design parameters.

6.4. Fabrication

The fabrication of the electrostatic switch uses the classical process of MEMS already existing at LAAS. To add stoppers, we add one mask to the process of 7 masks. The step for fabricating the stoppers needed to be developed and stabilized in order to control the depth of the stopper.

6.4.1. Stopper developement

We had many choices for the stopper fabrication depending on its compatibility with the process we want to use and the flatness of the final structure. The flatness of the structure is of big importance regarding its impact on the actuation voltage and on the quality of the capacitive contact. For this purpose, we used finite element modeling to investigate these effects (refer to chapter 6.2).

The stoppers can be either deposited on the dielectric which is the fixed part (figure 6.51) or on the movable bridge itself (figure 6.52 and 6.53). Depositing the stoppers on

the fixed part, will add a non uniformity in the topology under the sacrificial layer. Since the photoresist is conformal to the surface underneath, it follows the bumps and gaps and thus adding non uniformity to the bridge.

Two other existing options are both for the stopper fabricated on the moving beam. Either we can use two layers with different photoresist thicknesses as a sacrificial layer or use one layer with partial screening in the stoppers zone. The option with two photoresist layers showed problem of adhesion between them. The bad adhesion causes bad flatness as well as pealing of the layers during processing so this choice is rejected.

One last option that was studied is the partial screening of the photoresist. This method consist of a photolithography step where the exposure time is controled in a way that the radiation only affects a certain depth of the photoresist. The time of exposure for a stopper of 1.5 micron heigh is 5 seconds. This time is not fixed, it varies with surface exposed as well as the photoresist thickness. A reproducibility test was done on the height of the stopper (depth of the hole in the photoresist) for a circle of 10μm in diameter and a thickness of 2.5μm. The photoresist used is the AZ1529. The measurments obtained by mechanical profiler, for different tests, are shown in figure 6.54. The stopper height obtained for 5 seconds exposure is 1.5μm$\mp$100nm.

6.4.2. Switch process

Step	Description	Param	Scheme
♯1	High resistivity silicon substrate	250μm	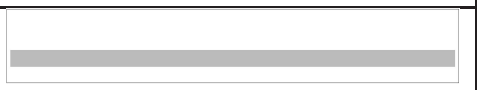
♯2	RCA cleaning		
♯3	Thermal Oxide??	800nm	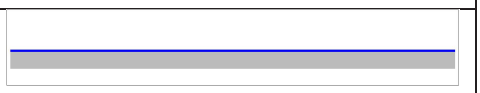
♯4	Metalization Ti/Cu (seed layer)	50nm	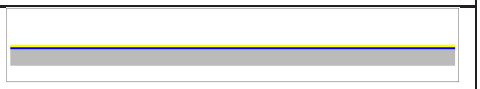
♯5	Spin coating of AZ4562	10μm	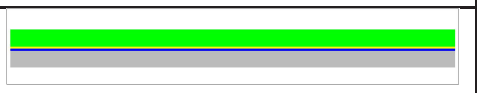
♯6	Lithography of CPW mold	Mask1	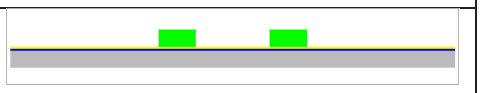
♯7	Gold electroplating	2.5μm	
♯8	Metalization Ti (adhesion layer for SiN)	50nm	
♯9	Spin coating of AZ1529	2.8μm	
♯10	Lithography for CPW gap etching	Mask2	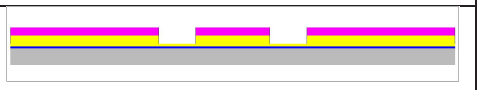
♯11	Ti/Au/Cu/Ti etching	90sec	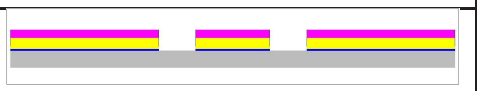
♯12	Dielectric deposition LF SiN	400nm	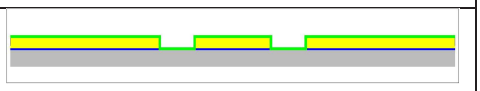
♯13	Spin coating of AZ1529		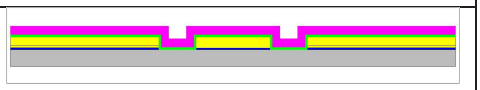
♯14	Lithography for dielectric etching	Mask3	
♯15	RIE for dielectric	180sec	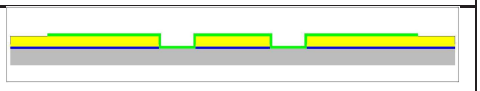

Continue on the next page . . .

Continued from previous page			
Step	Description	Param	Scheme
♯16	Wet etching (Buffer HF) of Ti		
♯17	HMDS for photoresist adhesion		
♯18	Spin coating of AZ1529	2.7μm	
♯19	Soft baking 105°C	60sec	
♯20	Lithography for gap filling	Mask2	
♯21	Developement		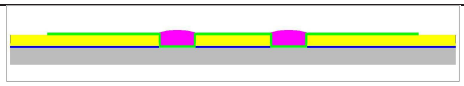
♯22	Post baking 150°C	120sec	
♯23	Spin coating of AZ1529	2.5μm	
♯24	Soft baking 105°C	60sec	
♯25	Lithography for anchors	Mask6 12sec	
♯26	Lithography for stoppers	Mask8 5sec	
♯27	Developement	28sec	
♯28	Post baking 150°C	60sec	
♯29	Metalization Au	100nm	
♯30	Gold electroplating	3μm	
♯31	Spin coating of AZ5214		
♯32	Lithography for bridge		
♯33	Gold etching		
♯34	Photoresist protection for dicing		
♯35	Dicing		
♯36	Bridge release (Acetone)	10min	
♯37	Bridge release (AZ100 remover)	2days	
♯38	Critical drying		

Table 6.14.: The MEMS switch process (LAAS).

6.4.3. Geometrical measurments

To verifie the reproducibility of the process, we measured the thicknesses of the important layers. The table below sumarizes the measured values and the targetted value of each parameter.

Description	targetted value	Measured value
High resistivity silicon substrate	250μm	253μm
CPW line thickness (step7)	2.5μm	2.4 to 3μm
Dielectric thickness	400 nm	395nm
Sacrificial layer thickness	2.5μm	2.7 to 2.8μm
Stopper height	1.5μm	1.7 to 1.88μm
Bridge thickness	3μm	3.5μm

Table 6.15.: Measured geometrical parameters versus targetted value

The uncertainties in the fabrication will be reconsidered in our design in order to estimate the shift in the results due to this offset in dimensions. The analytical expression of the pull-in voltage gives us [56]:

$$V_{in} = \sqrt{\frac{8Kg_0^3}{27\varepsilon_0 W_a W}} \tag{6.8}$$

A relative error study on the parameters of this expression will give the expression:

$$\frac{\Delta V_{in}}{V_{in}} = \frac{1}{2}(\frac{\Delta K}{K} + 3\frac{\Delta g_0}{g_0} - \frac{\Delta W}{W} - \frac{\Delta W_a}{W_a}) \tag{6.9}$$

Where W is the bridge width, W_a is the Actuation length (The same dimension as the signal line width), g_0 is the initial gap and K is the mechanical stiffness. The relative error on the bridge width comes from an over etching of the gold in step 33 of the process. The value of this over etch is estimated to the thickness of the etched gold that is 3μm from each side, giving a relative error of -7.5%. From measurments using the mechanical profilometer, we found that the actuation length is reduced from 100μm to 94μm due to the line over etching. The relative error on the actuation length is -6%. Always with a mechanical profilometer, we measured the initial gap g_0 to be 2.8μm instead of 2.5μm as designed. This error coming from the uncertainty on the sacrificial layer thickness leads to a relative error on the initial gap of 11%. The error on the stiffness is a bit more complicated to find, since it depends on the material properties which is already a difficult issue as well as the dimensions of the beam and the initial tensile stress. If we consider the only uncertainty on the stiffness is due to the bridge thickness, we have a relative error of 40%. Replacing the obtained values in the uncertainty equation we obtain a relative error in the pull-in voltage of 43%. If we neglect the effect of the actuation length and

the bridge width, we have a relative error of 36% which explains the 30% offset between 22.9V and 31.7V for the models in paragraph 6.2.7.

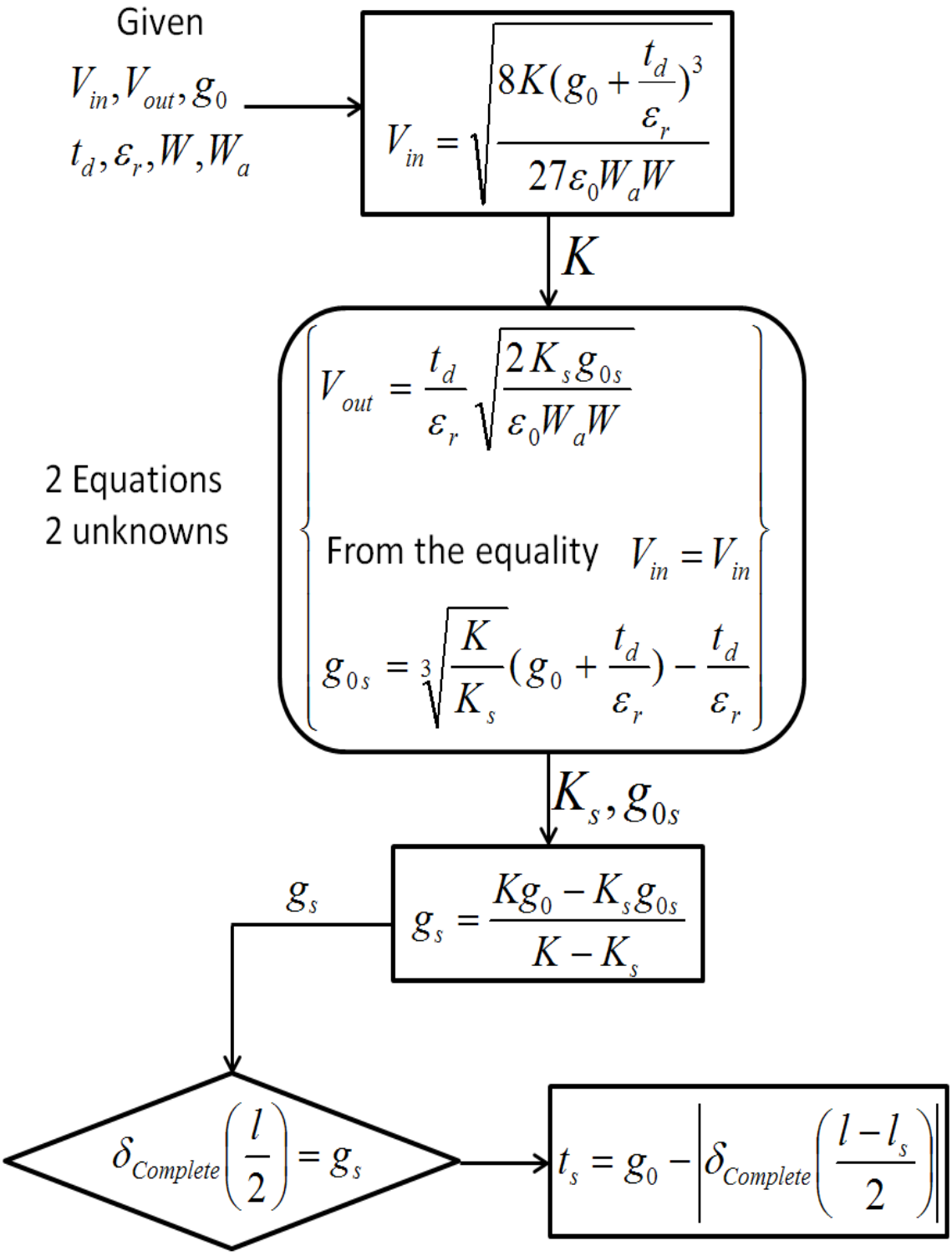

Figure 6.49.: Flow chart of the stopper design parameters.

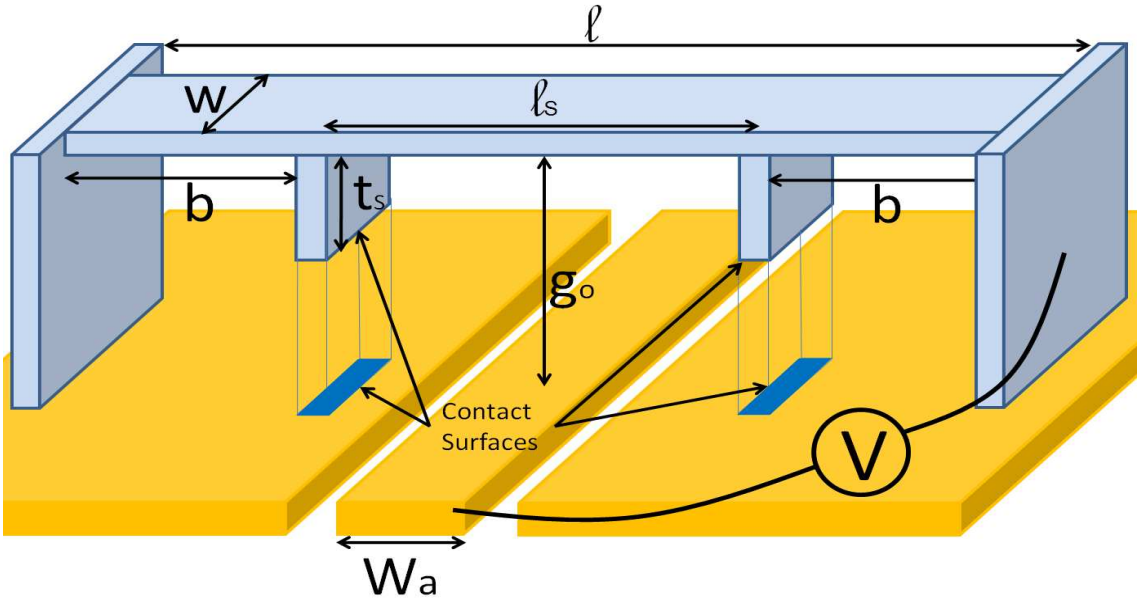

Figure 6.50.: Scheme of the design parameters.

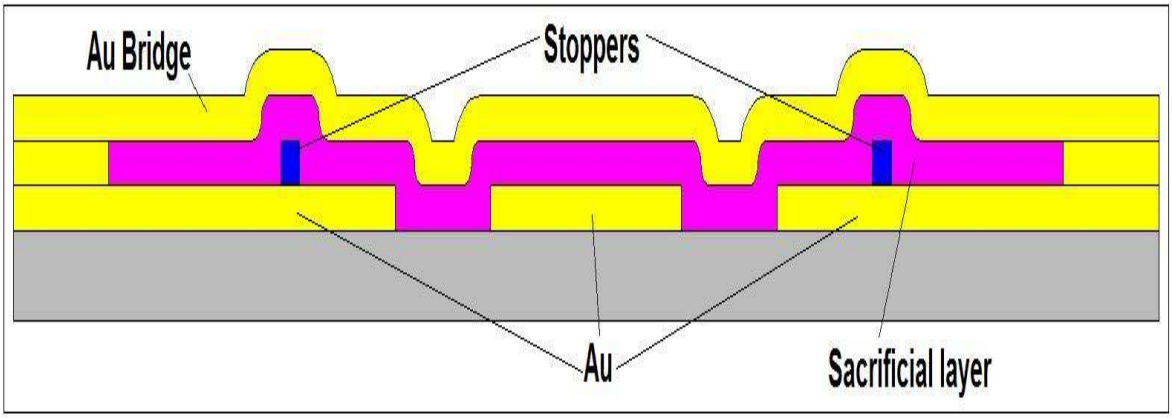

Figure 6.51.: First choice, depositing stoppers on the fixed part.

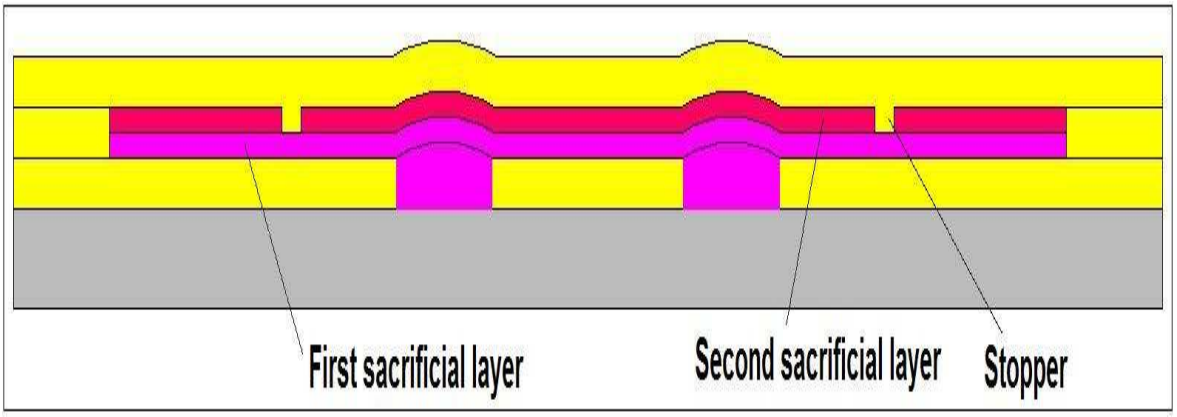

Figure 6.52.: Second choice, creating the stoppers in the bridge using two sacrificial layers.

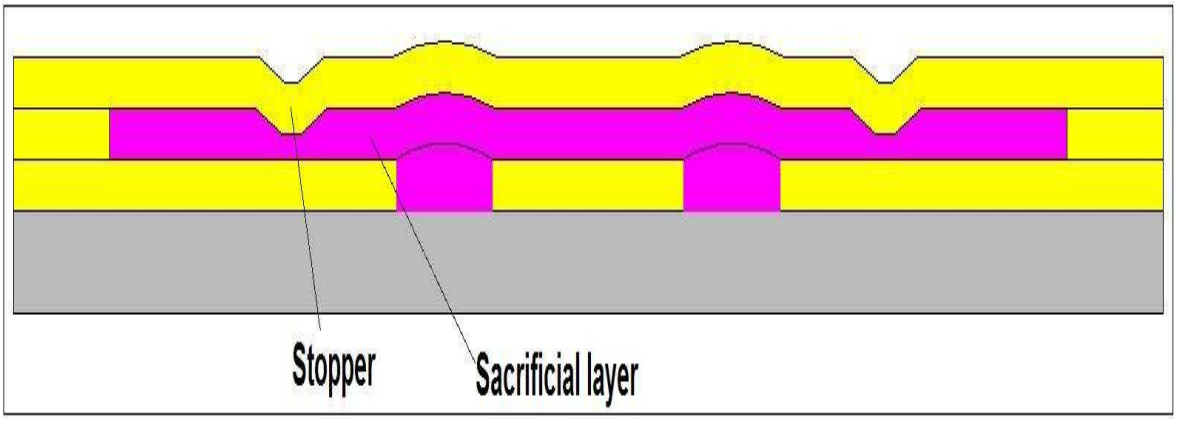

Figure 6.53.: Third choice, creating the stoppers in the bridge using partial screening.

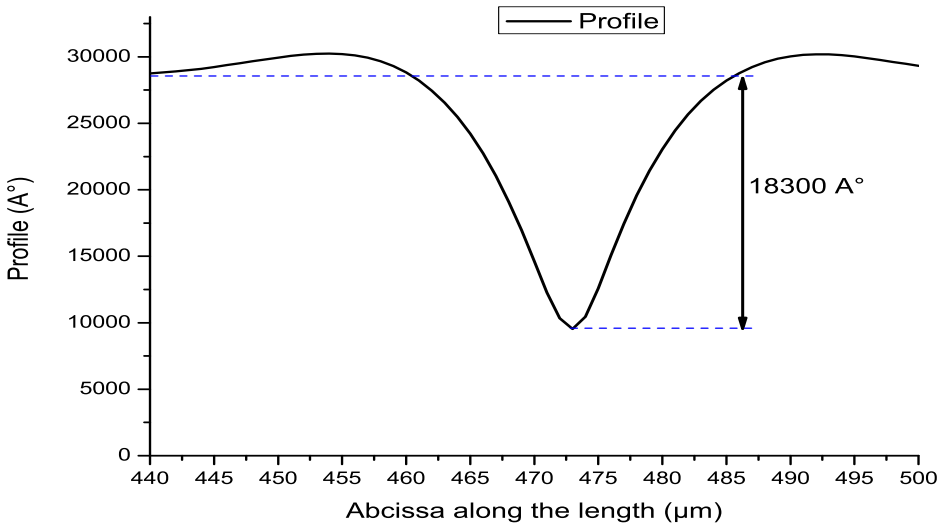

Figure 6.54.: Profile of the etched hole in the photoresist for stopper deposition.

Conclusion et perspective

Dans cette thèse, nous avons étudié les méthodes pour réduire l'effet de stiction dans les commutateurs RF MEMS capacitive a actionnement électrostatiques. Nous avons pris deux directions pour faire cela, premièrement changer la méthode d'actionnement tandis que l'autre s'agit d'ameleorer la force de rappel. Après avoir fait un aperçu général sur les méthodes pour améliorer la force de rappel, nous avons proposé un concept qui a été étudiée d'être efficace. Nous avions étudié aussi des possibilités différentes pour actionner le commutateur, et nous avons tirés la conclusion la plus commode à notre application, en termes de consommation de capacité et de vitesse de commutation, qui utilise un actionneur piézoélectrique.

Le différent simulateurs multiphysics ont été validé. Un modèle de contact construit sur COMSOL est comparé aux résultats analytiques et aux résultats numériques simulés utilisant ANSYS qui montre une différence négligeables. Ceci mène à une conclusion d'utiliser ANSYS pour toutes simulations de contact puisque il converge plus facile que COMSOL et contient plus de méthodes de résolution. L'actionnement piézoélectrique a été aussi validée en utilisant deux modèles différents, un modèle simple pour la validation avec les résultats analytiques et un autre plus compliqué pour le comparer à ANSYS. La conclusion tiré de cette étude est que COMSOL est plus commode pour résoudre des problèmes d'actionnement piézoélectriques car il est plus rapide dans le calcul qu'ANSYS. Enfin, nous avons validé l'actionnement électrostatique en utilisant un modèle de pont sur COMSOL et Coventor donnant des résultats tres proche et adoptant de cette façon Coventor pour ces études puisque c'est le seul logiciel qui offre l'option de calcul de la tension d'actionnement et obtenir l'hysteresis.

Dans la partie qui traite le changement de la méthode d'actionnement en actionnement piézoélectrique, nous avons fait une étude de faisabilité. Les différentes façons pour connecter la membrane à l'actionneur ont été étudié pour choisir la meilleure configuration. Les modèles II et IV était les plus intéressant en terme de la déflexion et vitesse de commutation. Le problème de planaéité de la membrane a été simulé montrant que l'actionneur est assez puissant pour plaquer la surface de la membrane contre l'électrode pour obtenir une surface plate. La déflexion initiale du a la variation de la température et au gradient des contraintes initiales a été equilibré en ajoutant une couche de compensation et en variant la température de recuit mais cela complique le processus de fabrication.

D'autre part, une conception pour améliorer la force de rappel dans les commutateurs électrostatique a été étudiée. Une structure offrant un double état de raideur a été obtenu, une raideur basse dans la phase d'actionnement et une haute raideur dans la phase de relachement. Ces deux état de raideursont été obtenue en ajoutant des plots qui change

la raideur une fois ils sont en contact avec la masse. Les plots ont eu un petit impact sur la déflexion initiale pour n'importe quelle position et n'importe quelle taille d'eux. Simulant ce concept sur Coventor, nous avons obtenu la courbe d'hysteresis montrant l'amélioration dans la tension de relachement qui augmente la force de rappel.

Dans la perspective à ce travail, nous avons l'intention de faire le suivant :

- Etudier l'application des plots conçu sur les cantilevers pour se débarrasser de l'effet des contraintes initiales sur la raideur.
- Etudier la possibilité de mettre plusieurs plots sur le même pont pour avoir les multi états de raideur (plus que deux) et bien d'augmenter plus la force de rappel.
- Etudier la profondeur de la hauteur du plot en fonction de temps d'insolation de la resine.
- Utiliser le polyimide comme couche sacrificiel.
- Mesurer le concept de switch a actionnement electrostatique bien que le piezoelectrique.

7. General conclusion and perspective

In this thesis, we studied the ways to reduce the stiction effect in electrostatic RF MEMS capacitive switches. We went in two directions in order to do that, first was changing the actuation method while the other was by ameliorating the restoring force. After having an overview on the methods used to ameliorate the restoring force, we have proposed a design that was studied to be efficient. We had also studied different possibilities to actuate the switch, and we came out with the conclusion that is convenient to our application, in terms of power consumption and speed of switching, which is using piezoelectric actuation.

The different multiphysics sowftwares were validated. A contact model built on COMSOL is compared to analytical results and to numerical results simulated using ANSYS and the results showed negligible difference. This leads to a conclusion to use ANSYS in order to run contact simulations since it converges easier than COMSOL and contains more resolution methods. Piezoelectric actuation was also validated using two different models, a simple model for validation with analytical results and a more complicated one to compare with ANSYS. This study lead to deduce that COMSOL is more convenient to solve piezoelectric actuation problems since its faster in calculation than ANSYS. Finally, we validated the electrostatic actuation using a bridge model on COMSOL and Coventor giving very near results and thereby adopting Coventor for these studies since it's the only software that offers the option to calculate the pull-out voltage and obtaining the hysteresis.

In the part dealing with changing the actuation method to piezoelectric actuation, we made a feasibility study. Different ways to connect the actuator to the membrane were designed in order to choose the best configuration. Models II and IV were the most interesting in terms of deflection and switching speed. The flatness problem of the membrane was simulated showing that the actuator have enough energy to push the membrane face to the electrode in order to obtain a flat surface. The initial deflection due to temperature and due to initial stress was equilibrated by adding a compensation layer and varying the annealing temperature but complicating the fabrication process.

On the other hand, a design to improve the restoring force in the electrostatic switch was studied. A structure offering a double state of stiffness was obtained, a low stiffness in the pull-in cycle and a high stiffness in the pull-out cycle. This two state stiffness was obtained by adding stoppers that changes the stiffness once they are in contact with the ground. The stoppers had a small impact on the initial deflection for any position or size of them. Simulating the design on Coventor, we obtained the hysteresis curve showing

amelioration in the pull-out voltage that is increasing the restoring force.

In perspective to this work, we planned to do the following:

- Study the application of the stoppers design on cantilevers in order to get rid of the effect of the initial stress on the stiffness.
- Study the possibility to put multiple stoppers on the same bridge in order to have multi stiffness states (more than two) and though increase more the restoring force.
- Study the depth of the height of the stopper as a function of exposure time.
- Use the polyimide as sacrificial layer.
- Test the electrostatic design as well as the piezoelectric designs.

A. Analytical model

A.1. Introduction

The mechanical structures deform under a certain load in order to store the work transmitted into potential energy. To simplify the model, we can replace the structure by a spring model, weather its stiffness is linear or not depending on the bending moment distribution and the structural behavior. Different parameters affects the stiffness of a structure such as, the Young mudulus, dimensions of the structure (thikness, length, width) and the point of application of the force. In microstructures, another factor becomes significant and increases the stiffness, it is the initial tensile stress.

In what follows, we present the equations governing the behavior of the structure, shown in figure A.1, used to deduce the expression of the total stiffness before contact (K) and after contact (K_s). The subscript s signifies that this stiffness state is after contact. Each stiffness state is a result of two sources, first the bending stiffness K_B of the structure and the seccond is the stiffness induced by the initial tensile stress (K_{IS}). Then we can write $K = K_B + K_{IS}$ and $K_s = K_{sB} + K_{sIS}$. Once we have the analytical expression of the stiffness before and after contact, it is then used to predesign the stoppers position and the bridge size.

A.2. Stiffness due to bending

Starting with the bending stiffness after contact KsB, we will consider few hypothesis. To model the structure with stoppers, we replace the contact of the stoppers by a reaction force at the same place as the stoppers. The loads acting on the beam are shown in figure A.1.

First, we will divide the forces into two groups (refer to figure A.2) and then by superposing the behavior of the beam respectively to each case, we obtain the overall behavior. First group is the reaction forces, R, replacing the contact of the stoppers and they are at the same distance from the anchor as the stoppers. Since the structure and the load are symmetrical, the stoppers reaction forces R are also equal and symmetrical with respect to the middle of the beam. A second group of forces is the actuation distributed load of intensity ξ symetrical with respect to the middle of the beam.

We start by writting the equations of a beam loaded with one concentrated charge P at any distance "a" from the anchor as in figure A.3. We consider that the stoppers before touching the ground, they don't affect the initial stiffness of the beam, this hypothesis

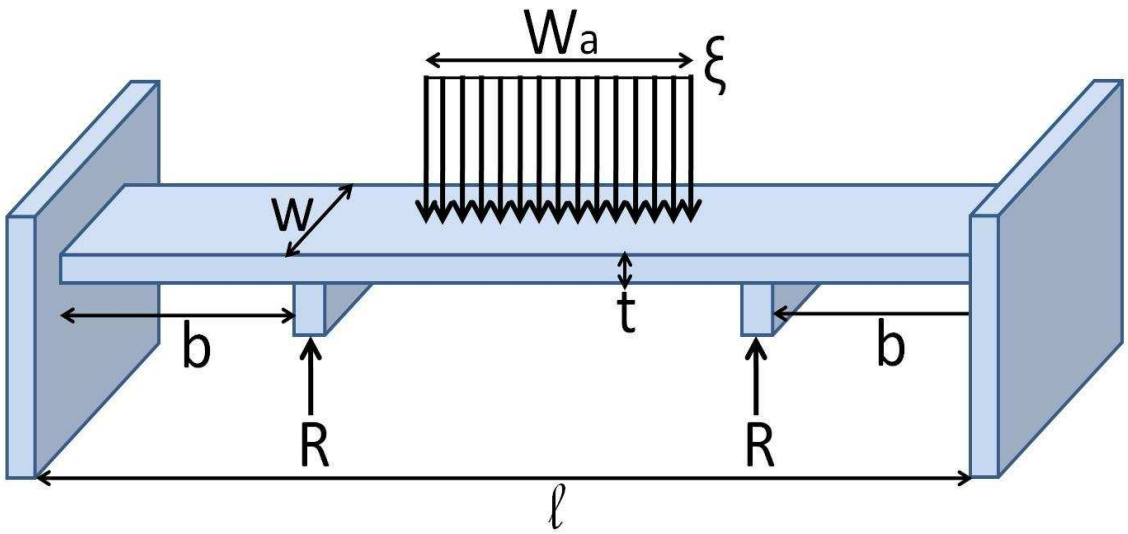

Figure A.1.: Forces diagram acting on the beam with stoppers

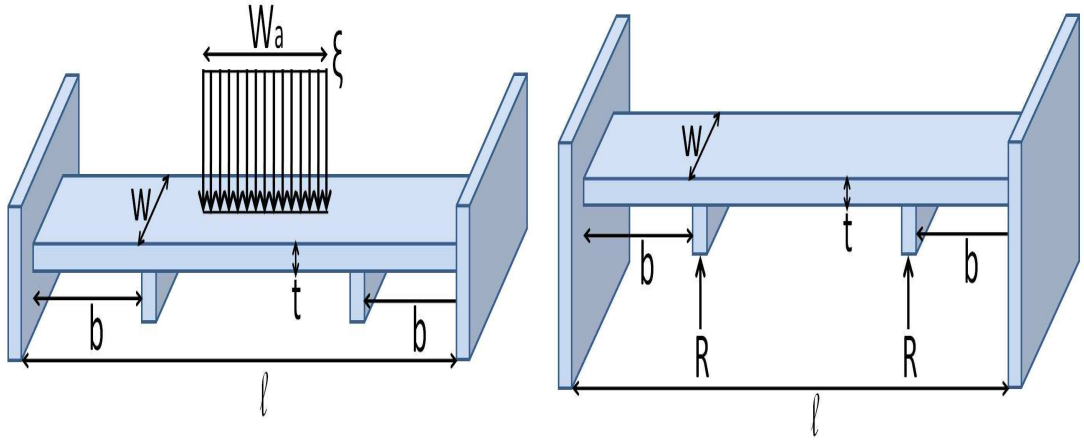

(a) The first group of forces, distributed load due to the actuation

(b) The second group of forces, two concentrated forces due to stoppers contact

Figure A.2.: The two load cases used for superposition.

which is validated by simulation in paragraph 6.2.5.

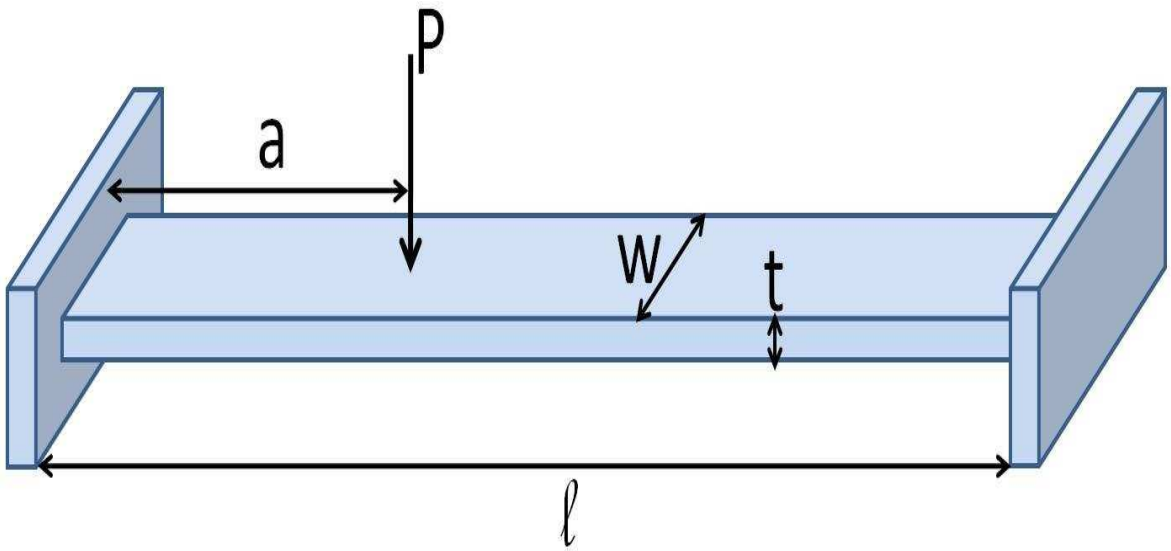

Figure A.3.: Scheme of the concentrated load.

The expression of the deformation of the beam at any point of distance x from the left anchor is given by:

$$\delta_1(x) = \frac{-Pa(l-a)^2x^2}{2l^2EI} + \frac{P(l+2a)(l-a)^2x^3}{6l^3EI} \qquad 0 \leqslant x \leqslant a \tag{A.1}$$

$$\delta_2(x) = \frac{-Pa^2(l-a)(l-x)^2}{2l^2EI} + \frac{Pa^2(3l-2a)(l-x)^3}{6l^3EI} \qquad a \leqslant x \leqslant l \tag{A.2}$$

Now considering a beam, like in figure A.4, loaded with two equal loads symetrical with respect to the middle of the beam.

Using equations (A.1) and (A.2) and the symmetry conditions , we can deduce the expression of the deflection due to the symetrical load by simply replacing x by (l-x). We obtain:

$$\delta_3(x) = \frac{-Pa^2(l-a)x^2}{2l^2EI} + \frac{Pa^2(3l-2a)x^3}{6l^3EI} \qquad 0 \leqslant x \leqslant l-a \tag{A.3}$$

$$\delta_4(x) = \frac{-Pa(l-a)^2(l-x)^2}{2l^2EI} + \frac{P(l+2a)(l-a)^2(l-x)^3}{6l^3EI} \qquad l-a \leqslant x \leqslant a \tag{A.4}$$

By superposing the two loads, we will obtain the deflection of the beam in the different intervals:

$$\delta_5(x) = \delta_1(x) + \delta_3(x) \qquad 0 \leqslant x \leqslant a \tag{A.5}$$

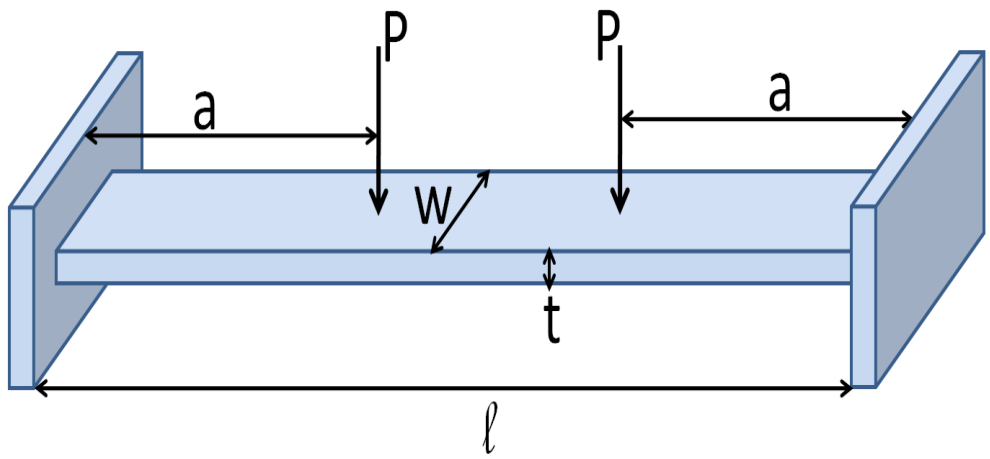

Figure A.4.: Scheme of the two symetrical concentrated loads.

$$\delta_6(x) = \delta_2(l-x) + \delta_3(x) \qquad a \leqslant x \leqslant l-a \tag{A.6}$$

$$\delta_7(x) = \delta_2(x) + \delta_4(x) \qquad l-a \leqslant x \leqslant l \tag{A.7}$$

We deduce the expression for $\delta_5(x)$, $\delta_6(x)$ and $\delta_7(x)$:

$$\delta_5(x) = \frac{-Pax^2(1-\frac{a}{l})}{2EI} + \frac{Px^3}{6EI} \qquad 0 \leqslant x \leqslant a \tag{A.8}$$

$$\delta_6(x) = \frac{-Pa^2(l-a)\Big((l-x)^2+x^2\Big)}{2l^2EI} + \frac{Pa^2(3l-2a)\Big((l-x)^3+x^3\Big)}{6l^3EI} \qquad a \leqslant x \leqslant l-a \tag{A.9}$$

$$\delta_7(x) = \frac{-Pa(l-x)^2(1-\frac{a}{l})}{2EI} + \frac{P(l-x)^3}{6EI} \qquad l-a \leqslant x \leqslant l \tag{A.10}$$

To model the stoppers now, we replace their contact by two concentrated loads. If the stoppers are at a distance "b" from each anchor, then we write the expression of the deflection due to the reaction force of the stopper by replacing P by -R and "a" by "b" in equations (A.8), (A.9) and (A.10).

$$\delta_8(x) = \frac{Rbx^2(1-\frac{b}{l})}{2EI} + \frac{-Rx^3}{6EI} \qquad 0 \leqslant x \leqslant b \tag{A.11}$$

$$\delta_9(x) = \frac{Rb^2(l-b)\Big((l-x)^2+x^2\Big)}{2l^2EI} + \frac{-Rb^2(3l-2b)\Big((l-x)^3+x^3\Big)}{6l^3EI} \qquad b \leqslant x \leqslant l-b \tag{A.12}$$

$$\delta_{10}(x) = \frac{Rb(l-x)^2(1-\frac{b}{l})}{2EI} + \frac{-R(l-x)^3}{6EI} \qquad l-b \leqslant x \leqslant l \tag{A.13}$$

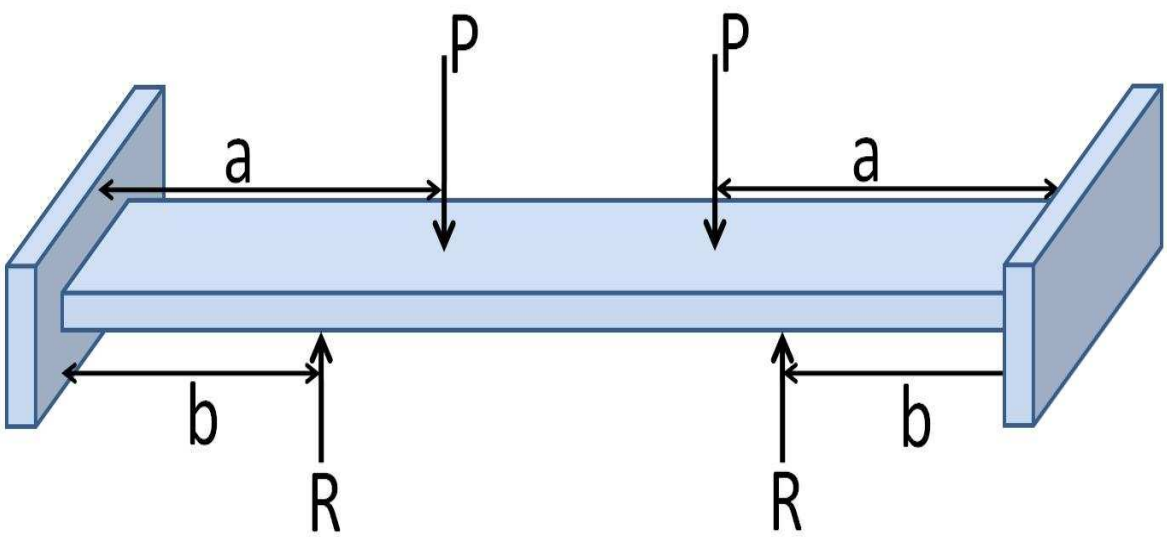

Figure A.5.: Superposition of two groupes of forces.

For the calculation of stiffness, we only need the value of the deflection at the center. For the boundary condition in order to solve for R, we need de deflection at the position of the stoppers. Now supperposing both effects to obtain the complete model as in figure A.5, we will add the expressions only on the points of interest. In our application, we have always the condition that:

$$b \leqslant a \leqslant \frac{l}{2}$$

With the corresponding expressions we obtain:

$$\delta_{Complete}(b) = \delta_6(b) + \delta_9(b) \tag{A.14}$$

$$\delta_{Complete}(\frac{l}{2}) = \delta_5(\frac{l}{2}) + \delta_8(\frac{l}{2}) \tag{A.15}$$

At x=b, the displacement is blocked by the stoppers. As a boundary condition we can write:

$$\delta_{Complete}(b) = g_o - t_s \tag{A.16}$$

So we can deduce the expression of R function of P.

$$R = P\frac{(a - \frac{a^2}{l} - \frac{b}{3})}{b(\frac{2}{3} - \frac{b}{l})} + 2(g_o - t_s)EI \tag{A.17}$$

Replacing R obtained from (A.17) in (A.15)

$$\delta_{Complete}(\frac{l}{2}) = \frac{P}{24EI(2l-3b)}(Term1 + Term2 + Term3 + Term4) + D \tag{A.18}$$

$$Term1 = a^3(8l - 12b) \tag{A.19}$$

$$Term2 = a^2(12b^2 - 6l^2) \tag{A.20}$$

$$Term3 = a(9l^2b - 12lb^2) \tag{A.21}$$

$$Term4 = (4b^3l - 3l^2b^2) \tag{A.22}$$

With D being a term constant independant from the charge P, coming from the displacement before reaching contact and given by:

$$D = \frac{b^2(g_o - t_s)(3l - 4b)}{12} \tag{A.23}$$

Going back to the real problem, we have a uniformly distributed load of intensity ξ centered over a distance W_a. The load is then ξda and we'll integrate this force over the half of the actuation width in order to get the total deflection.

$$\delta_T(l/2) = \int_{\frac{l-W_a}{2}}^{\frac{l}{2}} \underbrace{\frac{\xi}{24EI(2l-3b)}}_{Cst}(Term1 + Term2 + Term3 + Term4)\mathrm{d}a + D\mathrm{d}a \tag{A.24}$$

$$\int_{\frac{l-W_a}{2}}^{\frac{l}{2}} Term1.\mathrm{d}a = \frac{W_a(2l-3b)}{16}(-W_a^3 + 4lW_a^2 - 6l^2W_a + 4l^3) \tag{A.25}$$

$$\int_{\frac{l-W_a}{2}}^{\frac{l}{2}} Term2.\mathrm{d}a = \frac{4W_a(2b^2 - l^2)}{16}(W_a^2 - 3lW_a + 3l^2) \tag{A.26}$$

$$\int_{\frac{l-W_a}{2}}^{\frac{l}{2}} Term3.\mathrm{d}a = \frac{6W_alb(3l-4b)}{16}(-W_a + 2l) \tag{A.27}$$

$$\int_{\frac{l-W_a}{2}}^{\frac{l}{2}} Term4.\mathrm{d}a = \frac{8W_ab^2l(4b-3l)}{16} \tag{A.28}$$

$$\int_{\frac{l-W_a}{2}}^{\frac{l}{2}} D\mathrm{d}a = D\frac{W_a}{2} \tag{A.29}$$

$$\delta_T(l/2) = \frac{\xi W_a}{24EI(2l-3b)}(Term5 + Term6 + Term7) + D\frac{W_a}{2} \tag{A.30}$$

$$Term5 = W_a^3\frac{(3b-2l)}{16} \tag{A.31}$$

$$Term6 = W_a^2\frac{(4l^2-12bl+8b^2)}{16} \tag{A.32}$$

$$Term7 = \frac{l(-4l^3+24l^2b-48lb^2+32b^3)}{16} \tag{A.33}$$

$$K_{sB} = \frac{-\mathrm{d}P}{\mathrm{d}\delta_T(l/2)} = \frac{-\mathrm{d}\xi W_a}{\mathrm{d}\delta_T(l/2)} \tag{A.34}$$

We can see that the stiffness is independent from the displacement before reaching contact.

$$K_{sB} = \frac{-24EI(2l-3b)}{Term5 + Term6 + Term7} \tag{A.35}$$

The expression, given by [56], of the stiffness of a clamped-clamped beam without stoppers, or in other words before contact is:

$$K_B = \frac{32EWt^3}{W_a^3 - 2lW_a^2 + 2l^3} \tag{A.36}$$

With

$$I = \frac{Wt^3}{12} \tag{A.37}$$

When b=0, the beam will behave as if there are no stoppers and the stiffness obtained is that of a beam without stoppers, that is before contact. Equation (A.35) will then become the same as equation (A.36) as shown below in equation (A.38).

$$K_B = -384EI2l\frac{1}{-2lW_a^3 + 4l^2W_a^2 - 4l^4} = \frac{32EWt^3}{W_a^3 - 2lW_a^2 + 2l^3} \tag{A.38}$$

A.3. Stiffness due to initial stress

The model of the stiffness due to initial stress, K_{IS}, is derived from the wire theory. We consider that the beam when deflected, it behaves like a stretched wire as shown in figure A.6. The biaxial initial stress, σ, in the wire will act as a stretching force S pulling on both ends and is related to poisson's ratio, ν, of the material [57]. The expression of S is given by equation (A.39) obtained by multiplying the stress by the cross section area.

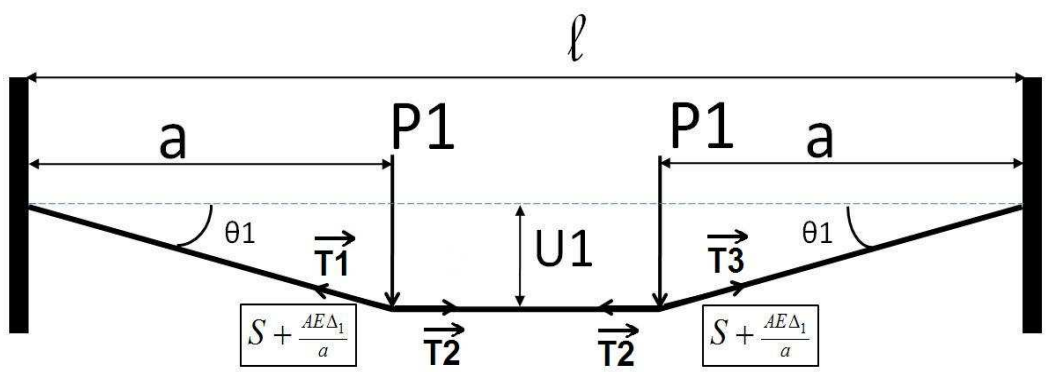

Figure A.6.: Modele of a beam like stretched wire with a concentrated load.

$$S = \sigma(1-\nu)tw \tag{A.39}$$

When we apply two vertical concentrated loads symetrical with respect to the center of the beam and at a distance "a" from the extrimity, the structure will be deflected by an amount of U as shown in figure A.6. Due to the deflection, the wire is streched and the axial stress in the structure is increased by an amount of EΔ/l. Where Δ is the elongation of the wire calculated by equation(A.40):

$$\Delta = 2\sqrt{a^2+U^2} - 2a = 2a\sqrt{1+\frac{U^2}{a^2}} - 2a \tag{A.40}$$

Since we are in small deflections, equation (A.40) becomes:

$$\Delta = 2a(1+\frac{U^2}{2a^2}) - 2a = \frac{U^2}{a} \tag{A.41}$$

Considering the case just before the contact of the stoppers, like the case in figure A.6, we have for a load P1 a deflection U1. The structure is at equilibrium when the sum of forces at any point is zero with $|\overrightarrow{T1}| = |\overrightarrow{T3}|$. If we isolate the point of application of the load and write the equilibrium equations we obtain:

$$\Sigma\overrightarrow{F} = \overrightarrow{P1} + \overrightarrow{T1} + \overrightarrow{T2} = \overrightarrow{0} \tag{A.42}$$

since we are in small deflections and small angles, we have

$$\sin(\theta 1) \simeq \tan(\theta 1) = \frac{U1}{a} \tag{A.43}$$

Now projecting (A.42) the forces on the vertical and neglecting the stress increase due to elongation, we obtain:

$$P1 = S\frac{U1}{a} \tag{A.44}$$

$$U1 = \frac{a.P1}{S} \tag{A.45}$$

we have a uniformly distributed load of intensity ξ centered over a distance W_a. The load is then $\xi_1 \mathrm{d}a$ and we'll use the symmetry to integrate this force over the half of the actuation width in order to get the total deflection.

$$U1_T(l/2) = \int_{\frac{l-W_a}{2}}^{\frac{l}{2}} \frac{a.\xi_1}{S}\mathrm{d}a = \frac{\xi_1 W_a}{8S}(2l - W_a) \tag{A.46}$$

$$K_{IS} = \frac{\xi_1 W_a}{U1_T(l/2)} = \frac{8S}{(2l - W_a)} = \frac{8\sigma(1-\nu)tw}{(2l - W_a)} \tag{A.47}$$

In the case where we have contact of the stoppers, we have a stiffness K_{sIS}, the case will be as shown in figure A.7. We have for a load P2 a deflection U2. The structure is at equilibrium, by projecting the equilibrium equations along the vertical and neglecting the effect of elongation, as we have done previously, we obtain:

$$P2 = S\sin(\theta 2) \tag{A.48}$$

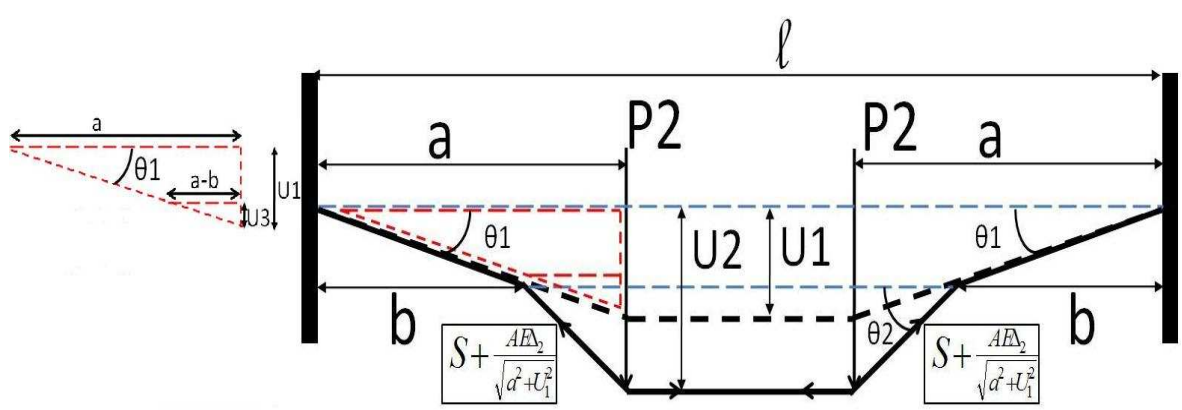

Figure A.7.: Model of a beam as a stretched wire with stoppers and two symetric concentrated loads.

Staying in the case of small deflections and small angles, we have:

$$\sin(\theta 2) \simeq \tan(\theta 2) = \frac{U2 - U1 + U3}{a - b} \tag{A.49}$$

where U3 is shown on the red dotted triangle to the left of the figure. Using Thales theorem, or the property of similar triangles we have:

$$\frac{U3}{U1} = \frac{a-b}{a} \Rightarrow U3 = U1\frac{a-b}{a} \tag{A.50}$$

$$\sin(\theta 2) \simeq \frac{aU2 - bU1}{a(a-b)} \tag{A.51}$$

and the expression of P2 becomes

$$P2 = S\frac{aU2 - bU1}{a(a-b)} \Rightarrow U2 = \frac{P2(a-b)}{S} + \frac{b}{a}U1 = \frac{P2(a-b)}{S} + \frac{bP1}{S} \tag{A.52}$$

now we will integrat the expression of U2 as we did for U1 by replacing P1 by $\xi_1 \mathrm{d}a$ and P2 by $\xi_2 \mathrm{d}a$ to obtain.

$$U2_T(l/2) = \int_{\frac{l-W_a}{2}}^{\frac{l}{2}} (\frac{\xi_2(a-b)}{S} + \frac{b\xi_1}{S})\mathrm{d}a \tag{A.53}$$

$$U2_T(l/2) = \frac{\xi_2 W_a}{8S}(2l - W_a - 4b) + \frac{b\xi_1 W_a}{2S} \tag{A.54}$$

We deduce the expression

$$U2_T(l/2) - U1_T(l/2) = (\xi_2 W_a - \xi_1 W_a)\frac{2l - 4b - W_a}{8S} \tag{A.55}$$

The stiffness due to initial stress after contact will be

$$K_{sIS} = \frac{\xi_2 W_a - \xi_1 W_a}{U2_T(l/2) - U1_T(l/2)} = \frac{8\sigma(1-\nu)tw}{2l - 4b - W_a} \tag{A.56}$$

Bibliography

[1] H. NATHANSON, W. NEWELL, R. WICKSTROM, and J. DAVIS, "The resonant gate transistor," *IEEE Transactions on electronic devices*, 1967.

[2] K. REBELLO, "Applications of mems in surgery," in *Proceedings of the IEEE*.

[3] "Novamems short course about mems."

[4] Y. developpement, "Mems buisness continues in growth," Yole Developpement, Tech. Rep., 2008.

[5] Y. Developpement, "Mems4mobile 06: updated analysis of the applications and markets of mems in mobile communications," Yole Developpement, Tech. Rep., 2006.

[6] F. CONSEIL, "Simulation, conception et realisation d'un commutateur en technologie microsysteme pour dispositifs logiques securitaires," Ph.D. dissertation, Universite des sciences et technologies de Lille, 2004.

[7] A. FLYNN, L. TAVROW, S. BART, R. BROOKS, D. EHRLICH, K. UDAYAKUMAR, and L. CROSS, "Piezoelectric micromotors for microrobots," in *Ultrasonics symposium*.

[8] Q. HUANG and N. LEE, "Analysis and design of polysilicon thermal flexure actuator," *Journal of micromechanics and microengineering*, 1999.

[9] CRAGUN and al, "Linear thermomechanical microactuators," in *ASME IMECE*.

[10] W. CHU, M. MEHREGANY, and R. MULLEN, "Analysis of tip deflection and force for bimetallic cantilever microactuator," *Journal of micromechanics and microengineering*, 1993.

[11] C. GOLDSMITH, D. FOREHAND, D. SCARBOURGH, Z. PENG, C. PALEGO, J. HWANG, and J. CLEVENGER, "Understanding and improving longevity in rf mems capacitive switches," in *SPIE*.

[12] J. SIMON, S. SAFFER, and C. KIM, "A liquid-filled microrelay with a moving mercury micro-drop," *Journal of Micro Electro Mechanical Systems*, 1997.

[13] P. BLONDY, A. CRUNTEANU, C. CHAMPEAUX, A. CATHERINOT, P. TRISTAN, O. VENDIER, J. CAZAUx, and L. MARCHAND, "Dielectric less capacitive mems switch," *Microwave symposium Digest, 2004 IEEE MTT-S international*, 2004.

[14] D. MARDIVIRIN, D. BOUYGE, A. CRUNTEANU, A. POTHIER, and P. BLONDY, "Study of residual charging in dielectric less capacitive mems switches," *Microwave symposium Digest, 2008 IEEE MTT-S international*, 2008.

[15] D. MARDIVIRIN, A. POTHIER, A. CRUNTEANU, and P. BLONDY, "Charging effect in rf mems switches with dielectric less actuators," in *MEMSWAVE 2008*.

[16] P. EKKELS, X. ROTTENBERG, R. PUERS, and H. TILMANS, "Simple and robust air gap-based mems technology for rf-applications," in *MEMSWAVE 2008*.

[17] P. SEUNGHOON, "A study on buckled-beam actuators for rf mems applications," Master's thesis, Dong-A university (KOREA) and Louisiana State University, 2007.

[18] A. VALENTINI, "Conception et realisation d'un micro-actionneur piezoelectrique," Master's thesis, Universite Libre de Bruxelle with Politecnico di Milano, 2001.

[19] "www.memsinvestorjournal.com/2007/10/fr-mems-switche.html."

[20] "www.ansys.com/industries/mems-what-is.asp."

[21] Y. Developpement, "Memsfoundries: Analysis of the market and business trends of mems foundries and contract manufacturers," Yole Developpement, Tech. Rep., 2006.

[22] "www.en.wikipedia.org/wiki/rf_mems."

[23] *RF MEMS: Theory, Design, and Technology.* John Wiley & Sons, 2003.

[24] M. POTIN, "Rf mems switch market, analysis of the market potential of rf mems switches based products in defence, industrial, automotive and telecom applications," Yole Developpement, Tech. Rep., 2007.

[25] W. van SPENGEN, R. PUERS, and I. DE WOLF, "A physical model to predict stiction in mems," *Journal of micromechanics and microengineering (IEEE)*, 2002.

[26] R. MABOUDIAN and R. HOWE, "Critical review: adhesion in surface micromechanical structures," *J. Vac. Sci. Thechnol.*, 1997.

[27] V. AGACHE, E. QUEVY, D. COLLARD, and L. BUCHAILLOT, "Stiction-controlled locking system for three-dimensional self-assembled microstructures: theory and experimental validation," *Appl. Phys. Lett.*, 2001.

[28] M. YAMAGUCHI and K. KAWAMURA, "Distributed electrostatic microactuator," in *MEMS93*.

[29] T. AKIYAMA and K. SHONO, "A new step motion of polysilicon microstructures," in *MEMS93*.

[30] I. SCHIELE and B. HILLERICH, "Comparison of lateral and vertical switches for application as microrelays," *Journal of micromechanics and microengineering*, 1999.

[31] J. Wright and Y. TAI, "Micro-miniature electromagnetic switches fabricated using mems technology," in *46th annual int. relay conference, NARM '98*.

[32] J. KO, M. LEE, D. LEE, C. CHOI, and Y. KIM, "Development and application of a laterally driven electromagnetic microactuator," *Applied physics letter*, 2002.

[33] L. LAGORCE, O. BRAND, and M. ALLEN, "Magnetic microactuators based on polymer magnet," *Journal of MEMS*, 1999.

[34] M. BECK, M. AHMED, C. BRIERLEY, A. NEEDHAM, and S. MARSH, "Microwave filters and switch produced using micro-machining techniques," in *Int. microwave symposium 2000*.

[35] S. ZHOU, S. XI-QING, and N. WILLIAM, "A micro variable inductor chip using mems relays," in *Digest Int. Conference on solide-state sensors and actuators (Transducer '97)*.

[36] R. PLANA and al, "Integrated rf-mems switch based on a combination of thermal and electrostatic actuation," in *Transducer 2003*.

[37] Y. WANG and al, "Low-voltage lateral-contact microrelays for rf applications," in *MEMS '02*.

[38] Q. HUANG and N. LEE, "Analysis and design of polysilicon thermal flexure actuator," *Journal of micromechanics and microengineering*, 1999.

[39] J. CORNTOIS and V. BRIGHT, "Applications for surface-micromachined polysilicon thermal actuators and arrays," *Sensors and actuators A*, 1997.

[40] K. ARAI and T. HONDA, "Micromagnetic actuators," *Robotica*, 1996.

[41] "http://en.wikipedia.org/wiki/shape_memory_alloy."

[42] *SHAPE MEMORY MATERIAL*. CAMBRIDGE university press, 2002.

[43] L. BRINSON, "One-dimensional constitutive behavior of shape memory alloys: thermomechanical derivation with non-constant material functions and redefined martensite internal variable," *Journal of intelligent material systems and structures*, 1993.

[44] C. LEXCELLENT and E. GIBEAU, "A short review of shape memory alloys thermomechanical models," *Solid state phenomena*, 2008.

[45] P. KRULEVITCH, A. LEE, P. RAMSEY, J. TREVINO, J. HAMILTON, and M. NORTHRUP, "Thin film shape memory alloy microactuators," *Journal of MEMS*, 1996.

[46] D. MARDIVIRIN, D. BOUYGE, A. CRUNTEANU, A. POTHIER, and P. BLONDY, "Contactless dielectric charging mechanisms in rf-mems capacitive switches," *Proceedings of the 36th European microwave conference*, 2006.

[47] T. LISEC, C. HUTH, and B. WAGNER, "Dielectric material impact on capacitive rf mems reliability," in *34th European microwave conference*.

[48] R. HERFST, P. STEENEKEN, and J. SCHMITZ, "Time and voltage dependence of dielectric charging in rf mems capacitive switches," *IEEE 07CH37867 45th annual international reliability physics symposium*, 2007.

[49] P. CZARNECKI, X. ROTTENBERG, P. SOUSSAN, P. NOLMANS, P. EKKELS, P. MULLER, H. TILMANS, W. DE RAEDT, R. PUERS, L. MARCHAND, and I. DE WOLF, "New insights into charging in capacitive rf mems switches," *IEEE CFP8RPS-CDR 46th annual international reliability physics symposium*, 2008.

[50] P. ZHEN, Y. XIAOBIN, J. HWANG, I. FOREHAND, and C. GOLDSMITH, "Superposition model for dielectric charging of rf mems capacitive switches under bipolar caontrol-voltage waveforms," *IEEE transactions on microwave theory and techniques*, 2007.

[51] T. IKEHASHI, T. MIYAZAKI, H. YAMAZAKI, A. SUZUKI, E. OGAWA, S. MIYANO, T. SAITO, T. OHGURO, T. MIYAGI, Y. SUGIZAKI, N. OTSUKA, H. SHIBATA, and Y. TOYOSHIMA, "An rf mems variable capacitor with intelligent bipolar actuation," in *2008 IEEE international solid-state circuits conference (ISSCC 2008)*.

[52] W. SHEN, R. EDWARDS, and C. KIM, "Electrostatically actuated metal-droplet microswitches integrated on cmos chip," *Journal of Micro Electro Mechanical Systems*, 2006.

[53] J. SIMON, S. SAFFER, F. SHERMAN, and C. KIM, "Lateral polysilicon microrelays with a mercury microdrop contact," *IEEE transactions on industrial electronics*, 1998.

[54] L. DeVoe and A. PISANO, "Modeling and optimal design of piezoelectric cantilever microactuators," *Journal of microelectromechanical systems (IEEE)*, 1997.

[55] S. KRYLOV, S. SERETENSKY, and D. SCHREIBER, "Pull-in behavior and multistability of a curved microbeam actuated by a distributed electrostatic force," in *MEMS 2008*.

[56] *RF MEMS: Theory, Design, and Technology.* John Wiley & Sons, 2003.

[57] *Mechanics of Materials.* PWS Publishing Company, Boston, 1997.

[58] "www.wtec.org/loyola/mems."

[59] "www2.parc.com/spl/projects/smart-matter/structural-enhance.html."

[60] "www.gmu.edu/departments/seor/student_project/syst101_00b/team07/applications.html."

[61] "www.mems-exchange.org/mems/applications.html."

[62] "www.eng.cam.ac.uk/~yf229/mems%20introduction.htm."

[63] "www.microlab.net."

[64] D. PEYROU, "Etude theorique et experimental des techniques d'assemblage et de mise en boitier pour l'integration de microsystems radiofrequence," Ph.D. dissertation, Universite de Paul Sabatier de Toulouse, 2006.

[65] S. Mohamed, "Optimisation des circuits passifs micro-ondes suspendus sur membrane dielectrique," Ph.D. dissertation, Universite de Paul Sabatier de Toulouse, 2005.

[66] "Novamems short course about failure analysis."

[67] "Novamems short course about characterisation techniques."

[68] X. CHEN, C. FOX, and S. Mc WILLIAM, "Modeling of a tunable capacitor with piezoelectric actuation," *Journal of micromechanics and microengineering (IEEE)*, 2004.

[69] H. ROUABAH, C. GOLLASCH, and M. KRAFT, "Design optimisation of an electrostatics mems actuator with low spring constant for an atom chip," University of Southampton, Tech. Rep., 2006.

[70] S. GROSS, "Micromachined switches and cantilever actuators based on piezoelectric lead zirconate titanate (pzt)," Ph.D. dissertation, Pennsylvania State University, department of electrical engineering, 2004.

[71] L. LATORRE, J. KIM, C. LEE, P. DE GUZMAN, H. LEE, P. NOUET, and C. KIM, "Electrostatic actuation of microscale liquid-metal droplets," *Journal of Micro Electro Mechanical Systems*, 2002.

[72] S. MELLE, D. DE CONTO, D. DUBUC, K. GRENIER, O. VENDIER, J. MURARO, J. CAZAUX, and R. PLANA, "Reliability modeling of capacitive rf mems," *IEEE transactions on microwave theory and techniques*, 2005.

[73] X. ROTTENBERG, P. EKKELS, S. BREBELS, T. WEBERS, P. CZARNECKI, R. MERTENS, B. NAUWELAERS, R. PUERS, L. MARCHAND, I. DE WOLF, W. DE RAEDT, and H. TILMANS, "Novel effa-based thin-film rf-mems technology," in *IEEE 14th international conference on solid state sensors, actuators and microsystems (Transducers and Eurosensors)*.

[74] B. LAKSHMINARAYANAN, D. MERCIER, and G. REBEIZ, "High-reliability miniature rf-mems switched capacitors," *IEEE transactions on microwave theory and techniques*, 2008.

[75] X. ROTTENBERG, B. NAUWELAERS, W. DE RAEDT, and H. TILMANS, "Distributed dielectric chargingand its impact on rf mems devices," in *34th European microwave conference*.

[76] G. PAPAIOANNU, R. MARCELLI, G. BARTOLUCCI, S. CANTONI, G. DE ANGELIS, A. LUCIBELLO, E. PROIETTI, B. MARGESIN, F. GIACOMOZZI, and F. DEBORGIES, "Charging effects and related equivalent circuits for ohmic series and shunt capacitive rf mems switches," in *MEMSWAVE 2008*.

[77] V. LEUS and D. ELATA, "An efficient modeling method for simulating time-response of rf-mems switches," in *MEMSWAVE 2008*.

[78] M. SAKATA, Y. KOMURA, T. SEKI, K. KOBAYASHI, K. SANO, and S. HORIIKE, "Micromachined relay which utilizes single crystal silicon electrostatic actuator," in *MEMS99*.

[79] R. SATTLER, P. VOIGT, H. PRADEL, and G. WACHUTKAL, "Innovative design and modelling of a micromechanical relay with electrostatic actuation," *Journal of micromechanics and microengineering*, 2001.

[80] C. GOLDSMITH, J. RANDALL, S. ESHELMAN, T. LIN, D. DENNISTON, S. CHEN, and B. NORVELL, "Characteristics of micromachined switches at microwave frequencies," in *Tech. Digest, IEEE Microwave theory and techniques symposium*.

[81] C. CHANG and P. CHANG, "Innovative micromachined microwave switch with very low insertion loss," in *Digest Int. Conference on solide-state sensors and actuators (Transducer '99)*.

[82] J. YAO and M. CHANG, "A surface micromachined miniature switch for telecommunications applications with signal frequencies from dc up to 4 ghz," in *Transducer '95*.

[83] C. GOLDSMITH, T. LIN, B. POWERS, W. WU, and B. NORVELL, "Micromechanical membrane switches for microwave applications," in *IEEE Microwave theory and techniques symposium.*

[84] C. GOLDSMITH, Z. YAO, S. ESHELMAN, and D. DENNISTON, "Performance of low-loss rf mems capacitive switches," in *IEEE Microwave and guided wave letters.*

[85] J. Muldavin and G. REBEIZ, "High isolation cpw mems shunt switches part 1: Modeling," in *IEEE transaction on Microwave theory and techniques.*

[86] M. TANG, A. LIU, A. AGARWAL, Q. ZHANG, and P. WIN, "A new approach of lateral rf mems switch," in *Analog integrated circuits and signal processing.*

[87] M. TANG, A. LIU, and A. AGARWAL, "A compact dc-20ghz spdt switch circuit using lateral rf mems switches," in *APMC2005 proceedings.*

[88] J. Muldavin and G. REBEIZ, "Rf mems switches and switch circuits," *IEEE microwave magazine*, 2001.

[89] M. WUTTIG, J. LI, and C. CRACIUNESCU, "A new ferromagnetic shape memory alloy system," *Scripta materialia*, 2001.

[90] J. GAUTHIER, A. HUBERT, J. ABADIE, N. CHAILLET, and C. LEXCELLENT, "Nonlinear hamiltonian modelling of magnetic shape memory alloy based actuators," *Sensors and Actuators A Physical*, 2008.

Abstract Français

MEMS est un système électromécanique à l'échelle du micron comprenant des capteurs ainsi que des actionneurs (micro moteurs, micro miroirs, micro relais...) fabriqués avec les techniques de la micro-électronique conventionnelle (croissance d'oxyde, dépôt de matériaux, lithographie). Les plupart des commutateurs RF MEMS sont actionnés à l'aide des forces électrostatique pour faire changer la distance entre deux électrodes pour couper ou transmettre le signal. Ce type d'actionnement, malgré ces avantages, il a un inconvénient majeur qu'il s'agit du chargement du diélectrique qui mène à l'échec de ce commutateur. Pour résoudre ce problème, on a travaillé en parallèle sur deux axes différents. Le premier axe s'agit de changer le type d'actionnement qui est la raison du chargement en actionnement piézoélectrique tandis que le deuxième consiste à garder l'actionnement électrostatique mais en améliorant le comportement des structures utilisées en augmentant la force de rappel pour surmonter le phénomène du collage sans changer la tension d'actionnement. Une étape a succédé ce travail qui s'agissait d'une validation de la plateforme numérique avant de l'utiliser à modéliser nos structures.